ANNUAL REPORT

NOVEMBER 1993

Innovative Processing of Composites for Ultra-High Temperature Applications

by

Reza Abbaschian
Department of Materials Science and Engineering
University of Florida
Gainesville, Florida

Sponsored by: The Advanced Research Projects Agency

Monitored by: The Office of Naval Research

ARPA Grant No. N00014-91-J-4075

BOOK III OF III

Executive Summary

The overall objective of this program was to provide a fundamental understanding of the processing science and technology necessary to fabricate ceramic-matrix, intermetallic-matrix, and metal-matrix composites with superior mechanical properties in high temperature and oxidizing environments. The composites are intended for use as structural materials for advanced aerospace applications at temperatures exceeding 1200°C (2200°F).

In order to accomplish the program objective, interactive research groups were established in three key area of (a) Fiber Fabrication, (b) Coatings and Infiltration, and (c) Composite Fabrication. The objective of the fiber fabrication group was to develop new fibers which have superior strength and toughness at high temperatures and in oxidizing environments. The research effort focused on the development of two types of fibers: (1) glass-free mullite-based fibers, and (2) oxygen-free silicon carbide fibers. The coatings program had two primary objectives: (1) to control the characteristics of matrix/reinforcing phase interfaces (e.g., to control chemical reactions and bonding at a matrix/fiber interface) and (2) to develop coatings that will improve the oxidation resistance of metal-matrix and intermetallic-matrix composites. Coatings methods utilized included chemical vapor deposition, sol-gel processing, and solution coating with polymeric precursors to ceramics.

The composite fabrication group investigated various methods to incorporate reinforcing phases (i.e., fibers, whiskers, and particulates) into ceramic-, metal-, and intermetallic-matrices. Processing methods investigated included colloidal processing, chemical vapor infiltration, reactive hot-compaction and *in situ* coating, and microwave sintering. The objectives were not only to utilize innovative processing techniques, but also to develop an improved scientific understanding of processing-microstructure relationships in composites fabrication.

This annual report consists of seven sections compiled in three books as described below:

Book I

Section 1 Processing and Properties of Silicon Carbide Fibers
Principal Investigators: C.D. Batich
M.D. Sacks

Section 2 Processing of Mullite Composite Fibers
Principal Investigators: A.B. Brennan
J.H. Simmons

Section 3 Chemical Vapor Deposition (CVD) and Chemical Vapor Infiltration (CVI)
Principal Investigator: T. Anderson

Book II

Section 1 Processing and Properties of Intermetallic Matrix Composites
Principal Investigator: R. Abbaschian

Section 2 Mechanical Alloying of $MoSi_2$
Principal Investigator: M.J. Kaufman

Book III

Section 1 Processing of Ceramic Matrix Composites
Principal Investigator: M.D. Sacks

Section 2 Processing of $BaO\text{-}Al_2O_3\text{-}2SiO_2$ Fibers.
Principal Investigator: D.E. Clark

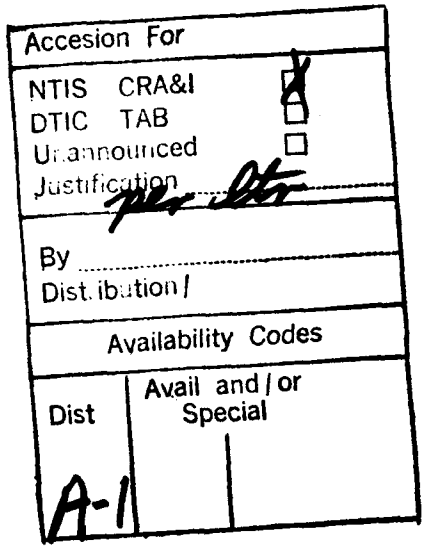

BOOK III

Section 1

Processing

of

Ceramic Matrix Composites

Principal Investigator: M.D. Sacks

Processing of Ceramic-Matrix Composites

Principal Investigator: **M.D. Sacks**

Objectives

The overall objectives of this program are:

- To develop improved processing methods for enhancing densification, controlling shrinkage and tailoring microstructure development in ceramic-matrix composites.

- To develop ceramic-matrix composites with high temperature properties (mechanical, chemical and dielectric) suitable for high temperature structural applications.

These objectives are currently being pursued throughout two projects:

(1) Viscous, Transient Viscous and Pressure-Assisted Transient Viscous Sintering of Ceramics and Composites Using Submicron Composite Particles.

(2) Processing of Ceramics and Composites by Liquid Infiltration Processing.

Project #1: Viscous, Transient Viscous and Pressure-Assisted Transient Viscous Sintering of Ceramics and Composites Using Submicron Composites Particles

Background and Approach

Powder compact densification is often hindered by the presence of "non-sinterable" inclusions (e.g., particles, whiskers). In particular, densification rates are severely impeded when the non-sinterable phase forms a connected network (i.e., when the concentration is large enough to form a percolation path). In conventional powder processing methods, inclusions can form connected networks at relatively low volume fraction (se Figure 1, left side). However, an effective method for avoiding the formation of percolation network is illustrated in the right side of Figure 1. The non-sinterable particles B are coated with a layer of A, thereby completely isolating them from each other.

Previous studies have shown that non-sinterable inclusions have less effect on the densification rate when the matrix phase sinters by viscous flow. Thus, it is anticipated that an especially effective method for enhancing densification rates would utilize composite

particles (as shown in Figure 1, right size) in which the outer coating is an amorphous material. This approach would not only allow fabrication of glass/ceramic composites at relatively low sintering temperature, but would also offer the possibility of developing novel microstructures in which a high concentration of crystalline phase is incorporated into a glassy matrix as isolated inclusions (Figure 2, top right). Furthermore, it is possible that the approach described above could also be applied to the fabrication of single-phase crystalline ceramics and crystalline ceramic-ceramic composites. This would require selection of appropriate core and coating materials that would react at elevated temperatures to eliminate the amorphous phase. An example is illustrated in Figure 2 (bottom) in which the core is alumina and the coating is silica. If the size of the composite particles is selected properly, this combination should viscously sinter at relatively low temperature to form an alumina/siliceous glass composite. At higher temperature, the core and coating would react to form mullite. This process is referred to as transient viscous sintering (TVS). This approach can also be used to fabricate other types of composites by mixing the silica-coated alumina particles with other silica-coated particles (i.e., with different crystalline core materials). In addition, by applying pressure during sintering, it should be possible to viscously densify fiber-reinforced composites. The approach illustrated in Figure 2 depends upon the availability of coated particles in the appropriate size range (i.e., colloidal dimensions).

Research Summary

(1) A process was developed for preparation of submicron composite particles. These particles consisted of inner cores of a crystalline material (e.g., alumina, silicon nitride, silicon carbide, zirconia) and an outer coating of amorphous silica. The volume ratio of amorphous silica/crystalline core could be readily varied over a wide range (see Figure 3). The formation of dense, uniform coatings was demonstrated using a variety of techniques, including SEM, TEM, microelectrophoresis, X-ray Photoelectron Spectroscopy (XPS), etc. (Detailed results are provided in the attached publications.) These particles were used to form a variety of bulk ceramics, glass/ceramic composites, and ceramic-ceramic composites using viscous sintering, transient viscous sintering (TVS) and pressure-assisted TVS.

(2) Glass/ceramic composites (alumina/silica, silica/silicon nitride) were fabricated by viscous sintering using silica-coated composite particles. As discussed below (research summary item #3), the silica/alumina sample were transformed into mullite and mullite-based composites. The silica/silicon nitride composites have potential for applications which require low dielectric constant and good high temperature mechanical properties. Enhanced densification was demonstrated by directly comparing the sintering behavior for compacts prepared with the silica-coated silicon nitride particles vs. a mixture of silica particles and silicon nitride particles (The green compact characteristics were similar to those schematically illustrated in Figure 1.). The increased densification rate for the samples prepared with composite particles can be attributed to 1) viscous flow of the amorphous coating and (2) avoiding the formation of a percolation network of the "non-sinterable" phase. A fully dense ~60 vol% silica/40 vol% silicon nitride composite

had an average dielectric constant value of ~5.0over the frequency range 10^3-10^7 Hz (see Figure 4) and a loss tangent value of ~3 x 10^{-4} at 1 MHz. Composite powder compacts were also prepared with a controlled addition of ~10-12 vol% latex particles. By appropriate choice of sintering schedule, it was possible to produce a microstructure in which isolated, closed pores (~2 μm dia.) were dispersed in a dense silica/silicon nitride matrix (see Figure 5). A ~60vol% silica/40 vol% silicon nitride sample with ~11% porosity had an average dielectric constant value of ~4.3 over the frequency range 10^3-10^7 Hz (see Figure 4) and a loss tangent value of ~2 x 10^{-4} at 1 MHz. Preliminary results show that samples with closed, isolated 2 μm pores have essentially the same flexural strength as the samples without porosity. This indicated that the strength-limiting flaws are larger than 2 μm.

(3) Mullite and mullite-based composites were fabricated by transient viscous sintering of amorphous silica-coated alumina particles. Compacts were sintered to near full density at relatively low temperatures (~1300°C) and subsequently heat treated at higher temperatures (~1500°C) in order to form mullite. The samples remained almost fully dense (i.e., almost zero porosity) after mullitization. (Detailed results are provided in the attached publications.) By using a "seeding" technique to control nucleation of mullite, it was also possible to lower the mullitization temperatures (to ~1400°C) and develop microstructures with a fine, equiaxed grain structure. The temperature needed to accomplish densification and mullitization was not much higher than that used for samples prepared by sol-gel techniques. One of the advantages of the present method was that processing difficulties normally associated with "sol-gel" routes (i.e., large weight losses and shrinkages during drying and sintering) were less of a concern due to the use of (i) considerably larger particles and (ii) alpha alumina (i.e., instead of an alumina precursor).

A variety of mullite-based composites were prepared using the TVS technique. For example, mullite/alumina and mullite/siliceous glass composites were fabricated by simply changing the alumina/silica ratio of the composite particles. Samples could be densified at ~1300°C,while mullitization was carried out at higher temperatures. A dense composite with ~55 vol% Mullite/45 vol% silica had a dielectric constant value of ~4.9and a loss tangent of ~7 x 10^{-4} at 1 MHz. Mullite/SiC_p composites were fabricated by sintering compacts prepared with mixtures of silica-coated particles, i.e.,in which the core materials were alumina and silicon as those processed without the second phase. Mullite/SiC_w composites were prepared using silica-coated alumina particles and uncoated whiskers. Samples with ≥96% relative density of the composite powders was largely controlled by viscous flow of the amorphous silica coating of the particles: (1) Samples with a wide range of alumina/silica weight ratios (i.e., 66/34 - 83/17) showed very similar densification behavior. (2) Samples prepared with coated second phase particles (i.e., silicon carbide) showed essentially the same densification behavior as samples prepared only with silica-coated alumina particles. (3) Samples despite the fact the whiskers were uncoated and their concentration exceeded the critical volume fraction for percolation. These samples densified at much lower temperatures compared to previous work on sintering of mullite/SiC whisker compacts. (Furthermore information is provided in the attached

publication.)

(4) Previous studies have shown that sialons and sialon-based composites have low dielectric constant, good oxidation resistance, and god high temperature mechanical properties. In this study, sialon-based composites were prepared by using mixtures of silica-coated alumina particles, silica-coated silicon nitride particles, and uncoated aluminum nitride particles. Samples were sintered under conditions to give almost fully crystalline samples that consisted primarily of one of the various sialon phases (J, β, or O). Dielectric constants in the range ~5.7-6.2 were observed for all samples. Figure 6 shows a plot of dielectric constant vs. frequency for a dense O-sialon/silicon nitride composite. (Detailed results will be provided in a forthcoming publication.)

(5) Sintered glass/ceramic composites prepared from silica-coated particles can be deformed viscously at elevated temperatures to high stains. This is illustrated in Figure 7 which shows compression stress-strain curves for dense composites prepared from silica-coated alumina particles. It was possible to deform samples to linear strains exceeding 80% without observing microcracking or cavitation (see Figure 8). Samples were subsequently converted to dense, fine-grained mullite by further heat treatment. Based on these results, work has been initiated to prepare fiber-reinforced composites by pressure-assisted TVS. Figure 9 shows stress-strain curve for a silica-coated alumina powder compact reinforced with ~10vol% Nicalon fibers. The sample was densified to ~97% at relatively temperature (1300°C) and pressure (~50MPa).

(6) Research has been initiated to produce composite particles having multicomponent silicate glass coatings. The objective is to lower the sintering temperature by lowering the viscosity of the silicate glass coating on the crystalline core particles. The initial studies have been directed toward preparation of silica coatings doped with boria. Borosilicate glass/alumina composite particles have been produced with ~5wt% $B_2\hat{}O_3$/95 wt% SiO_2 glass coatings. Compacts prepared with these particles had a sintering temperature ~150°C lower than compacts prepared with 100% SiO_2-coated alumina particles. (Figure 10 shows plots of open porosity vs. sintering temperature for the two types of compacts.) On-going work is directed toward forming multicomponent silicate coatings which can be fully crystallized after densification is completed.

Publications

(1) M.D. Sacks, N. Bozkurt and G.W. Scheiffele, "Fabrication of Mullite and Mullite-Matrix Composites by Transient Viscous Sintering of Composite Powders," J. Am. Ceram. Soc., 74 (10) 2428-2437 (1991).

(2) M.D. Sacks, G.W. Scheiffele, N. Bozkurt and R. Raghunathan, "Fabrication of Ceramics and Composites by Viscous and Transient Viscous Sintering of Composite

Particles, "pp. 437-55 in Ceramic Powder Science IV, Ceramic Transactions, Vol. 23, edited by S.-I Hirano, G.L. Messing and H. Hausner, American Ceramic Society, Westerville, OH, 1991.

(3) M.D. Sacks, M.S. Randall, G.W. Scheiffele and J.H. Simmons, "Processing of Silicate Glass/Silicon Nitride Composites with Controlled Microporosity," pp. 407-20 in Advanced Composite Materials, Ceramic Transactions, Vol. 19, edited by M.D. Sacks, American Ceramic Society, Westerville, OH, 1991.

(4) M.D. Sacks, N. Bozkurt and G.W. Scheiffele, "Transient Viscous Sintering of Mullite and Mullite-Matrix Composites," pp. 111-23 in Advanced Composite Materials, Ceramic Transactions, Vol. 19, edited by M.D. Sacks, American Ceramic Society, Westerville, OH, 1991.

(5) M.D. Sacks, G.W. Scheiffele, N. Bozkurt, R. Raghunathan and A.E. Bagwell, "Processing of Composite Powders: Fabrication of Ceramics and Composites by Viscous Sintering and Transient Viscous Sintering," Chapter 50 in Chemical Processing of Advanced Materials, edited by L.L. Hench, J. West and D.R. Ulrich, Wiley, NY, 1992.

Copies of publications 1-4 are attached.

Figure 1

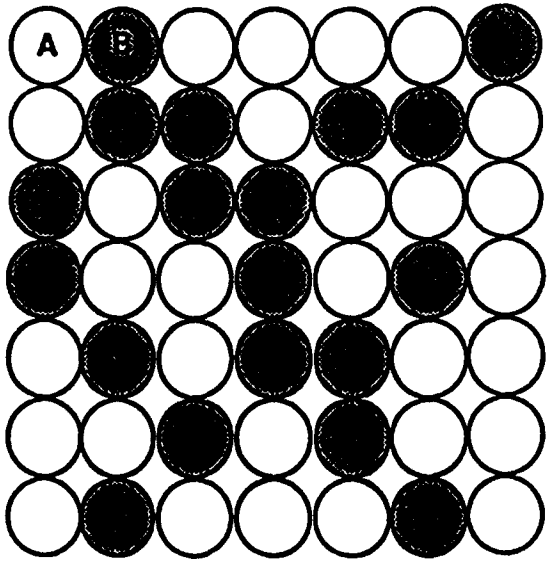

Mixture of A and B Particles

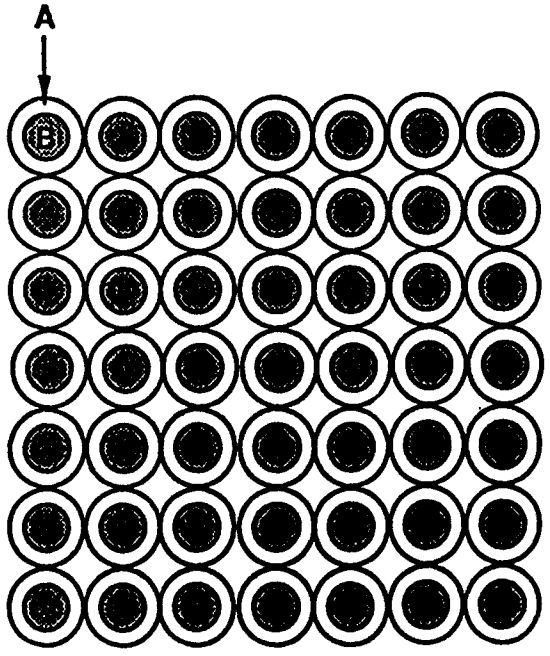

B Particles Coated with A

Figure 3

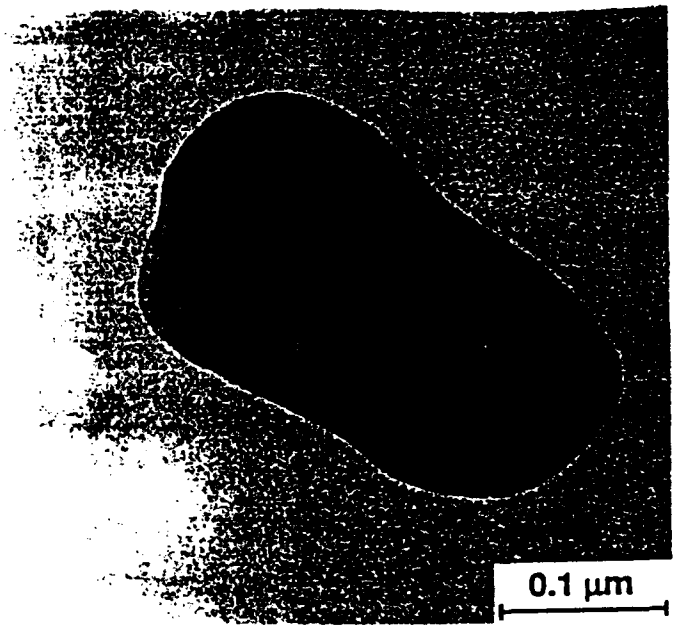

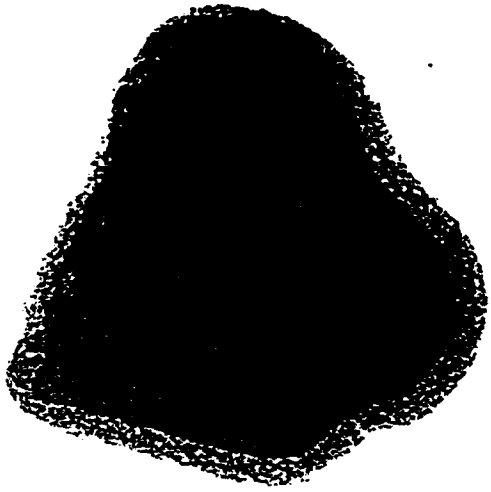

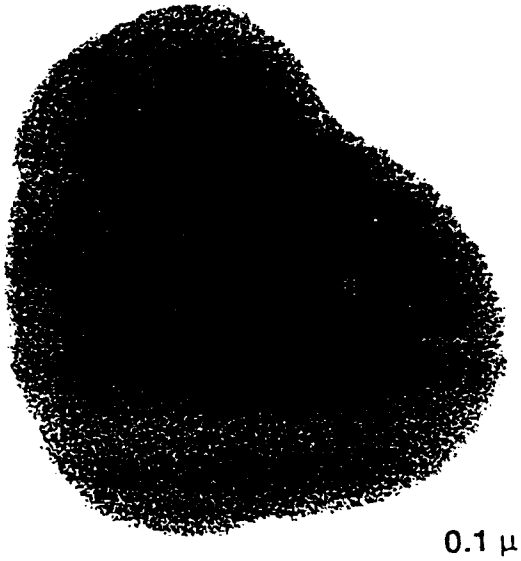

Figure 2

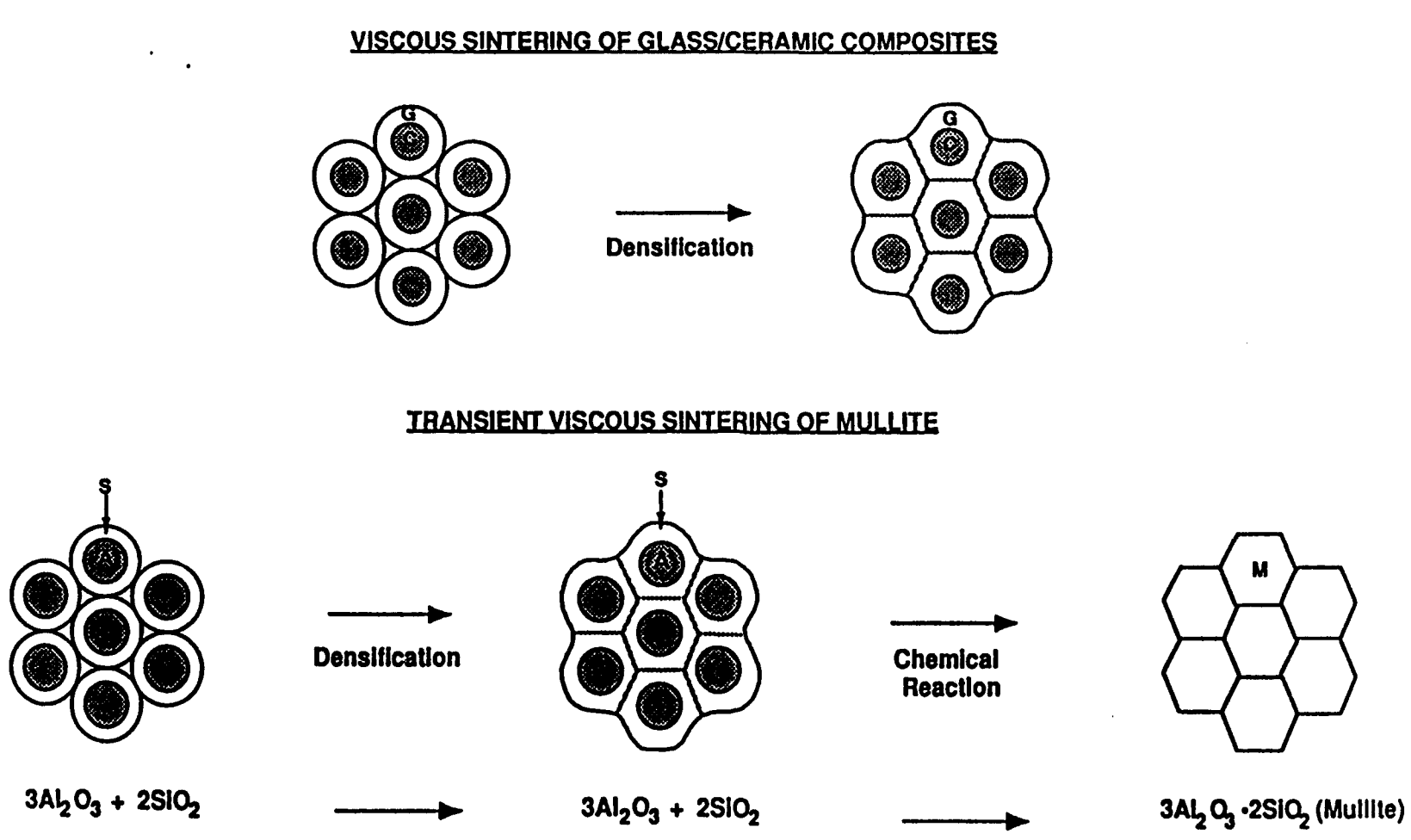
VISCOUS SINTERING OF GLASS/CERAMIC COMPOSITES
G
C
Densification
G
C
TRANSIENT VISCOUS SINTERING OF MULLITE
S
Densification
S
Chemical Reaction
M
3Al2O3 + 2SiO2
3Al2O3 + 2SiO2
3Al2O3·2SiO2 (Mullite)

Figure 4

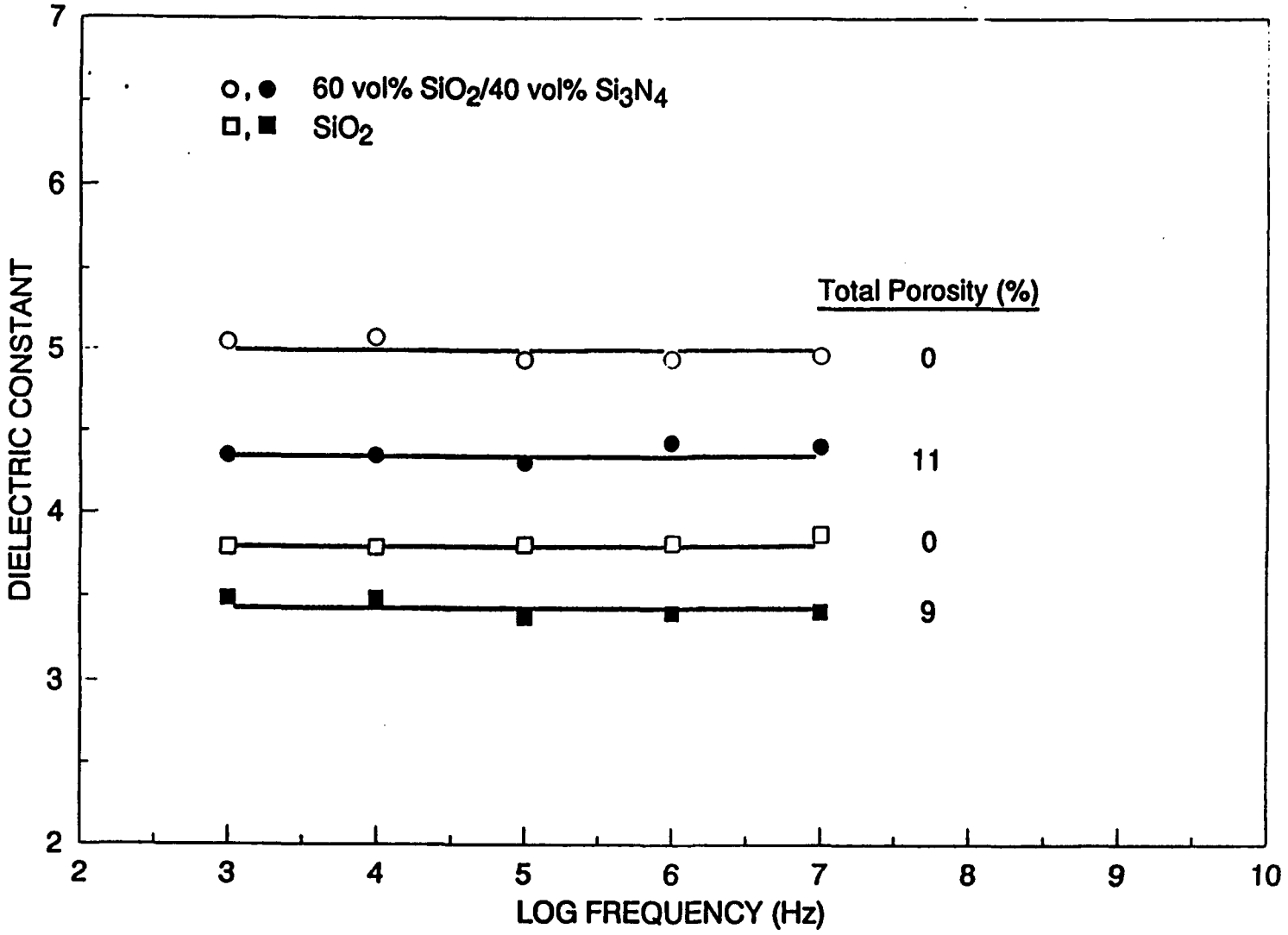
○, ● 60 vol% SiO2/40 vol% Si3N4
□, ■ SiO2
Total Porosity (%)
0
11
0
9
DIELECTRIC CONSTANT
LOG FREQUENCY (Hz)
2
3
4
5
6
7
8
9
10

Figure 5

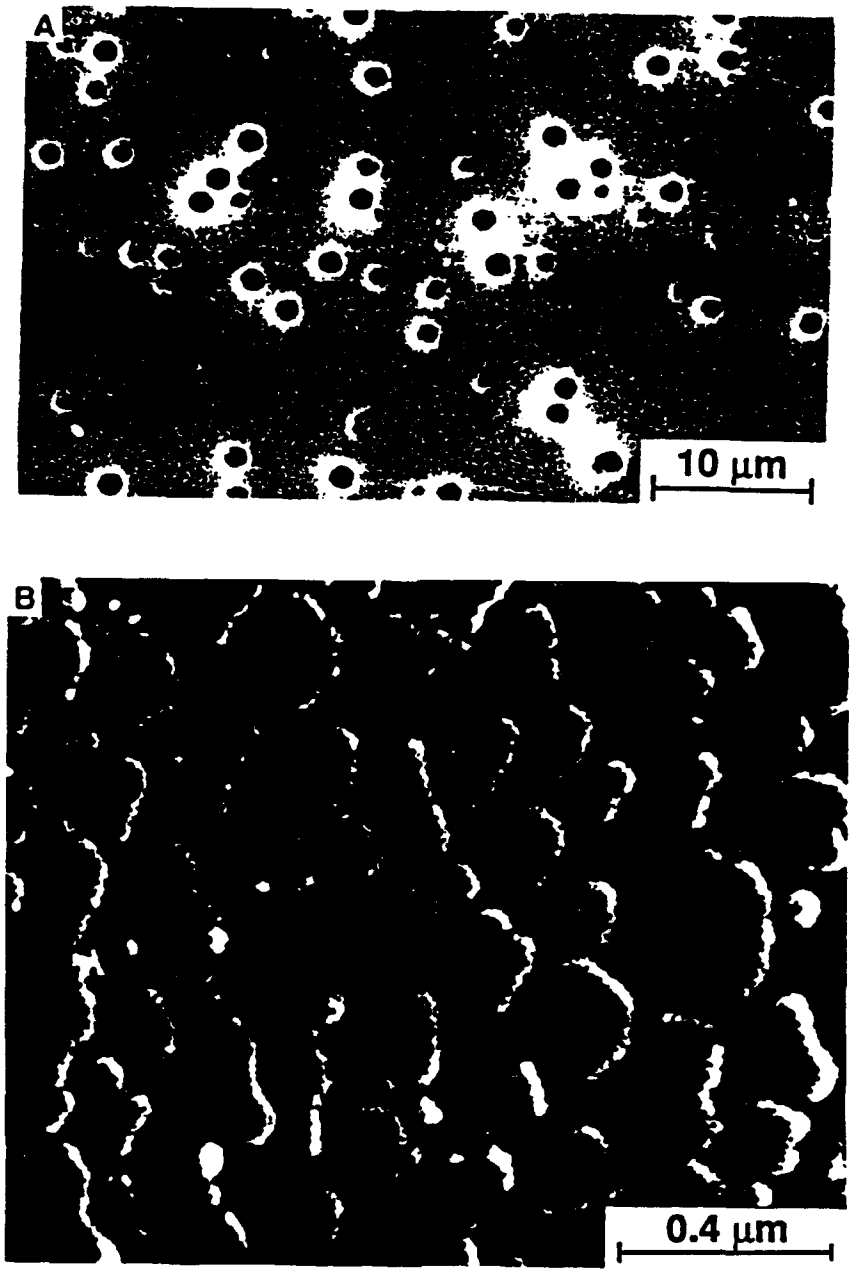

Figure 6

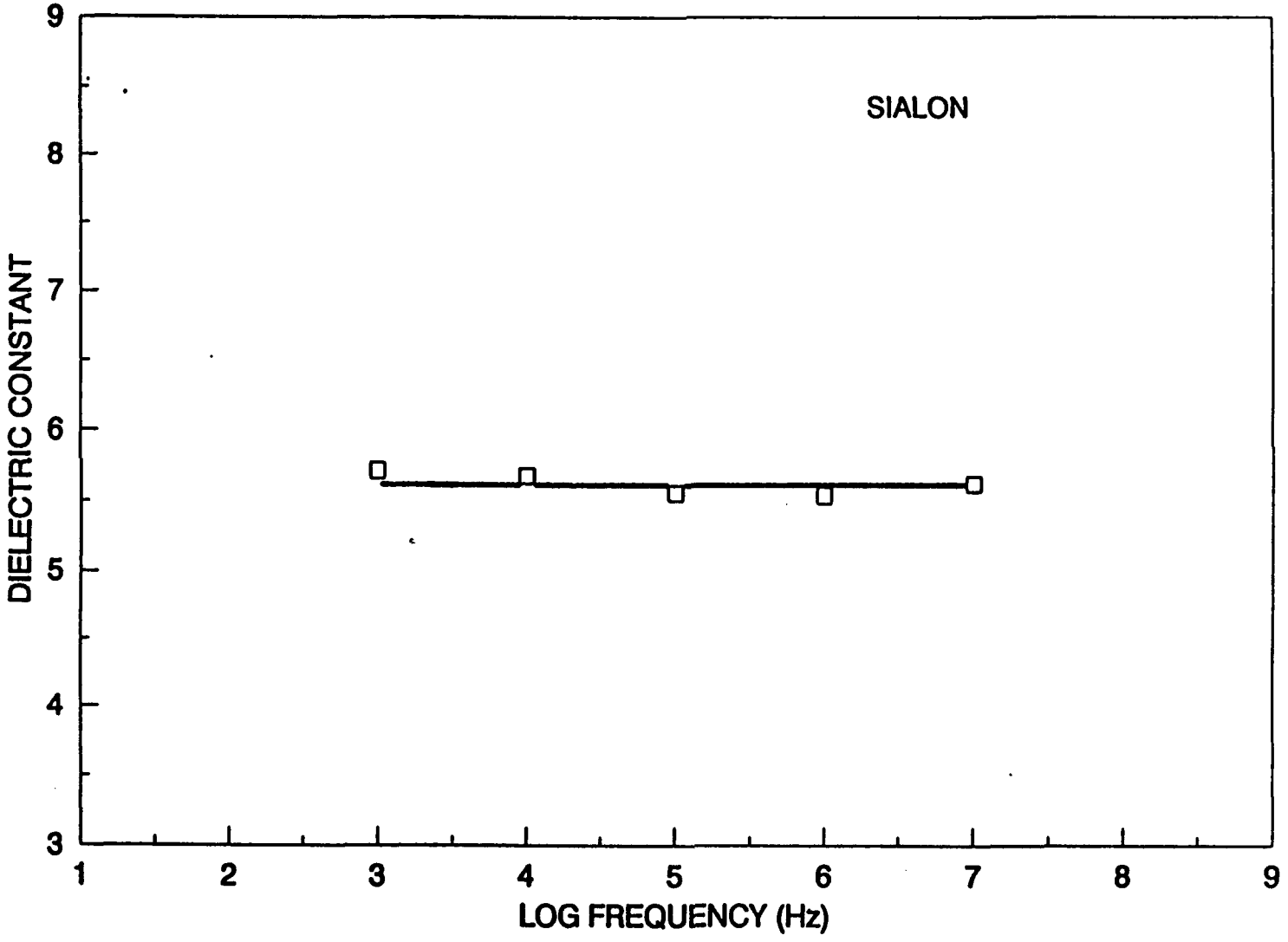
SIALON
DIELECTRIC CONSTANT
LOG FREQUENCY (Hz)
9
8
7
6
5
4
3
1
2
3
4
5
6
7
8
9

Figure 7

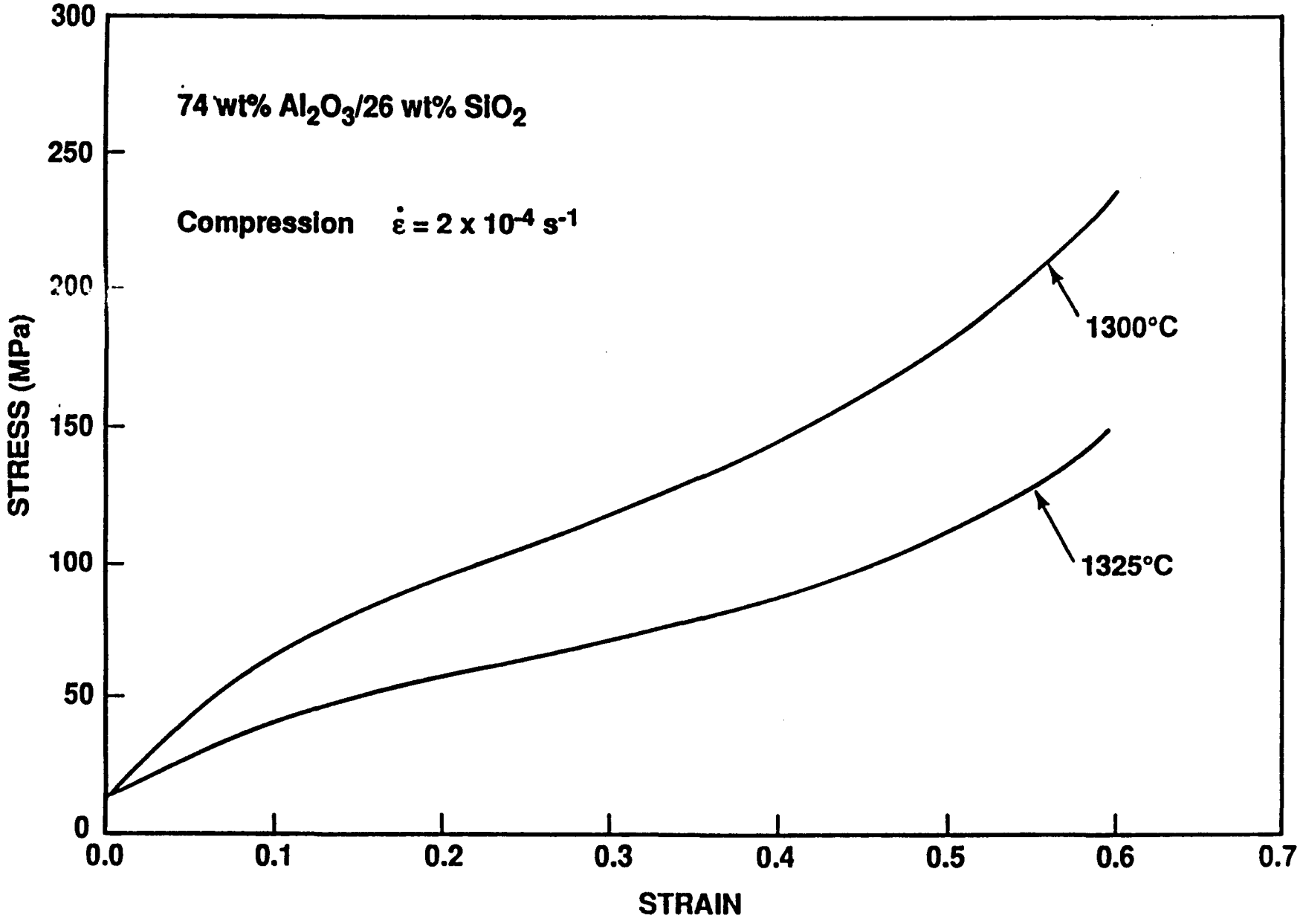
74 wt% Al_2O_3/26 wt% SiO_2
Compression $\dot{\varepsilon} = 2 \times 10^{-4}\ s^{-1}$
1300°C
1325°C
STRESS (MPa)
STRAIN
300
250
200
150
100
50
0
0.0
0.1
0.2
0.3
0.4
0.5
0.6
0.7

Figure 8

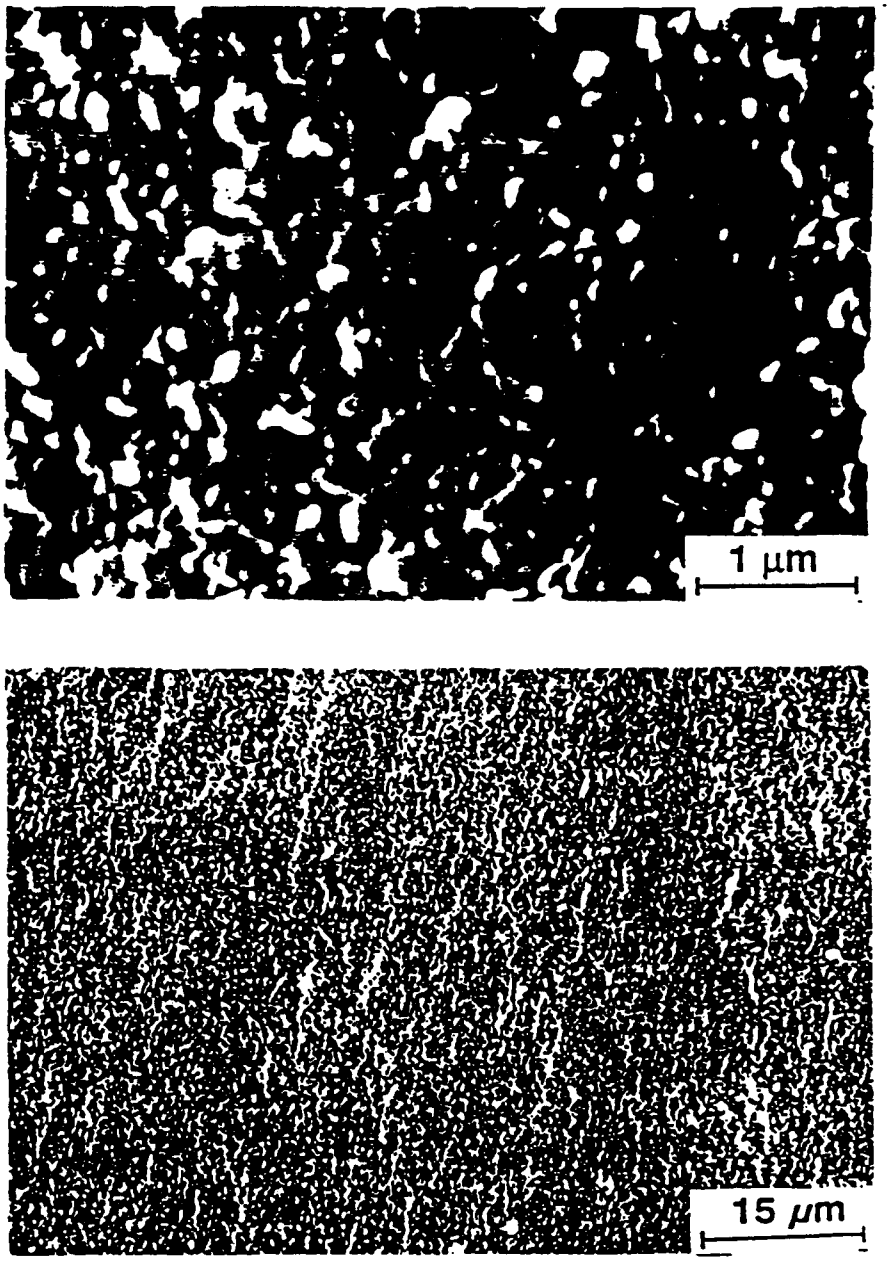

Figure 9

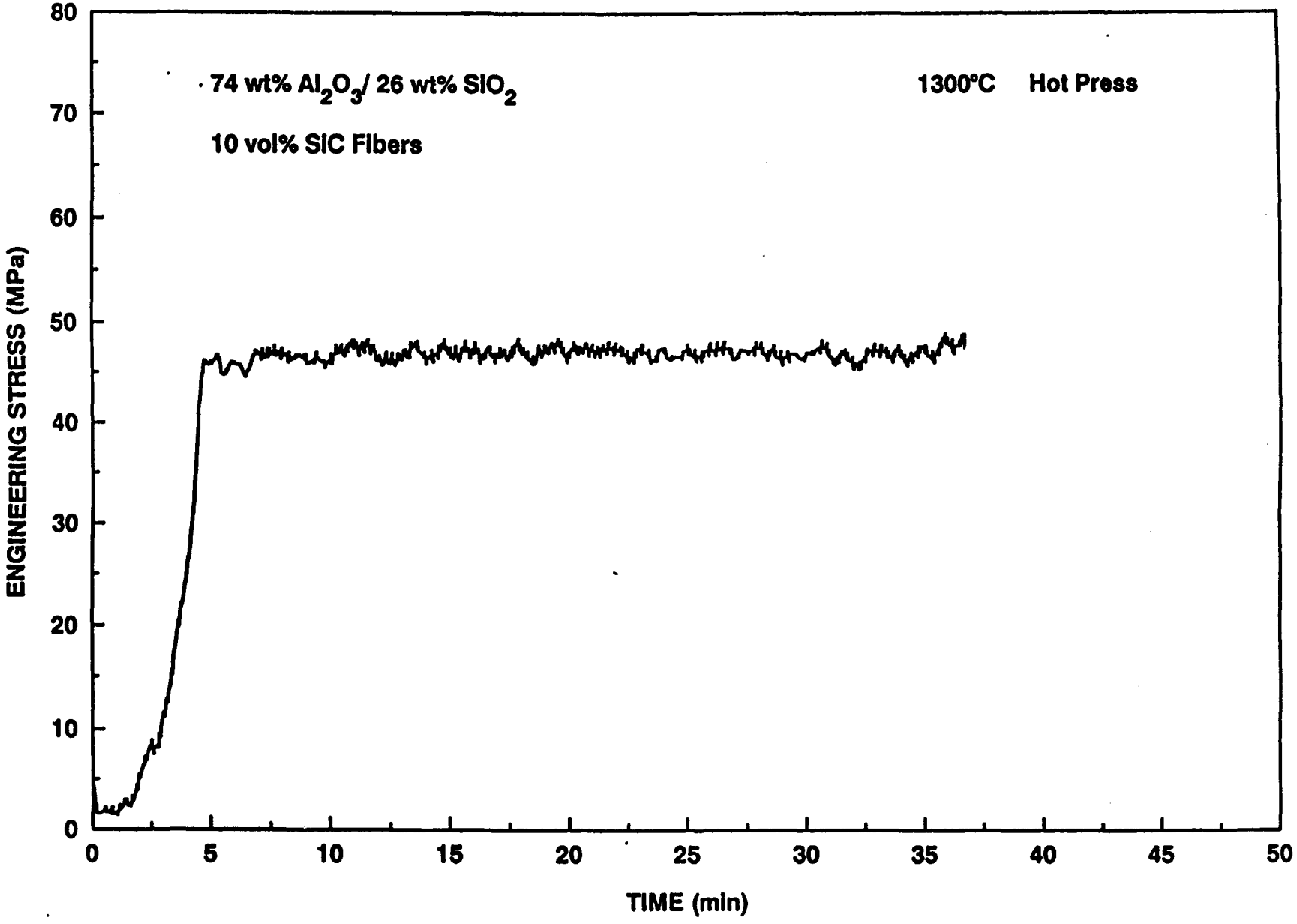
74 wt% Al2O3/ 26 wt% SiO2
10 vol% SiC Fibers
1300°C Hot Press
ENGINEERING STRESS (MPa)
TIME (min)
0
10
20
30
40
50
60
70
80
0
5
10
15
20
25
30
35
40
45
50

Figure 10

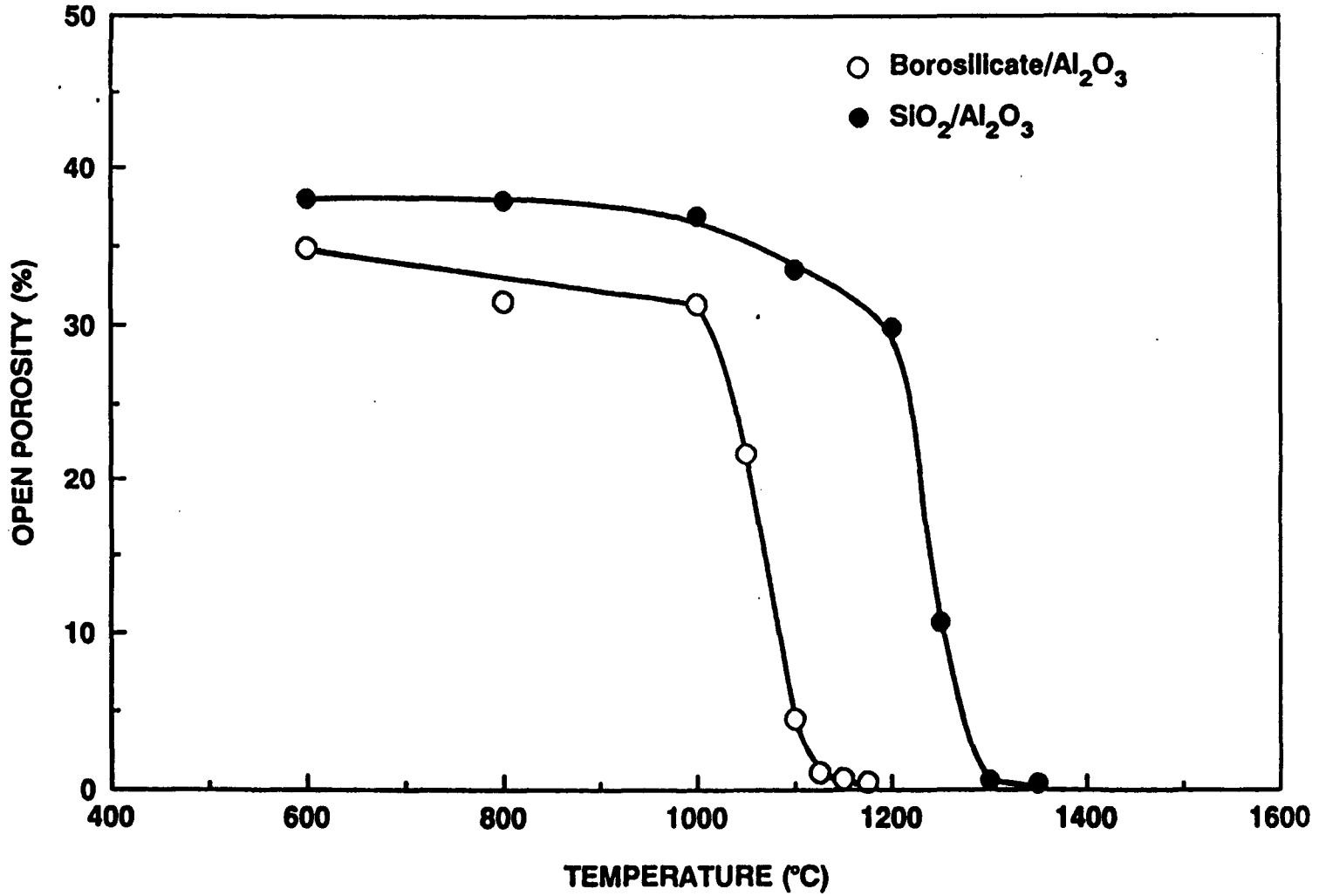
Borosilicate/Al_2O_3
SiO_2/Al_2O_3
OPEN POROSITY (%)
TEMPERATURE (°C)
0
10
20
30
40
50
400
600
800
1000
1200
1400
1600

Project #2: Processing of SiC-Based Composites by Infiltration Processing

Background and Approach

Infiltration processing has been investigated extensively for low cost, near-net-shape manufacturing of SiC. Reaction-bonded SiC is typically fabricated by infiltrating molten silicon into a compacted body of SiC and carbon powders. The molten silicon rises through the porous compact by capillary action and reacts with the carbon to form "new" SiC which bonds the original SiC particles together. The resultant material is a two-phase composite of silicon carbide and silicon. If no carbon exists in the initial porous compact, the silicon infiltration process involves only the filling of the pore channels. The resulting material is referred to as silconized silicon carbide. This material usually contains much more silicon as a second phase. However, the processing method is a relatively easy and cost effective method for fabricating large complex shapes. The major problem impeding the use of reaction-bonded or silconized silicon carbide as a structural material for high temperature applications is the presence of a large amount of free silicon phase in the final product. It is the free silicon phase which degrades the mechanical properties (strength, hardness, creep resistance, etc.).

The primary objective of this project was to improve mechanical properties and polishability of siliconized silicon carbide materials by increasing the SiC/Si ratio and reducing the size of silicon pockets in final microstructure (i.e., in addition to reducing the volume fraction of Si). The approach adopted in this study was to infiltrate extra silicon carbide or carbon into pore channels of the compact (prefrom) prior to the siliconization process. Both bulk and surface infiltration were investigated in order to modify bulk and surface properties of siliconized SiC composites. Infiltration involved filling the open pores of the porous SiC preform with the liquid precursor, solidifying the liquid "*in-situ*" at a lower temperature, and then decomposing it into SiC or C at a higher temperature. In the case of the carbon precursor, carbon formed after the lower temperature decomposition step would subsequently react with molten silicon to form extra SiC during the siliconization process. A key issue for successful application of characteristics for an ideal liquid precursor are: (1) The liquid precursor should infiltrate rapidly into the porous solid preform. (2) After infiltration has been accomplished, the liquid precursor should be immobilized in the porous solid. Transport of the liquid precursor by capillary action should be avoided during subsequent heat treatment steps (e.g., drying, pyrolysis) because this will result in concentration gradients within the porous solid. Solvents and liquid precursor decomposition products should be removed by vapor transport mechanisms in order to produce a pyrolyzed product with good compositional uniformity. (3) A high yield of the desired solid phase (i.e., high specific volume) should be produced after the heat treatment steps for precursor decomposition and phase transformation. The number of infiltration cycles needed for a given process can be reduced if the yield per cycle can be increased. (4) Simple, low cost processing steps are desirable. For example, it would be desirable to accomplish infiltration at room temperature and at low pressures. Similarly, precursor decomposition and phase transformation would be less costly if heat treatment temperatures were low. (5) Low cast infiltrant materials are desirable.

Research Summary

(1) Two suitable liquids with relatively low viscosity (which is important in obtaining reasonable infiltration rates) and relatively moderate weight loss upon pyrolysis (which is important in ultimately obtaining a high yield of SiC) were developed for infiltration into porous SiC preforms. One was a ceramic precursor, 1,3,5-trimethyl-1,3,5-trivinylcyclotrisilazane, which was polymerized by heat treatment (120-150°C) in the presence of a proper initiator and subsequently pyrolyzed at elevated temperature (1000-1650°C) to produce a silicon carbide/silicon nitride mixture. With proper control over atmosphere and temperature, the polymer can be pyrolyzed to form only silicon carbide. The other liquid was a carbon precursor, an organic resin solution, which was heat treated in the range of 90-150°C and subsequently pyrolyzed above 650°C to form glassy carbon. The glassy carbon in the pores of the sintered preform was reacted with molten silicon to form "new"silicon carbide during the siliconization process.

(2) The effect of liquid precursor infiltration on relative density and pore characteristics of the preforms was characterized by the Archimedes displacement method and mercury porosimetry measurements after each infiltration/polymerization/pyrolysis cycle. As the number of cycles increases (for both the ceramic and carbon precursors), the open porosity, median pore size, and apparent density decrease, while the bulk density increases.

(3) The infiltration parameters, including infiltration time, pyrolysis temperature and number of infiltrations, were optimized for the carbon precursor. The infiltration time depends mainly on the sample thickness and the pore size distribution of the preform to be infiltrated. For the 3 mm thick porous SiC preforms used in this study, the first infiltration was nearly completed within a few minutes, while the second infiltration could be accomplished in less than 1 hour. The optimum pyrolysis temperature was 800°C. In order to achieve dense, bulk composites with maximum SiC/Si ratio, two infiltration/pyrolysis cycles were used.

(4) After siliconization, both the apparent and bulk densities increase with increasing the number of infiltrations due to the increased SiC/Si ratio in the composites. Densities of siliconized SiC composites satisfy the "rule of mixtures" very well. Therefore, by measuring density values, the phase composition of the composite could be calculated. The phase composition of the final siliconized SiC composites can also be estimated from the open porosity of the SiC precursor above the pyrolysis temperature (i.e., the weight loss during the siliconization process).

(5) The carbon precursor infiltration was much more effective for increasing the SiC/Si ratio than the ceramic precursor. The SiC content of the siliconized composites was only increased 5-10 vol% after three or four successive infiltrations with the ceramic precursor. In contrast, the SiC content was increased ~14 and ~25 vol% after using only one and two carbon precursor infiltrations, respectively. The highest SiC contents achieved were in the range of ~91-93 vol%. In addition, lower pyrolysis

temperatures (650-1000°C) were used for the carbon precursor compared to the ceramic precursor (1000-1650°C). For these reasons, the carbon precursor infiltration/pyrolysis process has better potential for commercial application.

(6) Surface regions of porous SiC preforms were infiltrated with the carbon precursor to produce siliconized composites which had a dense surface layer of SiC content (~95 vol%). The best results were obtained using three of four infiltration/pyrolysis cycles.

(7) The mechanical properties, including flexural strength, Young's elastic modulus, Vickers hardness and fracture toughness, were increased by about 20-25% and 35-50% with one and two carbon precursor infiltrations, respectively. The average four-point flexural strength, Vickers hardness, elastic modulus and fracture toughness for siliconized samples with two carbon precursor infiltrations were ~280MPa, ~25GPa and ~4.0MPa·$m^{1/2}$, respectively. Also, the polishability of siliconized samples with carbon precursor infiltrations was improved significantly.

(8) From the strength and fracture toughness data, the maximum flaw size was estimated to be ~150 μm which was independent of the number of carbon precursor infiltrations. It is believed that the large flaws originated from the bubbles incorporated in the original SiC preforms (which were supplied by an industrial collaborator). Therefore, efforts are currently being directed toward improving the initial forming process so that bubbles (and other large processing flaws) are eliminated.

(9) Work has been initiated using an Si-Mo alloy for reactive infiltration into carbon/SiC preforms in order to created $MoSi_2$/SiC composites. (Molybdenum disilicide has much better mechanical properties at high temperatures than silicon.) Investigations are currently directed toward determining the appropriate alloy composition and heat treatment conditions (temperature, time and atmosphere) which will produce composites with minimal residual silicon. Future work will also be directed toward preparation of fiber-reinforced composites using reactive infiltration of silicon alloys. The work will focus on (1) reducing the siliconization temperatures by appropriate alloy selection and (2) developing an appropriate fiber coating to protect the fiber and improve the fiber-matrix interfacial properties.

Publications

(1) K. Wang, "Processing of Improved Siliconized Silicon Carbide by Liquid Infiltration Methods," M.S. Thesis, University of Florida, 1992.

Portions of the above publication are attached.

Fabrication of Mullite and Mullite-Matrix Composites by Transient Viscous Sintering of Composite Powders

Michael D. Sacks,* Nazim Bozkurt, and Gary W. Scheiffele*

Ceramics Division, Department of Materials Science and Engineering, University of Florida, Gainesville, Florida 32611

Mullite was fabricated by a process referred to as transient viscous sintering (TVS). Composite particles which consisted of inner cores of α-alumina and outer coatings of amorphous silica were used. Powder compacts prepared with these particles were viscously sintered to almost full density at relatively low temperatures (~1300°C). Compacts were subsequently converted to dense, fine-grained mullite at higher temperatures (≥1500°C) by reaction between the alumina and silica. The TVS process was also used to fabricate mullite/zirconia/alumina, mullite/silicon carbide particle, and mullite/silicon carbide whisker composites. Densification was enhanced compared with other recent studies of sintering of mullite-based composites. This was attributed to three factors: viscous flow of the amorphous silica coating on the particles, avoidance of mullite formation until higher temperatures, and increased threshold concentration for the development of percolation networks. [Key words: mullite, composites, sintering, powders.]

I. Introduction

There has been considerable interest in mullite and mullite-matrix composites in recent years due to their desirable properties, such as excellent high-temperature strength and creep resistance, good chemical and thermal stability, low thermal-expansion coefficient, and good dielectric properties. Optimization of the physical properties of mullite-containing materials requires careful control over the various stages of processing. Powder preparation techniques, consolidation (i.e., shape-forming) methods, and densification procedures for fabrication of mullite bodies with high relative density (i.e., low porosity) have been reviewed recently.[1] In conventional processing methods, mullite powders are shape formed and sintered. However, sintering of mullite powders to high densities normally requires relatively high temperatures because of the low bulk and grain-boundary diffusion coefficients for mullite. Thus, a large number of studies[1,2] have been directed toward preparation of mullite powders which have fine particle size (high specific surface area) to reduce diffusion distances and to increase the driving force for sintering. In addition to particle size reduction, it is well recognized that densification can be enhanced by utilizing homogeneous powder compacts in which particles are packed to high relative density and large pores and powder agglomerates are absent. Thus, efforts to enhance densification of mullite by improving the green microstructure have also been reported.[1,3] With optimum processing, mullite powder compacts can be pressureless sintered to high relative density (≥98%) and fine average grain size (≤1 to 2 μm) at temperatures of ~1550°C.

Bulk mullite bodies can be prepared at lower sintering temperature by using precursor materials which react to form mullite after densification has occurred. This approach requires control over the scale of mixing of the reactants.[1] If the aluminum- and silicon-bearing species are mixed on the molecular level, then mullitization occurs at low temperatures (~1000°C) and subsequent densification at low temperatures is very limited. In contrast, if the level of mixing is too coarse (i.e., micrometer scale), then high temperatures (≥1650°C) are required to accomplish both mullitization and densification. An analysis[1] of results reported by Yoldas,[4] Roy *et al.*,[5,6] Shinohara *et al.*,[7] Somiya,[8] and Rahaman *et al.*[9] indicates that the lowest sintering temperatures are achieved when the scale of mixing is in the approximate range of 5 to 50 nm. In these studies, soluble and/or colloidal aluminum- and silicon-containing materials were used to prepare either sol–gel monolithic samples or sol–gel powders which were subsequently pressed into pellets. Bulk samples could be substantially densified at temperatures in the approximate range of 1200° to 1300°C,[5–9] whereas the reaction to form mullite was typically observed at slightly higher temperatures (i.e., approximately 1250° to 1350°C[5–9]). The low sintering temperature can be attributed to two factors: (i) the small size (high specific surface area) of the mullite–precursor particulates (which results in larger driving forces and shorter transport distances for densification) and (ii) the amorphous or weakly crystalline character of the mullite-precursor powder (which results in densification by the viscous flow mechanism).

Although sintering temperatures are lowered by using sol–gel approaches, there are clearly several difficulties associated with the method when processing bulk shapes. "Wet" gels undergo large shrinkages during drying and substantial stress gradients can arise. Thus, gel monoliths tend to warp and/or crack during drying unless liquid removal is conducted at slow rates or by using special conditions such as supercritical drying. To overcome these difficulties, Roy *et al.*,[5,6] Somiya,[8] and Rahaman *et al.*[9] prepared bulk samples by compaction of gels which had been dried at low temperatures. Although dry-pressing operations generally produce compacts with relatively large interagglomerate pores, the gels dried at low temperatures were sufficiently deformable to produce compacts with fine pore sizes and relatively homogeneous structure. Nevertheless, the compact green densities were low; therefore, shrinkages during sintering were large. In addition, relatively large weight losses occurred during sintering because of dehydroxylation and elimination of residual organic groups. For example, Rahaman *et al.*[9] observed a 13% weight loss during sintering, even though gels were calcined at 800°C for 4 h prior to sintering. The large shrinkages and weight losses that occur during processing of gel monoliths

FABRICATION OF CERAMICS AND COMPOSITES BY VISCOUS AND TRANSIENT VISCOUS SINTERING OF COMPOSITE PARTICLES

Michael D. Sacks, Gary W. Scheiffele, Nazim Bozkurt, and Ramesh Raghunathan, Department of Materials Science and Engineering, University of Florida, Gainesville, FL 32611

ABSTRACT

Ceramics and composites were fabricated by sintering composite particles. These particles consisted of cores of crystalline materials (i.e., alumina, silicon nitride, silicon carbide, zirconia) with outer coatings of amorphous silica. Powder compacts prepared with composite particles showed enhanced densification due to viscous flow of the amorphous coating and the increased threshold concentration for percolation of the crystalline phase. Dense glass/ceramic composites (i.e., silica/silicon nitride, silica/alumina) with high concentrations of isolated crystalline phase could be prepared at low sintering temperature ($\leq$1300°C). In samples prepared with silica-coated alumina particles, it was possible to fabricate glass-free mullite and mullite-matrix composites by *transient viscous sintering (TVS)*. Powder compacts were sintered to almost full density at low temperature (~1300°C) and subsequently heated to higher temperature (~1500-1600°C) to form mullite. Dense, fine-grained mullite-matrix composites (i.e., mullite/zirconia/alumina, mullite/silicon carbide) having homogeneous second-phase distribution were also prepared at relatively low temperatures by the TVS process.

INTRODUCTION

In the past decade or so, a large body of literature[1] has appeared in the area of processing of ceramics, glasses, and composites and much of it has concerned (directly or indirectly) methods to improve sintering behavior and to produce sintered microstructures with desirable features, e.g., high relative density (low porosity), controlled size and spatial distribution of phases, etc. In this paper, we describe a novel approach for enhancing densification and controlling microstructure development which is based on the processing of composite particles. As discussed below, judicious selection of the composition, structure, and size of the composite particles not only provides a method for developing novel microstructures, but also allows two different approaches for increasing densification rates to be used in combination, i.e., utilizing viscous flow and controlling the spatial distribution of phases.

Consider the case in which a composite is fabricated using two different materials, A and B, where B is relatively non-sinterable compared to A (i.e., a powder compact prepared with pure B particles would have a much lower densification rate compared to a powder compact prepared with pure A particles). In a conventional processing route, A and B particles would be mixed, consolidated into a compact, and sintered. The green compact structure for this processing route is schematically illustrated in Fig. 1, left side. If the particles are equal-sized spheres which are randomly mixed, the B particles will form a connected network (percolation path) when the concentration reaches ~16 vol%.[2] Studies have shown that powder compact densification rates are severely impeded when this critical (threshold) concentration of the non-sinterable phase is exceeded.[3-6] One approach to minimizing the effect of the non-sinterable inclusions on densification is to deliberately control the spatial distribution of the phase, i.e., in order to increase the critical volume fraction required for percolation. The most effective method for avoiding the formation of a percolation network is illustrated in the right side of Fig. 1. The non-sinterable particles B are coated with a layer of A, thereby completely isolating them from each other.

Previous studies have shown that non-sinterable inclusions have less effect on the densification rate when the matrix phase sinters by viscous flow.[4] Thus, it is anticipated that an especially effective method for enhancing densification rates would utilize composite particles (of the type shown in Fig. 1) in which the outer coating is an amorphous material. This approach would not only allow fabrication of glass/ceramic composites at relatively low sintering temperatures, but would also offer the possibility of developing novel microstructures in which a high concentration of crystalline phase is incorporated into a glassy matrix as isolated inclusions (Fig. 2, top right).

It is possible that the approach described above could also be applied to the fabrication of single-phase crystalline ceramics and crystalline ceramic-ceramic composites. This would require selection of appropriate core and coating materials that would react at elevated temperatures to eliminate the amorphous phase. An example is illustrated in Fig. 2 (bottom) in which the core is alumina and the coating is silica. If the size of the composite particles is selected properly, this combination should viscously sinter at relatively low temperature to form an alumina/siliceous glass composite. At higher temperature, the core and coating would react to form mullite.* This process is referred to as *transient viscous sintering (TVS)*. This approach can also be used to fabricate mullite-matrix composites by mixing the silica-coated alumina particles with other silica-coated particles (i.e., with different crystalline core materials).

The approach illustrated in Fig. 2 depends upon the availability of coated particles in the appropriate size range (i.e., colloidal dimensions). Particles with these characteristics have been of interest for many years in several areas of

---

* Depending on the alumina/silica ratio chosen, the final composition could be single-phase mullite, mullite + siliceous glass, or mullite + alumina.

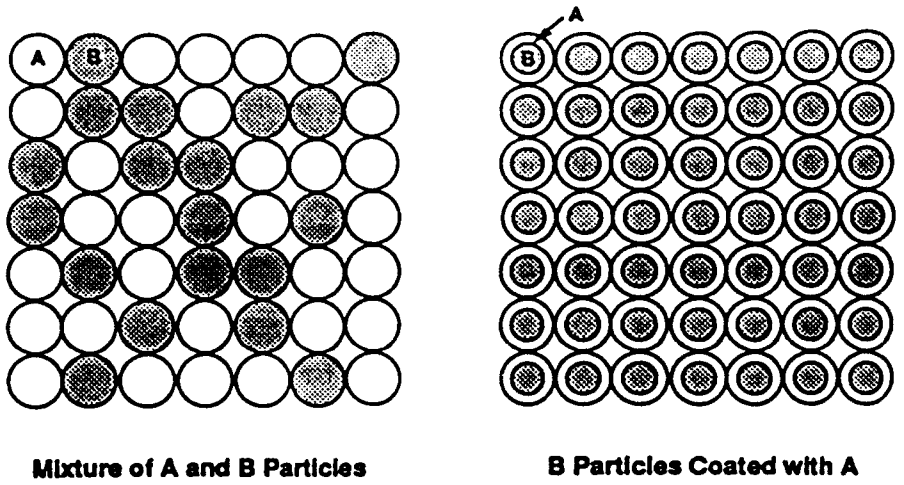

FIG. 1. Schematic illustration of two different powder compacts. Left side: compact is formed from a mixture of two different types of particles. Right side: compact is formed using composite particles which are composed of a core of one material and an outer coating of another material.

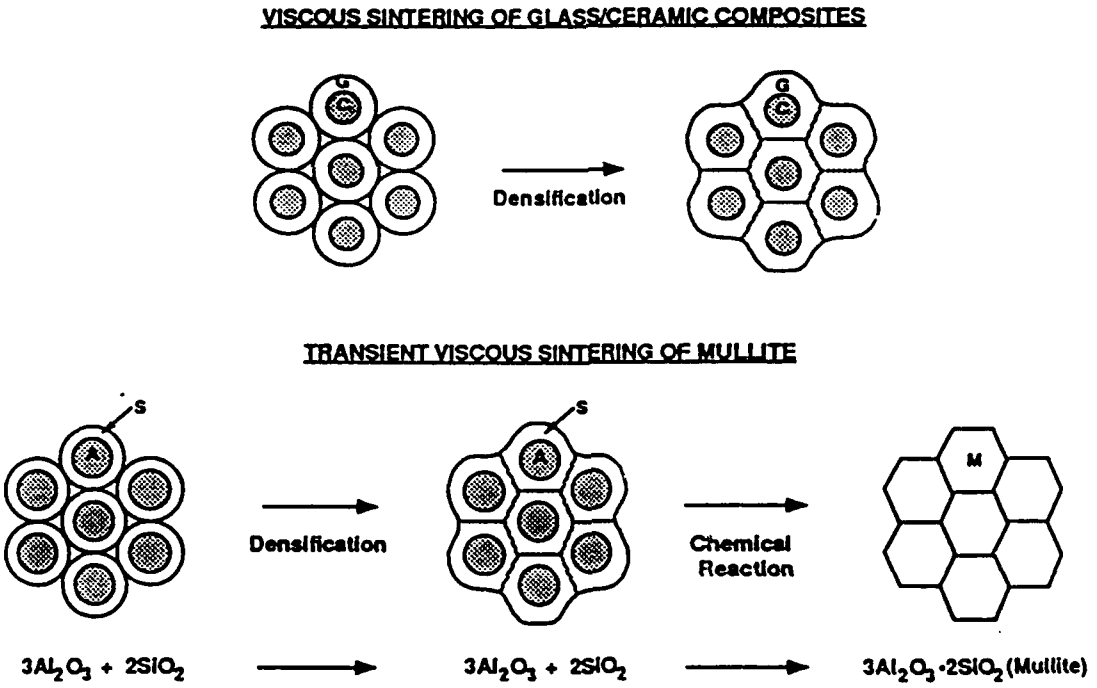

FIG. 2. Top: Schematic illustration of viscous sintering of glass (G)/crystalline ceramic (C) composites using compacts prepared with composite particles. Bottom: Schematic illustration of transient viscous sintering (TVS) of mullite using amorphous silica-coated alumina particles.

colloid technology (e.g., pigments used in paint, magnetic particles used in recording media, etc.).[6-10] A wide variety of coated particles have been synthesized in recent years[6-17] and some coated powders have been used to process bulk ceramics.[15-17] In most cases, the stated goal for using coated powders in ceramic processing is to achieve a uniform sintered microstructure, i.e., a homogeneous mixture of the phases comprising the coated particles. Only recently have coated particles been used to demonstrate that densification can be enhanced via the mechanism illustrated in Fig. 2.[17] In this paper, fabrication of ceramics and composites by viscous sintering and transient viscous sintering of amorphous silica-coated particles is described.

EXPERIMENTAL

Experimental procedures are described briefly, as details are provided elsewhere.[17,18] Composite powders were prepared using alumina,♦ silicon nitride,◂ silicon carbide,† and zirconia particles▲ as core materials. Silica coatings were deposited using tetraethylorthosilicate, TEOS,■ as the starting material. Prior to deposition of the coating, as-received core powders were fractionated using standard fluid classification techniques[18] in order to remove hard agglomerates. Depending on the particular material, average core particle diameters were in the range ~0.1-0.3 μm as determined by gravitational X-ray sedimentation‡ and/or centrifugal photosedimentation▾ techniques. The composite powders were prepared by the following steps: (i) core particles were dispersed in ethanol, (ii) a TEOS/ethanol solution was added to the core particle/ethanol suspension, (iii) ammoniated water was added to the core particle/TEOS/ethanol suspension in order to precipitate the silica coating onto the core material, and (iv) coated particles were collected by filtration, washed with deionized water, and dried in an oven. Figure 3 shows typical transmission electron micrographs (TEM)¶ of particles from different powder batches in which the thickness of the silica coating was varied. X-ray photoelectron spectroscopy§ was used to confirm that the external layer of the particles was silica.[18] X-ray diffraction (XRD)♦♦ was used to show that the silica coating was amorphous.[18]

In order to prepare homogeneous compacts with high green density, composite powders were slip cast from well-dispersed aqueous suspensions. Particles

---

♦ AKP-50, Sumitomo Chemical America, New York, NY.
◂ SN-E-10, Ube Industries (America), Inc., New York, NY.
† A-2, Showa Denka, Tokyo, Japan.
▲ Super-Z, TOSOH USA, Inc., Atlanta, GA. This powder is actually yttria-stabilized zirconia/alumina. The manufacturer reports the following composition: 75.7 wt% ZrO_2, 20 wt% Al_2O_3, and 4.2 wt% Y_2O_3.
■ Fisher Scientific, Fair Lawn, NJ.
‡ Model SediGraph 5100, Micromeritics Instruments Corp., Norcross, GA.
▾ Model CAPA-700, Horiba Instruments, Inc., Irvine, CA.
¶ Model 200CX, Japan Electron Optics Co. Ltd., Tokyo, Japan.
§ Model XSAM800, Kratos Analytical, Manchester, United Kingdom.
♦♦ Model APD 3720, Philips Electronic Instruments Co., Mt. Vernon, NY.

were dispersed using (i) ultrasonication to break down agglomerates and (ii) pH adjustment (to ~9-10) in order to generate relatively large zeta potentials. Green compacts were dried at ~80°C and sintered at temperatures in the range 600-1600°C. Samples containing silicon nitride or silicon carbide were sintered in nitrogen, while all other samples were sintered in air.

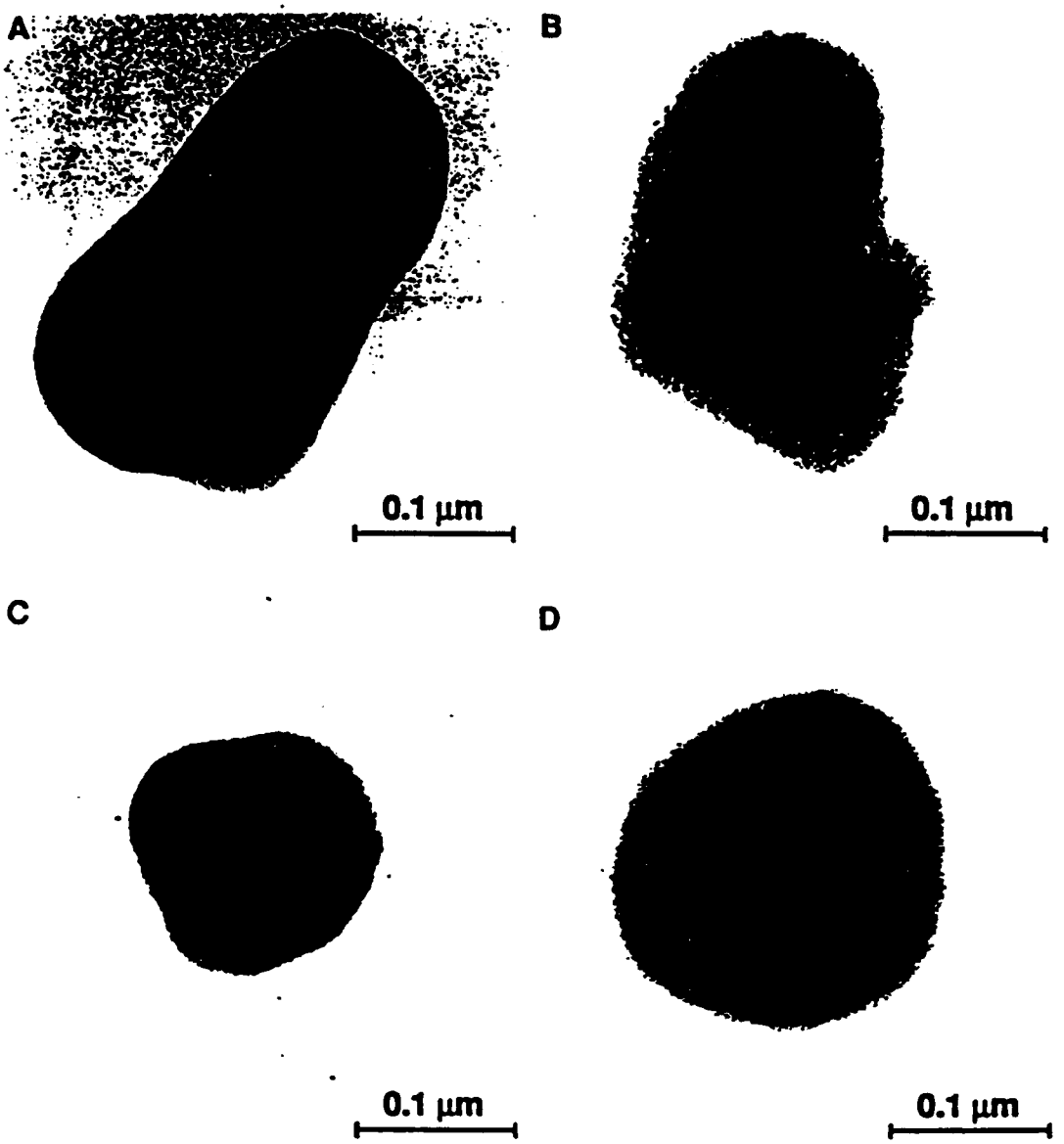

FIG. 3. TEM micrographs of composite particles from powder batches prepared with different amounts of amorphous silica coating. A and B have alpha alumina core particles, while C and D have alpha silicon nitride core particles.

The bulk density and open porosity of sintered samples were determined using the Archimedes method. Microstructure observations were made on polished samples using scanning electron microscopy (SEM).[◂◂] Phase analysis of sintered samples was carried out by XRD.

RESULTS AND DISCUSSION

Viscous Sintering of Glass/Ceramic Composites

An experiment was carried out in which densification behavior was compared for green compacts with characteristics similar to those schematically illustrated in Fig. 1. In order to isolate the effect of the spatial distribution of phases on densification behavior, an effort was made to avoid significant differences in particle sizes and particle packing densities of the compacts since these factors also affect sintering kinetics. Green compacts were prepared using (1) a mixture of silica particles plus silicon nitride particles and (2) silica-coated silicon nitride particles (such as shown in Fig. 3). The overall composition of the compacts was approximately 60 vol% SiO_2/40 vol% Si_3N_4. Compacts prepared with the composite particles had slightly higher packing density (~61% vs. ~57%) which would tend to slightly enhance densification. However, the median particle size was slightly larger (0.32 vs. 0.25 μm) and the specific surface area was slightly smaller (~15 vs. ~19 m^2/g) for the composite powder which would tend to slightly retard densification compared to the powder mixture.

Figure 4 shows plots of bulk density vs. sintering temperature (2 h) for the two types of compacts. The compact prepared with the composite powder starts to densify by 1000°C and reaches maximum density of ~2.51 g/cm^3 by 1275°C. Microstructure observations on a sample sintered at 1300°C showed very little residual porosity. Samples prepared with the composite powder also show that the silicon nitride particles remain well-separated from each other in the siliceous glass matrix (see Fig. 5). (XRD analysis of a 1300°C sintered sample shows that alpha silicon nitride is the only crystalline phase present. The pattern shows broadening in the range of $2\theta \approx 22°$ which is characteristic of amorphous silica.) In contrast to the results with the composite particles, the sample prepared from the mixture of silica and silicon nitride particles shows no densification until the temperature exceeds 1200°C. At 1275°C, the bulk density is only ~1.90 g/cm^3 and the open porosity is ~26%. It is evident that the controlled structure of the composite particles results in significant enhancement in the densification rate.

Glass/ceramic composites were also prepared by viscous sintering of silica-coated alumina particles. Figure 6 shows an SEM micrograph of a ~25 wt% alumina/75 wt% silica composite (~16 vol% alumina) prepared by sintering at 1250°C. The sample is fully dense and the alumina particles are extremely well-dispersed in the silica matrix.

◂◂ Models JSM 35-CF and JSM-6400, Japan Electron Optics Co. Ltd., Tokyo, Japan.

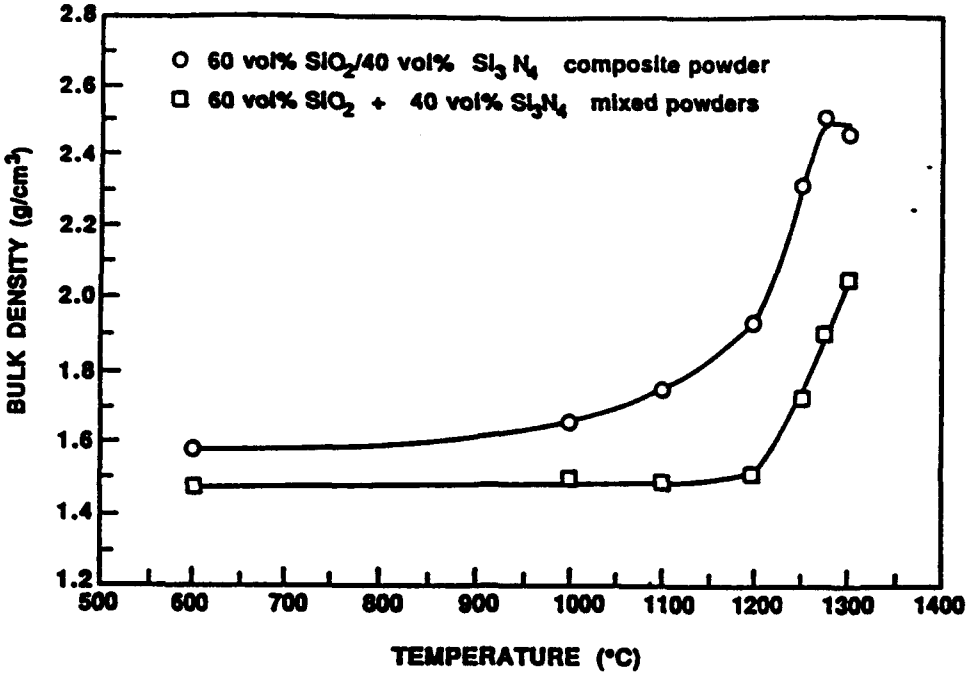

FIG. 4. Plots of bulk density vs. sintering temperature for two types of silicon nitride/silica powder compacts. Powder compacts were prepared from (i) a mixture of silica particles and silicon nitride particles and (ii) amorphous silica-coated silicon nitride particles.

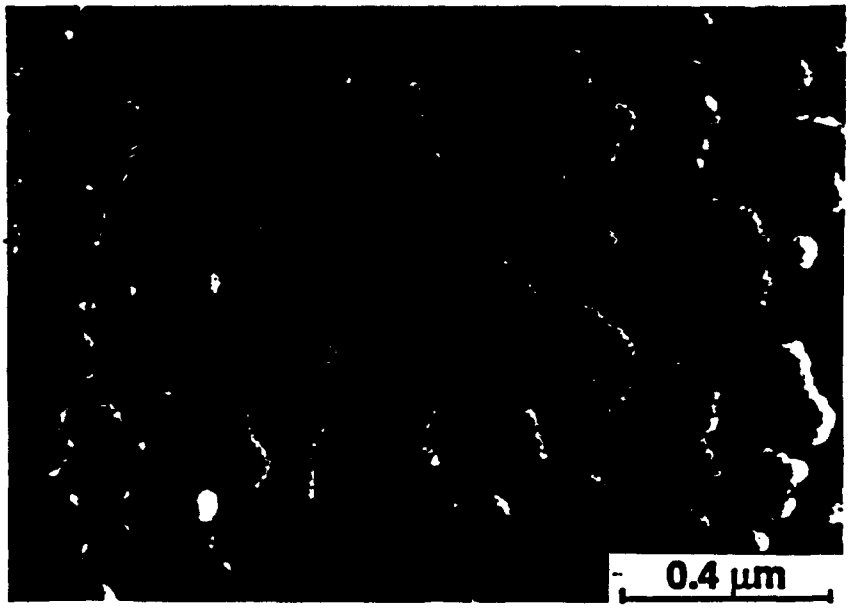

FIG. 5. SEM micrograph of a polished and etched silicon nitride/silica sample, prepared using composite particles, after sintering at 1300°C for 2 h.

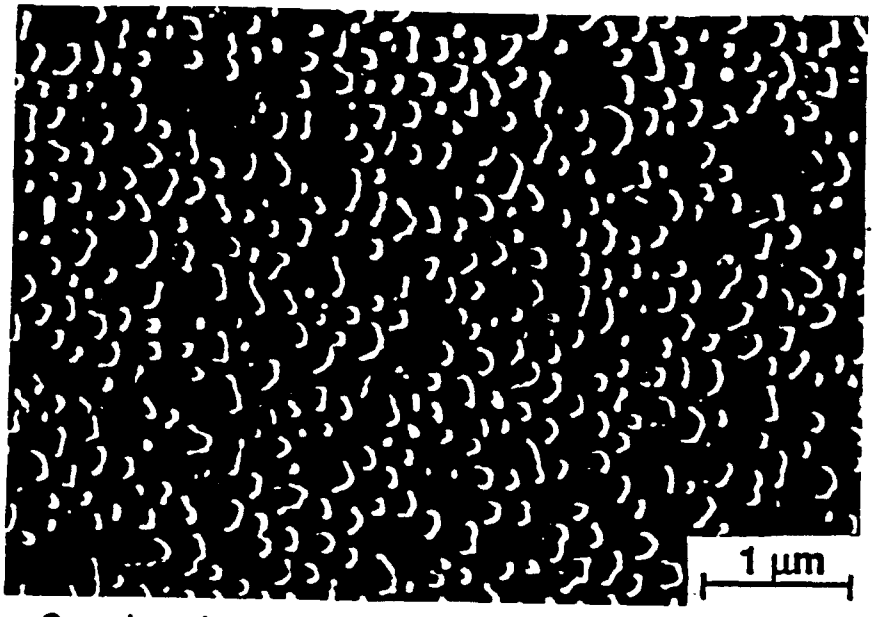

FIG. 6. Scanning electron micrograph of polished and etched 25 wt% alumina/75 wt% silica sample which was sintered at 1250°C for 8 h.

Transient Viscous Sintering of Mullite

Figure 7 shows plots of bulk density and open porosity as a function of sintering temperature (for 8 h) for samples prepared with a composite powder having an overall composition of ~74 wt% alumina/26 wt% silica (i.e., near the mullite/(mullite + alumina) phase boundary of the Al_2O_3-SiO_2 phase diagram). Most of the densification occurs in the range of ~1100-1300°C, as indicated by the large increase in bulk density and corresponding decrease in open porosity. Open porosity is completely eliminated by 1250°C and the bulk density reaches its maximum value by 1300°C. Figure 8A shows an SEM micrograph of a polished, but unetched, sample which had been sintered at 1300°C. The sample is almost fully dense, although some small pores (typically $\lesssim 1\mu m$) are occasionally observed. After etching with dilute hydrofluoric acid solution, the features of the original composite particles (i.e., alumina core particles and silica coatings) can be observed in the sintered sample (Fig. 8B). The small decrease in bulk density at sintering temperatures above 1300°C (Fig. 7A) reflects the volume expansion of the compact due to the reaction between alumina and silica to form mullite. Mullite formation at higher temperatures was confirmed by X-ray diffraction (Fig. 9). The XRD pattern for a sample sintered at 1300°C shows only alpha alumina. The siliceous phase remains amorphous in this sample, although cristobalite formation was observed after sintering at 1400°C.[17] Extensive mullite formation is observed in samples sintered at 1500°C, although a somewhat higher temperature is required for "complete" reaction.[17] Microstructure observations on a sample sintered at 1600°C show no residual siliceous phase (Fig. 8C), indicating that mullitization is complete by this temperature. (The XRD pattern

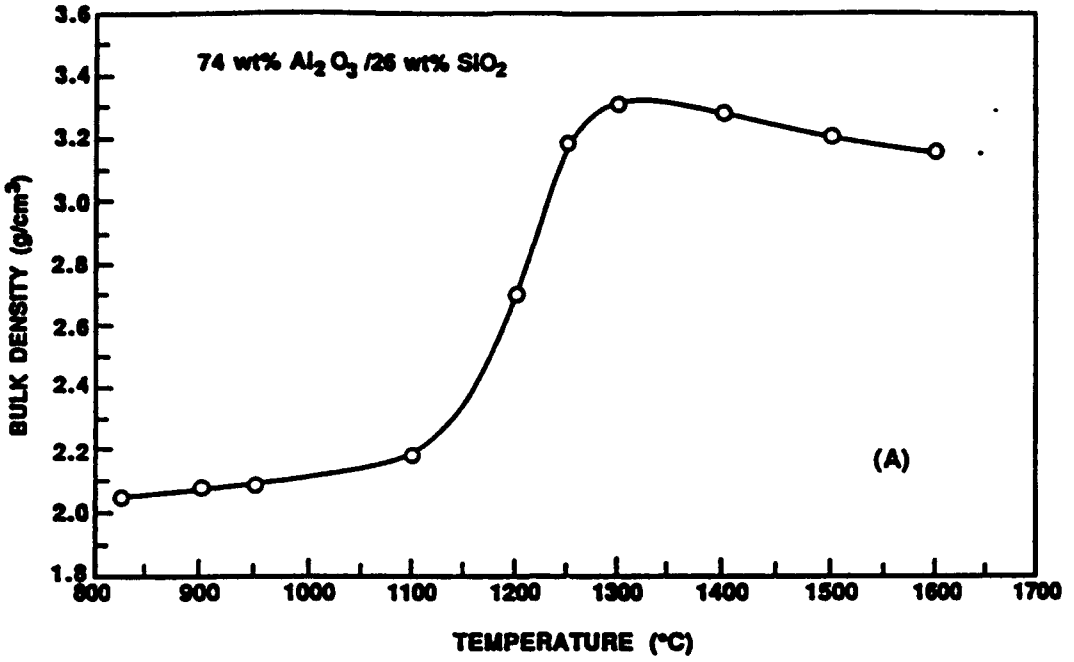

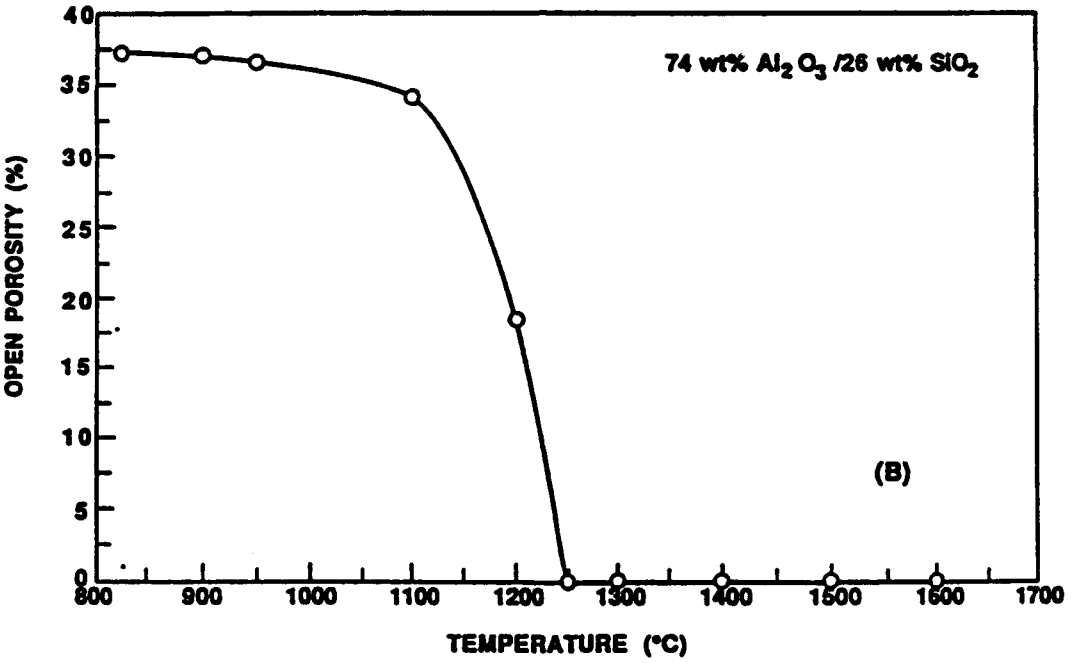

FIG. 7. Plots of bulk density (A) and open porosity (B) vs. sintering temperature for 74 wt% alumina/26 wt% silica samples.

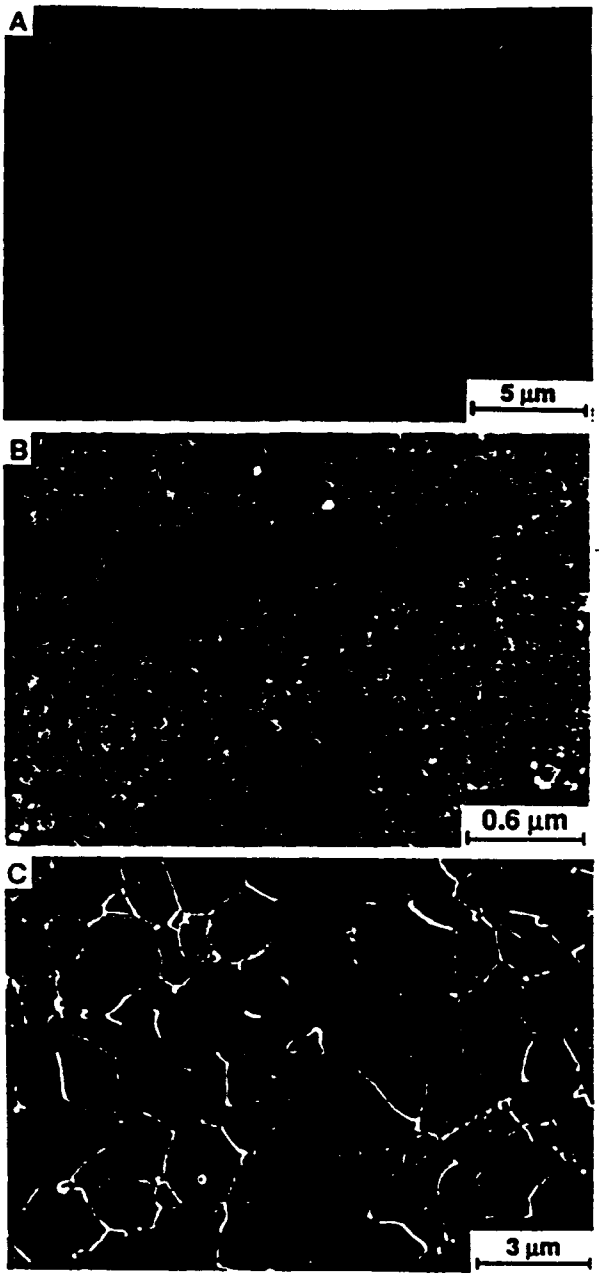

FIG. 8. A, B, and C show SEM micrographs of 74 wt% alumina/26 wt% silica samples sintered at 1300°C (A, B) and 1600°C (C). The 1300°C sample is almost fully dense, although small pores (upper right, A) are occasionally observed. The two-phase microstructure (alumina and siliceous glass) of the 1300°C sample was revealed by etching with a dilute hydrofluoric acid solution (B). The 1600°C sample has undergone reaction to form high-density, fine-grained mullite (C).

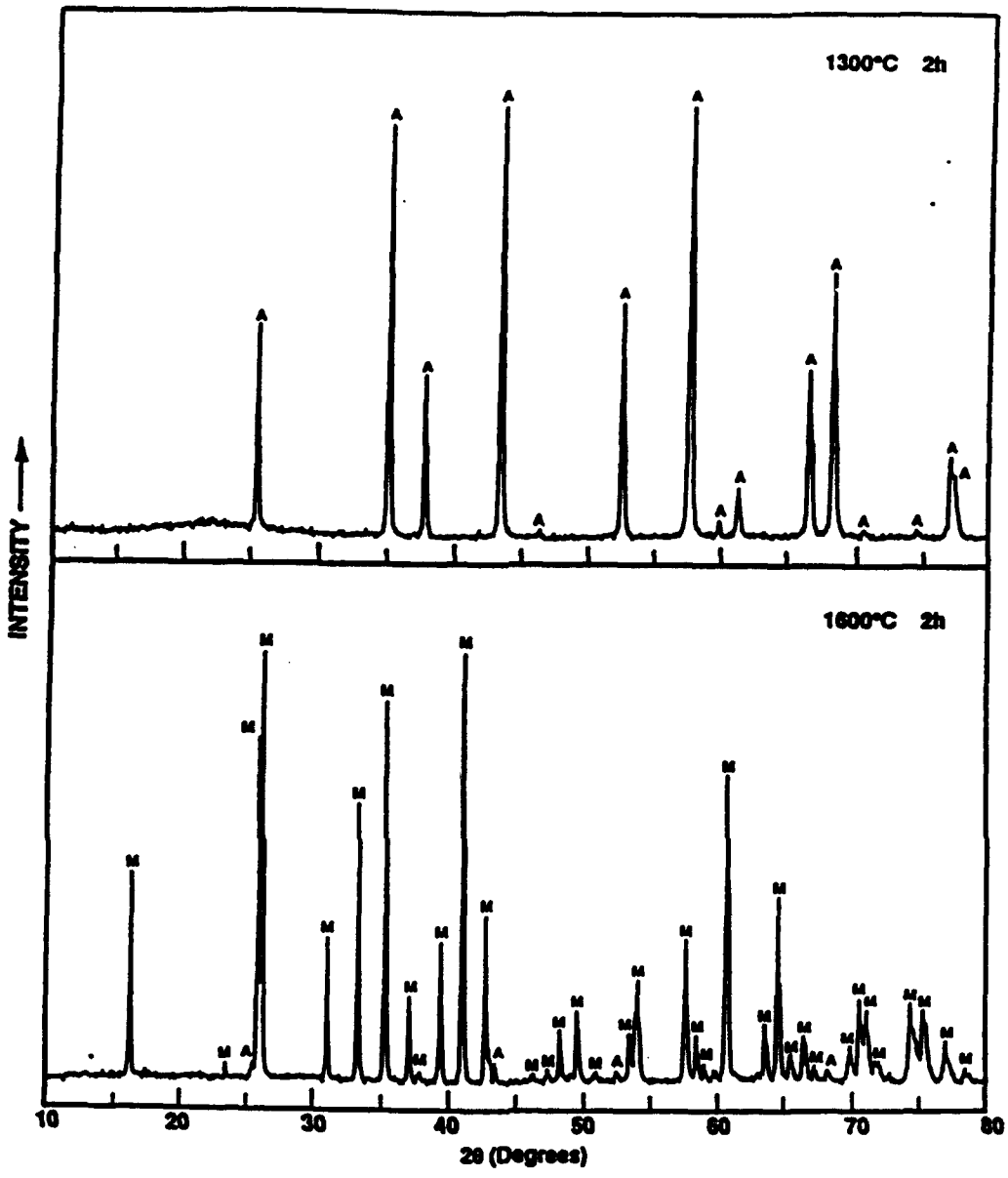

FIG. 9. X-ray diffraction patterns for 74 wt% alumina/26 wt% silica samples sintered at the indicated temperatures.

for the 1600°C sample (Fig. 9) does show a small amount of alumina, but this indicates that the overall composition (74 wt% alumina/26 wt% silica) fell just within the mullite + alumina phase field.) Figure 8C shows that a nearly pore-free microstructure is retained after conversion to mullite. Grains are equiaxed with an average intercept size of ~1.5 μm.

The powder compacts used in this study densify at temperatures that are not much higher than those used during sintering of "sol-gel" mullite-precursors, despite the fact that particulates prepared by the latter methods are approximately an order of magnitude smaller than the composite particles.[20-24] This can be attributed to viscous densification of the silica-coated alumina powders. By using larger particles and by using alpha alumina as a starting material, some of the difficulties normally associated with "sol-gel" techniques (i.e., large weight losses and large shrinkages during drying and sintering) are less of a concern in the current method. However, it is clear that the present method does require the use of considerably higher temperatures to form mullite (i.e., ~1500-1600°C vs. ~1250-1350°C for many sol-gel methods).[20-24] Thus, temperatures for fabricating bulk mullite from the composite particles are in the same range as used for sintering of homogenous green compacts prepared with fine-grained, deagglomerated mullite powders.[25,26] A potential advantage of the present method, however, is that compacts prepared with silica-coated particles could be used in hot forming of shapes. It is possible that samples densified at low temperatures (i.e., 1250-1300°C) could be shape-formed (at similar or lower temperatures) under pressure by viscous deformation.

Transient Viscous Sintering of Mullite-Matrix Composites

In a previous study by Rahaman et al.,[27] it was demonstrated that non-sinterable inclusions can significantly impede densification during fabrication of mullite-matrix composites. These investigators were able to densify "sol-gel" mullite-precursor powders to ~98% relative density at only ~1200°C. However, the relative density was only ~90% when 15 vol% silicon nitride particles were added to the mullite precursor powder, *even though the sintering temperature was increased to 1550°C.* In contrast, densification of composite powders by the TVS method is not affected as much by "non-sinterable" inclusions because these materials can also be coated with the amorphous phase. In the present study, mullite/zirconia and mullite/silicon carbide particle (SiC_p) composites were fabricated by sintering compacts prepared with mixtures of silica-coated particles, i.e., in which the core materials were alumina, silicon carbide, and/or zirconia. With this approach, densification and mullitization were accomplished at temperatures in the same range as those processed without the second phase particles. Several examples are discussed below.

Figure 10 shows a plot of bulk density vs. sintering temperature (2 h) for samples with an overall composition of ~63 wt% alumina/16.5 wt% silica/19.5 wt% zirconia/1 wt% yttria. (The composition was determined by electron microprobe analysis on a sample sintered at 1600°C.) The sintering behavior is essentially the same as observed in Fig. 7 in that densification occurs mostly in the range 1100-1300°C. The bulk density reaches its maximum value by 1300°C and the open porosity drops to zero by this temperature. The bulk density decreases at higher temperature due to mullite formation. XRD shows that mullitization is mostly completed by 1500°C.[17] The other crystalline phases present are alumina and tetragonal zirconia, as well as a small amount of monoclinic zirconia.[17] The

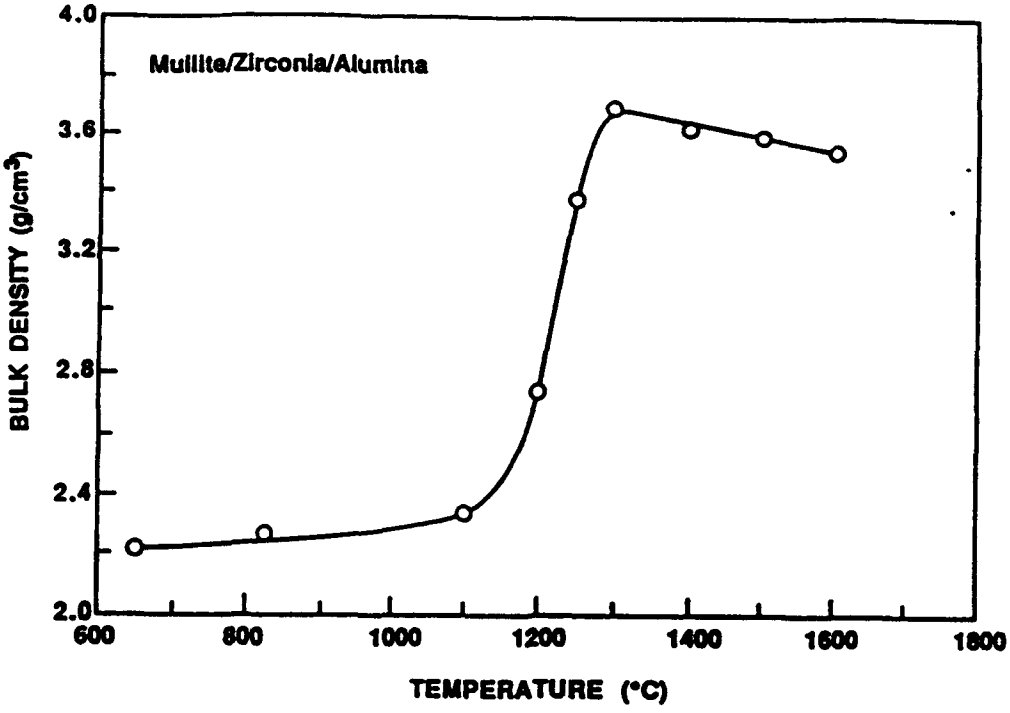

FIG. 10. Plot of bulk density vs. sintering temperature for ~63 wt% alumina/ 16.5 wt% silica/19.5 wt% zirconia/1 wt% yttria samples.

FIG. 11. SEM micrograph of polished and etched mullite/ zirconia/alumina sample sintered at 1500°C for 2 h.

sample contains residual alpha alumina because the alumina/silica weight ratio is ~79/21. (In the binary system, this would put the composition well within the mullite + alumina phase field.) Figure 11 shows the dense, fine-grained microstructure of a polished and etched mullite/zirconia/alumina sample which had been sintered at 1500°C. Zirconia (white phase) and alumina are present as submicrometer, uniformly-distributed inclusions. The very fine inclusions located within mullite grains are suspected to be original core particles that were not "consumed" during the mullite-forming reaction, although further study (e.g., by TEM analysis) is required to confirm this.

Figure 12 shows plots of bulk density and open porosity vs. sintering temperature for samples prepared with ~15 vol% silicon carbide particles (SiC_p) and an overall matrix composition of ~74 wt% alumina/26 wt% silica. The densification behavior is similar to that observed in Figs. 7 and 10, except that the temperature required to reach maximum bulk density is slightly higher.* However, the open porosity reached zero at 1300°C. XRD analysis for a sample sintered at 1550°C shows mullite, silicon carbide, and a trace amount of alumina.

Figure 12 also shows plots of bulk density and open porosity vs. sintering temperature for samples prepared with ~15 vol% silicon carbide whiskers (SiC_w).♦ The powder compacts in this case were prepared using a mixture of uncoated whiskers and silica-coated alumina powders with a composition of ~73 wt% alumina/27 wt% silica. Densification was inhibited compared to samples prepared with ~15 vol% SiC_p. This is not surprising since the whiskers were uncoated and their high aspect ratio would lead to the formation of a whisker network (which would resist the sintering stress). Nevertheless, substantial densification occurred in these samples; the open porosity reached zero by 1400°C and the calculated relative density was ≥96% at 1500°C. (The relative density was calculated assuming true densities of 3.19 g/cm^3 for the SiC_w[28] and 3.17 g/cm^3 for mullite.) These results can be compared with those of Rahaman et al.[27] in which mullite composites with 15 vol% SiC_w reached only ~85% relative density after sintering at 1550°C for 1 h despite the use of very fine powders prepared by a "sol-gel" method.† The results in Fig. 12 can also be compared to those reported by Tiegs et al.[29] in which isopressed mullite powder/SiC_w mixtures were sintered using a proprietary 2 wt% sintering aid. Despite the formation of a liquid phase during sintering, samples with 15 vol% SiC_w did not reach 95% relative density until sintering temperatures approached 1800°C.

---

* In contrast to the results in Figs. 7 and 10, samples prepared with silicon carbide particles and whiskers were sintered in nitrogen. It is not known if the densification rate for these samples is affected by the sintering atmosphere.

♦ SCW-1 S105, Tateho Chemical Industries, Hyogo-ken, Japan. The as-received whiskers were processed by the methods described in references 19 and 28 before they were mixed with the composite powders.

† Limited densification was observed until temperatures exceeded 1500°C because the "sol-gel" precursor powders converted to mullite at low temperature, i.e., ~1300°C.

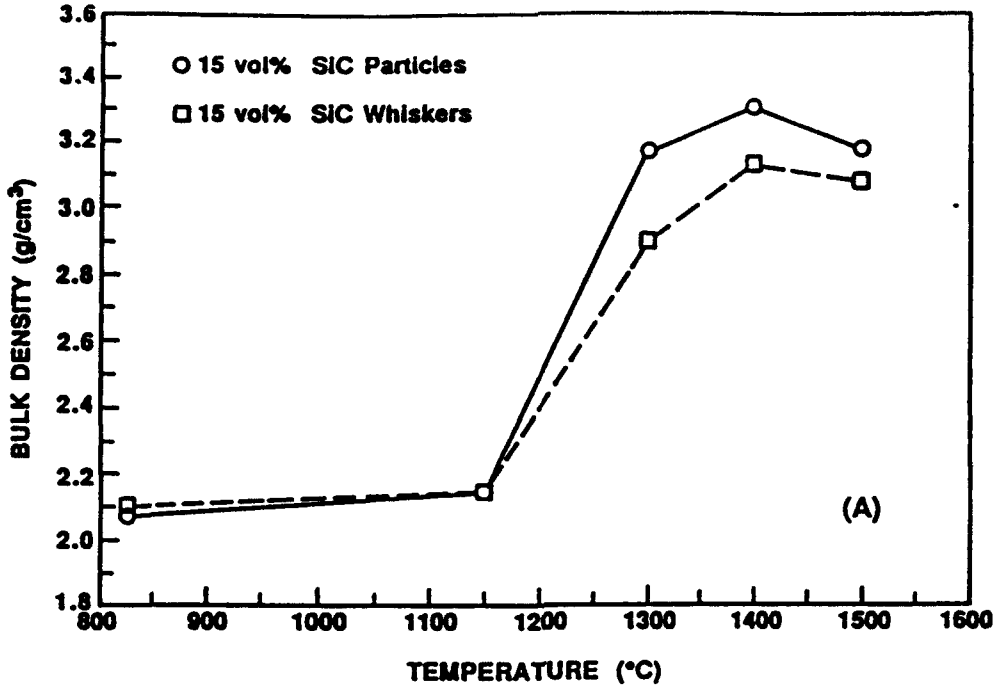

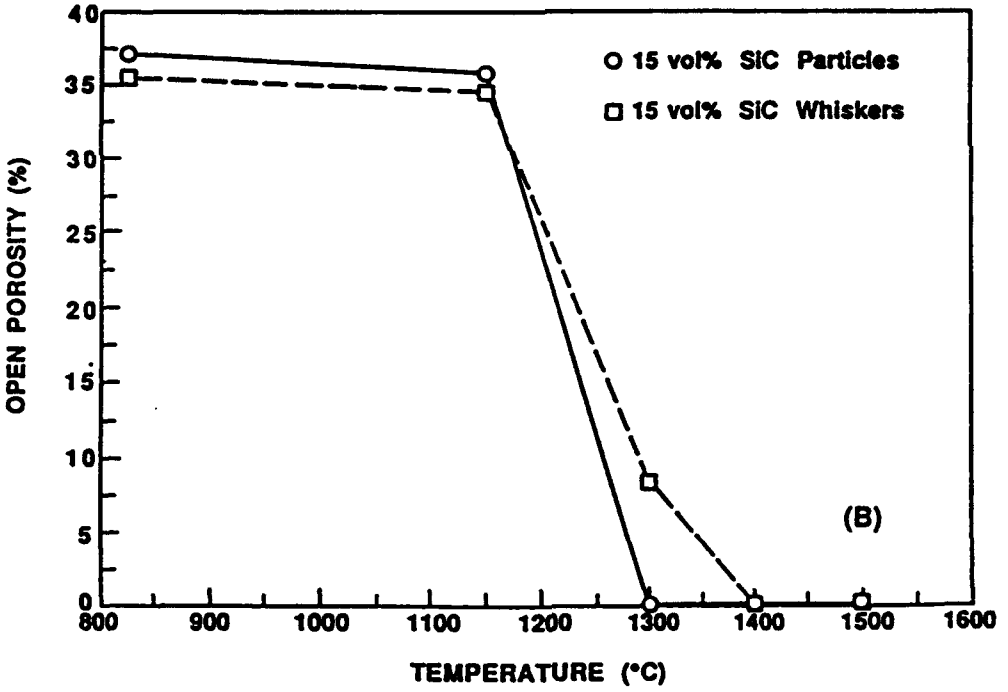

FIG. 12. Plots of bulk density (A) and open porosity (B) vs. sintering temperature for samples with ~15 vol% SiC_p (matrix: ~74 wt% alumina/26 wt% silica) and with ~15 vol% SiC_w (matrix: ~73 wt% alumina/27 wt% silica).

SUMMARY AND CONCLUSIONS

A novel process was developed in which ceramics and composites were fabricated using composite particles consisting of an inner core of a crystalline material and an outer coating of amorphous silica. These particles allowed increased powder compact densification rates due to (1) viscous flow of the amorphous coating and (2) increased threshold concentration for percolation of the "non-sinterable" phase. Enhanced densification was demonstrated by directly comparing sintering behavior for compacts prepared with silica-coated silicon nitride particles vs. a mixture of silica particles + silicon nitride particles.

Glass/ceramic composites prepared from coated particles also allowed the development of novel microstructures in that a high concentration of crystalline phase could be incorporated into the glassy matrix as isolated inclusions.

By choosing a core material that reacted at elevated temperatures with the silica coating, it was possible to fabricate glass-free ceramics and ceramic-ceramic composites by *transient viscous sintering (TVS).* For example, silica-coated alumina particles were sintered to almost full density at low temperature (~1300°C) and subsequently heated to higher temperature (~1500-1600°C) to form dense, fine-grained mullite.

Due to viscous densification of silica-coated alumina particles, it was possible to sinter mullite/silicon carbide whisker composites to high relative density (≥96%) at considerably lower temperature (1500°C) compared to previous studies. In addition, dense, fine-grained mullite-matrix composites having homogeneous second-phase distribution were fabricated using mixtures of composite particles having different crystalline cores (i.e., alumina, zirconia, silicon carbide). These samples showed essentially the same densification behavior as samples prepared only with silica-coated alumina particles.

ACKNOWLEDGMENT

Experimental assistance from C.S. Khadilkar, G. Norsworthy, Y.-J. Lin, A. Ulicny, M. Springgate are gratefully acknowledged. This work was supported by the Defense Advanced Research Projects Agency (MDA972-88-J-1006); National Science Foundation, Division of Materials Research (DMR-8451916); Florida High Technology and Industry Council; and IBM Corp.

REFERENCES

1. The following books are representative of progress in the field:
   a. Better Ceramics Through Chemistry, Mat. Res. Soc. Symp. Proc., Vol. 32, edited by C.J. Brinker, D.E. Clark, and D.R. Ulrich, Elsevier Science Pub. Co., New York, NY, 1984.
   b. Better Ceramics Through Chemistry II, Mat. Res. Soc. Symp. Proc., Vol. 73, edited by C.J. Brinker, D.E. Clark, and D.R. Ulrich, Materials Research Society, Pittsburgh, PA, 1986.

c. Better Ceramics Through Chemistry III, Mat. Res. Soc. Symp. Proc., Vol. 121, edited by C.J. Brinker, D.E. Clark, and D.R. Ulrich, Materials Research Society, Pittsburgh, PA, 1988.

d. Better Ceramics Through Chemistry IV, Mat. Res. Soc. Symp. Proc., Vol. 180, edited by B.J.J. Zelinski, C.J. Brinker, D.E. Clark, and D.R. Ulrich, Materials Research Society, Pittsburgh, PA, 1990.

e. Ultrastructure Processing of Ceramics, Glasses, and Composites, edited by L.L. Hench and D.R. Ulrich, John Wiley & Sons, New York, NY, 1984.

f. Science of Ceramic Chemical Processing, edited by L.L. Hench and D.R. Ulrich, John Wiley and Sons, New York, NY, 1986.

g. Ultrastructure Processing of Advanced Ceramics, edited by J.D. Mackenzie and D.R. Ulrich, John Wiley & Sons, New York, NY, 1988.

h. Ceramic Powder Science, Advances in Ceramics, Vol. 21, edited by G.L. Messing, K.S. Mazdiyasni, J.W. McCauley, and R.A. Haber, American Ceramic Society, Inc., Westerville, OH, 1987.

i. Ceramic Powder Science II, Parts A and B, Ceramic Transactions, Vol. 1, edited by G.L. Messing, E.R. Fuller, and H. Hausner, American Ceramic Society, Inc., Westerville, OH, 1988.

j. Ceramic Powder Processing Science, edited by H. Hausner, G.L. Messing, and S. Hirano, Deutsche Keramische Gesellschaft, Koln, FRG, 1989.

k. Ceramic Powder Processing Science III, Ceramic Transactions, Vol. 12, edited by G.L. Messing, S.I. Hirano, and H. Hausner, American Ceramic Society, Inc., Westerville, OH, 1990.

2. R. Zallen. The Physics of Amorphous Solids. Wiley, New York, 1983.

3. L.C. De Jonghe, M.N. Rahaman, and C.H. Hsueh, "Transient Stresses in Bimodal Compacts during Sintering," Acta Metall., 34 (7) 1467-1471 (1986).

4. M.N. Rahaman and L.C. De Jonghe, "Effect of Rigid Inclusions on the Sintering of Glass Powder Compacts," J. Am. Ceram. Soc., 70 (12) C-348 - C-351 (1987).

5. G.W. Scherer and A. Jagota, "Effect of Inclusions on Viscous Sintering," to be published in Processing, Microstructure, and Properties of Composite Materials, Ceramic Transactions, edited by M.D. Sacks, American Ceramic Society, Inc., Westerville, OH, 1991.

6. P.B. Howard and G.D. Parfitt, "The Precipitation of Silica/Alumina on Titanium Dioxide Sufraces," Croat. Chem. Acta, 50 15-30 (1977).

7. M. Bruni and M. Visca, "Precipitation of Aluminosilicates on the Surface of Titanium Dioxide," Ind. Eng. Chem. Prod. Res. Dev., 24 (4) 579-586 (1985).

8. A.M. Homolo, M.R. Lorenz, C.J. Mastrangelo, and T.L. Tilbury, "Novel Magnetic Dispersions Using Silica Stabilized Particles," IEEE Trans. Magn., Mag.-22 (5) 716-719 (1986).

9. T. Sueyoshi, "Morphology and Porous Texture of Iron Fine Particles with Relation to Their Magnetic Properties," J. Mater. Sci., 22 860-866 (1987).

10. T. Ishikawa and E. Matijevic, "Formation of Monodispersed Pure and Coated Spindle-Type Iron Particles," Langmuir, 4 (1) 26-31 (1988).

11. S. Kratohvil and E. Matijevic, "Preparation and Properties of Coated, Uniform, Inorganic Colloidal Particles: I, Aluminum (Hydrous) Oxide on Hematite, Chromia, and Titania,"

Adv. Ceram. Mater., 2 (4) 798-803 (1987).

12. A. Garg and E. Matijevic, "Preparation and Properties of Uniform Coated Inorganic Colloidal Particles. II. Chromium Hydrous Oxide on Hematite," Langmuir, 4 (1) 38-44 (1988).

13. A. Garg and E. Matijevic, "Preparation and Properties of Uniform Coated Inorganic Colloidal Particles III. Zirconium Hydrous Oxide on Hematite," J. Colloid Interface Sci., 126 (1) 243-250 (1988).

14. A.K. Garg and L.C. De Jonghe, "Microencapsulation of Silicon Nitride Particles with Yttria and Yttria-Alumina Precursors," J. Mater. Res., 5 (1) 136-142 (1990).

15. H. Okamura, E.A. Barringer, and H.K. Bowen, "Preparation and Sintering of Monosized Al_2O_3-TiO_2 Composite Powder," J. Am. Ceram. Soc., 69 (2) C-22 - C-24 (1986).

16. S.-I. Hirano, T. Hayashi, T. Kojima, and C. Kato, "Chemical Processing of Zirconia-Containing Oxide Composites by a Colloidal Method," pp. 55-61 in MRS Int'l Mtg. on Adv. Mats., Vol. 3, 55-61, Materials Research Society, 1989.

17. M.D. Sacks, N. Bozkurt, and G.W. Scheiffele, "Fabrication of Mullite and Mullite-Matrix Composites by Transient Viscous Sintering of Composite Powders," to be published in J. Am. Ceram. Soc.

18. M.D. Sacks, G.W. Scheiffele, N. Bozkurt, and C.S. Khadilkar, "Synthesis and Characterization of Composite Particles: Silica-Coated Alumina," to be submitted to J. Colloid Interface Sci.

19. H.-W. Lee "Suspension Processing and Pressureless Sintering of Silicon Carbide Whisker-Reinforced Alumina-Matrix Composites," Ph.D. Dissertation, University of Florida, 1990.

20. S. Komarneni, Y. Suwa, and R. Roy, "Application of Compositionally Diphasic Xerogels for Enhanced Densification: The System Al_2O_3-SiO_2," J. Am. Ceram. Soc., 69 (7) C-155 -C-156 (1986).

21. R. Roy, Y. Suwa, and S. Komarneni, "Nucleation and Epitaxial Growth in Diphasic (Crystalline + Amorphous) Gels"; pp. 247-258 in Science of Ceramic Chemical Processing. Edited by L.L. Hench and D.R. Ulrich. Wiley, New York, 1987.

22. N. Shinohara, D. M. Dabbs, and I. A. Aksay, "Infrared Transparent Mullite Through Densification of Monolithic Gels at 1250°C"; pp. 19-24 in Infrared and Optical Transmitting Materials. SPIE Vol. 683 (1986).

23. B. Sonuparlak, "Sol-Gel Processing of Infrared-Transparent Mullite," Adv. Ceram. Mat., 3 (3) 263 (1988).

24. M.N. Rahaman, L.C. De Jonghe, S. Shinde, and P.H. Tewari, "Sintering and Microstructure of Mullite Aerogels," J. Am. Ceram. Soc., 71 (7) C-338 - C-341 (1988).

25. M.D. Sacks, H.-W. Lee, and J.A. Pask, "A Review of Powder Preparation Methods and Densification Procedures for Fabricating High Density Mullite," pp. 167-207 in Mullite and Mullite Matrix Composites, Ceramic Transactions, Vol. 6. Edited by S. Somiya, R.F. Davis, and J.A. Pask. The American Ceramic Society, Inc., Westerville, OH, 1990.

26. Y. Hirata, I.A. Aksay, R. Kurita, S. Hori, and H. Kaji, "Processing of Mullite with Powders Processed by Chemical Vapor Deposition," pp. 323-338 in Mullite and Mullite Matrix Composites, Ceramic Transactions, Vol. 6. Edited by S. Somiya, R.F. Davis, and J.A. Pask. The American Ceramic Society, Inc., Westerville, OH, 1990.

27. M.N. Rahaman and D.-Y. Jin, "Sintering of Mullite and Mullite Matrix Composites"; pp. 753-766 in Sintering of Advanced Ceramics, Ceramic Transactions, Vol. 7. Edited by C.A. Handwerker, J.E. Blendell, and W.A. Kaysser. The American Ceramic Society, Inc., Westerville, OH, 1990.

28. H.-W. Lee and M.D. Sacks, "Pressureless Sintering of SiC-Whisker-Reinforced Al_2O_3 Composites: I, Effect of Matrix Powder Surface Area," J. Am. Ceram. Soc., 73 (7) 1884-1893 (1990).

29. T.N. Tiegs, P.F. Becher, and P. Angelini, "Microstructures and Properties of SiC Whisker-Reinforced Mullite Composites"; pp. 463-472 in Mullite and Mullite Matrix Composites, Ceramic Transactions, Vol. 6. Edited by S. Somiya, R.F. Davis, and J.A. Pask. The American Ceramic Society, Inc., Westerville, OH, 1990.

TRANSIENT VISCOUS SINTERING OF MULLITE AND MULLITE-MATRIX COMPOSITES

Michael D. Sacks, Nazim Bozkurt, and Gary W. Scheiffele, Ceramics Division, Department of Materials Science and Engineering, University of Florida, Gainesville, FL 32611

ABSTRACT

Mullite was fabricated by *transient viscous sintering (TVS)* of composite powders. In this process, powder compacts were prepared using particles which consisted of inner cores of alpha alumina and outer coatings of amorphous silica. The compacts could be viscously sintered to almost full density at relatively low temperature (~1300°C). Samples were subsequently converted to dense, fine-grained mullite at higher temperatures (≥1500°C) by reaction between the alumina and silica. The TVS process was also used to fabricate mullite/SiC particle and mullite/SiC whisker composites. Densification was enhanced compared to other recent studies of sintering of mullite-matrix composites.

INTRODUCTION

Mullite, an aluminum silicate compound with nominal composition $3Al_2O_3 \cdot 2SiO_2$, has a variety of attractive properties, including excellent high temperature strength and creep resistance, good chemical and thermal stability, low thermal expansion coefficient, and good dielectric properties. Consequently, the fabrication of mullite bodies with high relative density (low porosity) and fine grain size has been the subject of numerous investigations.[1,2] In conventional processing methods, mullite powders are shape-formed and sintered. However, sintering of powder compacts to high densities normally requires relatively high temperatures due to the low bulk and grain boundary diffusion coefficients for mullite. Various approaches have been used to enhance densification, including (i) reducing the particle size, (ii) improving the green microstructure (e.g., increasing particle packing density, eliminating agglomerates and other large processing flaws), (iii) applying external pressure (e.g., hot pressing, hot isostatic pressing), and (iv) using additives which form a liquid-phase during sintering.

Another approach to fabricating high density mullite involves using precursor materials.[1,2] The objective is to densify mixtures of alumina- and silica-bearing materials prior to the mullite-forming reaction. The success of this approach depends on the scale of mixing of the reactants. When mixing occurs at the

molecular level, mullitization occurs at low temperature (~1000°C) and subsequent densification (at low temperatures) is very limited. In contrast, if the level of mixing is too coarse (e.g., micrometer scale), then high temperatures (≥1650°C) are required to accomplish both mullitization and densification. The lowest sintering temperatures are usually achieved when scale of mixing is in the approximate range of 5-50 nm (i.e., the typical size range for "sol-gel" processes). Substantial densification of bulk samples can be achieved at temperatures in the approximate range of 1200-1300°C,[3-7] while the reaction to form mullite occurs at slightly higher temperatures (i.e., approximately 1250-1350°C).[3-7] The low sintering temperature can be attributed to two attributes of the mullite-precursor particulates: (i) the small size (high specific surface area) and (ii) the amorphous or weakly crystalline character (which favors densification by the viscous flow mechanism). Despite the advantage of low temperatures for densification and mullitization, "sol-gel" methods present other processing problems which make it difficult to fabricate bulk mullite samples, i.e., relatively large weight losses and shrinkages occur during drying and sintering.

Fabrication of mullite-matrix composites generally presents even greater processing difficulties. It is well-known that the addition of "non-sinterable" inclusions to a matrix material can significantly decrease the densification rate.[8,9] In samples prepared with crystalline matrix materials, bulk densification may be completely arrested once the inclusion concentration exceeds a critical volume fraction.[8] (According to percolation theory, the threshold concentration to establish a connected network is ~16 vol% in a random mixture of two types of equal-sized, spherical particles.[10]) Samples prepared with amorphous matrix materials also exhibit reduced densification rates when "non-sinterable" inclusions are present, but the effect is not as severe as observed for crystalline matrix materials.[9]

In the present study, a novel processing technique was developed for fabricating mullite and mullite-matrix composites which combines several approaches for achieving enhanced densification: (i) colloidal processing to prepare homogenous green compacts with high relative density and fine pore sizes, (ii) use of an amorphous phase to allow viscous densification, and (iii) controlled spatial distribution of phases in order to minimize the development of rigid networks of non-sinterable phases. The overall approach is schematically illustrated in Fig. 1. To fabricate mullite, the starting material would be composite particles having an inner cores of alpha alumina and an outer coatings of amorphous silica. Particles would be in the ~0.1-1.0 μm size range so that colloidal processing methods could be used to produce homogeneous, high density green compacts. It is anticipated powder compacts could be densified at moderate sintering temperatures because of the fine particle size and the outer coating of amorphous silica on the particles. Samples would subsequently be heated to higher temperatures so that the alumina core and silica coating of each particle could react to form mullite. The overall process is referred to as *transient viscous sintering (TVS)*. The process could also be used to fabricate mullite-matrix composites by mixing the silica-coated alumina particles with second-phase particulates.

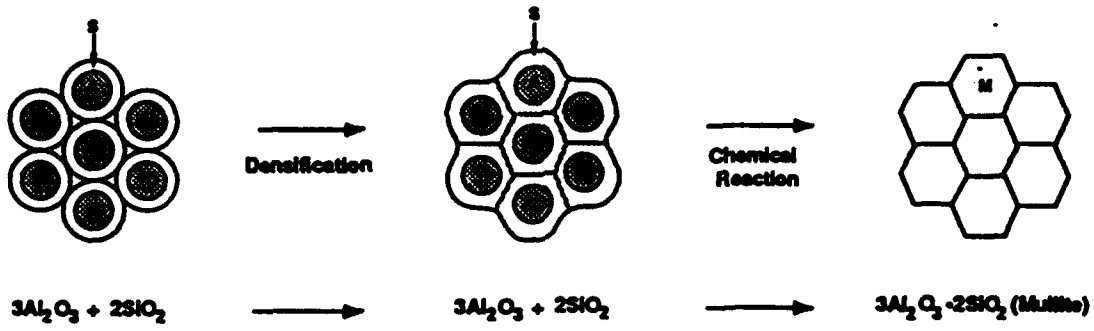

FIG. 1. Schematic illustration of the formation of single-phase mullite by transient viscous sintering (TVS).

EXPERIMENTAL

Experimental procedures are described briefly, as details have been provided elsewhere.[11-13] Coated powders were prepared using alpha alumina (AKP-50, Sumitomo Chemical America) and silicon carbide particles, SiC_p, (A-2, Showa Denka) as the core materials and tetraethylorthosilicate, TEOS, (Fisher Scientific) as the source of silica. Prior to deposition of the coating, as-received core powders were fractionated using standard fluid classification techniques[14] in order to remove hard agglomerates. The average particle sizes of the fractionated powders were in the range of ~0.1-0.2 μm. The core particles were then suspended in TEOS/ethanol solutions and silica coatings were subsequently deposited by hydrolysis of the TEOS. The thickness of the coating could be varied by changing the ratio of the core material/TEOS in the initial suspension.[11] For example, Fig. 2 shows transmission electron micrographs (Model 200CX, JEOL) of silica-coated alumina particles with different thickness of the coating. X-ray photoelectron spectroscopy (Model XSAM800, Kratos Analytical) was used to confirm that the external layer of the particles was silica.[15] The amorphous nature of the silica coating was shown by X-ray diffraction.[13]

Mullite samples were prepared using composite particles with an overall composition of ~74 wt% alumina/26 wt% silica (designated 74/26).* This

* The alumina/silica ratios reported in this study were not determined directly from composite powders, but instead were measured by electron microprobe analysis (Superprobe 733, JEOL) on bulk samples prepared by sintering composite powder compacts at 1600°C.

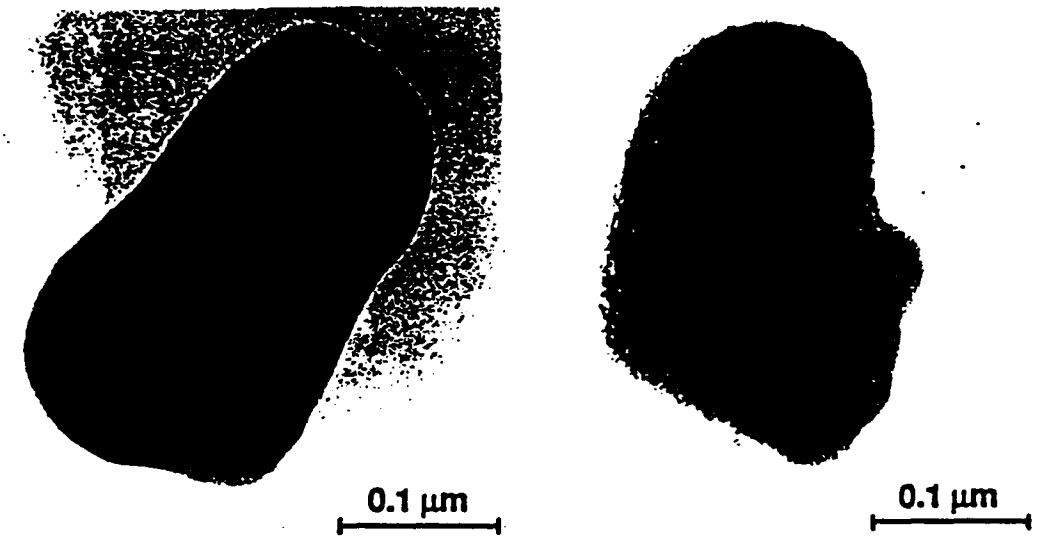

FIG. 2. Transmission electron micrographs of composite particles prepared with different amounts of amorphous silica coating on alpha alumina core particles.

composition is near the mullite/(mullite + alumina) phase boundary and was chosen to avoid residual siliceous glass after the mullite reaction was completed. Mullite-matrix composites with ~15 vol% SiC_p composites were prepared using mixtures of silica-coated alumina and silica-coated SiC_p particles. The overall alumina/silica weight ratio in the composites was ~74/26. Mullite/~15 vol% silicon carbide whiskers, SiC_w, (SCW-1 S105, Tateho Chemical Industries) composites were prepared using silica-coated alumina particles (~73/27 weight ratio) and uncoated whiskers.[11]

Disk-shaped green compacts (~2-3 mm thick, ~19 mm diameter) were prepared by slip casting well-dispersed aqueous suspensions into plastic rings set upon a plaster block. Good dispersion was achieved by using ultrasonication to break down powder agglomerates and pH adjustment to generate sufficiently high surface charge for electrostatic stabilization. After drying at ~80°C, compacts were sintered at temperatures in the range 825-1600°C using an air atmosphere for mullite samples and a nitrogen atmosphere for mullite/SiC samples.

The bulk density and open porosity were determined on sintered samples using the Archimedes method with deionized water as the liquid medium. Microstructure observations were made on polished samples using scanning electron microscopy, SEM, (Models JSM 35-CF and JSM-6400, JEOL). Phase analysis was carried out by X-ray diffraction, XRD, (Model APD 3720, Philips Electronic Instruments Co.) using Ni-filtered Cu $K\alpha$ radiation. XRD measurements were made on bulk sintered samples which were ground to a 30 μm surface finish.

RESULTS AND DISCUSSION

Aqueous suspensions of silica-coated alumina particles were electrostatically stabilized against flocculation using pH adjustment. Figure 3 shows a plot of electrophoretic mobility vs. pH for the composite particles used to prepare 74/26 mullite samples. Due to the surface coating of amorphous silica, the electrokinetic behavior of the composite particles is very similar to that observed for silica particles prepared by a similar solution-precipitation method, i.e., the isoelectric point is at pH≈2.5 and the mobility becomes increasingly negative as the pH increases. Based on these results, suspensions were prepared at pH≈9 in order to ensure good stability against flocculation.

Mercury porosimetric analysis (Fig. 4A) showed that the 74/26 slip cast compact had a narrow distribution of fine pore channels (median radius ≈22 nm). These results indicated that the powder compact had a dense, homogenous packing of the composite particles. This was confirmed by SEM observations (Fig. 4B) of the green compact. Archimedes measurements were carried out on a sample which had been heated to 900°C in order to develop sufficient handling strength. The open porosity was ~38% and the bulk density was ~2.03 g/cm^3. From the latter value, the calculated relative density was ~62%. (This was calculated assuming true densities of 2.2 and 3.98 g/cm^3 for amorphous silica and alpha alumina, respectively.)

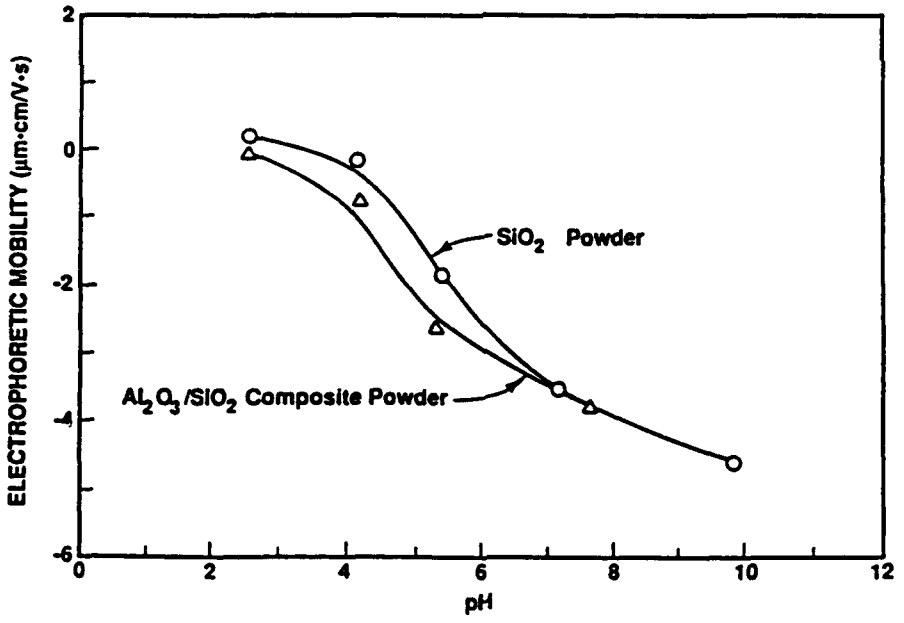

FIG. 3. Plots of electrophoretic mobility vs. pH for silica-coated alumina particles and silica particles.

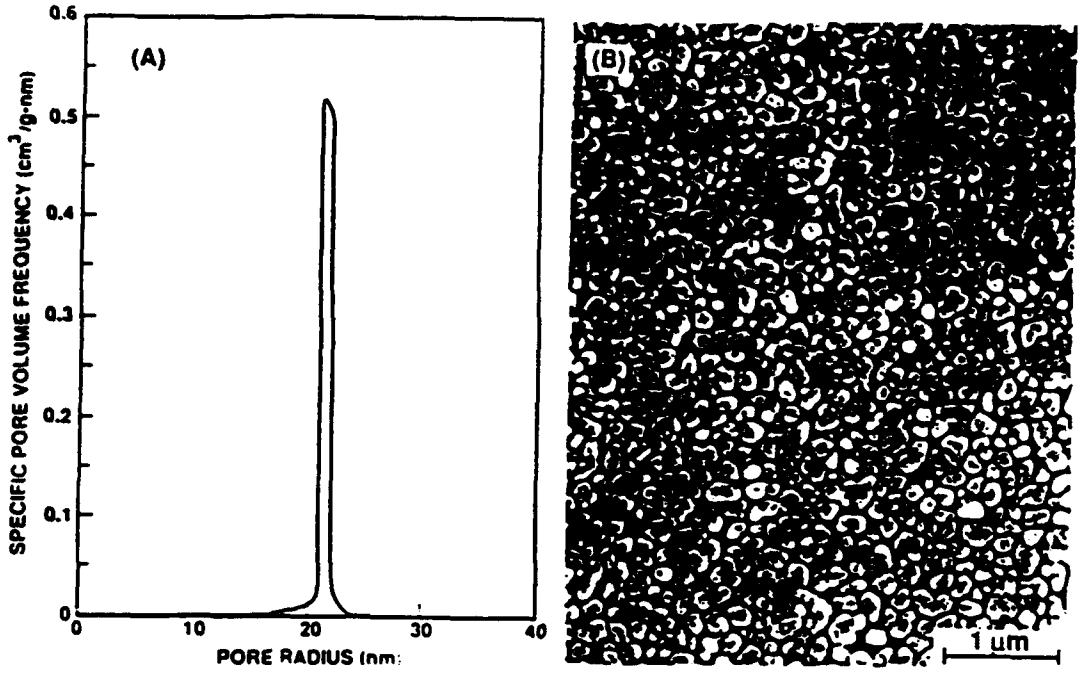

FIG. 4. (A) Mercury porosimetric plot of specific pore volume frequency vs. pore radius and (B) SEM micrograph which were both obtained from a slip cast green compact of composite particles.

Figure 5 shows plots of bulk density and open porosity vs. sintering temperature for 74/26 samples. Most of the densification occurs in the range of ~1100-1300°C. The open porosity is completely eliminated by 1250°C and the bulk density reaches a maximum at 1300°C. These temperatures are not much higher than those used to densify "sol-gel" samples, despite the fact that the particulates prepared by the latter methods are approximately an order of magnitude smaller than the composite particles.[3-7] This indicates that viscous flow is an important mechanism in densification of compacts prepared with the amorphous silica-coated alumina powder. The homogeneous, high density green microstructure of the composite powder compacts is also beneficial in achieving a low densification temperature.

The decrease in bulk density of compacts at sintering temperatures above 1300°C (Fig. 5) is attributed to the reaction between alumina and silica to form mullite. (This reaction results in a volume expansion of ~4%.) Mullite formation at higher temperatures was confirmed by XRD analysis. Figure 6 shows that the only crystalline phase in a sample sintered at 1300°C is alpha alumina. Substantial mullite formation occurs in the range 1400-1500°C, although higher temperature is required for complete reaction.[17] The sample sintered at 1600°C

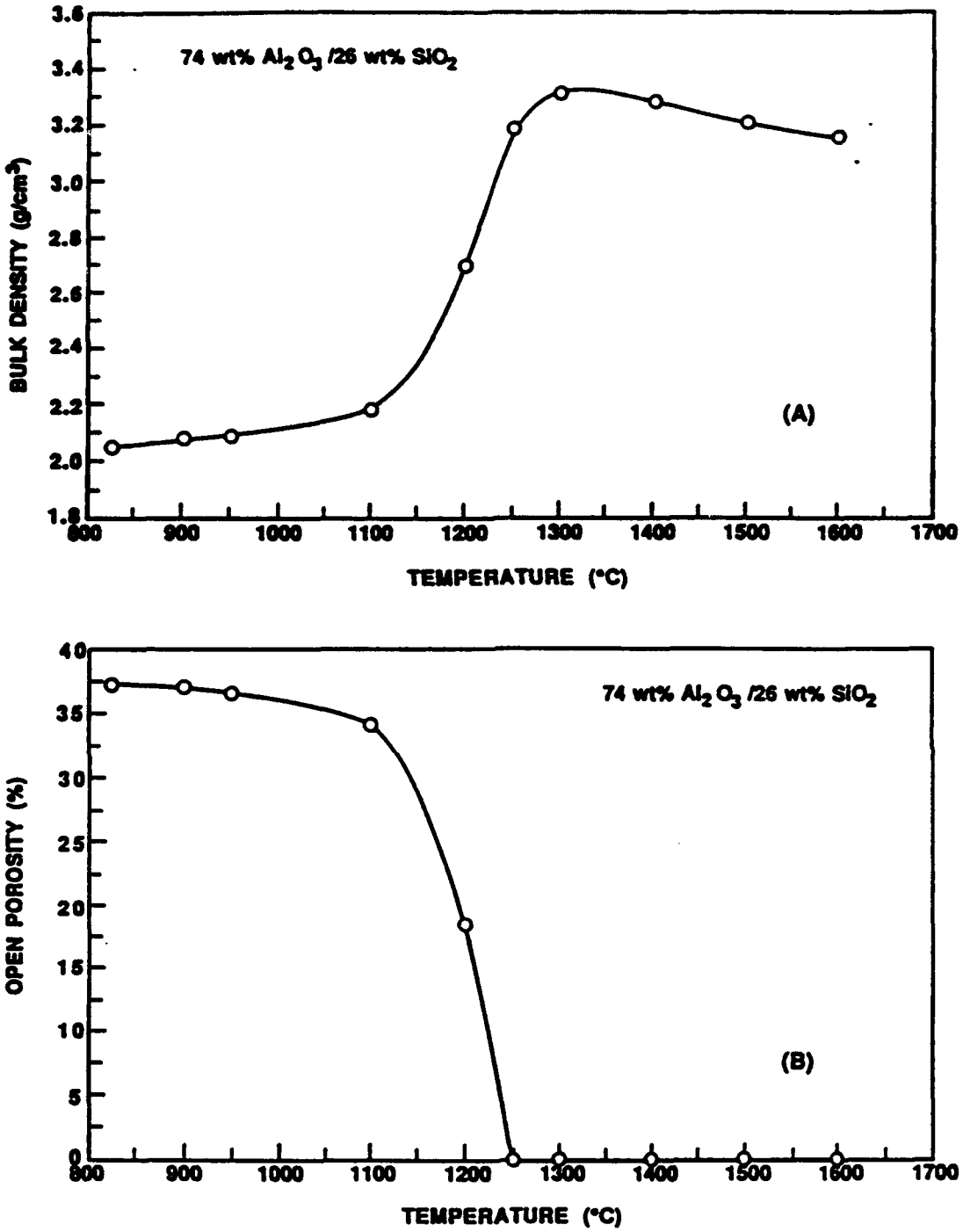

FIG. 5. Plots of bulk density (A) and open porosity (B) vs. sintering temperature for 74 wt% alumina/26 wt% silica samples.

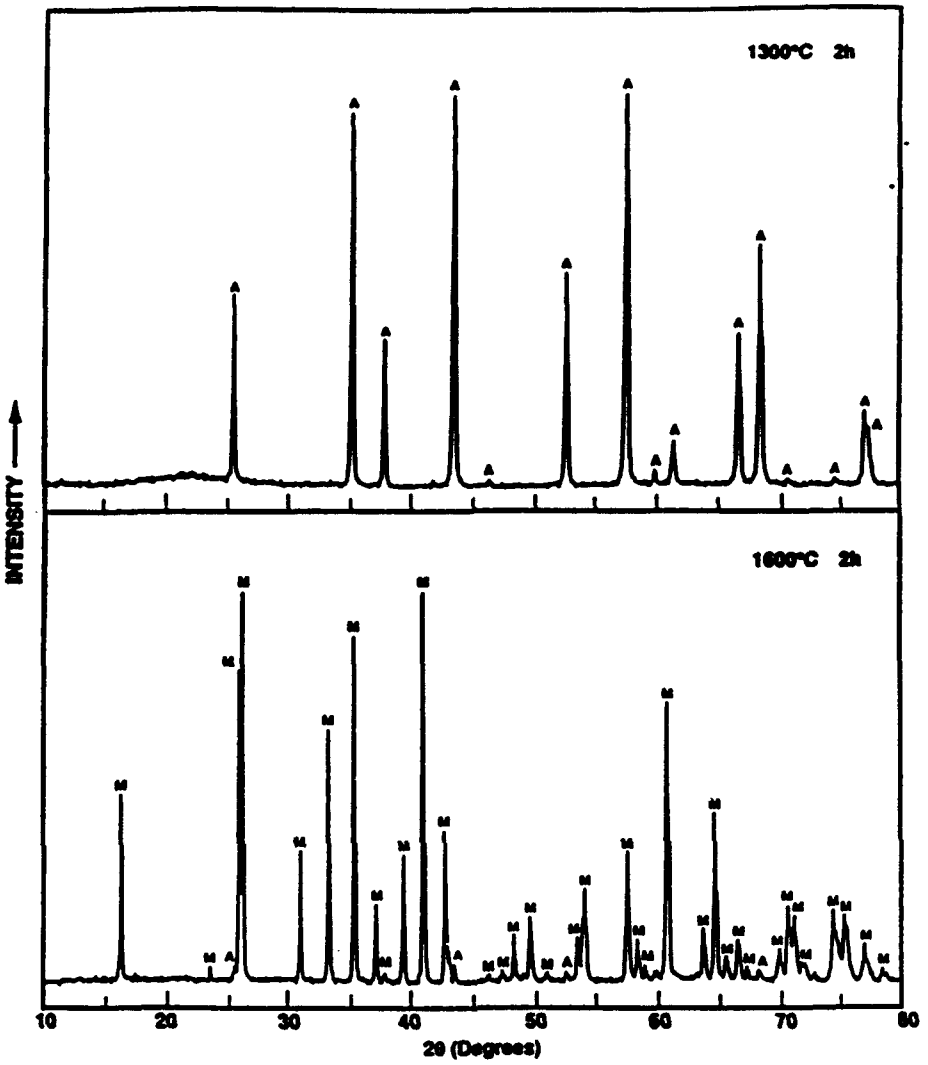

FIG. 6. X-ray diffraction patterns for 74 wt% alumina/26 wt% silica samples sintered at the indicated temperatures.

sample was mostly mullite, but a small amount of alumina was detected in the XRD pattern (Fig. 6).* Samples remain essentially pore-free after conversion to mullite. The bulk density value (~3.16 g/cm^3) for the 1600°C sample indicates that the relative density is >99%.

* As noted earlier, the overall composition of the 74/26 samples lies near the boundary between the single-phase (mullite) and two-phase (mullite + alumina) regions of the Al_2O_3 - SiO_2 phase diagram. The presence of a small amount of alumina suggests that the composition fell just within the latter phase field.

SEM observations on sintered samples are consistent with the results described in Figs. 5 and 6. Figure 7A shows an SEM micrograph of a polished, but unetched, sample that had been sintered at 1300°C. The sample is almost 100% dense, although some small pores (~1 μm or less) are occasionally observed. Figure 7B shows the same sample after chemical etching with dilute hydrofluoric acid. The sample retains features of the original composite particles, i.e., core alumina particles and siliceous coatings are evident. Figure 7C shows a polished and thermally-etched microstructure of a sample sintered at 1600°C. The sample is nearly pore-free with equiaxed grains having an average intercept size of ~1.5 μm. No residual siliceous phase was detected in the sintered samples, indicating that essentially full conversion to mullite occurred.

Figure 8 shows plots of bulk density and open porosity vs. sintering temperature for samples containing ~15 vol% SiC_p and ~15 vol% SiC_w. As noted earlier, the former samples were prepared using a mixture of silica-coated alumina and silica-coated SiC_p particles. The densification rate for these samples may be slightly lower compared to the compacts prepared only with silica-coated alumina particles (Fig. 5). The maximum bulk density in Fig. 8 is observed at a higher temperature (1400°C), while zero open porosity is also reached at slightly higher temperature (by 1300°C). This difference in densification behavior may reflect the fact that the average thickness of the amorphous silica coating on the core particles is thinner in the samples containing the 15 vol% SiC_p. (The average coating thickness must be lower since the overall matrix composition - 74 wt% alumina/26 wt% silica - remains the same.) However, further study is needed to confirm that is the cause for the slightly lower densification rate, since other processing variables (e.g., the use of a nitrogen sintering atmosphere for samples with SiC_p) could have also affected the densification behavior.

Densification of samples prepared with 15 vol% SiC_w is inhibited to a greater extent compared to samples containing 15 vol% SiC_p. This is not surprising considering the fact that these samples were prepared by mixing uncoated SiC_w with silica-coated alumina particles. Furthermore, due to the high aspect ratio of the whiskers,[14] the SiC_w concentration exceeds the critical volume fraction for percolation. Nevertheless, substantial densification is observed in these samples at relatively low temperatures. The open porosity is zero at 1400°C and the calculated relative density is $\geq$96% at 1500°C. (The relative density was calculated assuming true densities of 3.19 g/cm^3 for the SiC_w[14] and 3.17 g/cm^3 for mullite.)

It is interesting to compare the results in Fig. 8 to other studies of sintering of mullite-matrix composites. Rahaman et al.[18] prepared composites using "sol-gel" derived mullite-precursor powders as the matrix phase. With no second-phase inclusions, the amorphous, fine-sized powders could be sintered to ~98% relative density at only 1200°C. However, the addition of 15 vol% silicon nitride particles or 15 vol% silicon carbide whiskers resulted in substantially lower relative densities (~90% and ~85%, respectively), despite a considerably higher sintering temperature (i.e., 1550°C). The poor densification behavior for these samples could be attributed to the fact that mullite conversion occurred at low

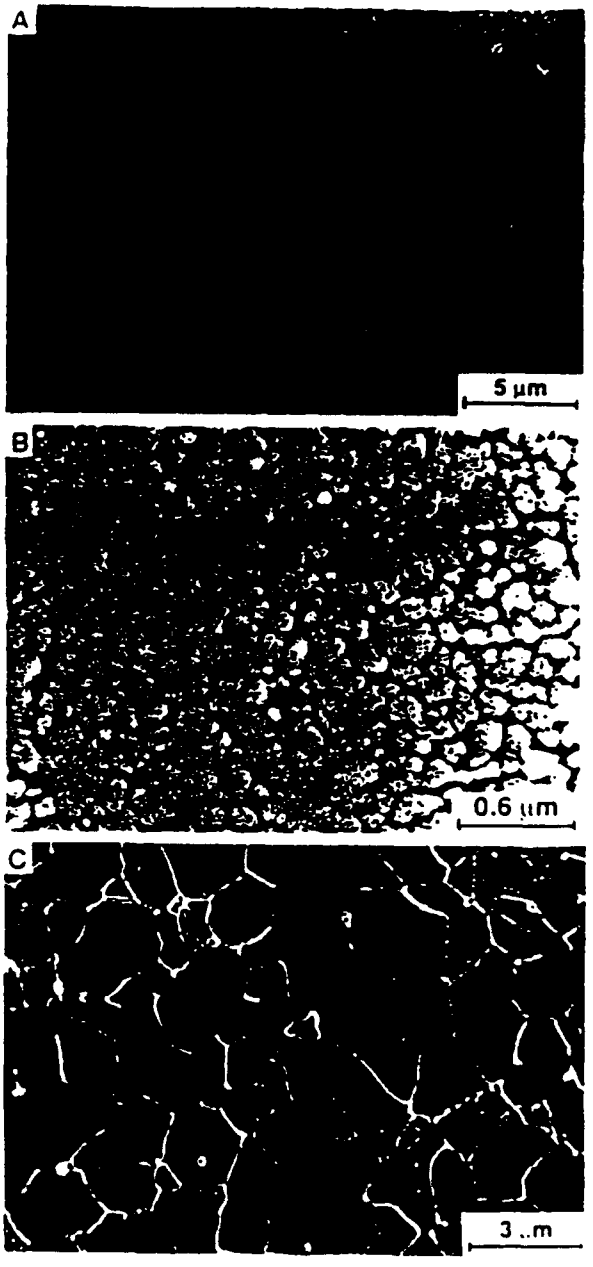

FIG. 7. A, B, and C are SEM micrographs of sintered 74 wt% alumina /26 wt% silica samples. A sample sintered at 1300°C is almost fully dense, although small pores (upper right) are occasionally observed (A). The two-phase microstructure of alumina and siliceous glass of the 1300°C sample is revealed after chemical etching with a dilute HF solution (B). A sample sintered at 1600°C converts to almost fully dense mullite having a fine, equiaxed grain structure (C).

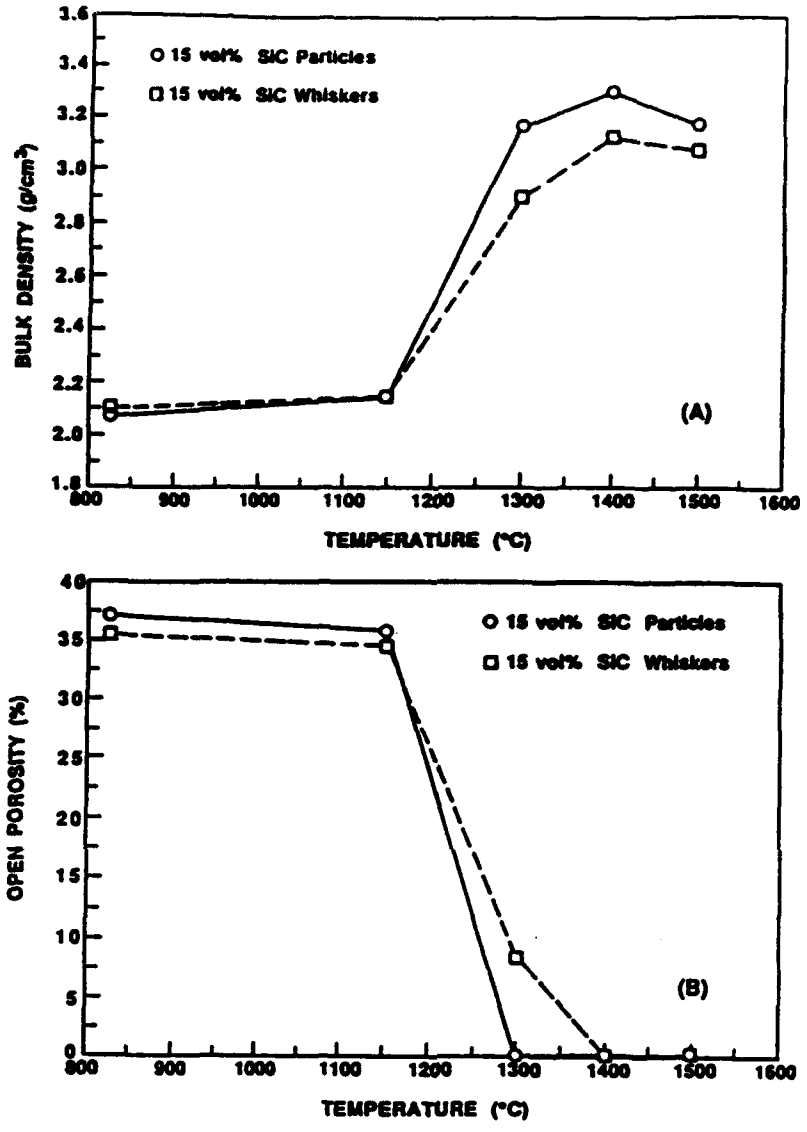

FIG. 8. Plots of (A) bulk density and (B) open porosity vs. sintering temperature for samples with ~15 vol% silicon carbide (either particles or whiskers).

temperature (~1300°C). Once mullitization occurred, densification of samples containing the second-phase inclusions was arrested until considerably higher temperatures were reached.[16] The results in Fig. 8 can also be compared to those reported by Tiegs et al.[17] in which isopressed mullite powder/SiC_w mixtures were densified using a proprietary sintering additive. Despite the formation of a liquid phase, samples with 15 vol% SiC_w still required a sintering temperature of 1800°C in order to achieve ~95% relative density.

SUMMARY AND CONCLUSIONS

Mullite was fabricated by a novel process referred to as *transient viscous sintering (TVS)*. Powder compacts were prepared using composite particles consisting of inner cores of alpha alumina and outer coatings of amorphous silica. These compacts were sintered to almost full density at relatively low temperature (~1300°C) and subsequently heat treated at higher temperature (~1500-1600°C) to form mullite. Samples remained almost fully dense (i.e., almost zero porosity) after mullitization and had a fine, equiaxed grain structure. Densification temperatures for composite powder compacts were only slightly higher than those used in various "sol-gel" processes, despite the considerably larger size of the particles used in the TVS process. This is attributed to the importance of the viscous flow mechanism in densification of the amorphous silica-coated particle compacts and the use of colloidally-processed compacts with homogeneous microstructure, high relative density, and fine pore sizes.

High density mullite/SiC_p composites were fabricated by sintering compacts prepared with a mixture of silica-coated particles, i.e., in which the core materials were alumina and silicon carbide. The sintering temperature for these samples was only slightly higher than that used for samples prepared without SiC_p. By coating the second-phase inclusions with amorphous silica, it was possible to avoid the formation of a rigid (deformation-resistant) percolation network of SiC_p.

Samples prepared by the TVS process required considerably higher temperature for complete mullitization ($\geq$ 1500°C) compared to "sol-gel" processes. (This is due to the coarser scale of mixing of the alumina and silica in the composite particles.) However, this was an advantage in processing of mullite-matrix composites, since the viscous flow mechanism for densification remained operative to considerably higher temperatures. This advantage was particularly evident in the fabrication of mullite/SiC_w composites prepared using silica-coated alumina particles and uncoated whiskers. Although densification was inhibited compared to samples prepared without whiskers, it was still possible to achieve $\geq$96% relative density after sintering at 1500°C. Thus, densification was enhanced considerably compared to studies in which "sol-gel" mullite-precursor powders or mullite powders containing liquid-phase sintering aids were used.

ACKNOWLEDGMENT

Experimental assistance from Y.-J. Lin and M. Springgate are gratefully acknowledged. This work was supported by the Defense Advanced Research Projects Agency (MDA972-88-J-1006); National Science Foundation, Division of Materials Research (DMR-8451916); Florida High Technology and Industry Council; and IBM Corp.

REFERENCES

1. M.D. Sacks, H.-W. Lee, and J.A. Pask, "A Review of Powder Preparation Methods and Densification Procedures for Fabricating High Density Mullite," pp. 167-207 in Mullite and Mullite Matrix Composites, Ceramic Transactions, Vol. 6. Edited by S. Somiya, R.F. Davis, and J.A. Pask. The American Ceramic Society, Inc., Westerville, OH, 1990.

2. See various articles in Mullite and Mullite Matrix Composites, Ceramic Transactions, Vol. 6. Edited by S. Somiya, R.F. Davis, and J.A. Pask. The American Ceramic Society, Inc., Westerville, OH, 1990.

3. S. Komarneni, Y. Suwa, and R. Roy, "Application of Compositionally Diphasic Xerogels for Enhanced Densification: The System Al_2O_3-SiO_2," J. Am. Ceram. Soc., 69 (7) C-155 - C-156 (1986).

4. R. Roy, Y. Suwa, and S. Komarneni, "Nucleation and Epitaxial Growth in Diphasic (Crystalline + Amorphous) Gels"; pp. 247-258 in Science of Ceramic Chemical Processing. Edited by L.L. Hench and D.R. Ulrich. Wiley, New York, 1987.

5. N. Shinohara, D. M. Dabbs, and I. A. Aksay, "Infrared Transparent Mullite Through Densification of Monolithic Gels at 1250°C"; pp. 19-24 in Infrared and Optical Transmitting Materials, SPIE Vol. 683 (1986).

6. B. Sonuparlak, "Sol-Gel Processing of Infrared-Transparent Mullite," Adv. Ceram. Mat., 3 (3) 263 (1988).

7. M.N. Rahaman, L.C. De Jonghe, S. Shinde, and P.H. Tewari, "Sintering and Microstructure of Mullite Aerogels," J. Am. Ceram. Soc., 71 (7) C-338 - C-341 (1988).

8. L.C. De Jonghe, M.N. Rahaman, and C.H. Hsueh, "Transient Stresses in Bimodal Compacts during Sintering," Acta Metall., 34 (7) 1467-1471 (1986).

9. M.N. Rahaman and L.C. De Jonghe, "Effect of Rigid Inclusions on the Sintering of Glass Powder Compacts," J. Am. Ceram. Soc., 70 (12) C-348 - C-351 (1987).

10. R. Zallen. The Physics of Amorphous Solids. Wiley, New York, 1983.

11. M.D. Sacks, N. Bozkurt, and G.W. Scheiffele, "Fabrication of Mullite and Mullite-Matrix Composites by Transient Viscous Sintering of Composite Powders," to be published in J. Am. Ceram. Soc.

12. M.D. Sacks, G.W. Scheiffele, N. Bozkurt, and R. Raghunathan, "Processing of Ceramics and Composites by Viscous Sintering and Transient Viscous Sintering," to be published Ceramic Powder Science IV, Ceramic Transactions. Edited by G.L. Messing, S.-I. Hirano, and H. Hausner. American Ceramic Society, Westerville, OH, 1991.

13. M.D. Sacks, G.W. Scheiffele, N. Bozkurt, R. Raghunathan, A.E. Bagwell, "Processing of Composite Powders: Fabrication of Ceramics and Composites by Viscous Sintering and Transient Viscous Sintering," to be published Ultrastructure Processing of Ceramics, Glasses, Composites, Ordered Polymers, and Advanced Optical Materials. Edited by L.L. Hench and J.K. West. John Wiley & Sons, New York, NY, 1991.

14. H.-W. Lee "Suspension Processing and Pressureless Sintering of Silicon Carbide Whisker-Reinforced Alumina-Matrix Composites," Ph.D. Dissertation, University of Florida, 1990.

15. M.D. Sacks, G.W. Scheiffele, and N. Bozkurt, unpublished research.

16. M.N. Rahaman and D.-Y. Jin, "Sintering of Mullite and Mullite Matrix Composites"; pp. 753-766 in Sintering of Advanced Ceramics, Ceramic Transactions, Vol. 7. Edited by C.A. Handwerker, J.E. Blendell, and W.A. Kaysser. The American Ceramic Society, Inc., Westerville, OH, 1990.

17. T.N. Tiegs, P.F. Becher, and P. Angelini, "Microstructures and Properties of SiC Whisker-Reinforced Mullite Composites"; pp. 463-472 in Mullite and Mullite Matrix Composites, Ceramic Transactions, Vol. 6. Edited by S. Somiya, R.F. Davis, and J.A. Pask. The American Ceramic Society, Inc., Westerville, OH, 1990.

PROCESSING OF SILICATE GLASS/SILICON NITRIDE COMPOSITES WITH CONTROLLED MICROPOROSITY

Michael D. Sacks, Michael S. Randall, Gary W. Scheiffele, Ramesh Raghunathan, and Joseph H. Simmons, Ceramics Division, Department of Materials Science and Engineering, University of Florida, Gainesville, FL 32611

ABSTRACT

Methods for fabricating silicate glass/silicon nitride composites with closed, isolated pores were investigated. Glass/ceramic matrices were developed using green compacts prepared from (1) mixtures of silicate glass and silicon nitride powders and (2) composite particles which consisted of inner cores of silicon nitride and outer coatings of amorphous silica. Significant enhancement in densification rate was demonstrated using the latter compacts. Polymer particles were incorporated into green compacts in order to introduce controlled porosity into samples. By appropriate selection of the heat treatment schedule, it was possible to form sintered bodies with closed, isolated micropores. Preliminary characterization of sintered samples demonstrated the feasibility of producing porous glass/ceramic composites with low dielectric constant (≤ 4.5).

INTRODUCTION

The ideal ceramic material for microelectronics packaging applications would have the following characteristics: (1) excellent electrical properties (high resistivity, low dielectric constant, low loss tangent), (2) high thermal conductivity, (3) coefficient of thermal expansion (CTE) that matches the metallizing and/or chip materials, (4) resistance to corrosion (e.g., due to moisture), (5) adequate mechanical properties (strength, fracture toughness) to prevent failure (e.g., due to CTE mismatch), (6) good surface smoothness (e.g., to allow the use of fine conductive lines), and (7) low sintering temperature (i.e., to allow co-firing with low resistivity interconnect materials such as copper, silver, etc.). It is clear that no single material can provide optimum properties for all of the above requirements. However, the trend toward increasing signal propagation speed and higher circuit density has resulted in numerous investigations[1-6] directed toward the development of glass/ceramic materials* with low dielectric constant

* This includes (1) glass-ceramics prepared by controlled crystallization of a glass and (2) mixtures of glass and crystalline powders which are subsequently densified by sintering.

(typically in the range ~5-8) and co-firing compatibility with low resistivity metals. Despite the successful application of such materials in microelectronics packaging, there is still considerable interest in achieving further reductions in the dielectric constant value. This is generally accomplished by using hybrid ceramic/polymer packaging materials[9] or by introducing porosity (with dielectric constant ≈1) into the ceramic material.[10,11]

The present investigation focuses on the development of silicate glass/silicon nitride composites with controlled microporosity. Although this type of composite has been identified as a potential candidate for low-dielectric-constant packaging applications,[7] investigations of the processing behavior and dielectric properties have not been reported. Silicate glasses were chosen as the composite matrix material in this investigation because of (1) low dielectric constants (~4) and (2) low sintering temperatures. Silicon nitride was selected as the crystalline phase in the composite because of (1) low dielectric constant (~6), (2) good thermal and mechanical properties (e.g., compared to other low-dielectric-constant materials such as cordierite), and (3) availability of high purity powders with fine particle sizes. In order to compensate for the increase in dielectric constant that results from adding silicon nitride to a silicate glass, it is desirable to incorporate controlled microporosity into the composite. The micropores should be closed (i.e., inaccessible from the surface) so that the material will not be susceptible to property degradation due to infiltration of moisture or other contaminants.

PROCESSING APPROACHES

Development of Glass/Ceramic Matrix

Two different approaches were used to form glass/ceramic composites. In one case, a conventional processing method was used in which green compacts were formed from mixtures of glass (silica or borosilicate glass) and ceramic (silicon nitride) powders. A schematic illustration of a green compact formed from a mixture of powders is shown in Fig. 1, left side. A potential problem with this approach is that powder compact densification rates usually decrease when a crystalline ceramic phase is added to a glassy matrix.[12] In particular, studies have shown that densification is severely impeded when the concentration of "non-sinterable" inclusions exceeds that required to establish a connected network (i.e., percolation path).[12] Thus, it may be difficult to fabricate glass/ceramic composites with high concentrations of the ceramic phase.

Another approach to fabricating bulk glass/ceramic composites involves processing of particles which are microcomposites. As illustrated in the right side of Fig. 1, the formation of a connected network of "non-sinterable" ceramic inclusions can be avoided by controlling the spatial distribution of the phases which comprise the composite particles. In this case, the "non-sinterable" ceramic particles are coated with a layer of glass phase, thereby completely isolating them from each other. By maintaining the amorphous phase as an outer coating, compacts can be densified by the viscous flow mechanism. This

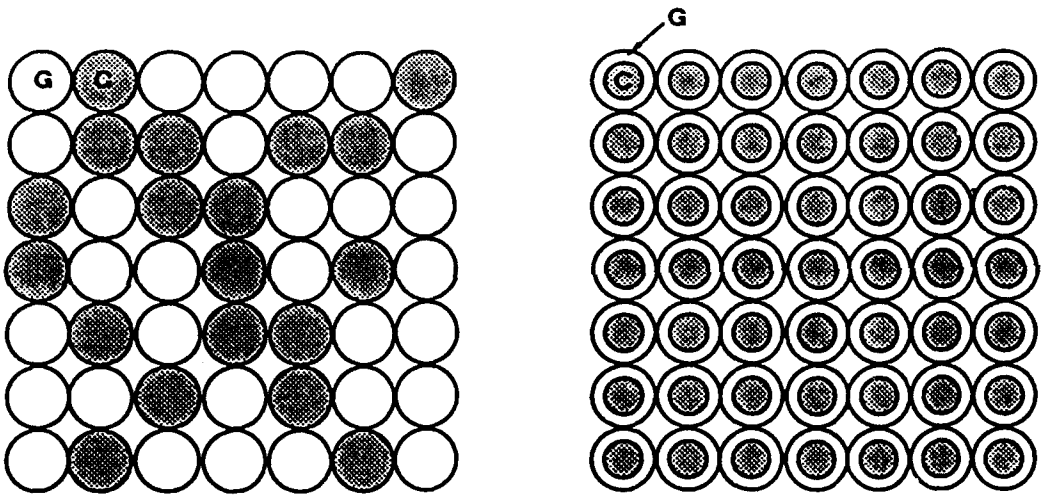

FIG. 1. Schematic illustration of two different types of glass/ceramic powder compacts. Left side: compact is formed from a mixture of glass and ceramic particles. Right side: compact is formed using composite particles which are composed of ceramic cores and outer coatings of glass.

approach would not only facilitate sintering of glass/ceramic composites at relatively low temperatures, but would also allow the development of novel composite microstructures in which a high concentration (i.e., above the percolation threshold) of the crystalline phase could be dispersed in a glassy matrix *as isolated inclusions*.

Introduction of Controlled Porosity

Isolated, closed pores can be incorporated in a glass or glass/ceramic matrix by using green compacts which contain polymer particles larger in size than the glass and/or ceramic particles. Pyrolysis of the polymer particles at relatively low temperatures (i.e., below sintering temperatures) would result in a powder compact with a bimodal distribution of pores, i.e., larger pores created by pyrolysis of the polymer particles and smaller pores associated with the glass or glass/ceramic particle packing arrangement. It is anticipated that the larger pores would undergo relatively little shrinkage if sintering was carried out using a temperature/time schedule just sufficient to shrink and eliminate the fine interparticle pores. However, as densification of the glass or glass/ceramic matrix occurred, the larger pores would begin to close (and become less accessible to infiltration from the surface). Furthermore, if the concentration of these larger pores was below the percolation threshold, they would remain isolated from each other after the matrix had densified.

EXPERIMENTAL PROCEDURES

Processing of Borosilicate Glass/Silicon Nitride Composites

Starting materials were commercially-available silicon nitride[♦] and borosilicate glass[†] powders. The former material was used as-received, but the glass powder was ball milled for 20 h in methanol to reduce the median particle size. Median Stokes' diameters (as determined by X-ray sedimentation[▾]) were ~1.8 and ~1.2 μm for the milled glass and silicon nitride powders, respectively.

Polymer particles were added to some of the suspensions in order to incorporate controlled porosity into glass and glass/ceramic compacts. Two types of polymer particles were used: (1) thin-walled, hollow spheres ("microballoons")[■] which were a vinylidene chloride/acrylonitrile co-polymer (PVDC) and (2) solid, spherical polystyrene (PS) particles which were prepared by a dispersion polymerization method.[13] The synthesized PS particles had an average number diameter of ~4.6 μm, as determined by scanning electron microscopy (SEM) measurements on 1000 particles.

Green compacts were prepared by suspension processing. Ethanol was used as the suspension liquid, except for samples containing PVDC microballoons which were prepared using a methyl isobutyl ketone/ethanol mixture (3:1 volume ratio). Well-dispersed suspensions were prepared using ultrasonication to break down powder agglomerates and an addition of ~1 wt% poly(vinyl pyrrolidone) as a deflocculant.

Disk-shaped samples (~3-6 mm thick, ~28 mm dia.) were slip cast in phenolic rings set upon absorbent plaster blocks. Samples were presintered in air at 550°C and subsequently sintered in air at temperatures in the range 625-820°C.

Processing of Silica/Silicon Nitride Composites

Green compacts having characteristics similar to those schematically depicted in Fig. 1 were prepared using (1) a mixture of silica particles plus silicon nitride particles and (2) silica-coated silicon nitride particles. In the first case, the starting powders were silica (prepared by solution-precipitation using tetraethyl-orthosilicate, TEOS,[‡] as the silica precursor material) and a commercially-available silicon nitride.[▲] The as-received silicon nitride was first fractionated by standard fluid classification techniques in order to remove hard agglomerates. The powders were then mixed in aqueous suspension in a ratio of ~60 vol%

♦ SN-E-03, Ube Industries (America), Inc., New York, NY.

† 7070, Corning Glass, Corning, NY. The composition reported by the manufacturer is 72 wt% SiO_2, 25 wt% B_2O_3, 1 wt% Al_2O_3, 1 wt% K_2O, 0.5 wt% Na_2O, and 0.5 wt% Li_2O.

▾ Sedi-Graph Particle Size Analyzer, Micromeritics Instrument Corp., Norcross, GA.

■ Expancel DE 461/20, Expancel Nobel Industries, Marietta, GA.

‡ Fisher Scientific, Fair Lawn, NJ.

▲ SN-E-10, Ube Industries (America), Inc., New York, NY.

silica/40 vol% silicon nitride. The mixed powder suspension was subjected to ultra-sonication to break down powder agglomerates and pH adjustment (to ~9-10) to achieve electrostatic stabilization. Suspensions were then slip cast, oven-dried (~80°C), pre-sintered at 600°C in air, and subsequently sintered in nitrogen at temperatures in the range 1000-1300°C for 2 h.

The second type of green compact was prepared using composite particles. The fractionated silicon nitride powder was used as a source of core particles and silica was deposited as an outer coating by aqueous precipitation from a TEOS precursor solution. Details of the method have been provided elsewhere.[14] Figure 2 shows typical transmission electron micrographs of composite particles from two different powder batches in which the thickness of the silica coating was varied. The amorphous nature of the silica coating was confirmed by X-ray diffraction measurements which showed that alpha silicon nitride was the only crystalline phase present. In the present study, green compacts were prepared using composite particles with a ratio of ~60 vol% silica/40 vol% silicon nitride. Subsequent processing was carried out in the same manner as described for the particle mixture.

In order to isolate the effect of the spatial distribution of phases on densification behavior, an effort was made to avoid significant differences in particle sizes and particle packing densities of the two types of compacts since these factors also affect sintering kinetics. The composite particles were slightly larger (median Stokes' diameter and specific surface area of ~0.3 μm and ~15 m^2/g, respectively, vs. values of ~0.25 μm and ~19 m^2/g, respectively, for the particle mixture). While this would tend to retard densification slightly, the effect may have been compensated for (at least partially) by the slightly higher packing density for compacts prepared with the composite particles (~61% vs. ~57%).

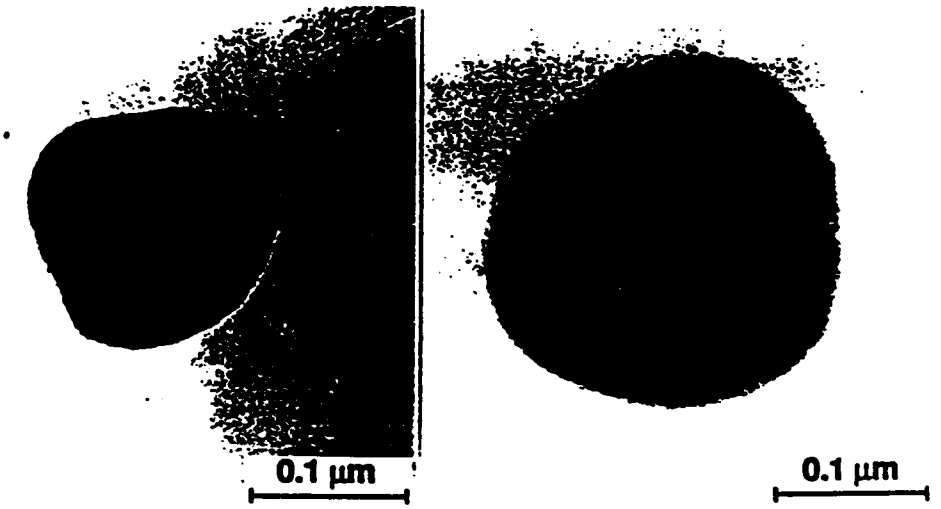

FIG. 2. Transmission electron micrographs of composite particles prepared with different amounts of amorphous silica coating on silicon nitride core particles.

Polystyrene (PS) particles, prepared by dispersion polymerization,[15] were used to demonstrate the feasibility of introducing a controlled pore phase into silica/silicon nitride composites. Composite particles (overall composition of ~60 vol% silica/40 vol% silicon nitride) were mixed in suspension with ~2 μm diameter, spherical PS particles. The volume ratio of composite particles/PS particles was ~90/10. Subsequent processing was carried out as described earlier for samples prepared without PS particles.

Characterization

The bulk density and open porosity of sintered samples were determined by the Archimedes displacement method. Microstructure observations were made on polished and fracture sections using SEM. Measurements of sample dielectric constant were made at 1 MHz using a non-contacting electrode method.[§]

RESULTS AND DISCUSSION

Borosilicate Glass/Silicon Nitride Composites

The initial experiments to develop microstructures with isolated, closed pores were carried out with compacts prepared with borosilicate glass and PVDC microballoons. Figures 3A and 3B show SEM micrographs of polished sections of a sintered sample prepared with ~0.25 wt% of the PVDC. The micrographs demonstrate the feasibility of producing a dispersion of isolated, closed pores in a dense matrix. However, due to the low density of the polymer microballoons (~0.05 g/cm^3), it was difficult to avoid segregation effects during slip casting of the ceramic/polymer suspensions. Thus, bulk compacts often had substantial gradients in pore volume fraction.

Another concern with using the PVDC microballoons was that the pore sizes in the sintered samples were relatively large. To lessen the adverse effects of porosity on the ceramic properties (e.g., strength, surface smoothness, etc.), additional experiments were carried out using the ~4.6 μm PS particles. Figures 3C and 3D show SEM micrographs of fracture surfaces of a sintered sample prepared using an ~90 vol% borosilicate glass/10 vol% PS mixture. The sample was sintered (625°C, 18 h) to ~90% relative density and essentially zero open porosity (<0.2%). The pores are relatively well-dispersed in the glass matrix, although some pore clusters are evident. Similar observations were made on a sample prepared using an ~81 vol% borosilicate glass/9 vol% silicon nitride/10 vol% PS mixture (Figs. 3E and 3F). In this case, the sample was sintered (625°C, 18 h) to ~89% relative density and ~1% open porosity. The amount of residual fine (interparticle) porosity appears to be slightly higher in this sample (Fig. 3F) compared to the borosilicate glass/PS sample shown in Fig. 3D.

---

§ HP 4192A Impedance Analyzer and HP 16451B Dielectric Test Fixture, Hewlett-Packard Co., Palo Alto, CA.

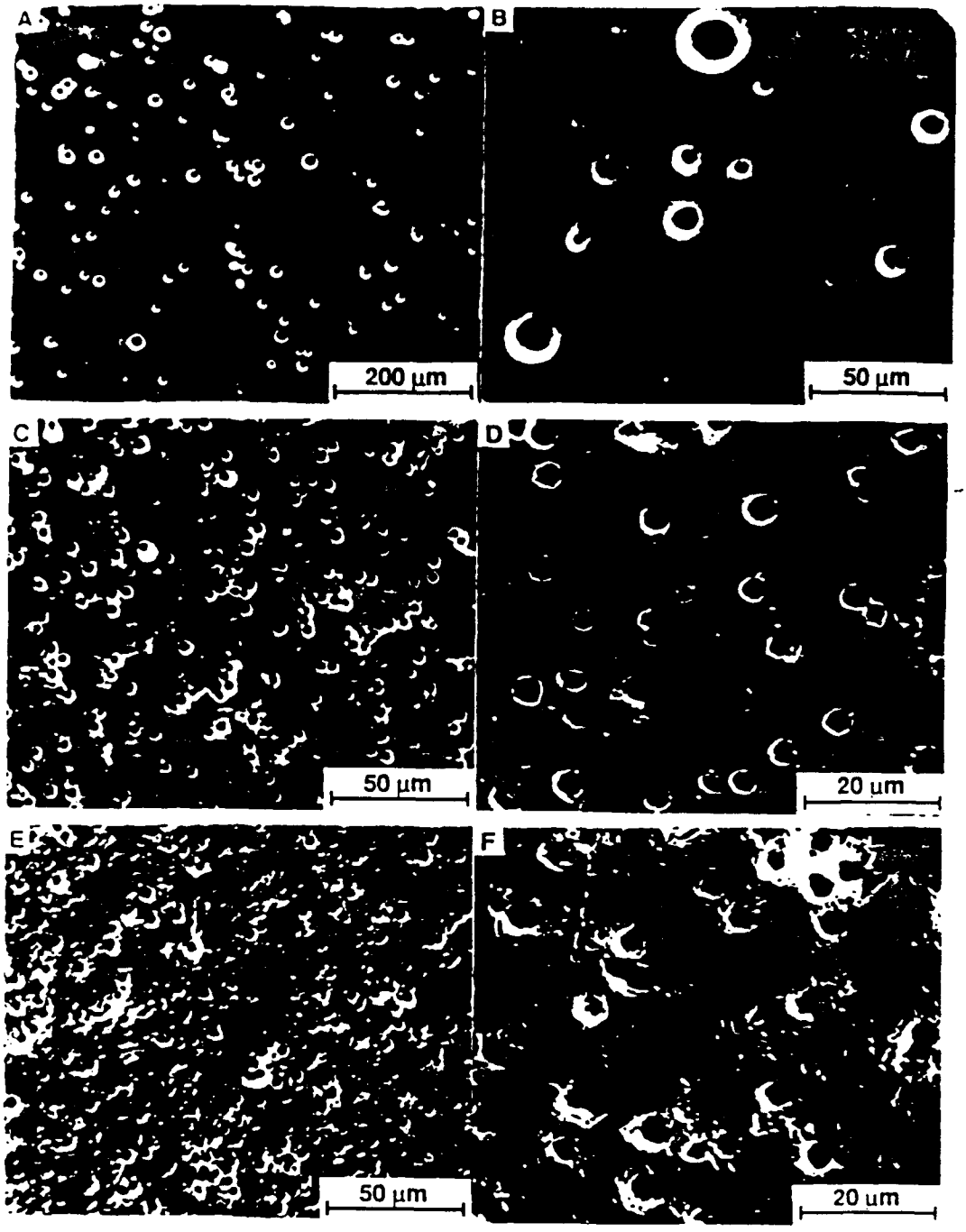

FIG. 3. SEM micrographs of samples containing closed pores. A, B: Polished surface of borosilicate glass sample prepared using PVDC microballoons. C, D: Fracture surface of borosilicate glass sample prepared using PS particles. E, F: Fracture surface of borosilicate glass/Si_3N_4 sample prepared using PS particles.

Figure 4 shows measurements of dielectric constant (at 1 MHz) as a function sintered relative density for samples with various borosilicate glass/silicon nitride ratios. Samples were prepared with 0, ~10, and ~20 vol% PS particle additions. The following observations can be made: (1) As expected, the dielectric constant increases as the relative density increases (i.e., total volume of porosity decreases). There was an approximately linear relation (correlation factors ≈0.98-0.99) between dielectric constant and relative density over the range of densities investigated. (2) As expected, the dielectric constant increases with silicon nitride content in the composite. (3) To a first approximation, the dielectric constant is dependent primarily upon the volume fraction of porosity, but not the type of porosity (i.e., open vs. closed, interparticle vs. polymer-derived). (4) The addition of PS particles allows zero open porosity to be reached at lower relative densities. The solid symbols plotted in Fig. 4 designate data collected on samples in which the open porosity was near zero (i.e., ≤1%). For samples prepared without PS particles, sintered relative densities above ~95% were required in order to achieve ≤1% open porosity. However, two of the borosilicate glass samples prepared with PS additions reached near zero open porosity at considerably lower relative densities, i.e., ~90% and ~87%.* These samples have dielectric constant values of ~3.6 (Fig. 4A). Similarly, an ~80 vol% borosilicate glass/20 vol% silicon nitride sample prepared with PS particles was sintered to ~89% relative density with only ~0.3% open porosity. The dielectric constant for this sample is ~4.3 (Fig. 4B).

Available evidence indicates that it is more difficult to control the pore characteristics of samples having high silicon nitride content because densification of the glass/ceramic matrix is severely inhibited in these samples. The effect of silicon nitride content on isothermal (650°C) sintering behavior is shown in Fig. 5. As observed by other investigators,[12] the densification rate decreases as the concentration of the "non-sinterable" phase increases. Also consistent with previous studies is the observation that densification is not significantly inhibited until the inclusion volume fraction exceeds the concentration required to form a connected network (i.e., percolation path).[12] (For a random mixture of equal-sized spherical particles, the percolation threshold is ~16 vol%.[16]) The maximum relative density achieved in samples with ~40 vol% silicon nitride was only ~92% (Fig. 5). Even with higher sintering temperatures (up to 820°C), it was not possible to achieve a higher relative density.

---

* The two borosilicate samples were prepared using ~10 and ~20 vol% PS additions, respectively. An ~80 vol% glass/20 vol% silicon nitride sample with ~89% relative density and ~0.3% open porosity was prepared using ~20 vol% PS. In the compacts prepared with ~20 vol% PS, the volume fraction of particles was close to (and may have exceeded) the percolation threshold for forming a connected network. A connected pore network (i.e., after pyrolysis) would not be conducive to maximizing the amount of closed porosity in sintered samples. It may be possible to achieve zero open porosity at lower relative density than reported above by using (1) an intermediate concentration of polymer particles (e.g., ~15 vol%) or (2) a broader PS particle size distribution.

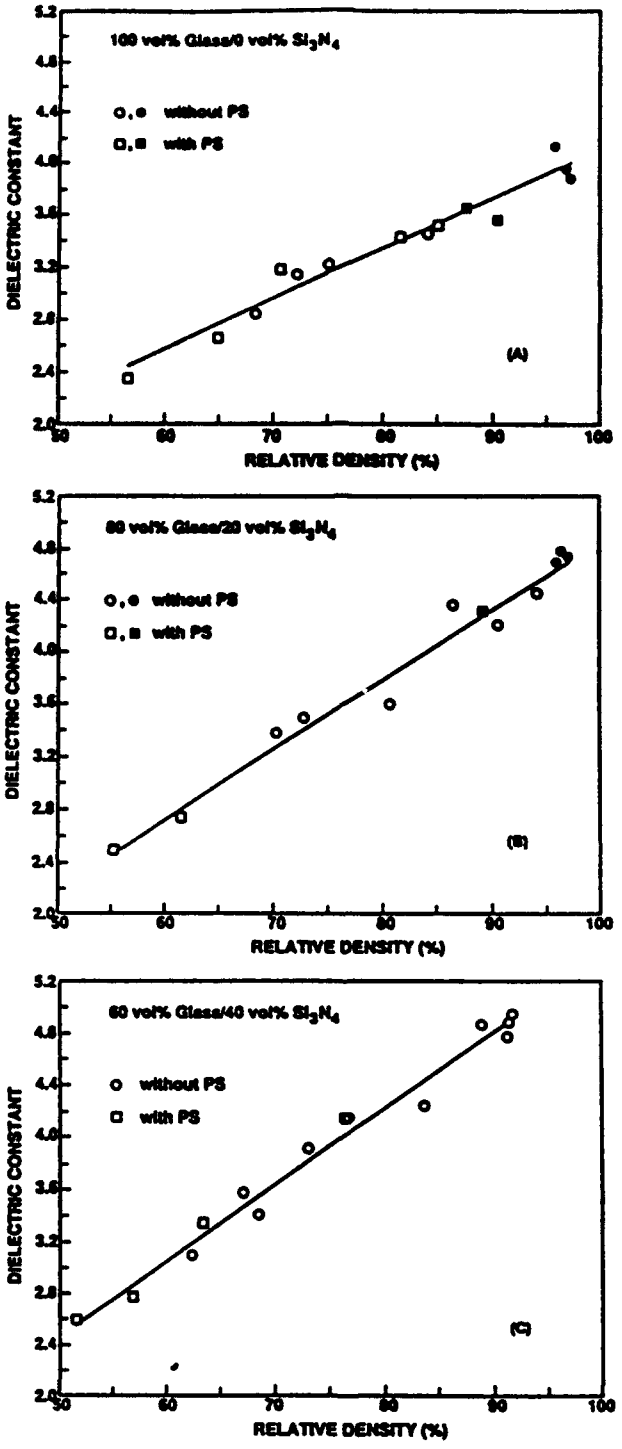

FIG. 4. Plots of ctric constant vs. sintered relative density for samples prepared with various borosilicate glass/silicon nitride ratios.

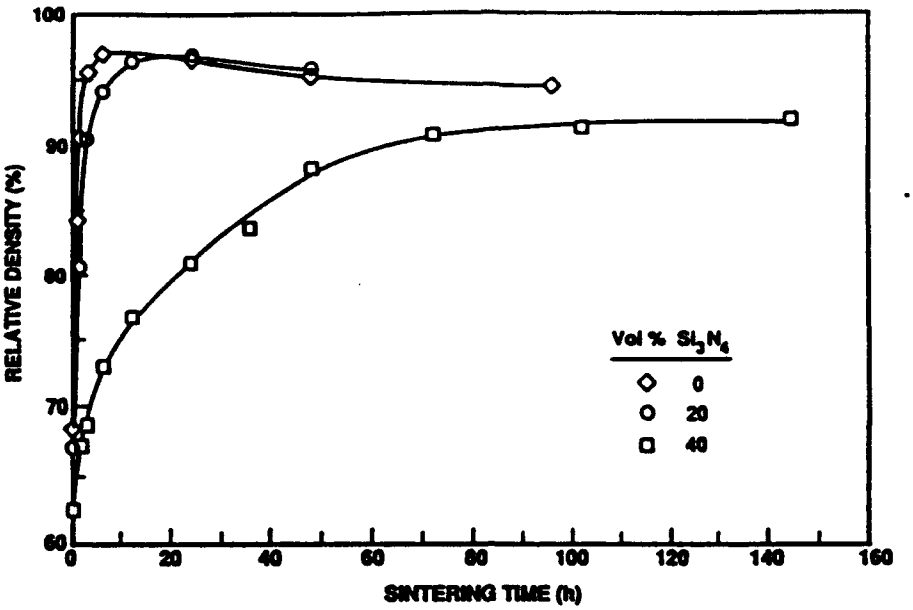

FIG. 5. Plots of relative density vs. sintering time for powder compacts prepared with various borosilicate glass/silicon nitride ratios. The sintering temperature was 650°C.

Silica/Silicon Nitride Composites

Figure 6 shows plots of bulk density and open porosity vs. sintering temperature for green compacts prepared with two different types of powders, i.e., the mixture of silica particles and silicon nitride particles vs. the silica-coated silicon nitride composite particles. The composite powder compact shows an increase in bulk density and decrease in open porosity by 1000°C, while the mixed powder compact shows essentially no changes until the temperature exceeds 1200°C.. The former sample reaches a maximum bulk density of ~2.51 g/cm^3 by 1275°C and the open porosity approaches zero at this temperature. In contrast, the bulk density of the particle mixture compact is only ~1.90 g/cm^3 at 1275°C and the open porosity is ~26%. These results clearly demonstrate that significant enhancement in powder compact densification rate can be achieved by using composite particles with controlled microstructure.

Based on the results in Fig. 6, a composite powder compact prepared with ~10 vol% addition of ~2 μm PS particles was sintered at 1300°C for 2 h in order to densify the silica/silicon nitride matrix. Figure 7 shows SEM micrographs of a polished surface of the sample. The lower magnification SEM micrograph (Fig. 7A) shows that the pores are closed and mostly isolated. The higher magnification micrograph (Fig. 7B) shows that the silica/silicon nitride matrix is almost fully dense (i.e., nearly pore-free) and that the silicon nitride particles are well-dispersed in the siliceous glass phase.

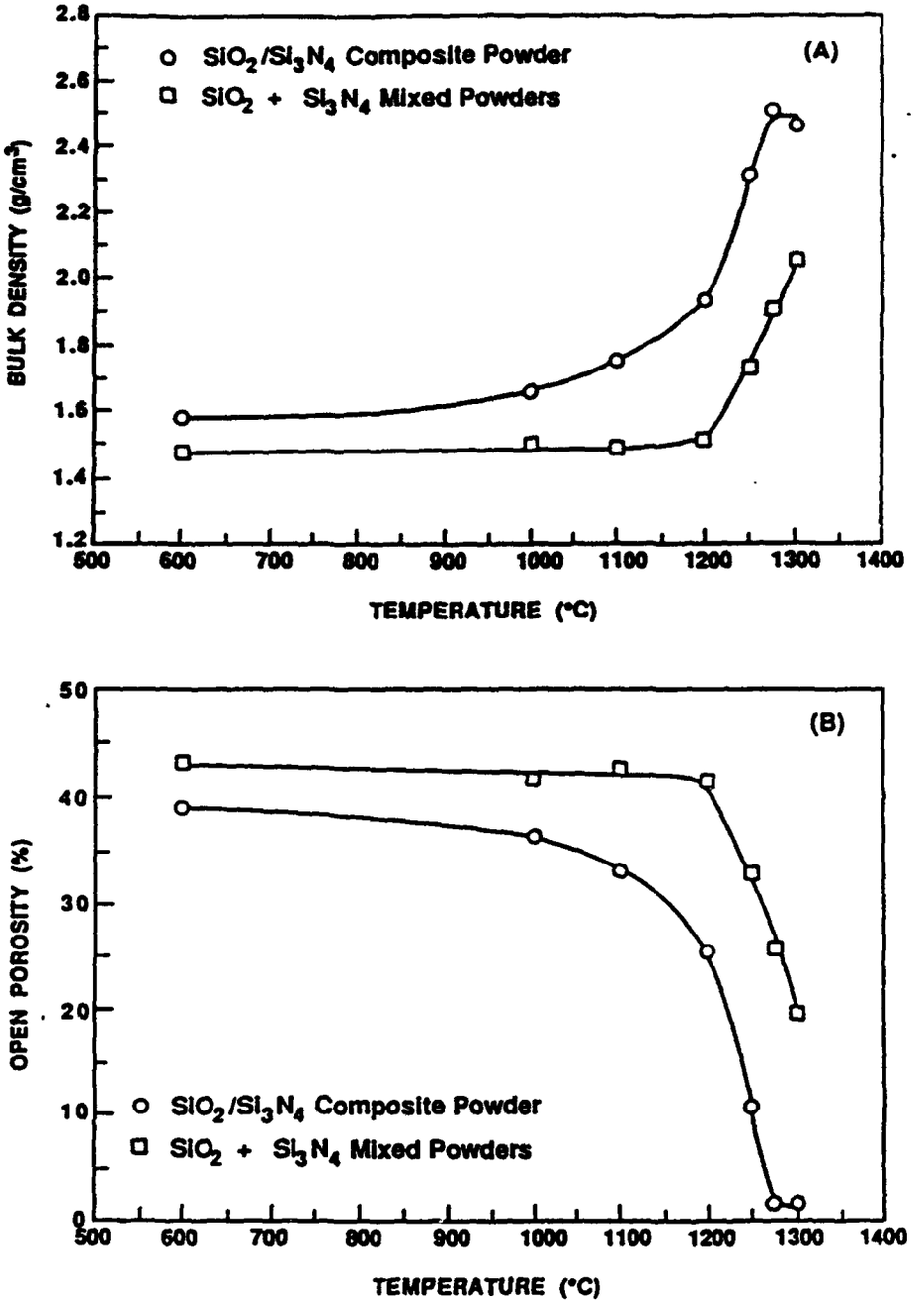

FIG. 6. Plots of (A) bulk density and (B) open porosity vs. sintering temperature for two types of silicon nitride/silica powder compacts. Powder compacts were prepared from (1) a mixture of silica particles and silicon nitride particles and (2) amorphous silica-coated silicon nitride particles.

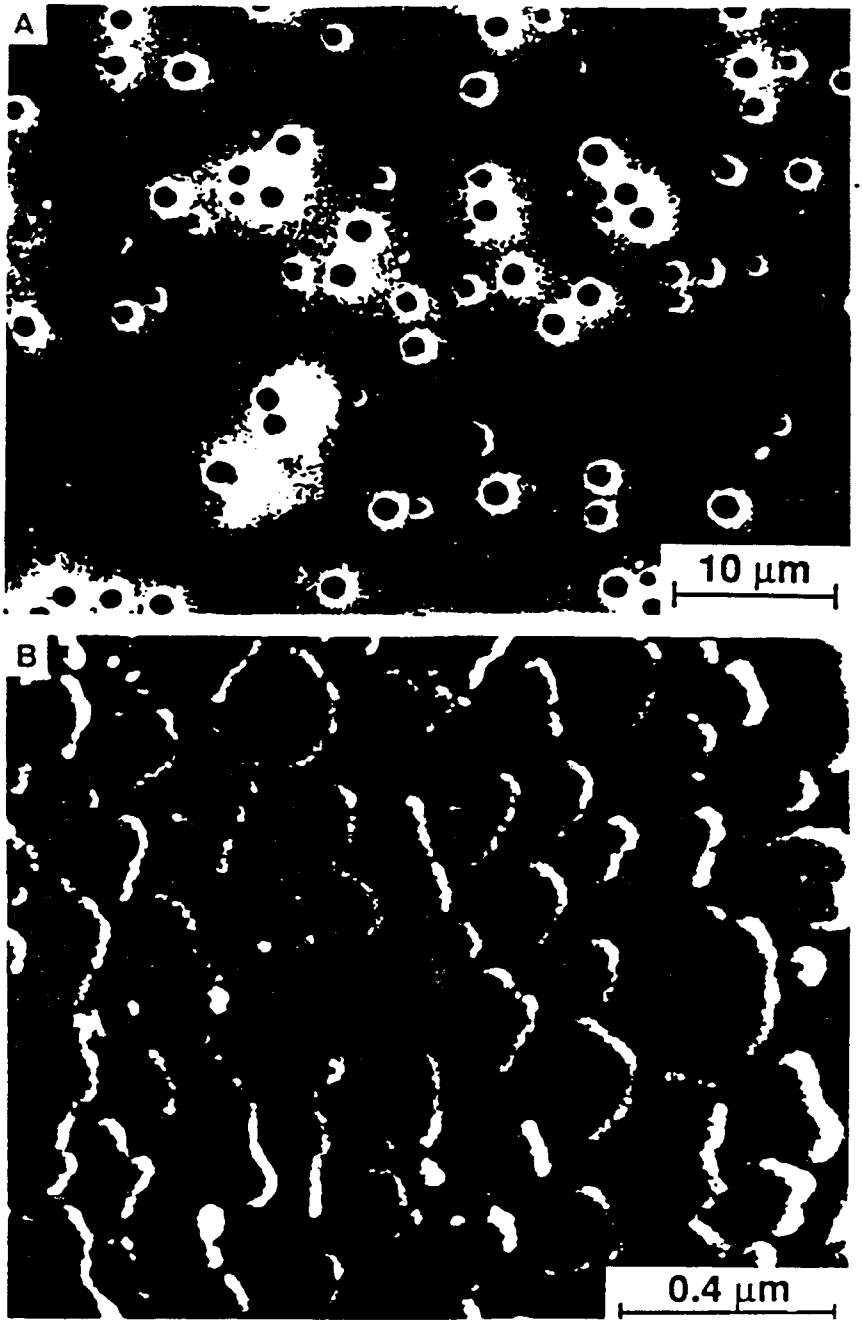

FIG. 7. SEM micrographs of a polished and etched silicon nitride/silica sample which was sintered at 1300°C (2 h). The lower magnification micrograph (A) shows closed, spheroidal pores obtained by incorporating ~10 vol% PS particles in the green compact. The higher magnification micrograph (B) shows the dense matrix in which silicon nitride particles are dispersed in the siliceous glass phase.

SUMMARY AND CONCLUSIONS

Composites with ~100-60 vol% borosilicate glass/0-40 vol% silicon nitride were fabricated by conventional processing of powder mixtures. The feasibility of using polymer particles to develop isolated, closed pores in a dense borosilicate glass or borosilicate glass/silicon nitride matrix was demonstrated. With this approach, it was possible to produce samples with near zero open porosity despite relative densities as low as ~87%. Borosilicate glass and ~80 vol% borosilicate glass/20 vol% silicon nitride samples with these characteristics had dielectric constants of ~3.6 and ~4.3, respectively. For samples with ~40 vol% silicon nitride, densification of the glass/ceramic matrix was severely inhibited and it was not possible to completely close interparticle pore channels. With improved processing (e.g., removal of powder aggregates, higher green densities, etc.), it may be possible to produce hermetic 60 vol% silicate glass/40 vol% silicon nitride composites with dielectric constant ≈4.5.

A novel process was developed in which glass/ceramic composites were fabricated using composite particles consisting of an inner core of silicon nitride and an outer coating of amorphous silica. Enhanced densification was demonstrated by directly comparing the sintering behavior for compacts prepared with the silica-coated silicon nitride particles vs. a mixture of silica particles and silicon nitride particles. The increased densification rate for the samples prepared with composite particles can be attributed to (1) viscous flow of the amorphous coating and (2) avoiding the formation of a percolation network of the "non-sinterable" phase. Composite powder compacts were also prepared with the addition of ~10 vol% polystyrene particles. By appropriate choice of sintering schedule, it was possible to produce a microstructure in which isolated, closed pores were dispersed in a dense silica/silicon nitride matrix.

Although the present study has demonstrated the feasibility of processing porous silicate glass/silicon nitride composites with low dielectric constant, a great deal of additional research is needed to determine if these composites would be useful in microelectronics applications. In particular, characterization of other composite properties (e.g., electrical resistivity, strength, thermal expansion coefficient, thermal conductivity, surface roughness, etc.) is needed. In the case of silica/silicon nitride composites, it is also desirable to lower the sintering temperatures to allow co-firing with low resistivity metals (e.g., copper, silver) Despite the fine size of the composite particles, these samples require relatively high sintering temperatures (~1300°C) due to the high viscosity of silica. Thus, it would be desirable to synthesize composite particles having a multicomponent silicate (e.g., borosilicate) coating that would flow viscously at lower temperature.

ACKNOWLEDGMENT

Experimental assistance from C.S. Khadilkar, Y.-J. Lin, and N. Bozkurt is gratefully acknowledged. This work was supported by the Defense Advanced Research Projects Agency (MDA972-88-J-1006); National Science Foundation, Division of Materials Research (DMR-8451916); Florida High Technology and Industry Council; and IBM Corp.

REFERENCES

1. A.H. Kumar, P.W. McMillan, and R.R. Tummala, "Glass-Ceramic Stuctures and Sintered Multilayer Substrates Thereof with Circuit Patterns of Gold, Silver, and Copper," U.S. Pat. No. 4 301 324, 1981.
2. N. Kamehana, K. Niwa, and K. Murakawa, "Packaging Material for High Speed Computers"; pp. 388-392 in IEEE 33rd Electronics Components Conference Proceedings, IEEE, Washington, DC, 1983.
3. Y. Shimada, K. Utsumi, M. Suzuki, H. Takamizawa, M. Nitta, and T. Witari, "Low Firing Temperature Multilayer Glass-Ceramic Substrate," IEEE Trans. Components, Hybrids, Manuf. Technol., 6 [4] 382-388 (1983).
4. S. Nishigaki, S. Yano, J. Fukuta, M. Fukuya, and T. Fuwa, "A New Multilayered, Low-Temperature-Fireable Ceramic Substrate, pp. 225-234 in Proceedings of the 1986 International Symposium on Microelectronics, ISHM, Reston, VA, 1985.
5. K. Kondo, M. Okuyama, and Y. Shibata, "Low Firing Temperature Ceramic Materials for Multilayer Ceramic Substrates"; pp. 77-87 in Advances in Ceramics, Vol. 19. Edited by J.B. Blum and W.R. Cannon. American Ceramic Society, Westerville, OH, 1986.
6. K. Kawakami, M. Takabatake, T. Minowa, J. Chiba, and M. Sasaki, "A Low-Temperature Cofired Multilayer Ceramic Substrate"; ibid., pp. 95-102.
7. R.R. Tummala, "Ceramics in Microelectronic Packaging," Am. Ceram. Soc. Bull., 67 [4] 752-758 (1988).
8. Y. Shimada, Y. Yamashita, Y. Shiozawa, M. Suzuki, and H. Takamizawa, "Low Dielectric Constant Multilayer Glass-Ceramic Substrate with Ag-Pd Wiring for VLSI Package"; pp. 398-405 in IEEE 37th Electronics Components Conference Proceedings, IEEE, Washington, DC, 1987.
9. Y. Iwata and S. Saito, "New Ceramic and Plastic Composite Substrate for Face Down Bonding and Large Size Silicon Chip Mounting"; ibid., pp. 392-397.
10. D.W. Kellerman, "The Development and Characterization of a Low Dielectric Constant Thick Film Material"; ibid., pp. 316-327.
11. W.A. Yarbrough, T.R. Gururaja, and L.E. Cross, "Materials for IC Packaging with Very Low Permittivity via Colloidal Sol-Gel Processing," Am. Ceram. Soc. Bull., 66 [4] 692-698 (1987).
12. M.N. Rahaman and L.C. De Jonghe, "Effect of Rigid Inclusions on the Sintering of Glass Powder Compacts," J. Am. Ceram. Soc., 70 (12) C-348 - C-351 (1987).
13. K.P. Lok and C.K. Ober, "Particle Size Control in Dispersion Polymerization of Polystyrene," Can. J. Chem., 63 209-216 (1985).
14. M.D. Sacks, G.W. Scheiffele, N. Bozkurt, and R. Raghunathan, "Processing of Ceramics and Composites by Viscous Sintering and Transient Viscous Sintering," to be published Ceramic Powder Science IV, Ceramic Transactions. Edited by G.L. Messing, S.-I. Hirano, and H. Hausner. American Ceramic Society, Westerville, OH, 1991.
15. Y.Y. Lu, M.S. El-Aasser, and J.W. Vanderhoff, "Dispersion Polymerization of Styrene in Ethanol: Monomer Partitioning Behavior and Locus of Polymerization," J. Polymer Sci., Part B: Polymer Physics, 26 1187-1203 (1988).
16. R. Zallen. The Physics of Amorphous Solids. Wiley, New York, 1983.

Processing of Improved Siliconized Silicon Carbide by Liquid Infiltation Methods

I. Infiltration with Ceramic Precursor

Characterization of Ceramic Precursor

The vinyl silazane ceramic precursor used in this study has low molecular weight, low viscosity and readily wets SiC preforms. Therefore, it is an excellent material for achieving rapid infiltration into porous preforms. Figure 1 shows plots of shear stress vs. shear rate and viscosity vs. shear rate for the vinyl silazane. The plots show that the flow behavior is Newtonian and viscosity is low (about 2.1 mPa s at 20°C).

Based on the chemical composition of the vinyl silazane precursor, a mixture of SiC and Si_3N_4 materials is expected to form after pyrolysis at high temperatures. Table 1 shows the elemental analysis results for samples heat treated at temperatures up to 1500°C [Tor90]. Obviously, the major elements present after pyrolysis are Si, C, and N. XRD analysis of samples heated at 650°C, 900°C, 1100°C showed no evidence of crystallinity. For the sample fired at 1500°C, XRD and TEM analysis showed that weakly crystalline α-Si_3N_4 was formed, but a significant amount of amorphous material was still present. As expected, the helium gas pycnometric density values for the amorphous samples (Table 1) were considerably lower than values reported for crystalline Si_3N_4 (3.19 g/cm^3) or SiC (3.21 g/cm^3). Table 1 shows that the density increases with increasing temperature as the polymer converts to a ceramic. In addition, the BET specific surface area decreases significantly with increasing temperature. This suggests that small, open pores which develop during the early stages of pyrolysis (i.e., when volatile species are evolving from the polymer) are eliminated (e.g., by shrinkage/densification) at the higher pyrolysis temperatures.

Table 1 Elemental Analysis, Pycnometry Density and BET Specific Surface Area of Pyrolyzed Polyvinylsilazane [Tor90]

Pyrolysis Temp.(°C)	C(wt%)	H(wt%)	N(wt%)	Si(wt%)	Density (g/cm^3)	BET Surface Area(m^2/g)
650	14.8	3.0	8.2	38.1	1.65	13.3
900	21.5	1.2	18.7	47.6	1.88	0.2
1100	26.3	<0.5	23.0	48.0	2.13	0.2
1500	23.2	<0.5	21.8	48.4		

Since the siliconization process is often carried out at temperatures above 1500°C, it is necessary to characterize the pyrolysis behavior and phase transformation of the ceramic precursor at higher temperatures than reported by Toreki et al. Therefore, the pre-ceramic polymer was characterized by TGA by heating at 10°C/min to 1575°C, followed by a 2 hour hold, in both nitrogen and argon atmospheres (Figure 2). As observed previously by Toreki et al., the vinyl silazane polymer undergoes most of its weight loss by ~800°C. Above this temperature, very little weight loss occurs until the 2 hour hold at 1575°C.

The weight loss at 1575°C was initially puzzling since both Si_3N_4 and SiC are stable in inert atmospheres to considerably higher temperatures. Inspection of the elemental composition in Table 1 indicates that a large amount of free carbon is probably present in the samples after the low temperature ($\leq$1500°C) decomposition reactions. Free carbon contents can be calculated for two

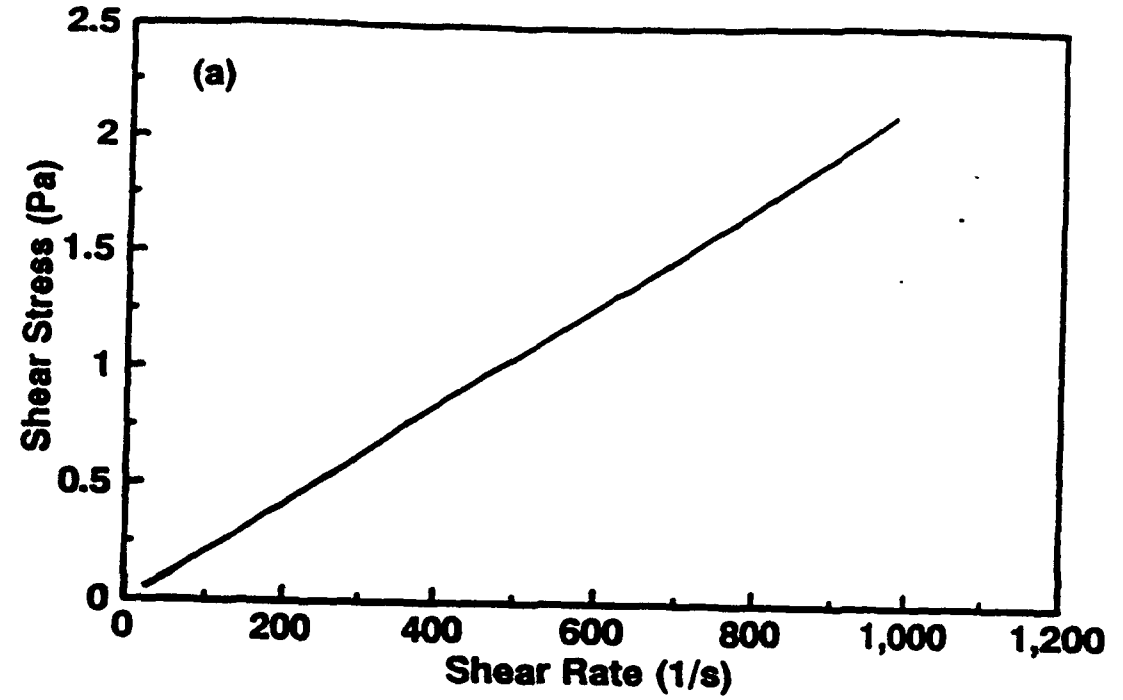

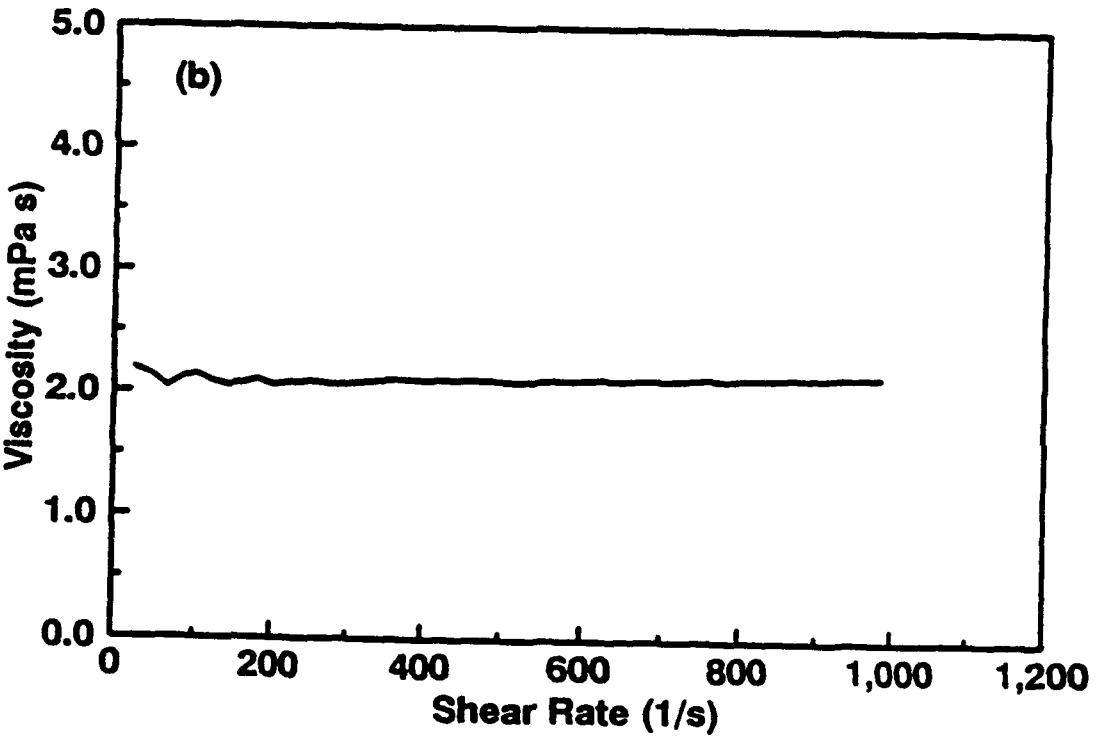

Figure 1 Plots for Vinyl Silazane (a) Shear Stress vs. Shear Rate (b) Viscosity vs. Shear Rate

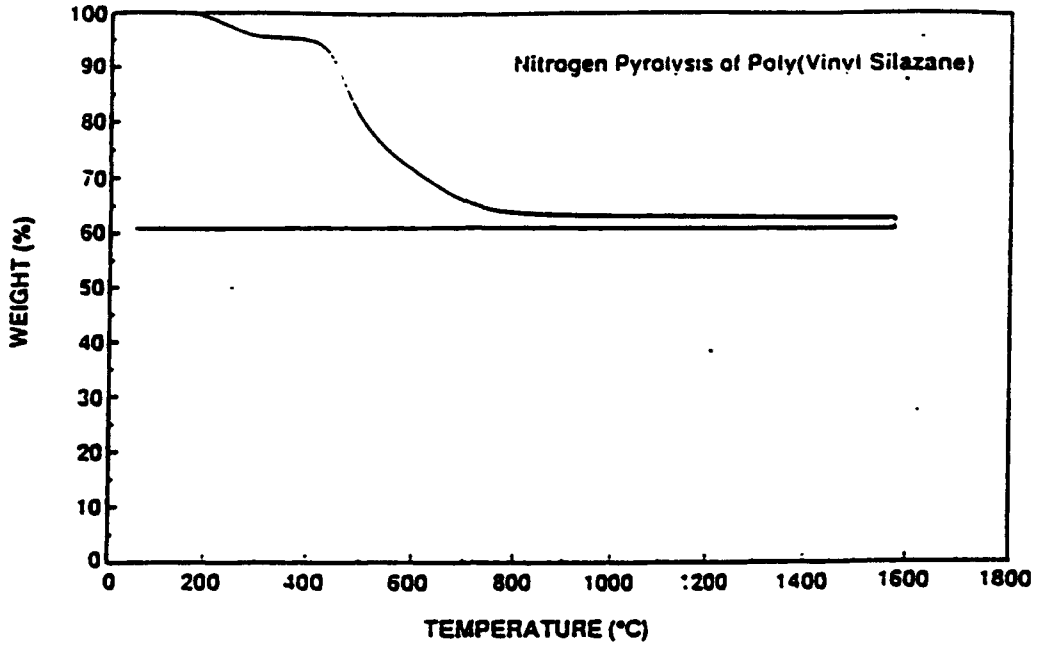

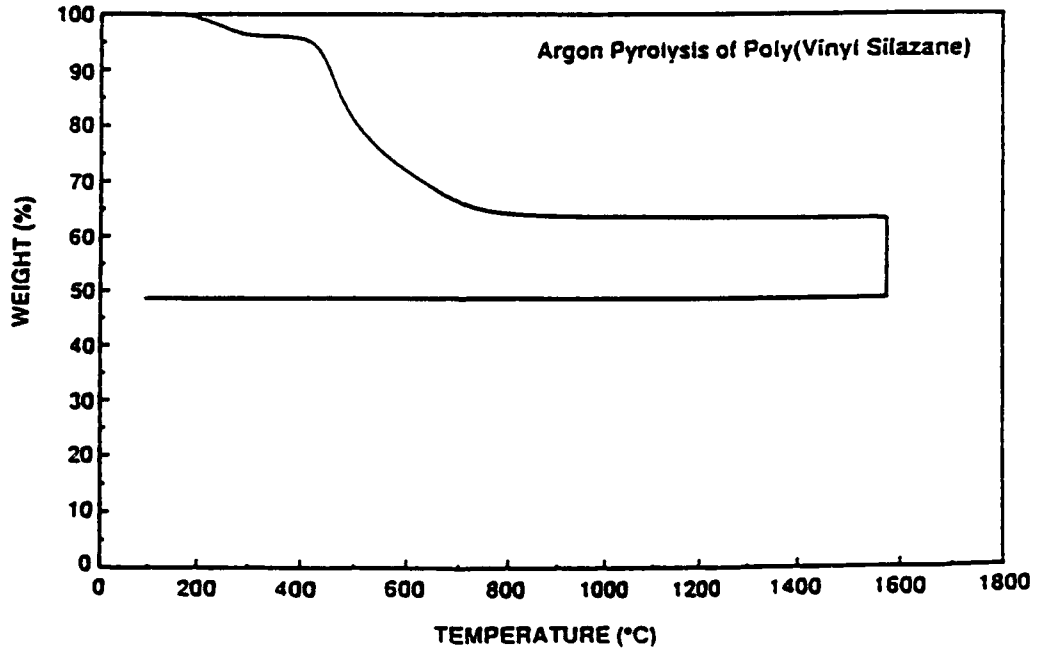

Figure 2 TGA Data for Polyvinyl Silazane Heated in (a) Nitrogen and (b) Argon. Samples were held for 2 h at 1575°C.

extreme cases. First, assume that every silicon atom bonds with one carbon atom to form SiC (i.e., no nitrogen atoms react with silicon). The free carbon content is then given by the equation:

$$\text{Free Carbon \%} = C(wt\%) - [Si(wt\%)\, W_C/W_{Si}] \quad (1)$$

where

C(wt%) = weight percentage of carbon in the sample
Si(wt%) = weight percentage of silicon in the sample
W_C = atomic weight of carbon
W_{Si} = atomic weight of silicon

Using this equation, the free carbon contents are calculated to be 5.7% and 2.5% for samples fired at 1100°C and 1500°C, respectively. In the second case, assume that the reaction of carbon with silicon occurs only after every four nitrogen atoms bond with three silicon atoms to form Si_3N_4. The free carbon content can then be calculated by the equation:

$$\text{Free Carbon \%} = C(wt\%) - \{[Si(wt\%) - R_{Si}]\, W_C/W_{Si}\} \quad (2)$$

where R_{Si} is weight percentage of silicon which binds with nitrogen. R_{Si} can be calculated from the following equation:

$$R_{Si} = N(wt\%)\, 3W_{Si}/4W_N \quad (3)$$

where N(wt%) is the weight percentage of nitrogen in the sample, and W_N is the atomic weight of nitrogen. From equation 2 and 3, the free carbon contents are calculated to be 20.6% and 16.5% for samples fired at 1100°C and 1500°C, respectively. These two sets of calculations give upper and lower limits for the free carbon content. In the actual samples, it is likely that the free carbon contents lie somewhere in between the extreme values.

Based on the above considerations, it is proposed that at 1575°C the following reaction occurs:

$$Si_3N_4 + 3C = 3SiC + 2N_2 \quad (4)$$

This hypothesis is supported by thermodynamic calculations which indicate the change in Gibbs free energy for this reaction at 1575°C is negative at standard conditions. Thus, the free carbon promotes decomposition of Si_3N_4 at higher temperatures. Figure 3 shows the change in standard Gibbs free energy ($\Delta G°$) vs. temperature (T) curves for reaction 4, as well as the reaction for direct decomposition of Si_3N_4:

$$Si_3N_4 = 3Si + 2N_2 \quad (5)$$

The thermodynamic data were obtained from the JANAF Thermochemical Tables [Cha85]. It is clear from Figure 3 that thermodynamics favors reaction 4 over the temperature range from about 1430°C (1703 K) to 1880°C (2150 K).

Reaction 4 is supported by XRD analysis on samples pyrolyzed at 1650°C (1 hour hold) in nitrogen and argon (Figure 4). Only SiC phases (primarily β-SiC and a small amount of α-SiC) were detected in both samples. The larger weight loss during TGA analysis in argon (Figure 2(b)) (i.e., compared to the TGA result in nitrogen) is also consistent with the decomposition reaction 4. In addition, both samples heated to 1650°C (in argon and nitrogen) showed the same residual weight of ~49%. (This was also the approximate residual weight for the sample heated in argon for 2 hours at 1575°C, Figure 2(b).) This residual weight value is very close to the calculated value (48 wt%) if the vinyl silazane decomposed to pure SiC. The theoretical calculation assumes that all nitrogen and hydrogen atoms are eliminated, all silicon atoms are retained, and the amount of carbon atoms

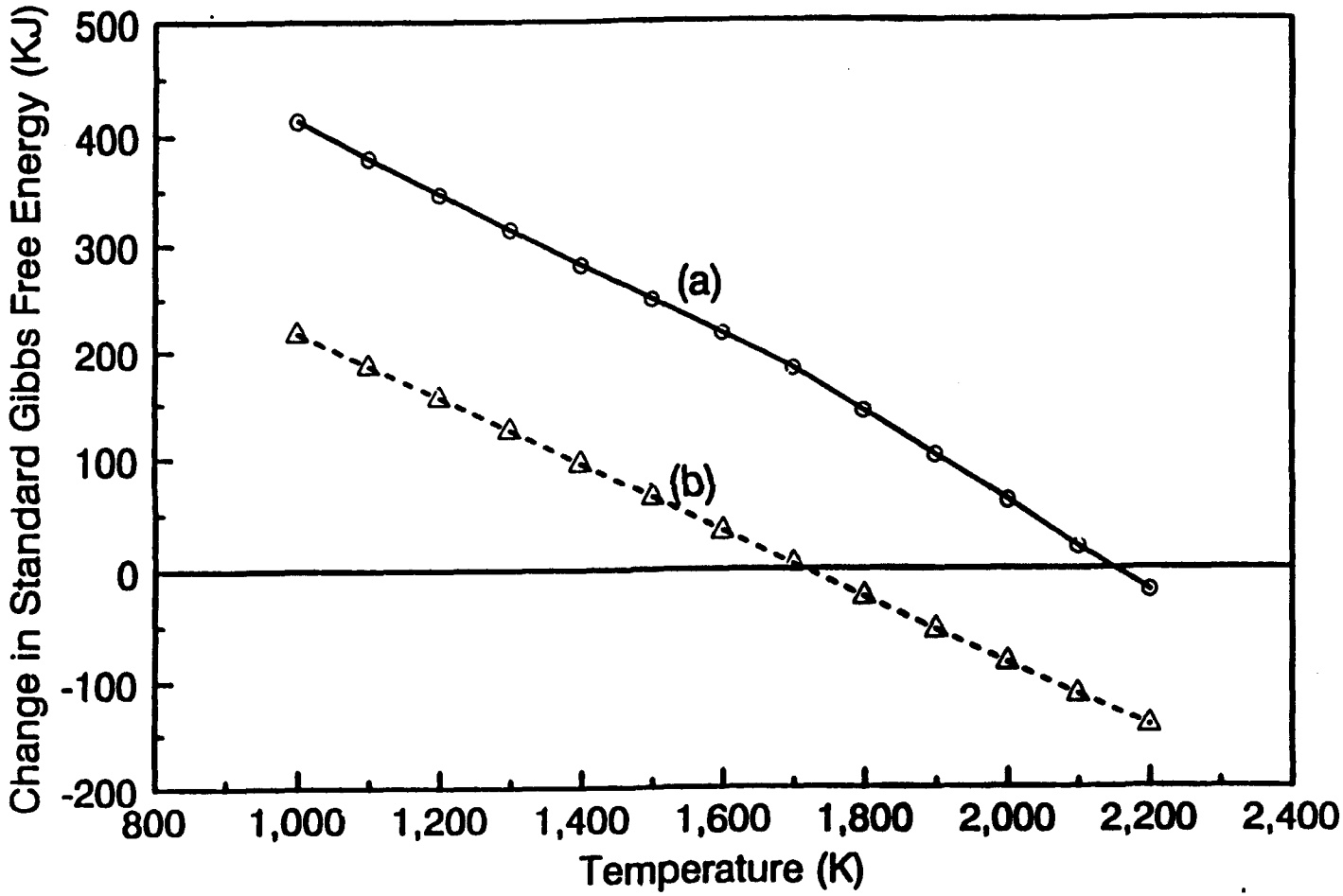

Figure 3 Plots of Change in Standard Gibbs Free Energy vs. Temperature for Reactions (a) $Si_3N_4 = 3Si + 2N_2$ and (b) $Si_3N_4 + 3C = 3SiC + 2N_2$

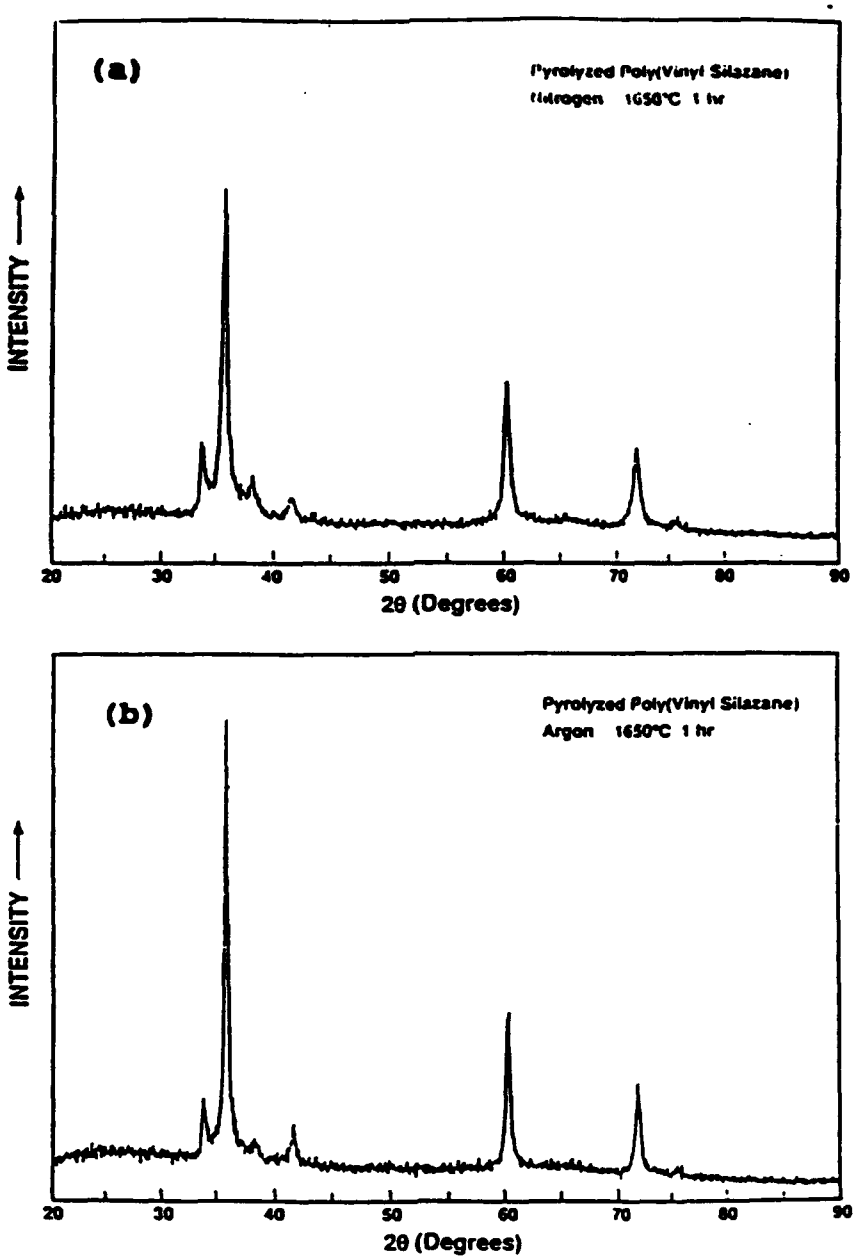

Figure 4 XRD Results for Samples of Polyvinyl Silazane after Pyrolysis at 1650°C for 1 hr in (a) Nitrogen and (b) Argon

retained equals to the number of silicon atoms. This calculation was made using the following equation:

$$SiC_{wt\%} = (N_{Si}W_{Si} + N_{Si}W_C)/(N_{Si}W_{Si} + N_C W_C + N_N W_N + N_H W_H) \quad (6)$$

where

N_{Si} = number of silicon atoms
W_{Si} = atomic weight of silicon
N_C = number of carbon atoms
W_C = atomic weight of carbon
N_N = number of nitrogen atoms
W_N = atomic weight of nitrogen
N_H = number of hydrogen atoms
W_H = atomic weight of hydrogen

Thus, it appears that complete decomposition of the vinyl silazane to nearly stoichiometric SiC can be accomplished either by heat treatment in argon (or other inert atmosphere except nitrogen) for 2 hours at 1575°C or by heat treatment in nitrogen (or other inert atmosphere) for 1 hour at 1650°C. Since using nitrogen during siliconization will allow the silicon to react to form Si_3N_4, the atmosphere for siliconization process is usually argon or vacuum. Therefore, the effective yield for the vinyl silazane is about 48-49 wt%.

Infiltration and Pyrolysis of the Ceramic Precursor

Two processing variables--number of infiltrations and pyrolysis temperature--were investigated in order to obtain maximum ceramic yield after pyrolysis and subsequent siliconization.

Tables 2, 3, and 4 show density and porosity results obtained by Archimedes immersion measurement for various samples with different number of infiltrations and pyrolysis temperatures (i.e., 1100, 1400, and 1575°C, respectively). The average values of open porosity, bulk density, and apparent density for these samples vs. number of infiltrations are plotted in Figures 5, 6, and 7, respectively.

Figure 5 shows that the bulk density increases, while the apparent density and open porosity decrease with increasing number of infiltration and pyrolysis (at 1100°C) cycles. It is clear that the bulk density increases and the open porosity decreases because the pore channels in the original porous sintered SiC preform have been filled with new ceramic material. There are two reasons for the decrease in the apparent density: (1) the true density of the 1100°C-pyrolyzed ceramic is lower than that of the SiC preform (~ 3.20 g/cm^3) and (2) closed porosity (i.e., porosity that is inaccessible to penetration of water during the Archimedes density measurement) develops after the infiltration/pyrolysis process.

Figure 6 shows the same trends as observed in Figure 5. However, the bulk density increases more slowly, while apparent density and open porosity decrease more slowly during the infiltration/pyrolysis process. There are several possible reasons for this behavior:

1. Greater volumetric shrinkage of the ceramic precursor is expected when the pyrolysis temperature is increased to 1400°C. The greater amount of shrinkage during pyrolysis results, at least in part, from the increase in true density of the material, i.e., conversion to higher-density crystalline SiC and Si_3N_4 begins to occur at pyrolysis temperatures above 1100°C. It is also possible that some additional weight loss may occur after repeated pyrolysis at 1400°C and this would also result in additional volumetric shrinkage. In any case, the smaller amount of ceramic volume incorporated in the SiC preform during the infiltration/pyrolysis process leads to lower bulk density values and more residual open pore volume. Furthermore, the incorporation of less new ceramic (but with higher true density) is consistent with smaller decrease in apparent density during the infiltration/pyrolysis process.

Table 2 **Properties Determined by the Archimedes Immersion Method for Samples Infiltrated with Ceramic Precursor and Pyrolyzed at 1100°C**

Sample	A	Q	C	B	G3	G4
Uninfiltrated						
% Open Porosity	34.1	34.0	33.7	33.7	36.4	36.3
Bulk Density	2.11	2.11	2.12	2.12	2.03	2.03
Apparent Density	3.20	3.19	3.20	3.20	3.19	3.19
1st Infiltration						
% Open Porosity	24.8	24.6	24.6	24.4	25.6	25.4
Bulk Density	2.29	2.30	2.31	2.30	2.24	2.25
Apparent Density	3.04	3.05	3.06	3.04	3.02	3.01
Cumul. Wt. Gain%	8.5	9.0	9.0	8.5	10.3	10.8
2nd Infiltration						
% Open Porosity		17.6	17.6	17.5	18.6	19.6
Bulk Density		2.45	2.45	2.44	2.39	2.37
Apparent Density		2.97	2.97	2.96	2.94	2.95
Cumul. Wt. Gain%		16.1	15.6	15.1	17.7	16.7
3rd Infiltration						
% Open Porosity			12.5	12.0	13.2	13.4
Bulk Density			2.55	2.58	2.50	2.49
Apparent Density			2.91	2.93	2.88	2.88
Cumul. Wt. Gain%			20.3	21.7	23.2	22.7
4th Infiltration						
% Open Porosity				4.1		
Bulk Density				2.63		
Apparent Density				2.74		
Cumul. Wt. Gain%				24.1		

Table 3 Properties Determined by the Archimedes Immersion Method for Samples Infiltrated with Ceramic Precursor and Pyrolyzed at 1400°C

Sample	G1	G2
Uninfiltrated		
% Open Porosity	36.5	36.3
Bulk Density	2.03	2.03
Apparent Density	3.19	3.19
1st Infiltration		
% Open Porosity	27.6	27.1
Bulk Density	2.23	2.24
Apparent Density	3.07	3.07
Cumul. Wt. Gain%	9.9	10.3
2nd Infiltration		
% Open Porosity	23.3	21.6
Bulk Density	2.32	2.36
Apparent Density	3.02	3.01
Cumul. Wt. Gain%	14.3	16.3
3rd Infiltration		
% Open Porosity	20.1	15.9
Bulk Density	2.38	2.45
Apparent Density	2.98	2.91
Cumul. Wt. Gain%	17.2	20.7

Table 4 Properties Determined by the Archimedes Immersion Method for Samples Infiltrated with Ceramic Precursor and Pyrolyzed at 1575°C

Sample	S	R	T	U
Uninfiltrated				
% Open Porosity	33.9	33.8	34.1	33.9
Bulk Density	2.11	2.11	2.11	2.11
Apparent Density	3.20	3.19	3.20	3.19
1st Infiltration				
% Open Porosity	28.0	28.4	28.4	28.3
Bulk Density	2.28	2.27	2.26	2.27
Apparent Density	3.16	3.17	3.16	3.17
Cumul. Wt. Gain%	8.1	7.6	7.1	7.6
2nd Infiltration				
% Open Porosity		26.2	26.3	25.9
Bulk Density		2.33	2.33	2.33
Apparent Density		3.16	3.16	3.15
Cumul. Wt. Gain%		10.4	10.4	10.4
3rd Infiltration				
% Open Porosity			24.2	24.0
Bulk Density			2.40	2.40
Apparent Density			3.16	3.16
Cumul. Wt. Gain%			13.7	13.7
4th Infiltration				
% Open Porosity				22.0
Bulk Density				2.44
Apparent Density				3.14
Cumul. Wt. Gain%				15.6

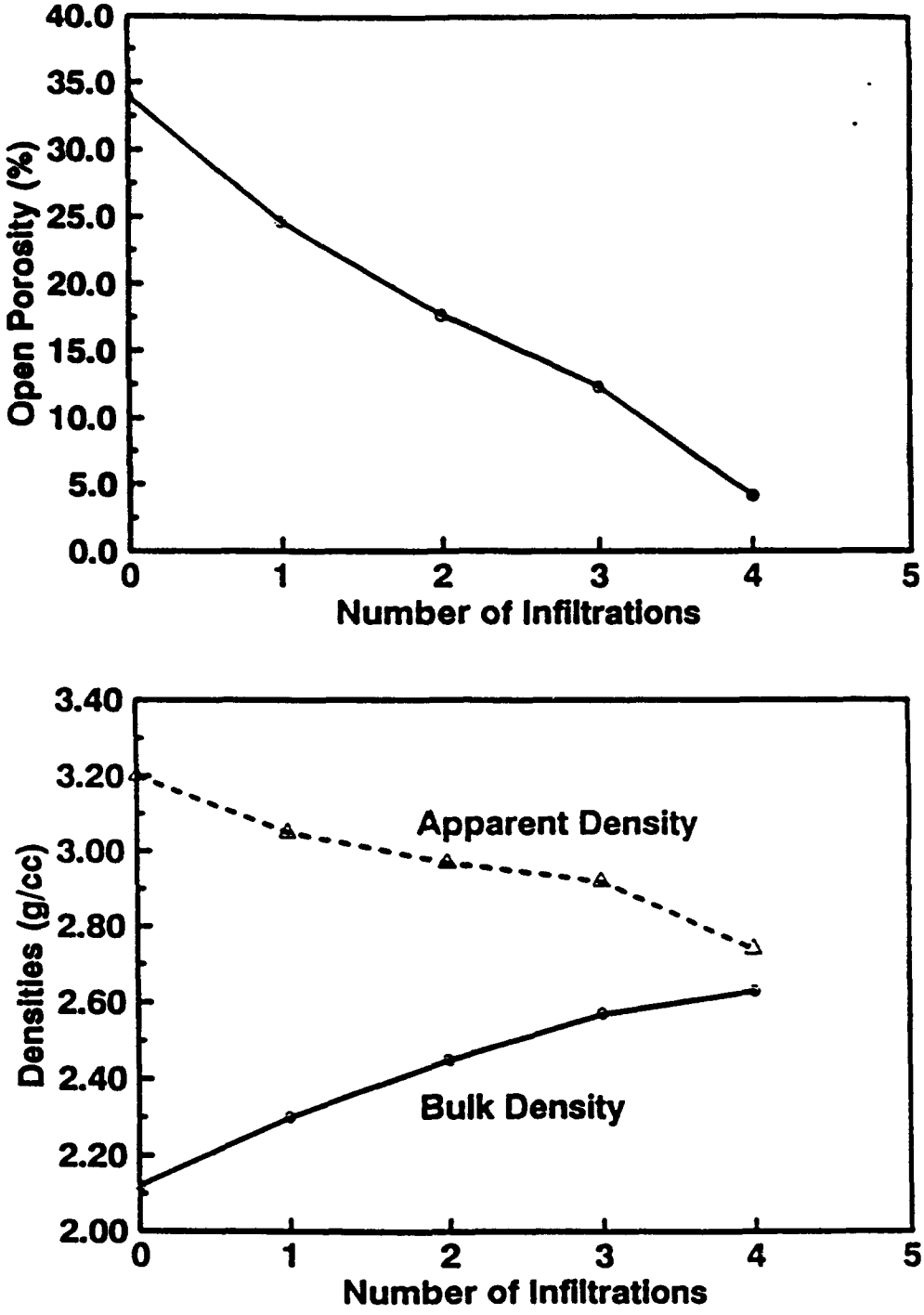

Figure 5 Plots of Average Open Porosity, Bulk Density, and Apparent Density as a Function of Number of Infiltrations for Samples Pyrolyzed at 1100°C

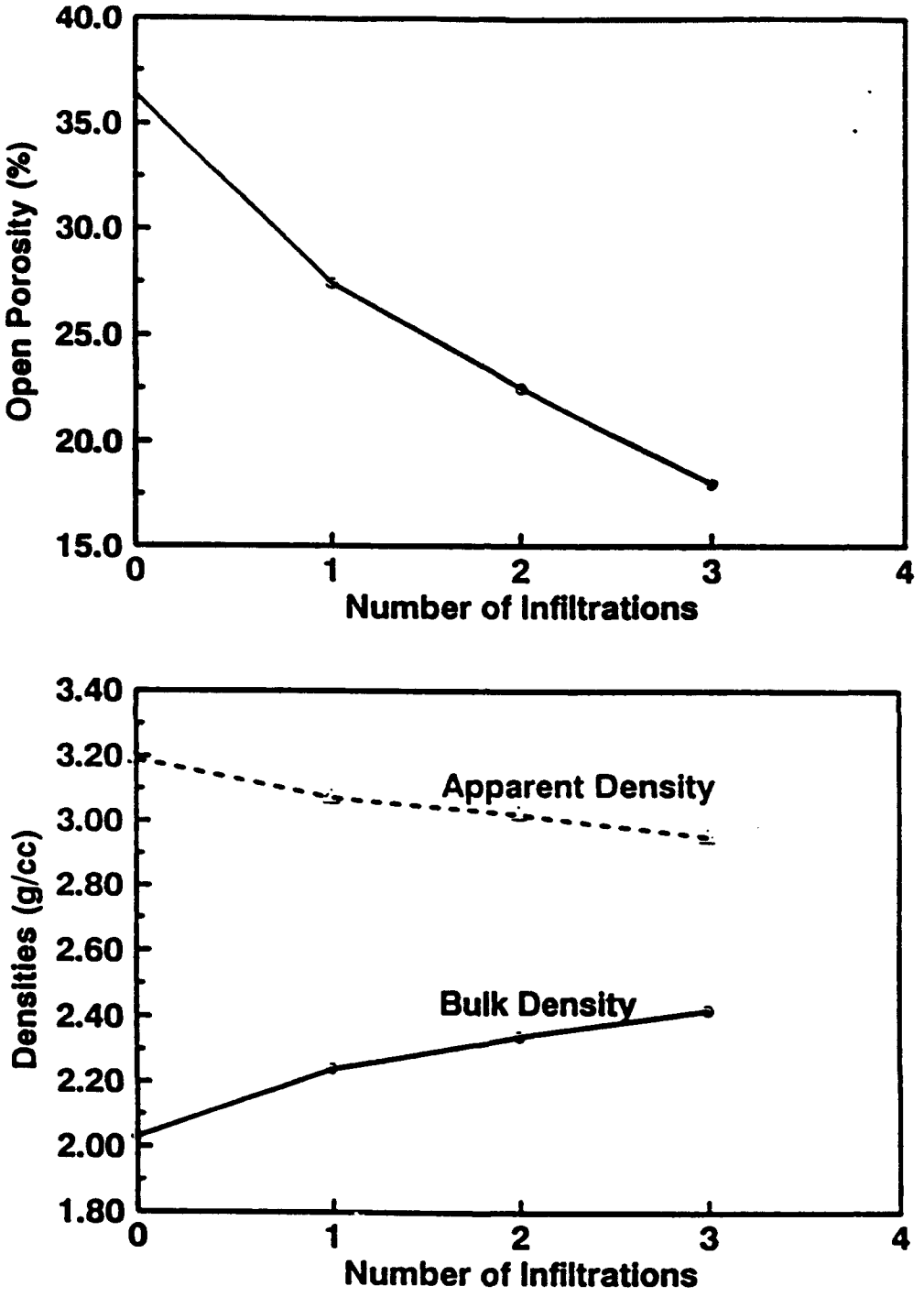

Figure 6 Plots of Average Open Porosity, Bulk Density, and Apparent Density as a Function of Number of Infiltrations for Samples Pyrolyzed at 1400°C

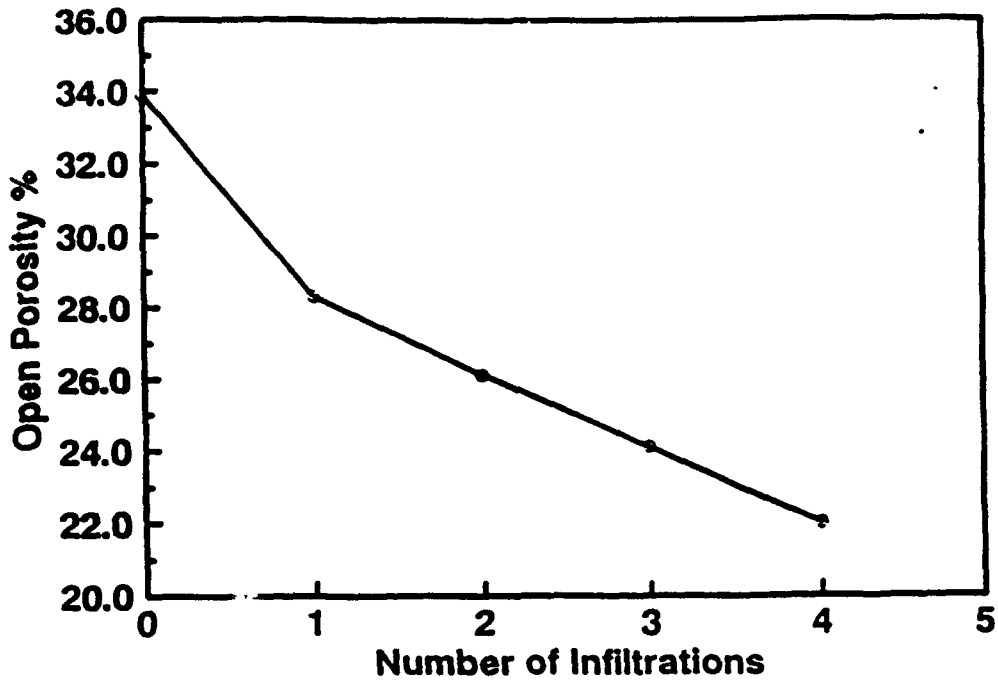

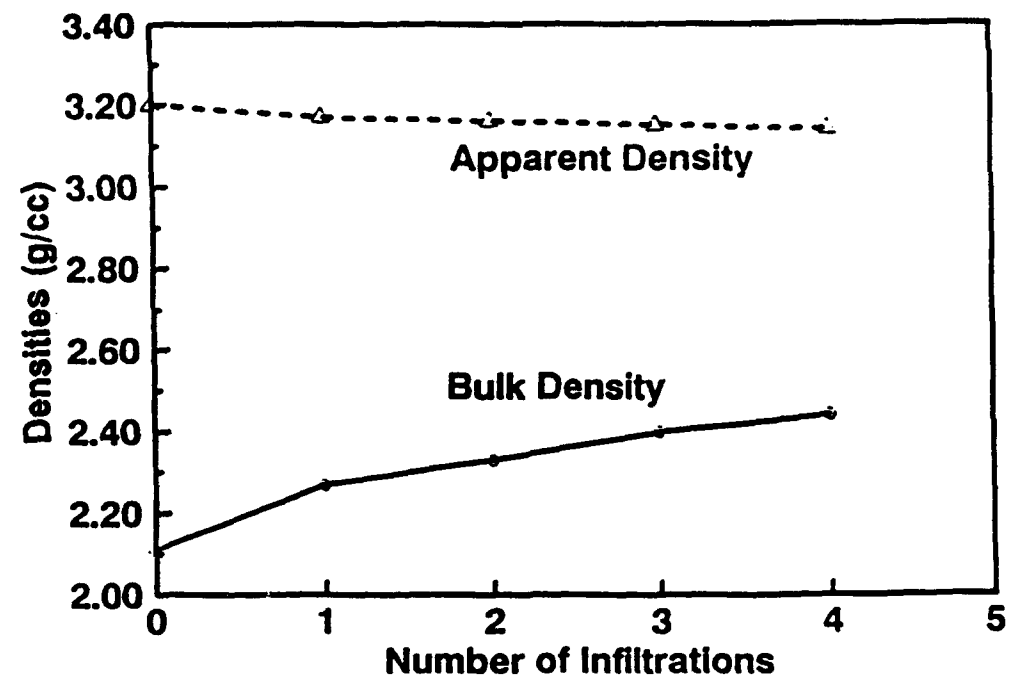

Figure 7 Plots of Average Open Porosity, Bulk Density, and Apparent Density as a Function of Number of Infiltrations for Samples Pyrolyzed at 1575°C

2. The efficiency of the infiltration process may be diminished after the first infiltration/pyrolysis treatment at 1400°C, i.e., a smaller volume of ceramic precursor may be infiltrated into the samples relative to the 1100°C-pyrolyzed samples. This would imply that samples pyrolyzed at higher temperatures develop a pore structure that is less amenable to infiltration (e.g., a structure with finer pore channels). This possibility is discussed later in this section in conjunction with results of Hg porosimetry analysis of samples pyrolyzed at 1100 and 1575°C.

Figure 7 shows the same tends as observed in Figure 6, although the bulk density increases more slowly, while apparent density and open porosity decrease more slowly during the infiltration/pyrolysis process. The explanation for this behavior is essentially the same as discussed above in regards to Figure 6:

1. There will be greater volumetric shrinkage for samples heat treated to 1575°C because of the increased true density of the new ceramic material formed and the increased weight loss at the higher temperature. (In this case, it is clear from the TGA results in Figure 2 that samples heat treated at 1575°C will have a higher weight loss compared to samples heat treated at 1100 or 1400°C.) At the higher temperature (1575°C), the true density of the pyrolyzed product is closer to the value for crystalline silicon carbide. Hence, the apparent density shows only a small decrease during the infiltration/pyrolysis process. (This also indicates that most of the porosity in the sample is open to penetration by water during the Archimedes density measurement.)
2. Mercury porosimetry experiments, which are discussed in more detail later in the section, suggest that some of the pore channels in 1575°C-pyrolyzed samples may be too small to be infiltrated by the ceramic precursor. Hence, less new ceramic material may be incorporated during infiltration compared to the samples pyrolyzed at lower temperatures.

The closed porosity after the infiltration/pyrolysis process can be determined by subtracting the open porosity (measured by the Archimedes method) from the total porosity. The total porosity can be calculated from the following equation:

$$P = 100\,[1 - d_o/d_{SiC} - (d_f - d_o)/d_e] \qquad (7)$$

where

d_o = initial bulk density (measured before infiltration/pyrolysis)
d_f = final bulk density (measured after infiltration/pyrolysis)
d_{SiC} = theoretical density of SiC (3.21 g/cm^3)
d_e = true density of the new ceramic material formed after the infiltration/pyrolysis process)
d_o/d_{SiC} = volume fraction of SiC in the original porous SiC preform (before the infiltration/pyrolysis process)
$(d_f-d_o)/d_e$ = volume fraction of the new ceramic material formed (after the infiltration/pyrolysis process)

For samples pyrolyzed to 1100°C, the true density value determined by Toreki et al. (2.13 g/cm^3, Table 1) was used to calculated the closed porosity from equation 7. The true density values were not available for samples pyrolyzed at 1400 and 1575°C; however, a value of 3.2 g/cm^3 was assumed for samples pyrolyzed at 1575°C. (The actual true density may be smaller than this value). Figure 8 shows plots of average open porosity and closed porosity (both as a percentage of the total porosity) vs. number of infiltration/pyrolysis cycles. As expected, the samples pyrolyzed at 1575°C show very little closed porosity, even after four infiltration cycles. In contrast, the samples pyrolyzed at 1100°C show a large increase in closed porosity after the fourth infiltration cycle. The development of closed pores is, of course, harmful to the subsequent siliconization process. However, there is a potential use for this type of sample if further infiltration/pyrolysis treatments could result in near zero open porosity. It might be possible to hot-isostatically press such samples without using a cladding. However, this would only have potential for densification of fine powder compacts. (The SiC preforms used in this study have too coarse a grain structure to undergo significant densification, even at very high HIPing temperatures).

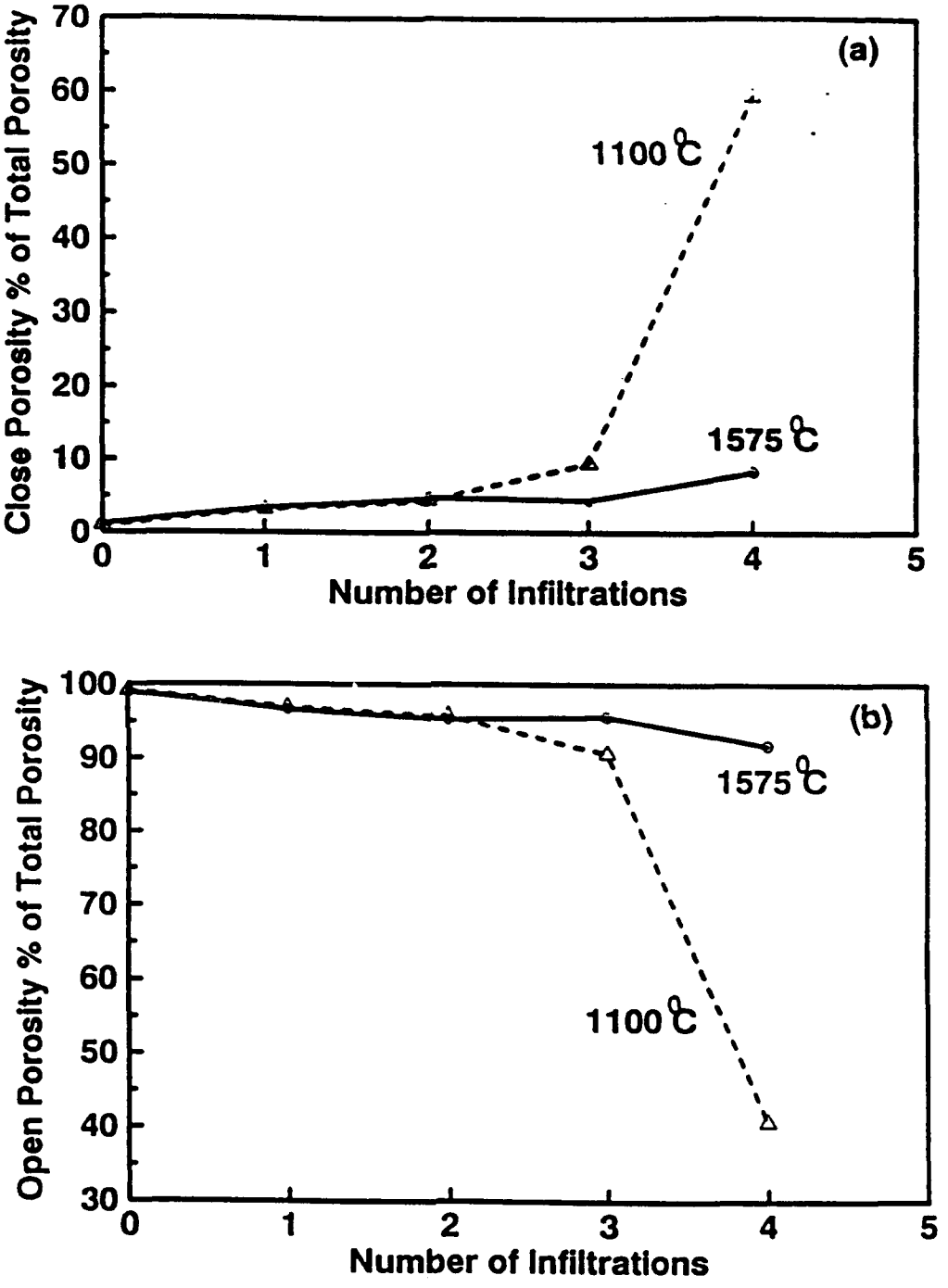

Figure 8 Plots of (a) Average Percent (Close Porosity/Total Porosity) and (b) Average Percent (Open Porosity/Total Porosity) vs. Number of Infiltration/Pyrolysis Cycles Using Indicated Pyrolysis Temperatures

Figures 9 and 10 show the Hg porosimetry results after successive infiltration/pyrolysis cycles at 1100°C and 1575°C, respectively. As expected, with an increased number of infiltrations, the pore size distribution curves shift to smaller channel radii and lower total intruded specific pore volume.

Table 5 compares the open porosity values determined from both Archimedes immersion and Hg porosimetry measurements. The median pore radii determined by mercury porosimetry are also included. The values are in relatively good agreement for the 1100°C pyrolyzed samples, although the differences increase with decreasing median pore size (i.e., increasing number of infiltration/pyrolysis cycles). The samples pyrolyzed at 1575°C show greater differences in open porosity values obtained by two methods. This is apparently due to very small pores which are formed during the densification and crystallization of the new ceramic material. These pores are accessible to water but not to mercury. Figure 11 shows that a significant fraction of these fine pores develops after the first infiltration/pyrolysis cycle for the samples that were pyrolyzed at 1575°C.

Table 5 Comparison of Open Porosity Values from Archimedes and Hg Porosimetry after Preceramic Infiltrations

Infiltration	Pyrolysis Temp.(°C)	Archimedes (%)	Porosimetry (%)	Median Pore Radius (μm)
None	None	34.0	33.8	3.21
First	1100	24.8	25.4	2.18
Second	1100	17.6	16.9	1.01
Third	1100	12.5	10.4	0.53
First	1575	28.0	25.9	1.82
Second	1575	26.2	18.7	0.94
Third	1575	24.5	17.3	0.81

Table 6 lists the measured percentage weight gains of different samples at different pyrolysis temperatures and Figure 12 shows the plots of cumulative weight gain vs. number of infiltrations for various pyrolysis temperatures.

The percentage weight gain for an infiltration is calculated from the following equation:

$$W\% = 100\ (W_f - W_i)/W_i \qquad (8)$$

where W_f is the final weight of sample (after infiltration/pyrolysis) and W_i is the initial weight of sample (before infiltration/pyrolysis). The percentage weight gain can also be predicted using the following equation if it is assumed that the open pore volume of the preform is completely filled by the liquid infiltrant:

$$W\% = 100\ d_i\ P\ (1-L)/d_b \qquad (9)$$

where

- d_i = density of infiltrant (0.95 for the ceramic precursor)
- P = fractional open porosity before infiltration (i.e., open pore volume/sample bulk volume)
- d_b = bulk density before infiltration
- L = fractional weight loss of polymer after pyrolysis

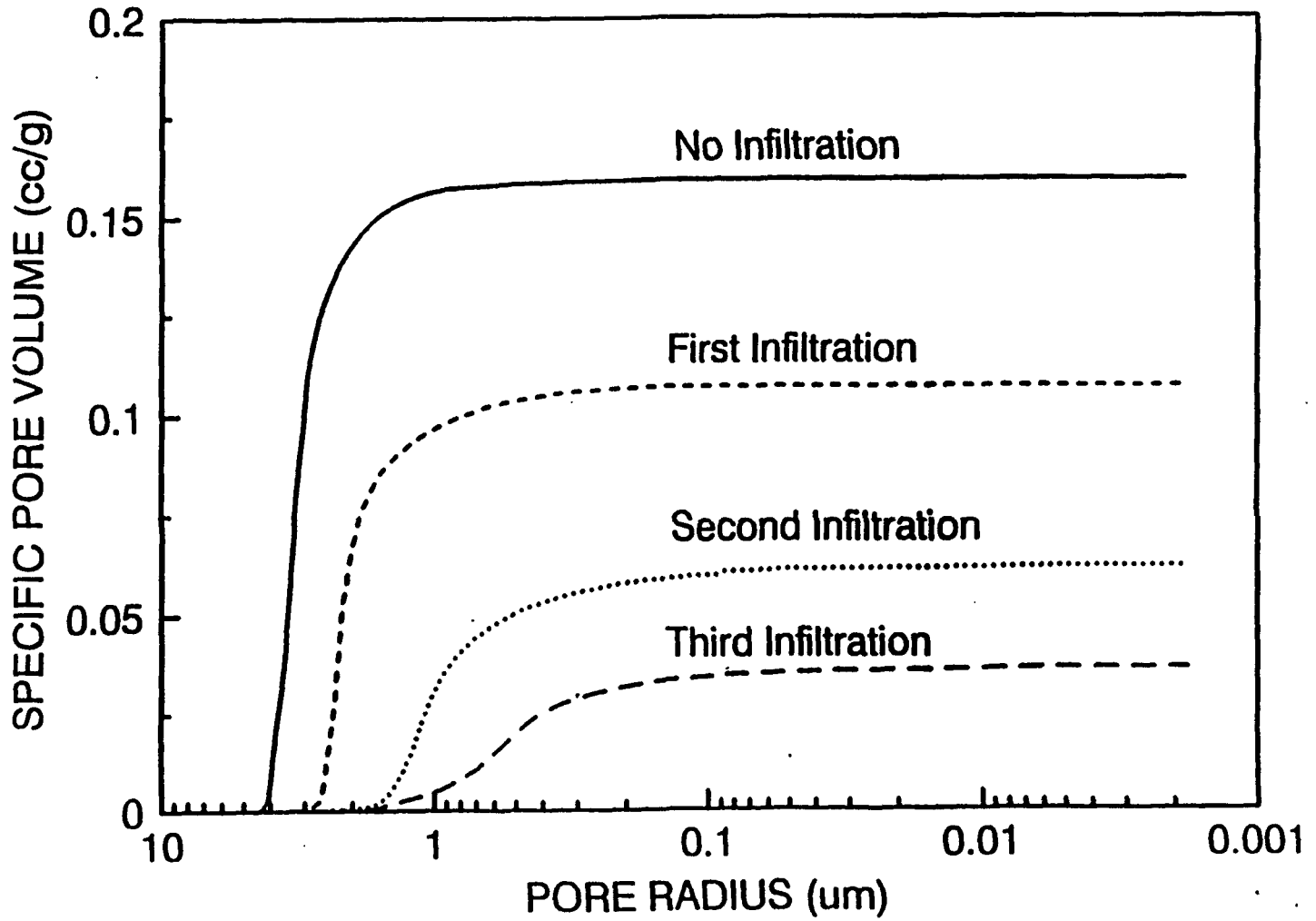

Figure 9 Plots of Specific Pore Volume vs. Pore Radius (Obtained by Mercury Porosimetry) for Samples with Indicated Number of Ceramic Precursor Infiltration/Pyrolysis (at 1100°C) Cycles

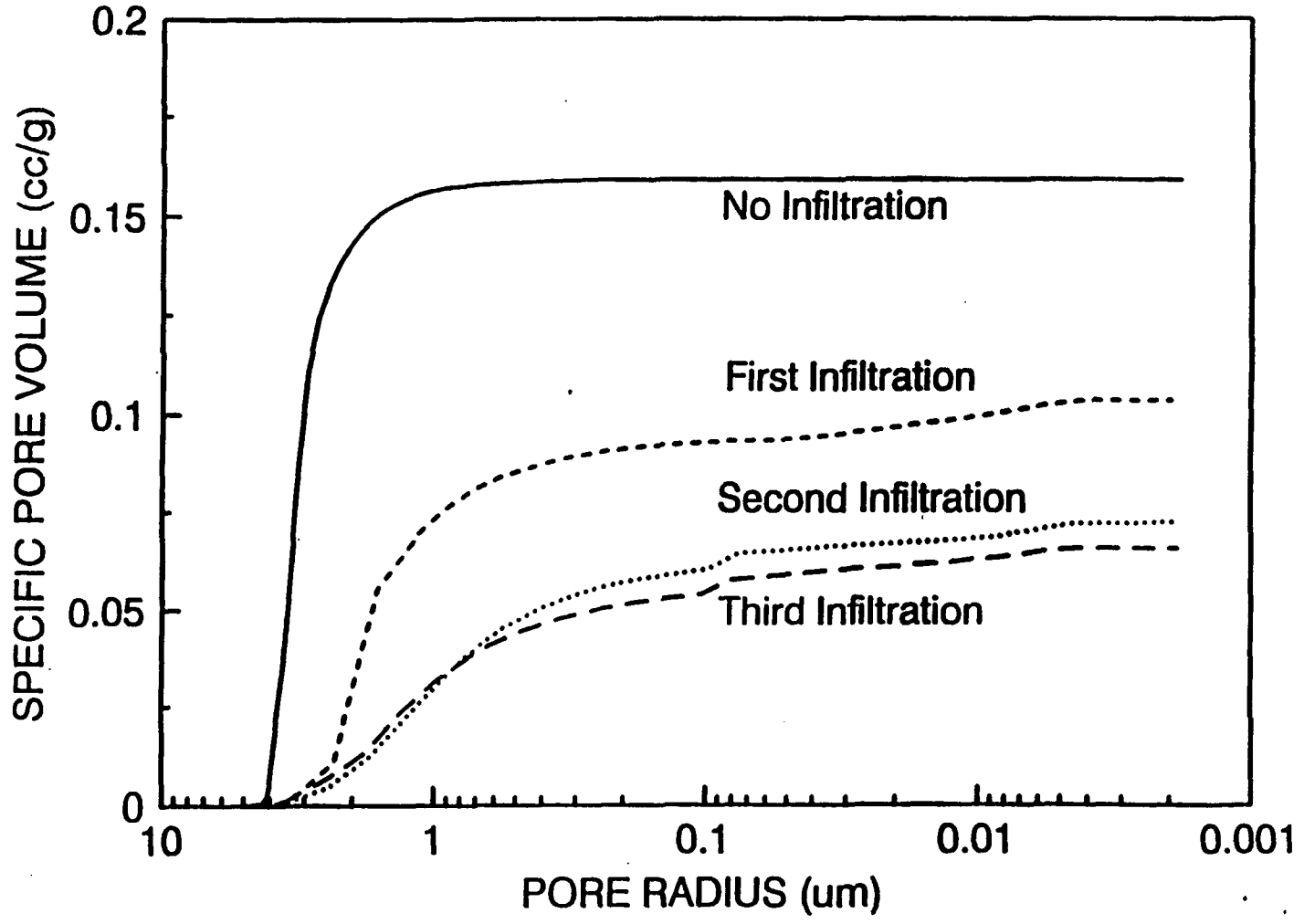

Figure 10 Plots of Specific Pore Volume vs. Pore Radius (Obtained by Mercury Porosimetry) for Samples with Indicated Number of Ceramic Precursor Infiltration/Pyrolysis (at 1575°C) Cycles

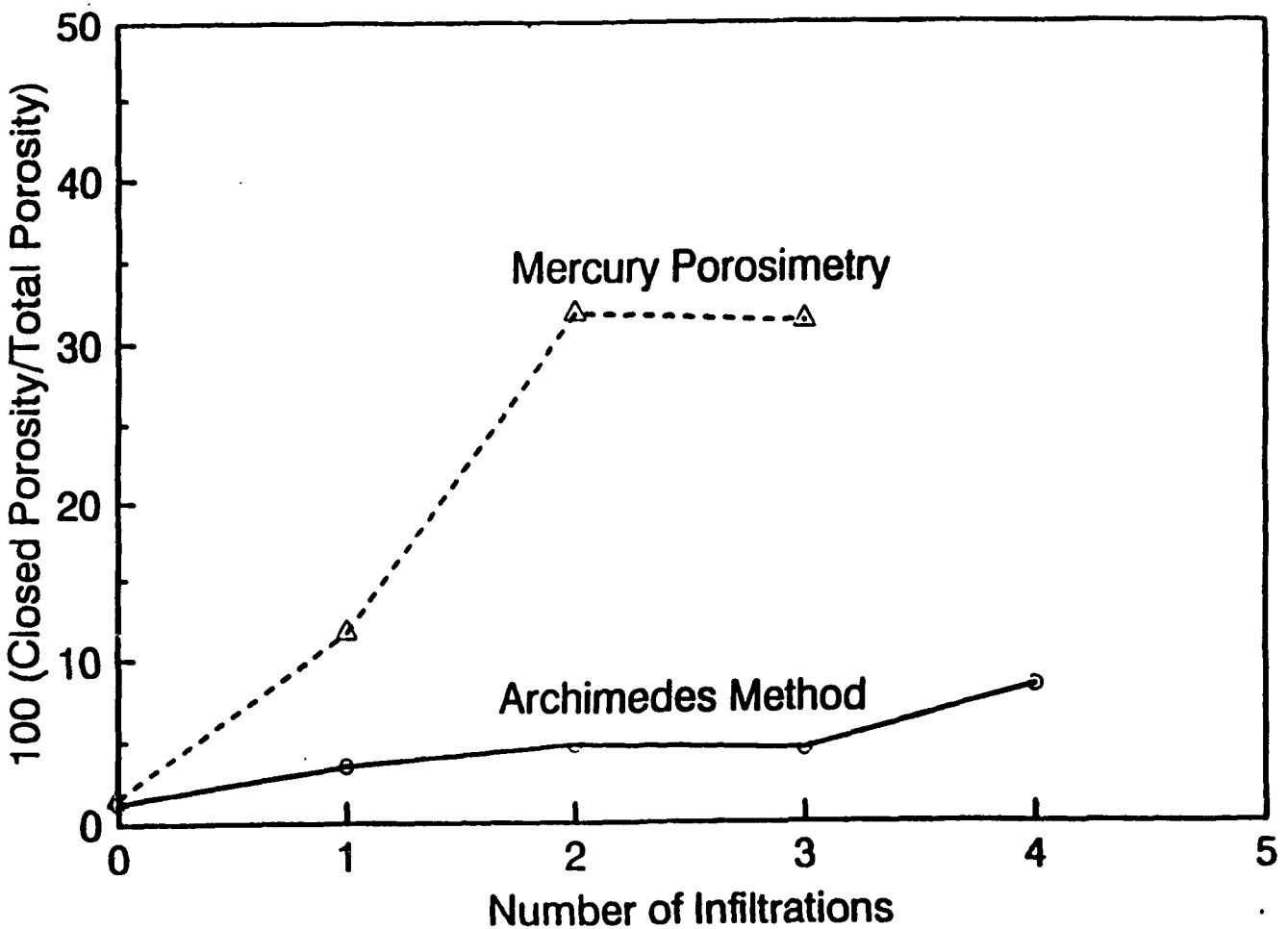

Figure 11 Plots of Average Percent (Closed Porosity/Total Porosity) vs. Number of Infiltration/Pyrolysis (at 1575°C) Cycles as Determined by Archimedes Immersion and Mercury Porosimetry Measurements

Table 6 Measured and Predicted Weight Gain Values for Infiltrated/Pyrolyzed Samples

After Pyrolysis at 1100°C

Sample	1 Infil.	2 Infil.	3 Infil.	4 Infil.
A	8.5 (9.7)			
Q	9.0 (9.6)	6.4 (6.4)		
C	9.0 (9.5)	6.6 (6.3)	4.5 (4.2)	
B	8.5 (9.5)	6.1 (6.3)	5.7 (4.3)	1.9 (2.8)
G3	10.8 (10.7)	6.5 (6.8)	4.9 (4.7)	
G4	11.1 (10.7)	5.6 (6.7)	5.6 (4.9)	

After Pyrolysis at 1400°C

G1	10.7 (10.8)	4.8 (7.4)	3.1 (6.0)	
G2	10.7 (10.7)	5.4 (7.3)	4.5 (5.5)	

After Pyrolysis at 1575°C

S	8.1 (9.2)			
R	7.6 (9.1)	2.6 (7.1)		
T	7.1 (9.2)	2.6 (7.2)	2.8 (6.4)	
U	7.6 (9.2)	2.6 (7.1)	3.0 (6.3)	1.8 (5.7)

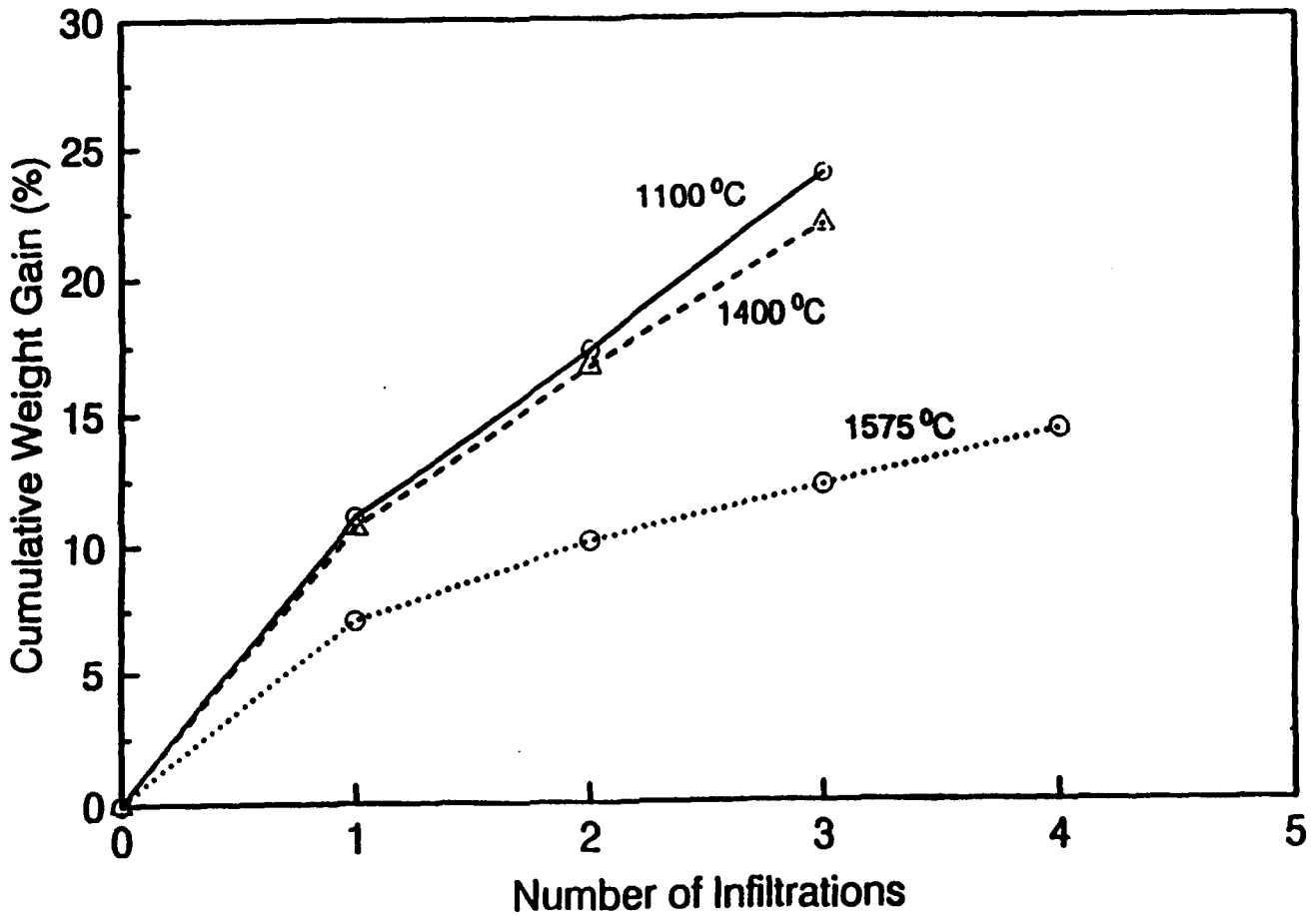

Figure 12 Plots of Cumulative Weight Gain vs. Number of Infiltration at Different Pyrolysis Temperatures

The calculated weight gains from equation 9 are given in parentheses in Table 6. Based on the TGA results in Figure 2, an L value of 0.35 was used for samples pyrolyzed at 1100 and 1400°C. An estimated value of L = 0.40 was used for samples pyrolyzed at 1575°C. (In reality, the L value for these samples probably depends on the number of infiltration cycles.)

The measured weight gain for samples pyrolyzed at 1100°C are in reasonably good agreement with the calculated weight gains. This suggests that the open pores are efficiently filled for each infiltration cycle. This seems reasonable based on the mercury porosimetry results in figure 9 and 10. Most of the pore volume accessible to mercury penetration retains a relatively large average pore channel size, even after three infiltration cycles. For samples pyrolyzed at 1400°C, the measured weight gains are lower than those calculated, except for the first infiltration cycle. The samples pyrolyzed at 1575°C show measured weight gains that are much lower than the calculated values for all infiltration cycles. The discrepancy between the measured and calculated weight gains may be due to inaccurate assumptions regarding the weight loss during pyrolysis. It is possible that the actual weight loss after the infiltration/pyrolysis process may be higher than the weight loss obtained by TGA (as reported in Figure 2). Several possible reasons for this are given below:

1. More "silica" (i.e., material with Si-O bonds) may be present in the infiltrated samples compared to the samples used for TGA measurement. The presence of silica and excess carbon (formed during pyrolysis of the vinyl silazane polymer) could lead to additional weight loss according to the reaction:

$$C + SiO_2 \rightarrow SiO(g) + CO(g) \qquad (10)$$

   This reaction occurs at >1000°C [Mil79]. There are several possible reasons why the samples used for the weight loss measurements may have more "silica" present compared to the samples used in the TGA experiments. The TGA measurements were carried out on "bulk" pieces of polymerized vinyl silazane, while the weight loss measurements were carried out on SiC preforms containing infiltrated vinyl silazane polymer. The SiC preform may have had some oxide contamination. (For example, the fine, high specific surface SiC particles used to prepare the preforms generally have a surface oxide layer.) However, this amount is expected to be small because the SiC preforms are sintered at very high temperatures in an non-oxidizing environment, i.e., under conditions in which SiO_2 should be unstable. SiO_2 may decompose to vapor species by the overall reaction: $2SiO_2 + SiC = 3SiO + CO$ [Pul66] or $SiO_2 = SiO + 1/2\ O_2$). Another possible reason for higher oxide content in the samples used for weight loss measurements is that the samples are boiled in water for several hours in order to carry out the Archimedes density/porosity measurements. This could results in hydroxylation (hydroxide formation) of the silazane polymer.
2. It is possible that the vinyl silazane does not crosslink as efficiently when infiltrated into the relatively small pores of the SiC preform. A greater weight loss would be expected during pyrolysis if the infiltrated material has a lower molecular weight and/or a lesser degree of crosslinking compared to the samples used in the TGA experiment.
3. The reaction given by equation 4 may be accelerated for the infiltrated samples compared to the TGA sample for several possible reasons. First, the vinyl silazane infiltrated into SiC preform probably has a higher specific surface area (due to the porous nature of the preform) compared to the TGA sample. The weight loss would be higher for the former samples if surface reaction kinetics are rate controlling. Second, the ingress of nitrogen into the preform and the egress of volatile products out of the preform may be impeded due to the fine pore sizes. Therefore, the partial pressure of nitrogen in the interior of the infiltrated samples may be lower than that used in the TGA experiment. This would lead to an acceleration of the weight loss reactions (as observed during argon pyrolysis, Figure 2).

The discrepancy between the measured and calculated weight gains reported in Table 6 (i.e., for samples with multiple infiltration/pyrolysis at 1400 and 1575°C) may also be caused, at least in part, by difficulties in achieving complete infiltration by the ceramic precursor. Small pore channels may develop during high temperature pyrolysis of the vinylsilazane-infiltrated SiC preforms. These

pores may be large enough for water to penetrate (i.e., for the Archimedes density/porosity measurements), but too small to permit infiltration of the vinyl silazane. This explanation cannot account for the low measured weight gain for the samples which are infiltrated once and then pyrolyzed to 1575°C, since mercury porosimetry (Figure 10) shows that all the pore channels are initially relatively large (i.e., radius >0.5 μm). However, Figure 10 also shows that relatively fine pore channels (radius <0.1 μm) develop after the first infiltration/pyrolysis cycle. (Such fine pore channels are less evident in Figure 9 for the 1100°C-pyrolyzed samples). Furthermore, Figure 11 shows that there is a significant fraction of porosity which is inaccessible to mercury penetration, but accessible to penetration by water in the 1575°C-pyrolyzed samples. The pore channel radii for this porosity must be <18 Å (i.e., the minimum size that can be detected at the maximum pressure of 60 ksi (410 MPa)). Thus, this explanation could be a contributing factor for the low weight gains observed in the samples that have been infiltrated more than once.

Siliconized SiC with Preceramic Infiltrations

Table 7 gives the Archimedes bulk density, apparent density, and open density results for siliconized samples after removing the excess silicon on the surface. The low open porosity values, together with microstructure observations discussed in section 1.4, indicate that the siliconized samples are almost fully dense. The silicon phase content listed in Table 7 was calculated by the "rule of mixtures", assuming that the measured apparent density was very close to the true density of the sample.

$$d_e = V_{SiC}d_{SiC} + V_{Si}d_{Si} \qquad (11)$$

where

d_e = true density of siliconized SiC composite (assumed equal to the measured apparent density)
V_{SiC} = volume fraction of SiC
d_{SiC} = true density of SiC (3.2 g/cm^3)
V_{Si} = volume fraction of Si
d_{Si} = true density of silicon (2.33 g/cm^3)

Table 7 shows that infiltrated samples have higher bulk and apparent densities compared to the uninfiltrated samples, indicating that the infiltration/pyrolysis process does indeed increase the final SiC/Si ratio.

Table 7 also shows that the calculated silicon content (column seven) for samples G1-G4 is approximately equal to the open porosity of the infiltrated/pyrolyzed samples prior to siliconization (column eight). These samples were heat treated at 1650°C for 2 hours. Thus, the pyrolysis products in the pores of the preform undergo additional weight loss and crystallization, thereby forming a relative dense, crystalline SiC product. The siliconization process only involves filling of the pores with molten silicon, i.e., the process is similar to siliconization of uninfiltrated SiC preform (sample X). In contrast, the other samples in Table 7 were pyrolyzed only at temperatures lower than the siliconization temperature. Therefore, during siliconization process, the precursor continues to undergo decomposition, densification, and crystallization reactions. Consequently, these samples show large differences between the silicon volume after siliconization and the open pore volume before siliconization.

The calculated volume percent of "new" SiC (see Table 8) formed due to the infiltration/pyrolysis is determined by subtracting the calculated Si content (Table 7) from the open porosity of the original porous SiC preform. The results show that 5-10 vol% new SiC can be formed by using three or four infiltration/pyrolysis cycles.

Table 7 Open Porosity, Bulk Density, Apparent Density, and Calculated Si Content for Siliconized Samples

Name	Number of Infil.	Initial Pyroly. T(°C)	Open Porosity (%)	Bulk Density (g/cm^3)	Apparent Density (g/cm^3)	Calculated Si Content (%)	Open Porosity (%) before Siliconization
X	0		0.3	2.89	2.90	34.5	34.2
G1	3	1400	0.2	2.93	2.93	31.0	30.5
G2	3	1400	0.0	2.96	2.96	27.6	28.0
G3	3	1100	0.2	2.95	2.95	28.7	29.4
G4	3	1100	0.0	2.95	2.95	28.7	29.9
U	4	1575	0.6	2.95	2.97	26.4	21.7
B	4	1100	0.7	2.97	2.99	24.1	4.1
C1	1	1000	0.3	2.90	2.91	33.3	18.4
C2	2	1000	0.4	2.93	2.95	28.7	11.4
C3	2	1000	0.3	2.95	2.96	27.6	11.0

Table 8 Volume Percent of "New" SiC Formed Due to the Infiltration/Pyrolysis Process

Name	G1	G2	G3	G4	U	B
Infiltration Number	3	3	3	3	4	4
Pyrolysis Temp. (°C)	1650	1650	1650	1650	1575	1100
Calculated New SiC Vol%	5.5	8.6	7.7	7.6	7.5	9.6
Predicted New SiC Vol%	6.5	8.6	6.9	6.6	8.2	12.1

Note: Samples G1 through G4 were treated at 1650°C for 2 hour in argon before siliconization. The values in last column for G1 through G4 represent the open porosity of samples after the 1650°C treatment.

Since the SiC preforms undergo little or no volume change during infiltration, pyrolysis, and siliconization treatments, the volume fraction of "new" SiC formed due to the infiltration/pyrolysis process, V_{NSiC}, can also be predicted from the bulk density of the original porous SiC preform, d_b, the fractional weight gain by successive infiltration/pyrolysis treatments, W, and the fractional weight loss, L, between the pyrolysis temperature and the siliconization temperature. For a 1 cm^3 bulk sample, the infiltration/pyrolysis treatments result in a weight gain of (Wd_b) grams. At the siliconization temperature, this weight reduces to [$Wd_b(1-L)$] grams. Assuming that all the weight converts to fully dense SiC during siliconization, the volume fraction of "new" SiC should be:

$$V_{NSiC} = \text{volume of "new" SiC/volume of bulk sample} = d_b W(1-L)/d_{th} \quad (12)$$

where d_{th} is the theoretical (true) density of silicon carbide (3.21 g/cm^3). The values calculated by equation 12 are shown in last row in Table 8. (The fractional weight loss between the pyrolysis temperature and the siliconization temperature, L, was estimated from the TGA data (Figure 2) or the final ceramic yield (~48%) measured after 1650°C heat treatment. The values used were L=0 for samples G1-G4, L=0.2 for sample U, and L=0.24 for sample B). The predicted values match fairly well with the values calculated from density measurements, except for the sample (B) pyrolyzed at 1100°C. As discussed in section 1.2, the actual weight loss, L, may be higher than predicted from the TGA data. This could account for the discrepancy between measured and calculated values for sample B.

X-ray diffraction patterns (Figure 13) for samples with and without preceramic infiltrations indicate that both samples consist of silicon, α-SiC, and β-SiC. No attempt was made to obtain a quantitative estimate of the relative content of the different SiC polytypes.

Microstructure Evolution

The microstructure of samples at various stages during processing were studied by optical and electron microscopy.

Porous SiC Preform

Figures 14-16 show the evolution of the SiC preform from the green state to the final sintered state. The green compact exhibits a microstructure of coarse particles embedded in fine powders (Figure 14). The pores at this stage are relatively small due to the close packing of the fine powders. (See Figure 17 which shows the pore size distribution obtained by mercury porosimetry). After sintering at 1850°C, regions of the compact with fine SiC particles show neck growth and local densification (Figure 15 (b)). Some large pores begin to develop due to local densification of the fine SiC particles in regions between the large SiC particles (Figure 15(a)). At higher sintering temperatures (>2050°C), the fine SiC powders have coalesced onto the coarse particles so that a strong SiC skeleton and a large open pore structure are formed (Figure 16). According to mercury porosimetry results, the median pore size for the sintered porous preform was 3.2 μm (Figure 9 and Table 5). Considerably larger pores are observed in Figure 16. The larger pores are not readily detected in mercury porosimetry because access to these pores is often restricted by smaller pore channels (i.e., an "ink-bottle" pore geometry is characteristic of many porous solids). (Ink-bottle shaped pores are also indicated by the large hysteresis observed during mercury intrusion/extrusion experiments. Thus, the pore size values obtained by mercury porosimetry tend to represent the accessible pore channels near the surface of the samples [Lee90].

SiC Preform after Preceramic Polymer Infiltration

Figure 18 shows typical microstructures of a polished sample after several preceramic polymer infiltration/pyrolysis treatments. The residue that forms in preform's open pore structure after 1000°C pyrolysis is an amorphous Si-C-N material (with small amounts of residual H and O). The

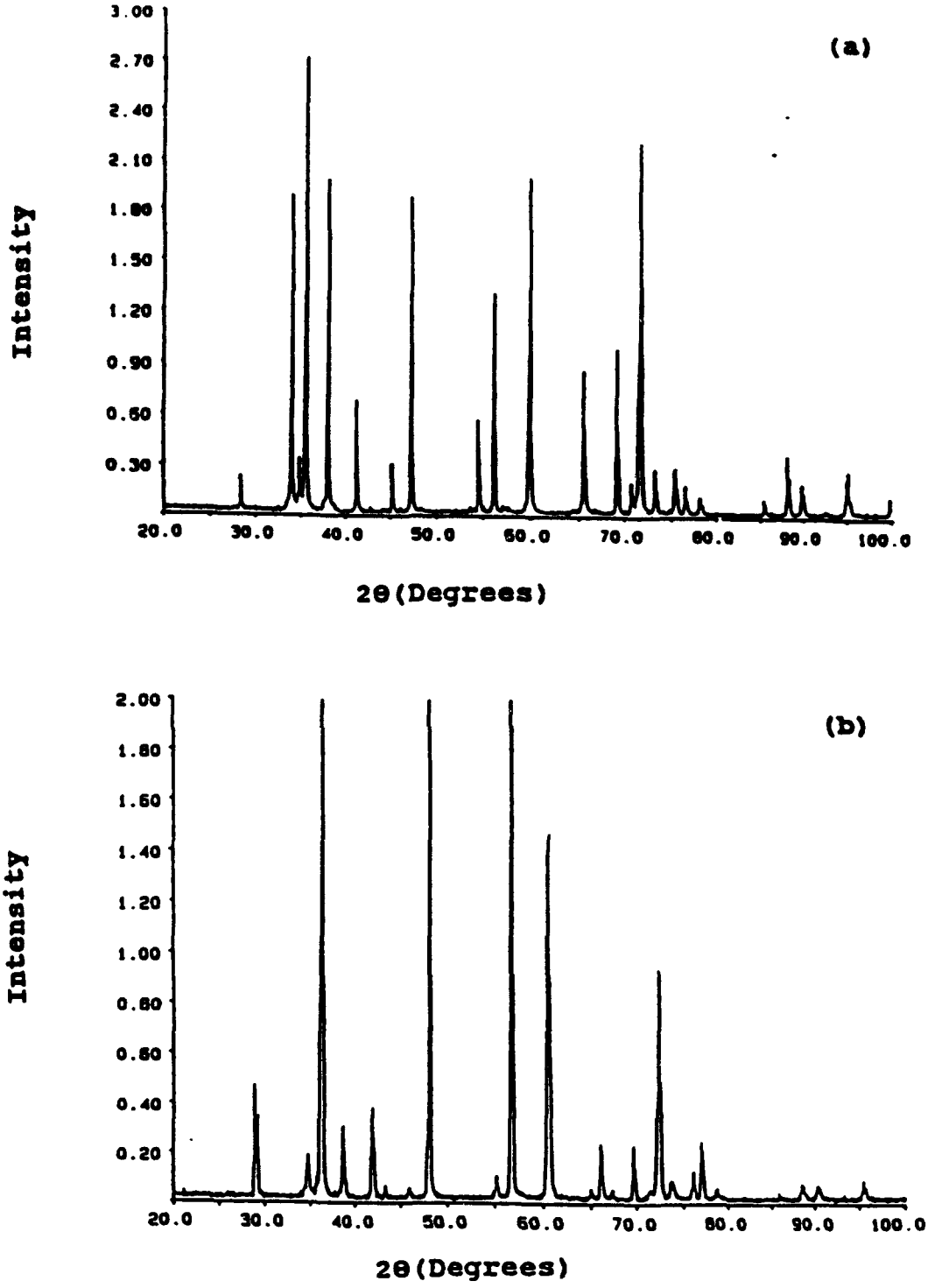

Figure 13 X-Ray Diffraction Patterns for the Siliconized Samples (a) without Preceramic Polymer Infiltrations (Sample X) and (b) with Preceramic Polymer Infiltrations (Sample G2)

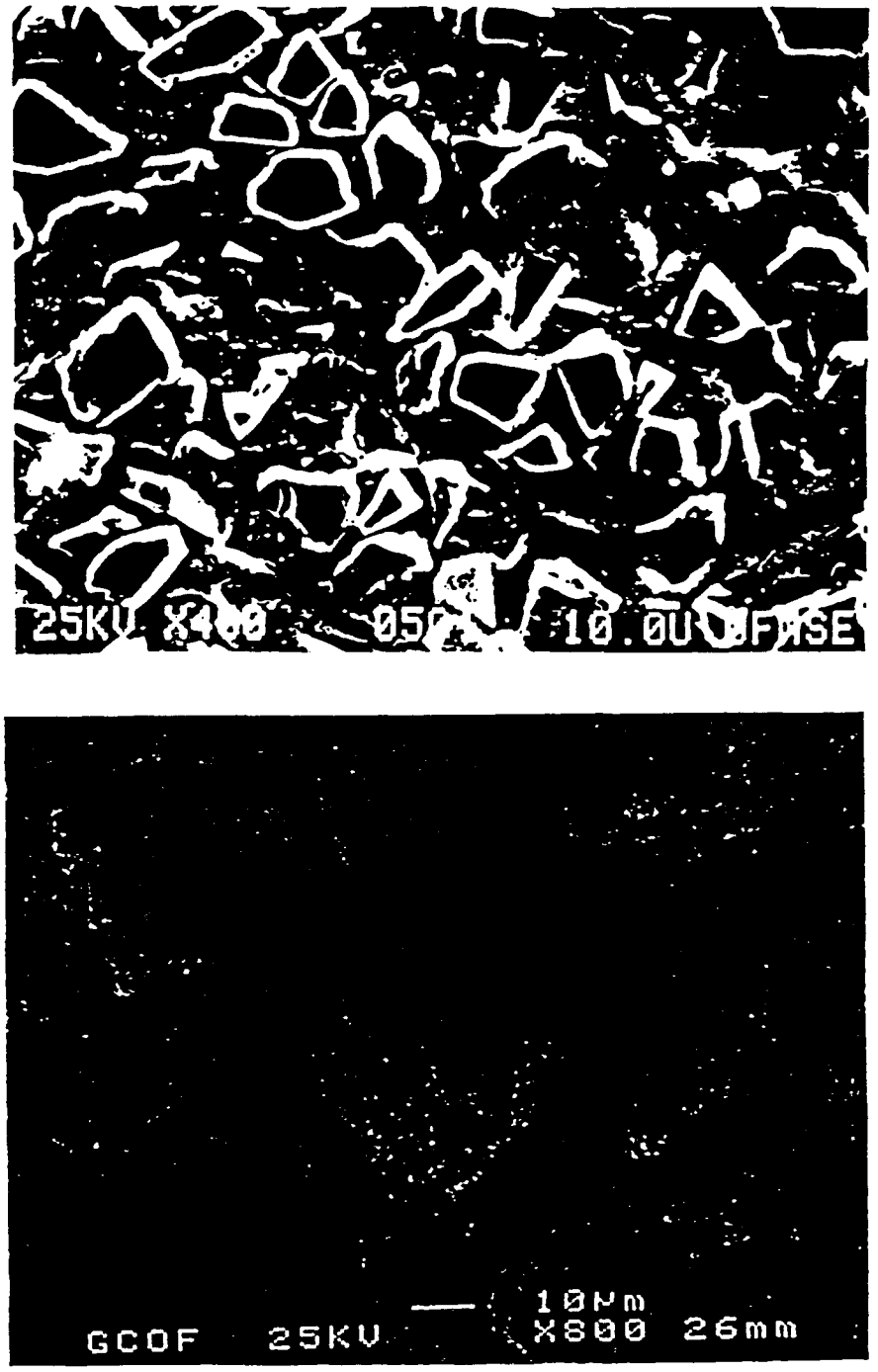

Figure 14 Scanning Electron Micrographs of a Cast SiC Green Compact at (a) Low and (b) High Magnification

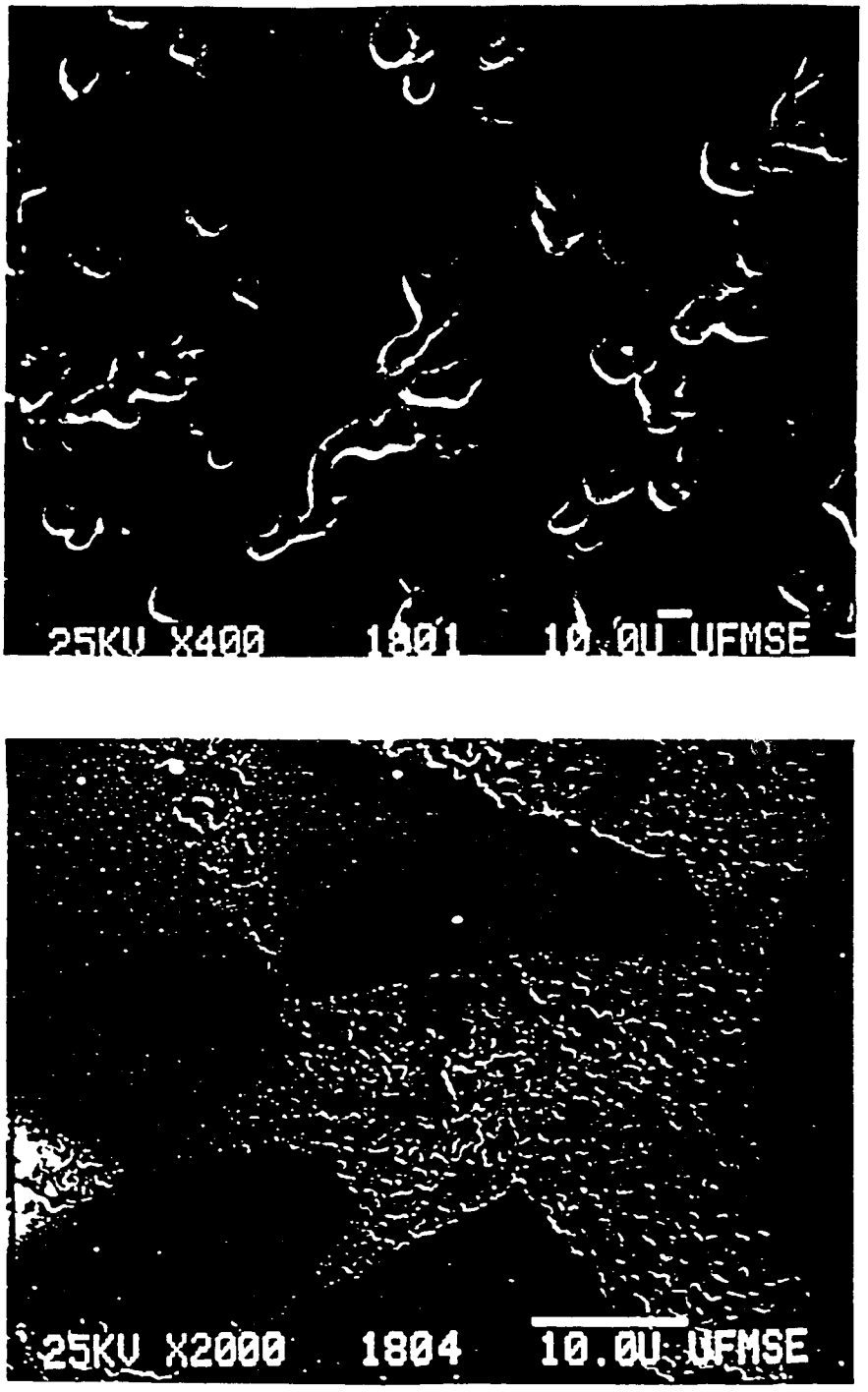

Figure 15 Scanning Electron Micrographs of an SiC Compact Sintered at 1850°C for 20 min. at (a) Low and (b) High Magnification

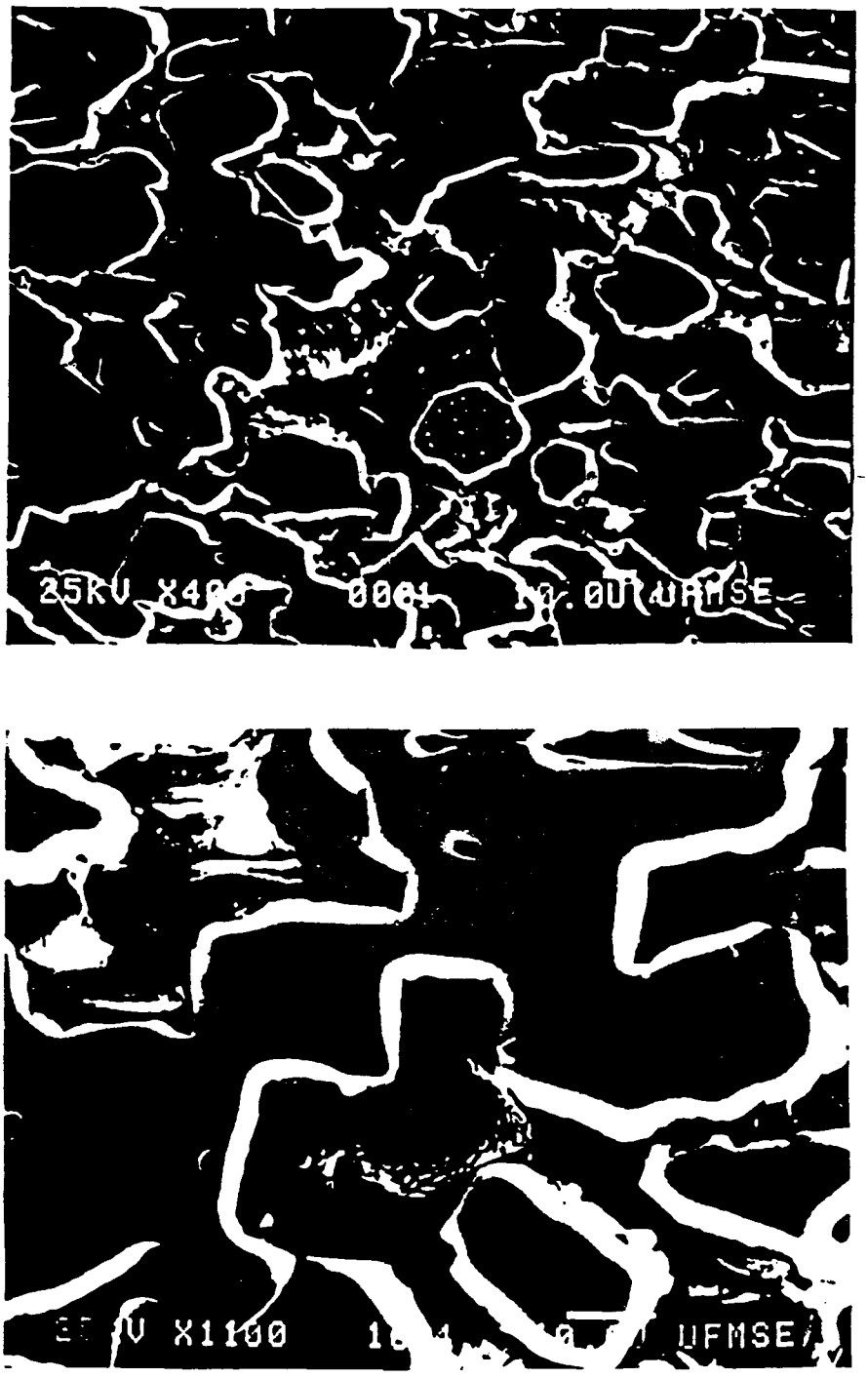

Figure 16 Scanning Electron Micrographs of a Porous SiC Preform Sintered at ~2050°C at (a) Low and (b) High Magnification

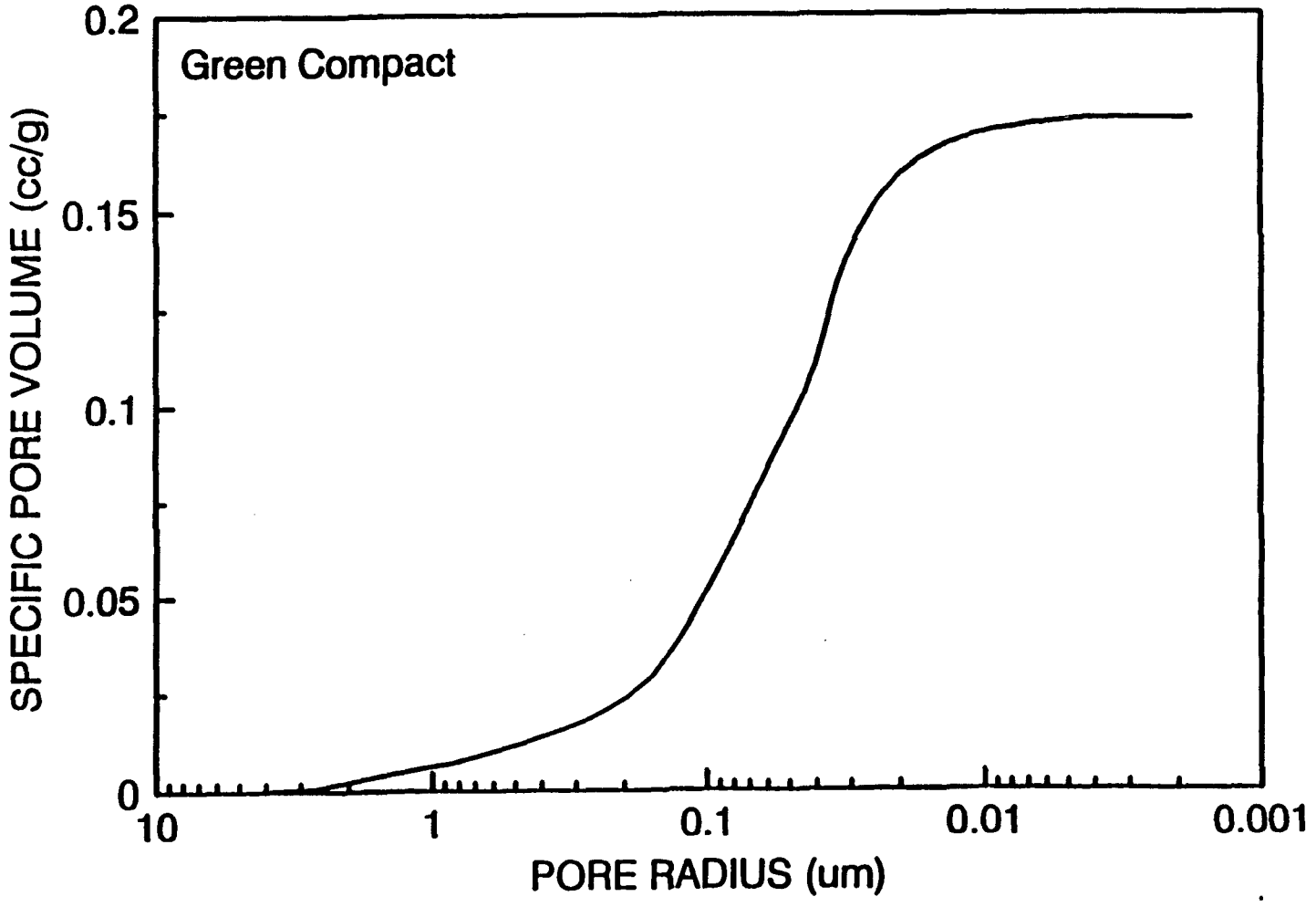

Figure 17 **Plot of Specific Pore Volume vs. Pore Radius (Obtained by Mercury Porosimetry) for a SiC Green Compact**

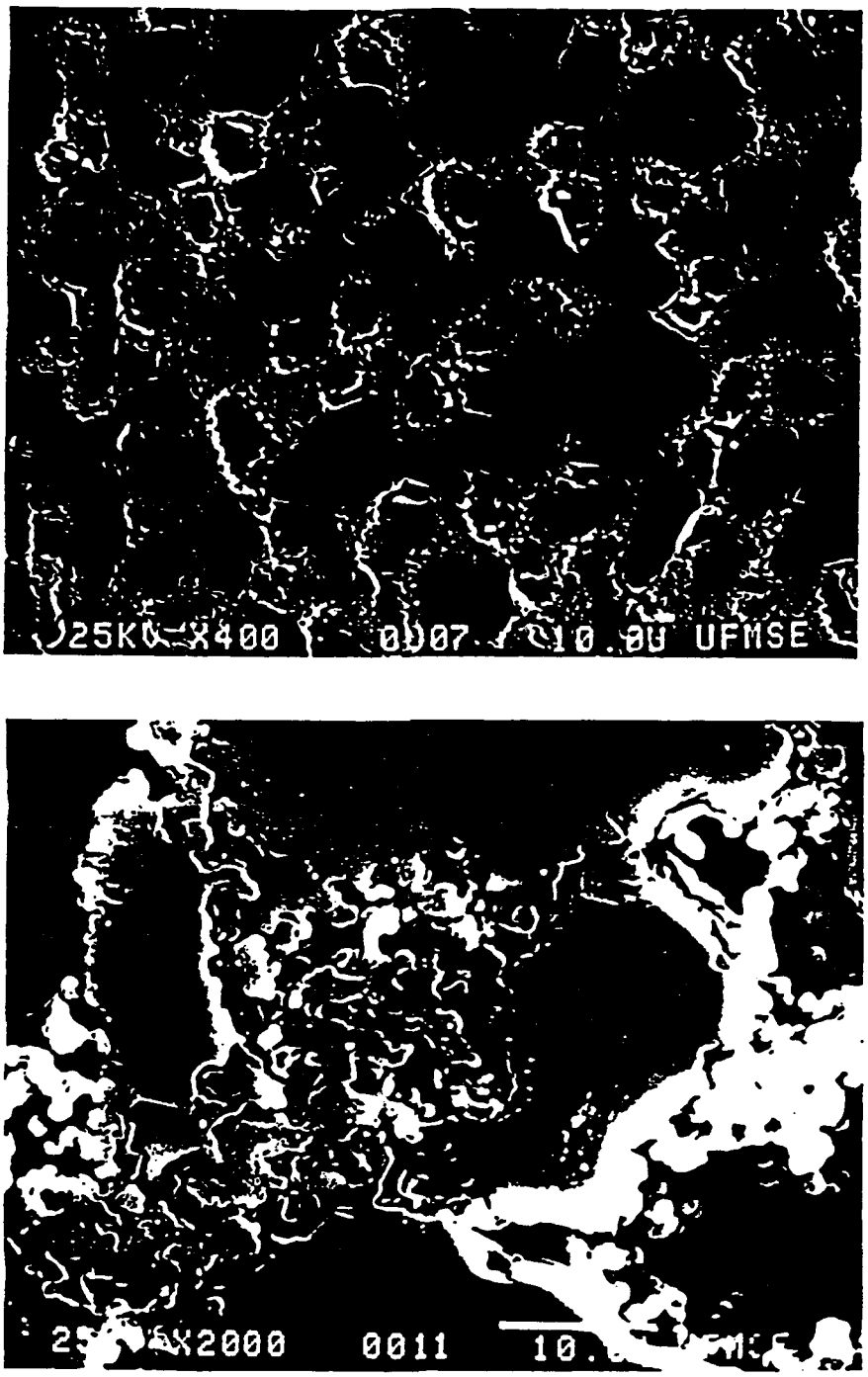

Figure 18 Scanning Electron Micrographs at (a) Low and (b) High Magnification of a Porous SiC Preform after Infiltration/Pyrolysis (1000°C) Cycles with Preceramic Polymer

density of the amorphous phase at this stage is ~2 g/cm^3 (Table 1) which is much higher than the liquid precursor density (0.95 g/cm^3). The volumetric shrinkage, coupled with the weight loss during decomposition of the precursor, means that a large amount of shrinkage (~70%) occurs during the heat treatment. The percentage volume shrinkage, S_v, for the ceramic precursor was estimated by the following equation:

$$S_v = 100\,[1-(d_i W/d_f)] \qquad (13)$$

where

d_i = density of ceramic precursor before pyrolysis (0.95 g/cm^3)
d_f = density of ceramic precursor after pyrolysis (~2 g/cm^3)
W = fractional weight remaining after pyrolysis of the ceramic precursor (i.e., the ceramic yield) =0.63 at 1000°C according to the TGA data (Figure 2)

Hence, the amount of SiC added during a single infiltration/pyrolysis is relatively small. A significant amount of open porosity is retained after only one or two infiltration/pyrolysis cycles. Through further infiltration and pyrolysis, an interlocking network structure of the amorphous phase is formed (Figure 18). However, as discussed in section 1.2, much of the residual porosity is closed after four infiltration/pyrolysis cycles.

Siliconized SiC with Preceramic Polymer Infiltrations

Figures 19(a) and (b) show typical microstructures of siliconized samples with and without preceramic infiltrations, respectively. The only obvious difference between them is the amount of silicon carbide phase which is darker in the micrographs. The small crystals embedded in silicon phase are also SiC. They are brighter in the micrographs due to the geometric contrast which results from the preferential removal of silicon phase during the etching treatment. Observations of unetched polished samples under an optical microscope showed that these small crystals had the same brightness as large SiC grains.

Microstructure studies also revealed some whisker-like crystals (Figure 20) in samples prepared with the ceramic precursor. Toreki et al. [Tor90] also detected some elongated grains in vinyl silazane samples pyrolyzed at 1500°C. Analysis in TEM by electron diffraction showed that these grains were β-Si_3N_4. In the present study, the observed whiskers may be either β-Si_3N_4 or SiC. It is proposed that SiC whisker could form by decomposition of the β-Si_3N_4 whiskers according to reaction 4.

Large pores were observed near the surface of some samples (Figure 21). The cause of these residual pores is not known at this time.

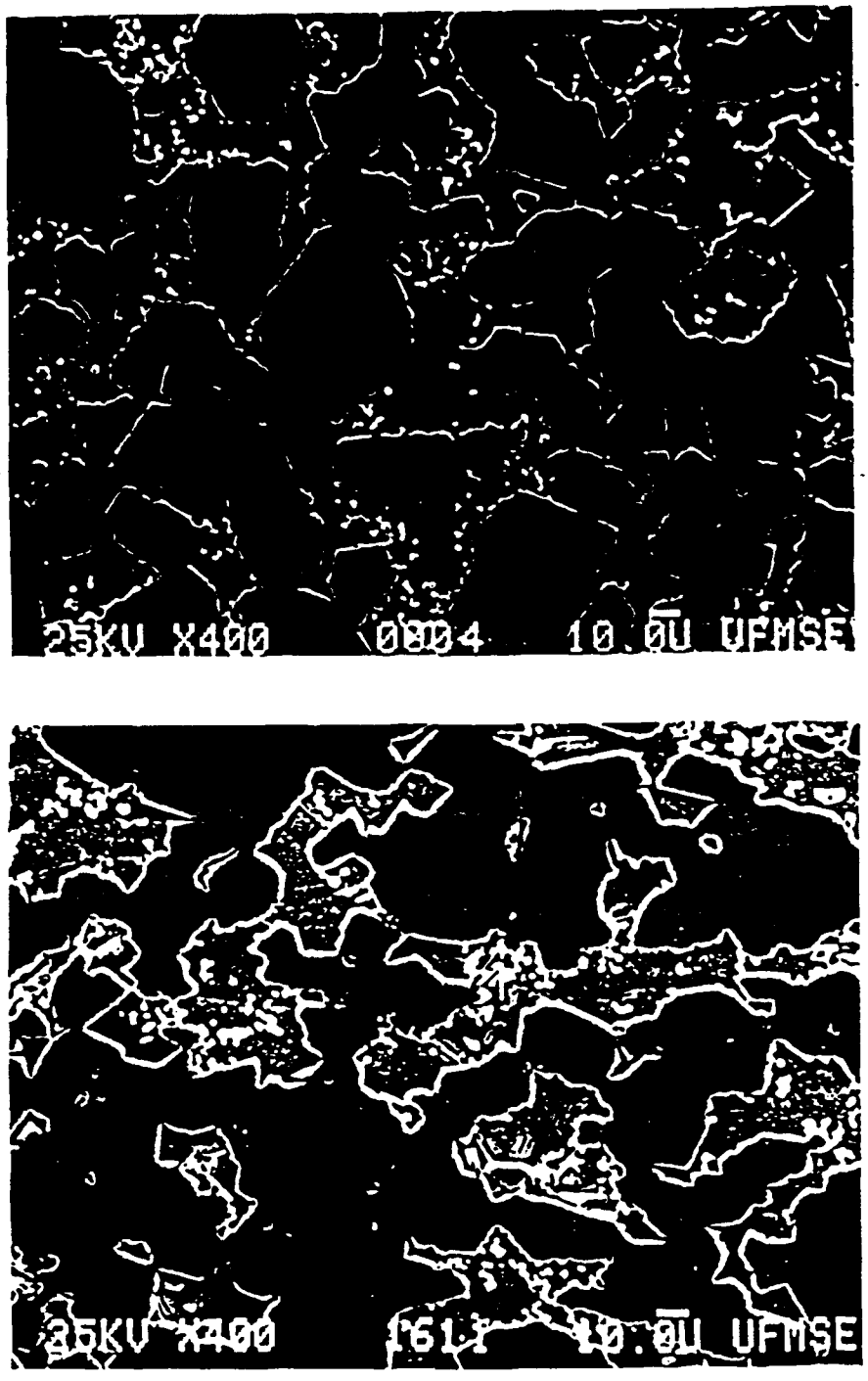

Figure 19 Scanning Electron Micrographs of Siliconized SiC Samples (a) without any Preceramic Polymer Infiltrations and (b) with Four Preceramic Polymer Infiltration/Pyrolysis (at 1575°C) Cycles

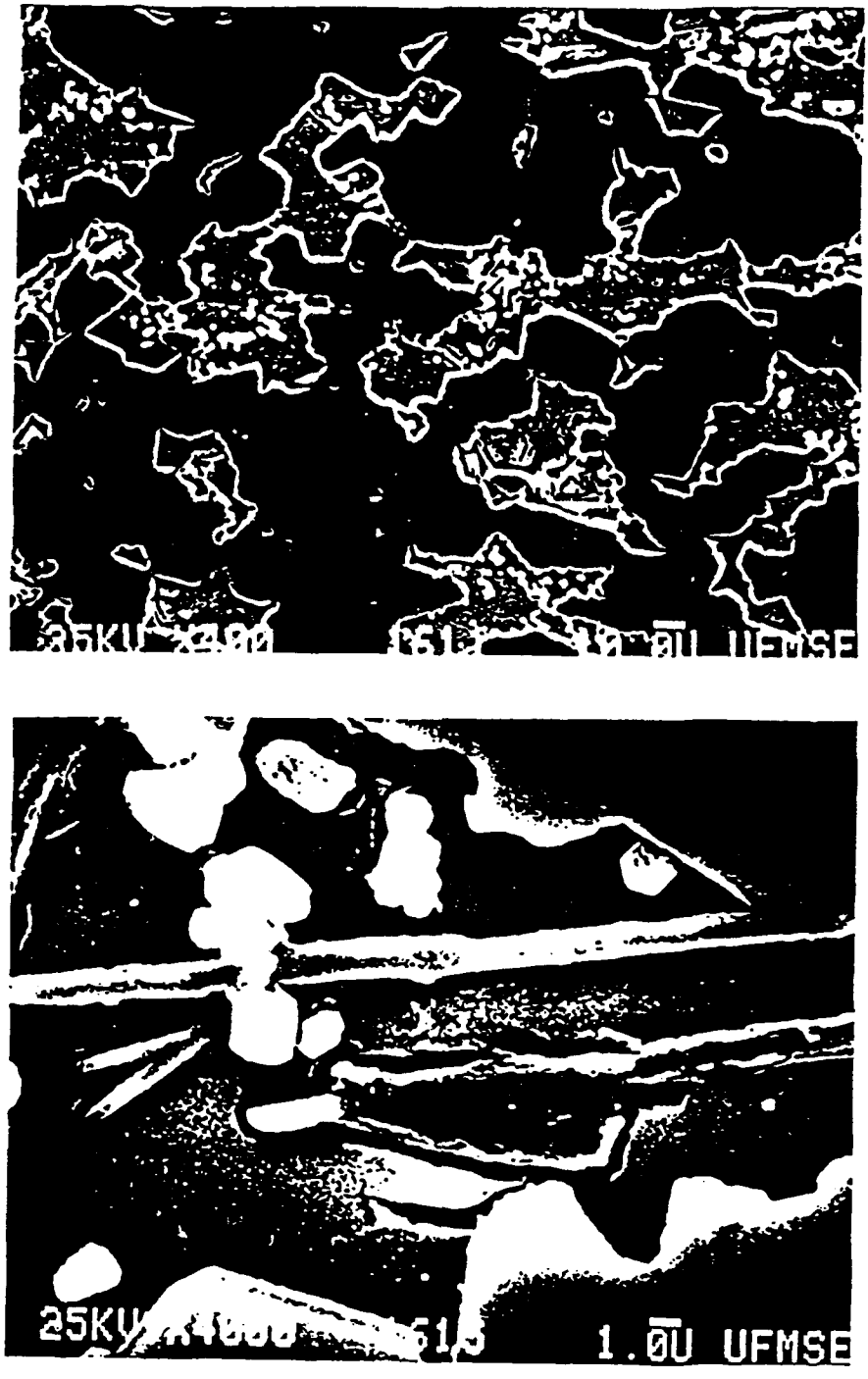

Figure 20 Scanning Electron Micrographs at (a) Low and (b) High Magnification of Whisker-Like Crystals in Siliconized SiC Samples Prepared with Four Preceramic Polymer Infiltration/Pyrolysis (at 1575°C) Cycles

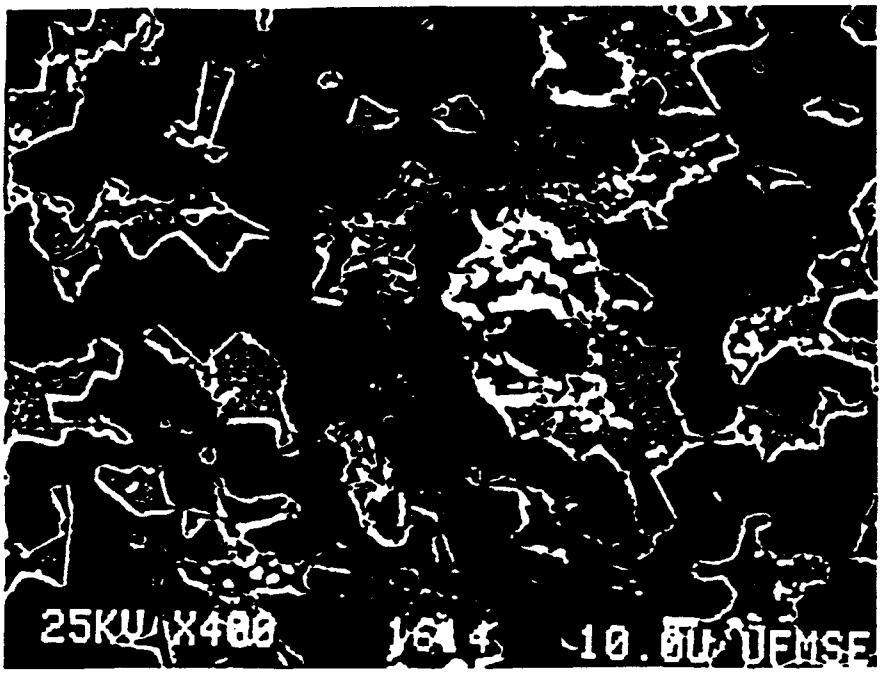

Figure 21 Scanning Electron Micrograph of Large Pores near the Surface of Siliconized SiC Sample with Four Preceramic Polymer Infiltration/Pyrolysis (at 1575°C) Cycles

II. Infiltration with Carbon Precursor

Characterization of Carbon Precursor

Figure 22 show the plots of shear stress vs. shear rate and viscosity vs. shear rate for the carbon precursor (organic resin solution). Except at very low shear rates, the flow behavior is approximately Newtonian and the viscosity is relatively low (although considerably higher than the ceramic precursor viscosity shown in Fig. 1).

Weight loss behavior was evaluated in order to determine the carbon yield. Low temperature heat treatment (95°C for 2 h, 140°C for 3 h) in air caused an ~21% weight loss due to solvent removal. Figure 23 shows TGA results (5°C/min in N_2) for the sample which had the initial low temperature heat treatment prior to analysis. The yield was ~62%, resulting in an overall yield (after both heating steps) of ~49% (Table 9).

Table 9 Residual Weight Percent after Heat Treatment

Max. Temp (°C)	Yield (Wt%) 1 atm Air	Yield (Wt%) 50-60 psi
140	79	96
1575	49	51

Another weight loss experiment was carried out in which the low temperature heat treatment was carried in a sealed container under a pressure of ~50-60 psi. The sample lost only ~4 wt% during this stage. This indicates that solvent removal is inhibited by using a closed container and a gas overpressure. The yield upon pyrolysis at high temperature (Figure 24) was ~53%, resulting in a similar overall yield (~51%) as in the first experiment (Table 9).

The advantage of using an overpressure during the low temperature heating stage was that bubble formation was minimized during solvent evaporation. This was considered desirable because bubbles could act as strength-degrading defects in final product. Thus, an overpressure of >50 psi was used in all subsequent experiments. In addition, a minimum temperature of 650°C was used in the subsequent pyrolysis step since Figures 23 and 24 show that a significant fraction of the weight loss occurs by this temperature.

The density of the carbon precursor was determined at various stages during processing. The as-received polymer solution had a density of ~1.24 g/cm^3. Table 10 gives the properties for bulk pyrolyzed samples which were initially heated for 3 hours at 140°C (under ~100 psi N_2) and then heated in nitrogen (at 5°C/min.) to the indicated temperatures and held at temperature for 2 hours.

It is apparent that a porous structure develops when solvent and other volatile products are removed during heat treatment. The open porosity and apparent density initially increase with the heat-treatment temperature, attain a maximum value at 800°C, and then decrease gradually at higher temperatures. The increase in the open porosity and apparent density in the region 600-800°C presumably results from increasing evolution of volatile products. The reason for decrease in the open porosity and apparent density above 800°C is unclear. The volume shrinkage measurement indicates that relatively little macroscopic densification occurs above this temperature. It is possible that open pore channels narrow and, to some extent, close off at the higher heat treatment temperatures.

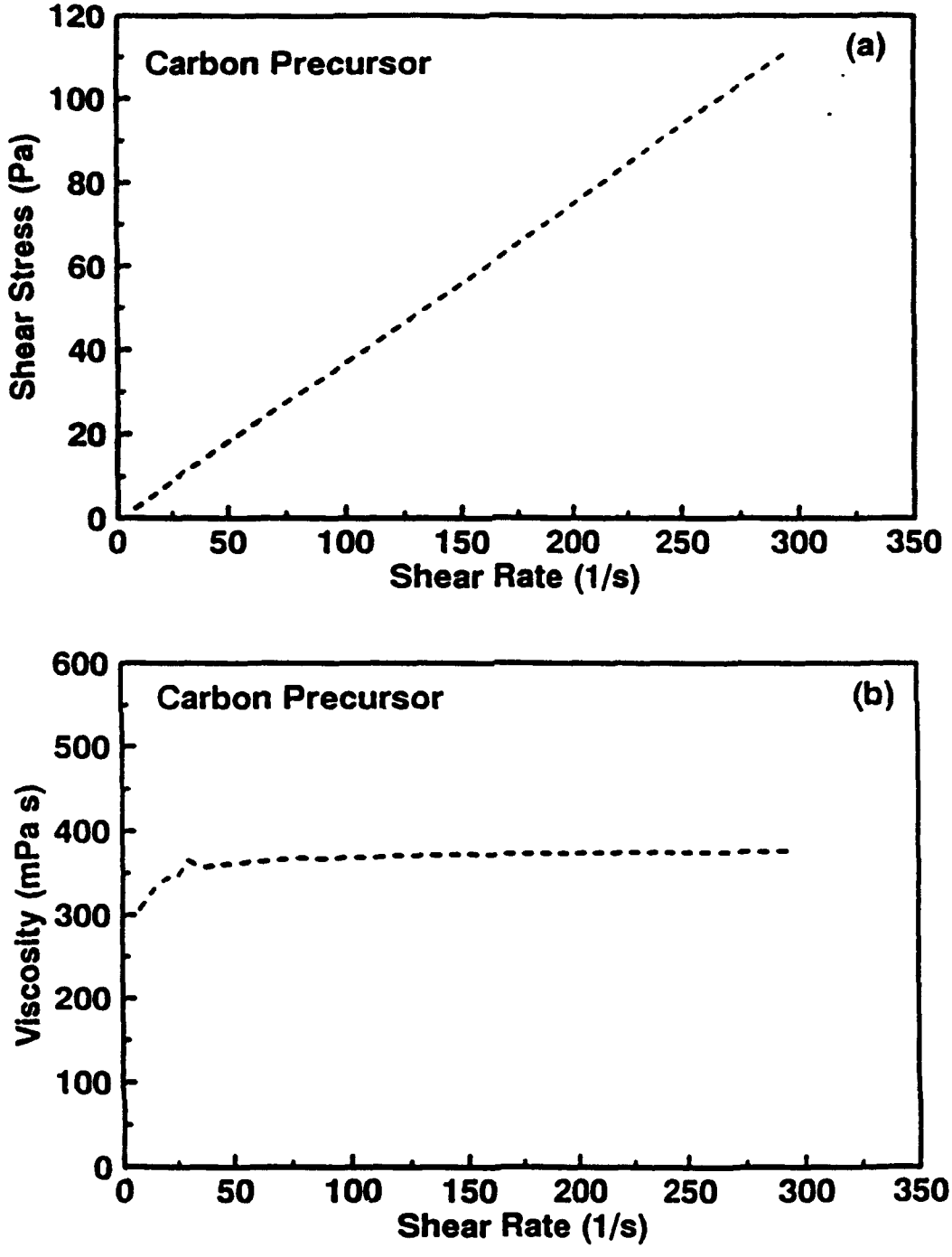

Figure 22 Plots of (a) Shear Stress vs. Shear Rate and (b) Viscosity vs. Shear Rate for Carbon Precursor

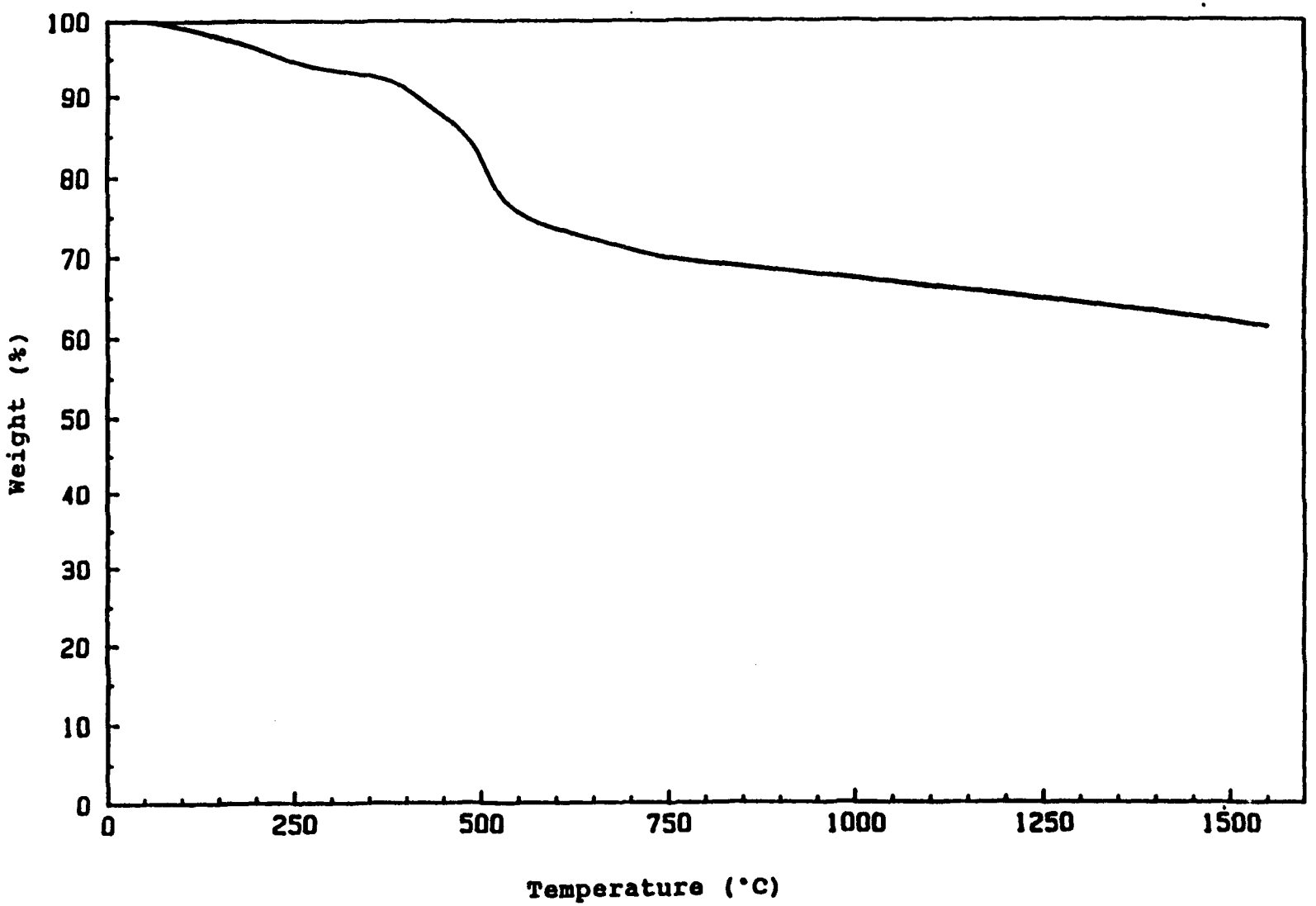

Figure 23 TGA Results for the Carbon Precursor (after Low Temperature Heat Treatment under Ambient (~1 atm) Pressure to Remove Solvent)

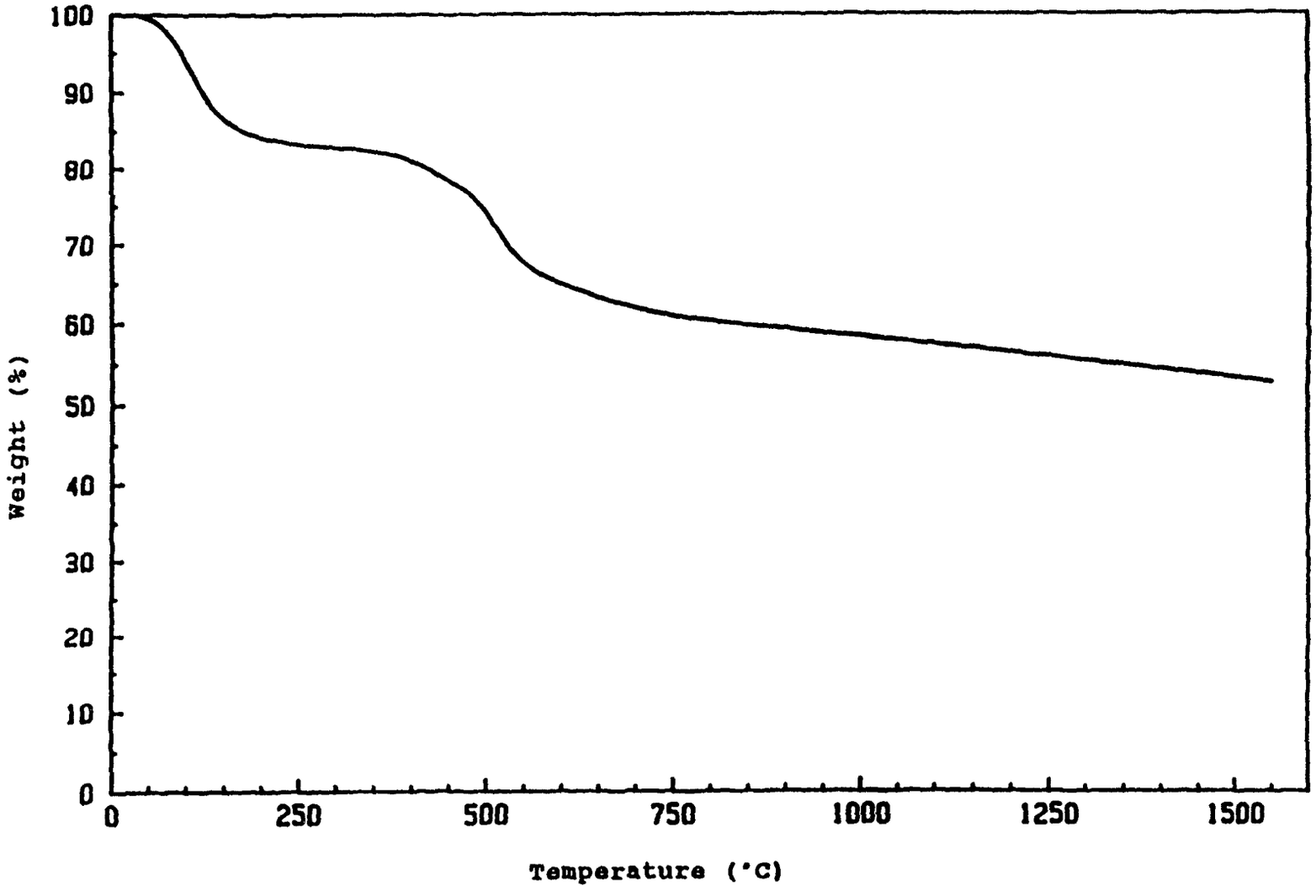

Figure 24 TGA Results for the Carbon Precursor (after Low Temperature Heat Treatment under a Pressure of 50-60 psi)

Table 10 Properties of Carbon Precursor after Pyrolysis at Different Temperatures in N_2

Pyrolysis Temp. (°C)	Open Porosity (%)	Bulk Density (g/cm^3)	Apparent Density (g/cm^3)	Volume Shrinkage (%)	Weight (%)
600	10.9	1.22	1.37	39.3	.53
800	19.2	1.40	1.73	50.1	49
1000	13.9	1.45	1.68	51.0	
1150	6.1	1.46	1.55	53.6	48

The results in Table 10 suggest that 800°C is a desirable pyrolysis temperature the following reasons: (1) The open porosity is near its maximum value. This is desirable if multiple infiltration cycles will be used. (2) Most of weight loss and volumetric shrinkage has occurred by this temperature. Thus, the final yield of SiC (after siliconization) is not likely to increase significantly by using a higher pyrolysis temperatures. (3) The low pyrolysis temperature allows one to use relatively inexpensive furnaces to accomplish decomposition of the carbon precursor.

Further experiments directed toward establishing the optimum pyrolysis temperature are described below.

Infiltration and Pyrolysis of Carbon Precursor

Effect of Multiple Infiltrations on Density, Porosity, and Weight Gain

The effects of the number of infiltrations and pyrolysis temperature on the density and porosity characteristics of the SiC preforms were investigated using the Archimedes displacement and mercury intrusion measuring techniques. The amount of time used to infiltrate the carbon precursor solution depended upon the number of infiltration cycles. In the initial experiments described below (Table 11-13), the times were 5 hours for the first infiltration, 15 hours for the second infiltration, and 45 hours for the third infiltration. These times were arbitrarily chosen. Later in this section, experiments designed to optimize the infiltration time are discussed.

Results for samples with different sizes are shown in Tables 11, 12, 13 and Figures 25, 26, 27. In Table 11, sample N was heat treated at 5°C/min in nitrogen to 650°C for 2 hours and samples K and M to 800°C for 2 hours. The values in parentheses represent the theoretical relative weight gains calculated using equation 9 in which the density of infiltrant, d_i, equals 1.24 g/cm^3 and the fractional weight loss, L, equals 0.49 and 0.51 for pyrolysis at 650°C and 800°C, respectively. The measured weight gains were smaller than the calculated values. This may be due to: (1) incomplete filling of the pores during infiltration and/or (2) higher weight losses during pyrolysis than observed in the experiments on the bulk samples.

In order to evaluate the effect of carbon precursor infiltrations on the flexural strength and fracture toughness, larger samples (25x13x3.5 mm) were infiltrated using the same procedures for the samples described in Table 11. Comparison of the results in Tables 11 and 12 shows that the carbon precursor infiltration process can be controlled so that consistent weight gain and density values are obtained for both smaller and larger samples.

Table 11 Properties of Small Size (10x10x2.5mm) Test Samples Infiltrated with Carbon Precursor*

Sample	N	K	M
Uninfil.			
Open Porosity	34.2	34.2	36.7
Bulk Density	2.10	2.10	2.02
App. Density	3.20	3.20	3.20
Infil. 1			
Open Porosity	22.7	24.7	26.4
Bulk Density	2.28	2.27	2.20
App. Density	2.95	3.01	2.99
Wt. gain(%)	8.6(10.3)	8.1(9.9)	8.9(11.0)
Infil. 2			
Open Porosity		17.5	19.5
Bulk Density		2.39	2.33
App. Density		2.90	2.89
Wt. Gain %		5.3(6.6)	5.9(7.3)
Cumul. Gain		13.8	15.3
Infil. 3			
Open Porosity			13.8
Bulk Density			2.42
App. Density			2.81
Wt. Gain %			3.9(5.1)
Cumul. Gain			19.8

* Low temperature heat treatment under ~50-60 psi N_2 followed by pyrolysis at 650°C or 800°C (see text).

Table 12 Properties of Flexural Test Bars (25x13x3.5mm) Infiltrated with Carbon Precursor*

Sample	N7	N6	N5	N3	N4	N8
Unifil.						
Wt.(g)	2.4012	2.4641	2.5850	2.2885	2.7670	2.6090
Open Porosity	34.2	34.0	34.2	34.2	34.1	34.3
Bulk Density	2.10	2.11	2.10	2.10	2.10	2.10
App. Density	3.20	3.19	3.20	3.19	3.19	3.19
Infil. 1						
Wt.(g)	2.5982	2.6632	2.7976	2.4643	2.9871	2.8192
Open Porosity	24.0	23.7	23.8	24.4	24.4	24.2
Bulk Density	2.28	2.29	2.28	2.27	2.28	2.27
App. Density	2.99	3.00	2.99	3.01	3.01	3.00
Cumu. Gain%	8.6	8.5	8.6	8.1	8.6	8.1
Infil. 2						
Wt. (g)				2.5971	3.1450	2.9590
Open Porosity				16.9	16.8	17.4
Bulk Density				2.39	2.40	2.39
App. Density				2.88	2.89	2.90
Wt Gain %				5.3	5.3	5.3
Cumu. Gain%				13.8	14.3	13.8

* Low temperature heat treatment under ~50-60 psi N_2 followed by pyrolysis at 800°C.

Table 13 Properties of Discs (~3.5 mm Thick, ~40 mm Diameter) Infiltrated with Carbon Precursor*

Atmosphere	1 Atm. Air		100 Psi N_2	
Sample	D1	D2	D5	D6
Unifil.				
Wt. (g)	16.6713	16.6777	18.8651	16.9090
Open Porosity	34.7	34.6	34.7	34.7
Bulk Density	2.09	2.10	2.09	2.09
App. Density	3.20	3.20	3.21	3.20
Infil. 1				
Wt. (g)	17.8313	17.7689	20.5083	18.3599
Open Porosity	26.2	26.7	24.1	24.1
Bulk Density	2.24	2.23	2.27	2.27
App. Density	3.04	3.04	2.99	3.00
Cumul. Wt Gain%	7.3	6.5	8.7	8.6
Infil. 2				
Wt. (g)	18.5023	18.3361	21.6827	19.3557
Open Porosity	21.6	22.6	16.4	16.5
Bulk Density	2.32	2.30	2.40	2.40
App. Density	2.96	2.97	2.88	2.87
Cumul. Wt Gain %	11.0	9.9	14.9	14.5

* Low temperature heat treatment followed by pyrolysis at 800°C.

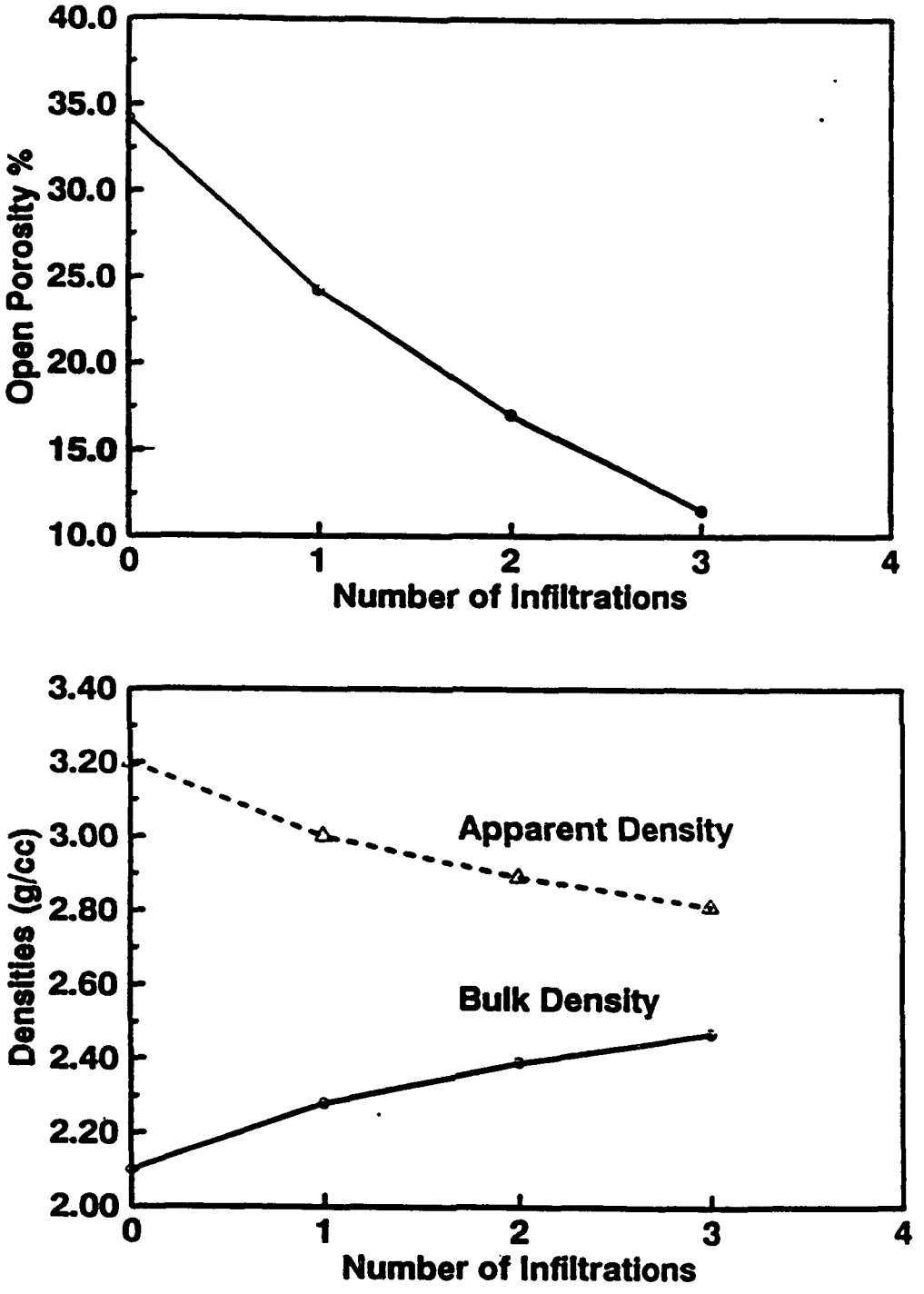

Figure 25 Plots of Average Open Porosity, Bulk Density, and Apparent Density as a Function of Number of Infiltrations for Samples Pyrolyzed at 800°C

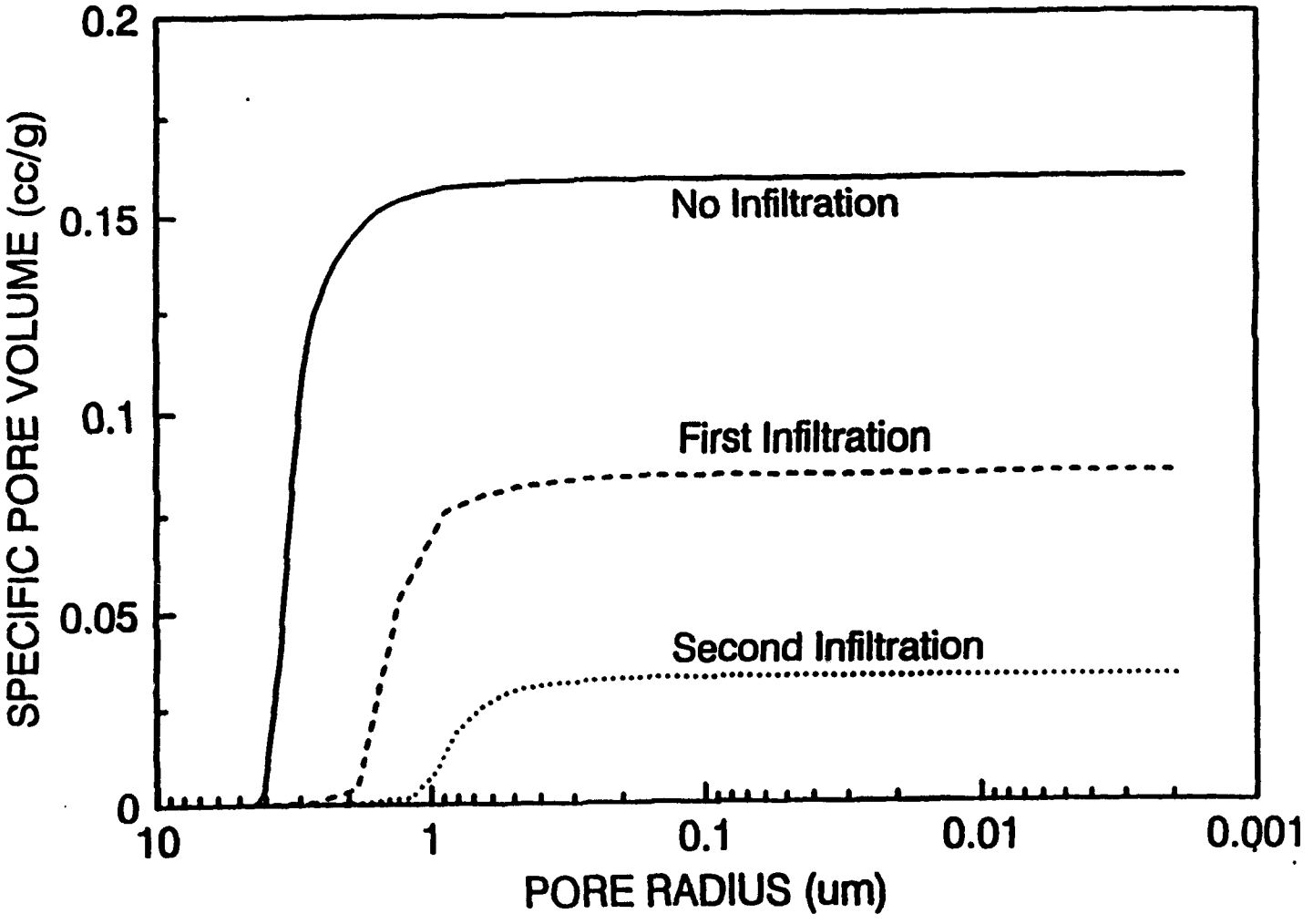

Figure 26 Plots of Specific Pore Volume vs. Pore Radius (Obtained by Mercury Porosimetry) for Samples with Indicated Number of Carbon Precursor Infiltration/Pyrolysis (at 650°C) Cycles

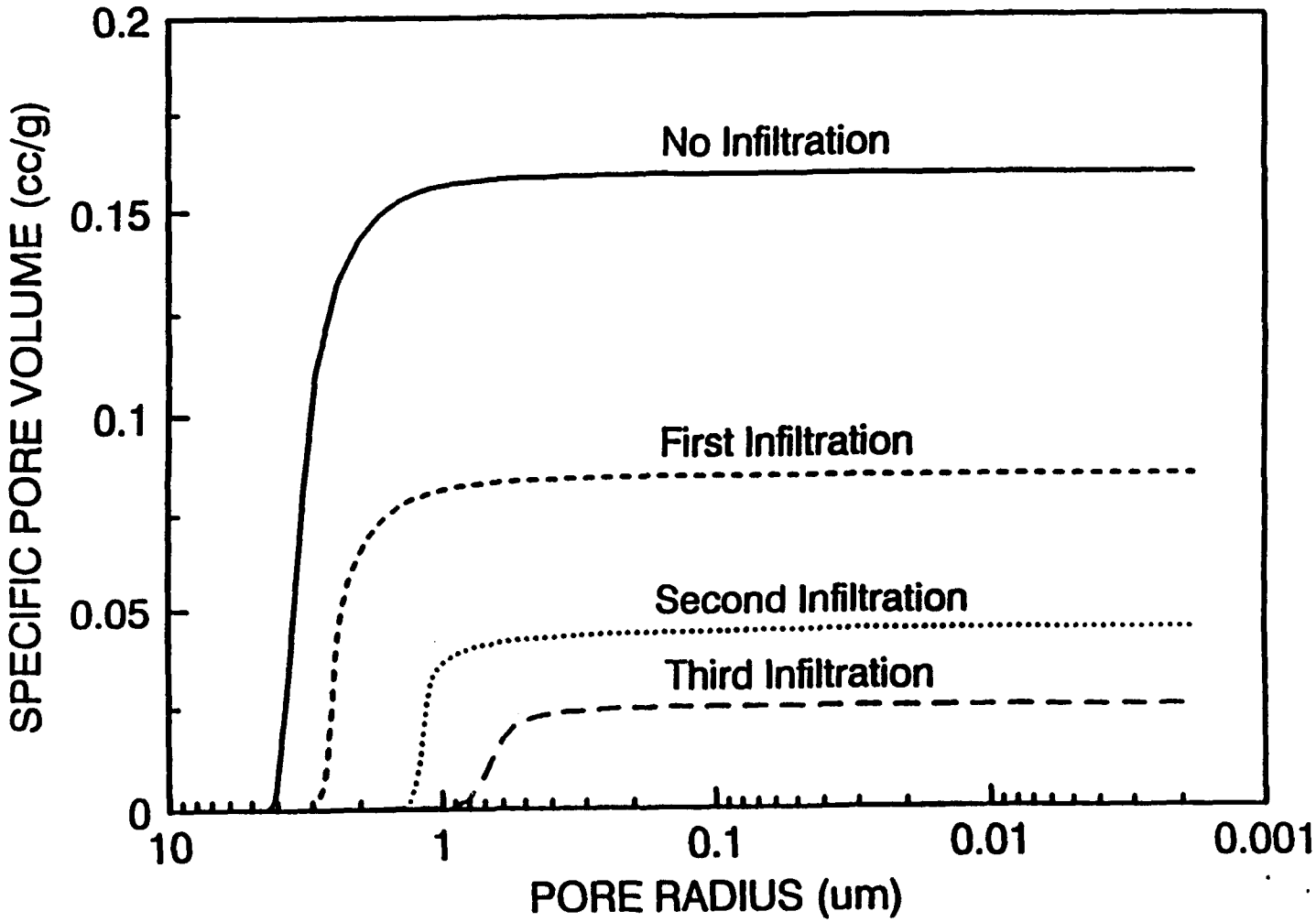

Figure 27 Plots of Specific Pore Volume vs. Pore Radius (Obtained by Mercury Porosimetry) for Samples with Indicated Number of Carbon Precursor Infiltration/Pyrolysis (at 800°C) Cycles

In order to evaluate the effect of carbon precursor infiltrations on the polishability of siliconized silicon carbide composites, four large disk-shaped samples (40x5.5mm) were infiltrated. Also, the effect of pressure during the low temperature (140°C) heat treatment step on the subsequent weight gain and density values after pyrolysis was investigated. Table 13 shows results for samples prepared using pressures of 1 atmosphere air (i.e., ambient conditions) and 100 psi N_2. It is evident that weight gain and bulk density values are larger if the low temperature heat treatment step is carried out under pressure. It is presumed that the higher pressure reduces the migration of polymer solution out of the preform pore channels during the heat treatment. Table 13 also shows that the density and weight gain values for the large samples (infiltrated under pressure) are consistent with values obtained for smaller samples (Table 11 and 12).

Figure 25 shows that the open porosity and apparent density decrease and the bulk density increases with increasing number of carbon precursor infiltrations for samples pyrolyzed at 800°C. These results are due to the incorporation of carbon in the pores after the infiltration/pyrolysis process.

Figures 26 and 27 show mercury porosimetry results for samples prepared with multiple carbon precursor infiltration/pyrolysis cycles; pyrolysis temperatures were 650°C and 800°C, respectively. As observed with the samples infiltrated with the ceramic precursor, the cumulative pore size distribution curves shift to smaller pore radii. Table 14 compares the porosity results determined by the Archimedes immersion technique and mercury porosimetry. The difference in open porosity values between the two methods increases with the number of carbon precursor infiltrations, suggesting that the pyrolyzed material has small pores which can not be filled by the mercury intrusion method. (At the maximum pressure (60,000 psi = 410 MPa) used in mercury porosimetry, the smallest pore channel diameter that can be penetrated is ~36 Å, assuming an Hg surface tension of 480 dyne/cm and a contact angle of 140°[1]). This hypothesis is supported by gas adsorption measurements on other glassy carbon materials prepared by pyrolysis [Fit70]. By using different adsorbents with various molecular size, Fitzer et al. found that the micropores in the pyrolyzed carbons were of uniform size, having a radius of ~12.5Å after heat treatment to 1200°C and of ~17.5Å after heat treatment to 3000°C. Most of the pore entrances were ~4-5Å. In the present study, it is interesting to note that virtually none of the open porosity detected by mercury porosimetry is smaller than ~0.1 μm. This is consistent with the hypothesis that pores formed within the pyrolyzed product are highly uniform and are all less than ~35Å diameter. The existence of these fine pores probably accounts for the observation (see Table 11) that the measured weight gains after infiltration/pyrolysis are less than the calculated weight gains. It is unlikely that the polymer solution (which has a relatively high viscosity) can penetrate the fine pores. Table 11 shows that the discrepancy between the measured and calculated weight gain is observed after the first infiltration/pyrolysis cycle. Thus, inaccessible pore channels develop after the first pyrolysis cycle. This is also illustrated by the results in Table 14.

Optimization of the Infiltration/Pyrolysis Process

The samples described in the previous section were prepared using arbitrary infiltration times. In order to improve the efficiency of the process, experiments were carried out to determine the optimum infiltration for samples given two infiltration/pyrolysis treatments. In addition, the effect of pyrolysis temperature on the subsequent infiltration rate was determined.

---

1 In fact, the minimum pore channel diameter accessible to mercury porosimetry may be larger than ~36Å because the contact angle may actually be larger than 140° for a carbon-infiltrated SiC preform. For example, Lowell and Shields [Low84] report a contact angle of ~155° for mercury on carbon substrates.

Table 14 Porosity Values for Carbon Infiltrated Samples from Archimedes Immersion and mercury Intrusion methods

Number of infil.	0	1	2	1	2	3
Pyrolysis Temp.(°C)		650	650	800	800	800
Open Porosity from Archimedes (%)	34.0	22.3	13.8	23.4	16.9	12.6
Open Porosity from Hg Intrusion (%)	33.8	20.0	8.5	20.4	11.3	6.5
Median Pore Size(μ) from Hg Intrusion	3.21	1.44	0.84	2.43	1.16	0.66
Total Porosity (%)	34.1	24.4	15.9	23.8	18.1	14.4
Open Pore Fraction from Archimedes	0.997	0.914	0.868	0.983	0.934	0.875
Open Pore Fraction from Hg Intrusion	0.991	0.820	0.535	0.857	0.624	0.451

Note: (1) The total Porosity was calculated by the equation:

$$P = 100\,[1 - (d_0/d_{SiC}) - (d_1-d_0)/d_c] \qquad (7)$$

where:

d_0 = bulk density before infiltrations
d_1 = bulk density after infiltrations
d_{SiC} = theoretical density of SiC (3.21 g/cm^3)
d_c = 1.77 g/cm^3 (density of carbon by helium pycnometry determined on a crushed powder sample pyrolyzed at 800°C)

(2) The apparent density values measured by the Archimedes method were used as the true density values in calculating the Hg intrusion open porosity values.

Theoretical estimates can be made for the (1) maximum amount of weight that can be gained during the infiltration process (i.e., before pyrolysis) and (2) amount of time required to complete the infiltration process.

Assuming that all pores in the preform are filled, the weight gain value after infiltration should be

$$\text{Wt\%} = 100 \text{ (weight of liquid infiltrated/weight of porous SiC preform)}$$

$$= 100\ P\ d_l/d_b \qquad (14)$$

where P is volume fraction of open pores, d_l is density of the liquid precursor (1.24 g/cm^3), and d_b is bulk density of the sample.

The approximate time needed to complete the infiltration can be estimated from the modified Washburn equation:

$$t = (2\ d^2\ \eta)/(r\ \sigma\ \cos\Theta) \qquad (15)$$

where

- d = infiltration depth (for complete infiltration d = 1/2 sample thickness)
- η = viscosity of the liquid precursor (~360 mPa s)
- r = average radius of pores
- σ = surface tension (or specific surface energy) of the liquid precursor
- t = infiltration time
- Θ = contact angle of the liquid precursor on the solid preform surfaces

Assuming that $\cos\Theta = 1$ (i.e., the liquid precursor completely wets the solid preform) and $\sigma = 40$ dyn/cm (= 0.04 J/m^2, estimated from published values for phenol solutions [Wea74]), the relationship between infiltration time and pore size for different thickness can be derived (Figure 28).

The weight gain as a function of time for the first infiltration is shown in Figure 29. Different symbols in the graph represent different samples. Each sample had ~34% open porosity and a thickness of ~3 mm. The dashed line represents theoretical weight gain calculated using equation 14. Clearly, the infiltration rate is very high due to the large pore sizes (3.2 μm median radius according to Figure 9) in the preforms. The weight gain reaches the theoretical value of about 20% after only 15 seconds. (The variations in weight gain at longer times are within the range of experimental errors.) However, to ensure complete filling of pores, an infiltration time of 5-10 minutes was used in future experiments, i.e., for first-time infiltrations into 3mm thick porous preforms.

The weight gain as a function of time was monitored during a second infiltration process on samples which were pyrolyzed at different temperatures (650-1000°C) after the first infiltration. The results (see Figure 30 and Table 15) show that the infiltration rate for second infiltration depends upon the temperatures at which the samples were pyrolyzed. This is because the pore size distribution and volume of porosity in the preform depend on the pyrolysis temperature.

Porosity and density characteristics determined by the Archimedes and mercury porosimetry methods are shown in Table 16 and Figure 31, respectively. The Archimedes measurements (Table 16) show that the open porosity and apparent density increase with increasing pyrolysis temperature after the first infiltration/pyrolysis process. A similar result can be observed in Table 11 by comparing samples N and K. The increase in apparent density can be attributed to the increased true density of the carbonaceous residue at higher pyrolysis temperatures. There are several possible reasons for the larger amount of open porosity. First, there is greater volumetric shrinkage during pyrolysis at higher temperatures due to (i) increase in true density of the carbonaceous residue and (ii) larger weight loss. Second, samples pyrolyzed at lower temperatures may form more

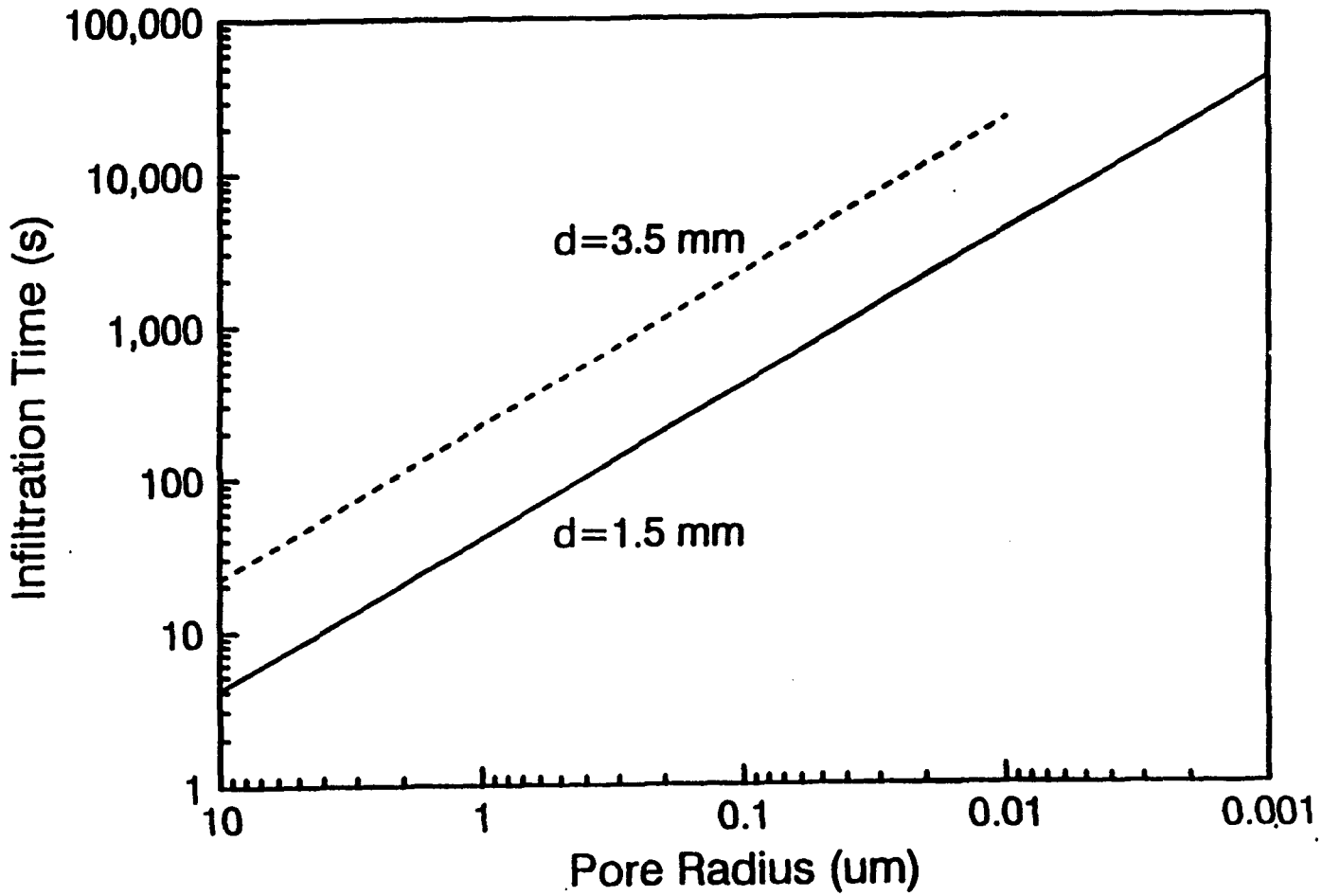

Figure 28 Plot of Time Required for Complete Infiltration as a Function of Pore Radius for Samples with Two Thicknesses (d = 1/2 of the Sample Thickness)

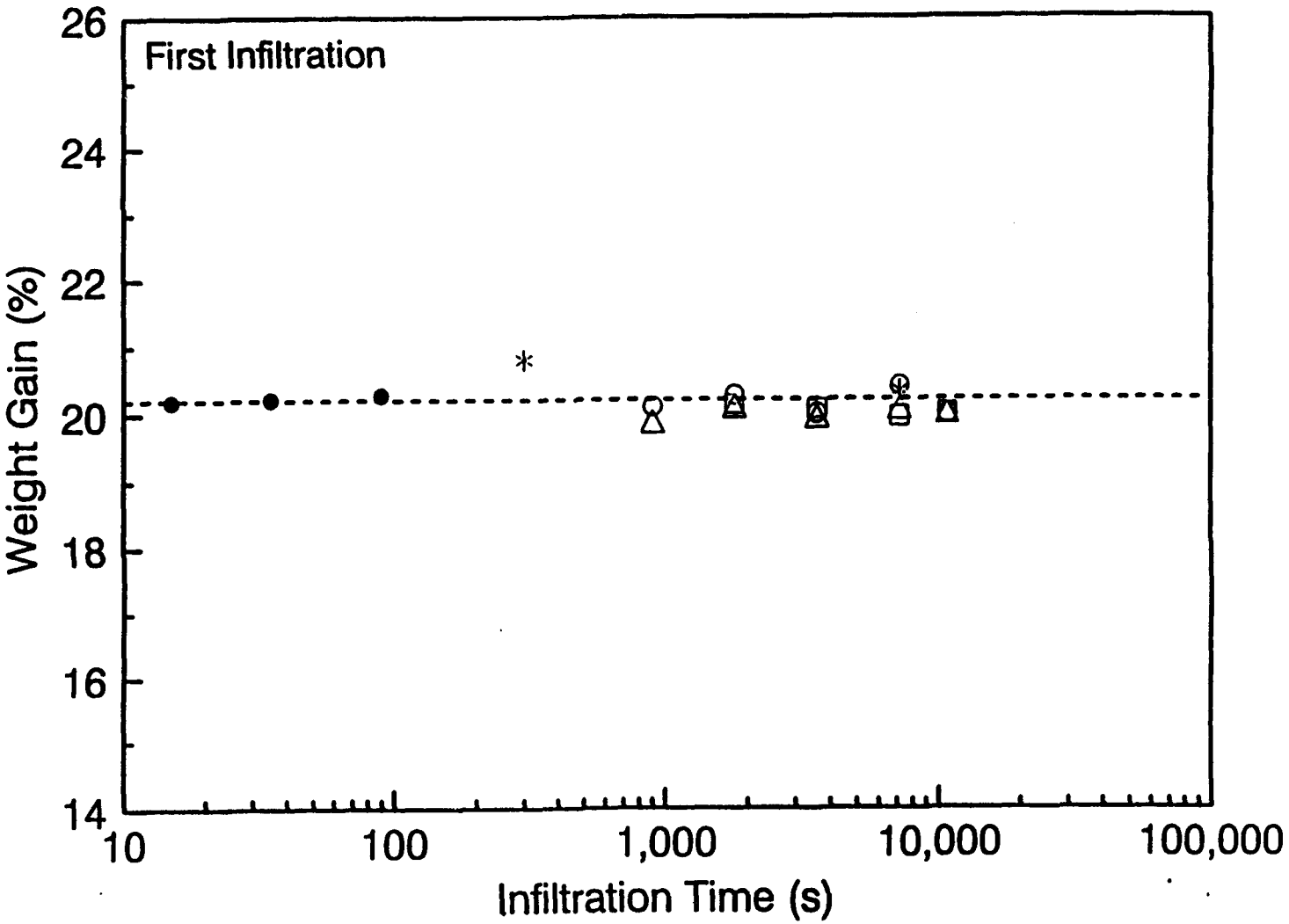

Figure 29 Plot of Weight Gain vs. Time for First Infiltration

Table 15 Effect of Infiltration Time and Pyrolysis Temperature on Weight Gain (%)

Sample	T1	T2	T3
Pyrolysis T (°C)	650	800	1000
25 sec	5.2	10.1	11.0
45 sec	5.7	10.3	11.4
1.5 min	6.3	10.7	11.7
3.5 min	6.4	10.9	12.1
15 min	7.5	11.3	11.8
1.5 hr	7.8	11.1	11.6
4 hr	9.1	11.2	11.9
20.5 hr	10.9	11.7	12.0
Theoretical Value	11.3	12.6	13.0
Time for >90% of theoretical value	12 h	15 min	1.5 min

Table 16 Effects of Number of Infiltrations and Pyrolysis Temperature on Properties

Sample	T1	T2	T3
Pyrolysis Temp. (°C)	650	800	1000
Before Infiltration			
Open Porosity %	34.1	34.2	34.2
Bulk Density	2.10	2.10	2.09
Apparent Density	3.19	3.19	3.18
1st Infiltration			
Open Porosity %	21.1	23.4	24.2
Bulk Density	2.30	2.30	2.30
Apparent Density	2.92	3.00	3.04
2nd Infiltration			
Open Porosity %	13.8	16.8	17.3
Bulk Density	2.43	2.42	2.42
Apparent Density	2.81	2.90	2.93
Hg Porosimetry			
Open Porosity (%)*	8.5	10.5	11.2
Median Pore Size(μm)	0.84	1.2	1.1

* Open porosity was calculated by assuming the true density was equal to the apparent density determined from the Archimedes immersion method.

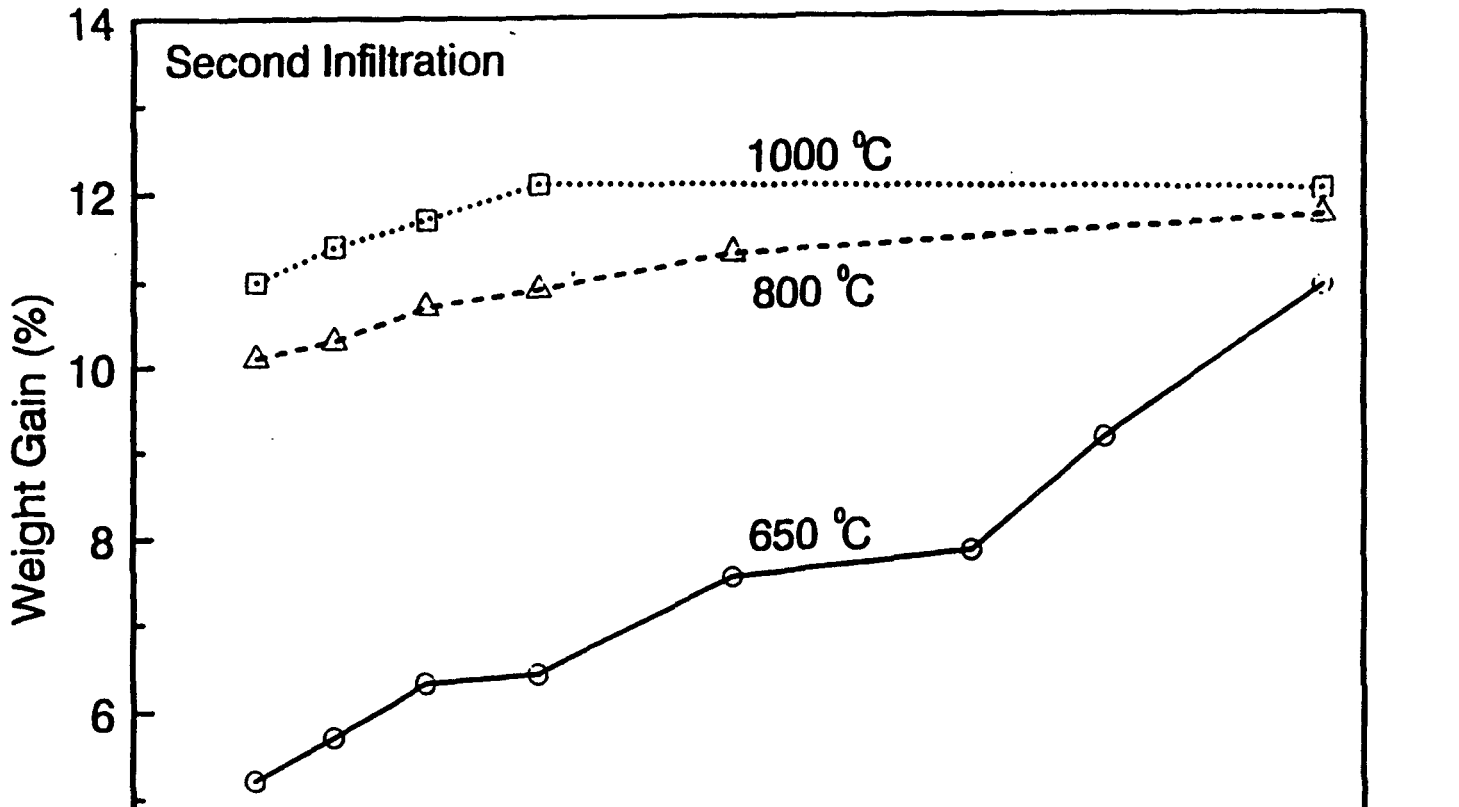

Figure 30 Plot of Weight Gain vs. Time for Second Infiltration after Different Pyrolysis Temperatures

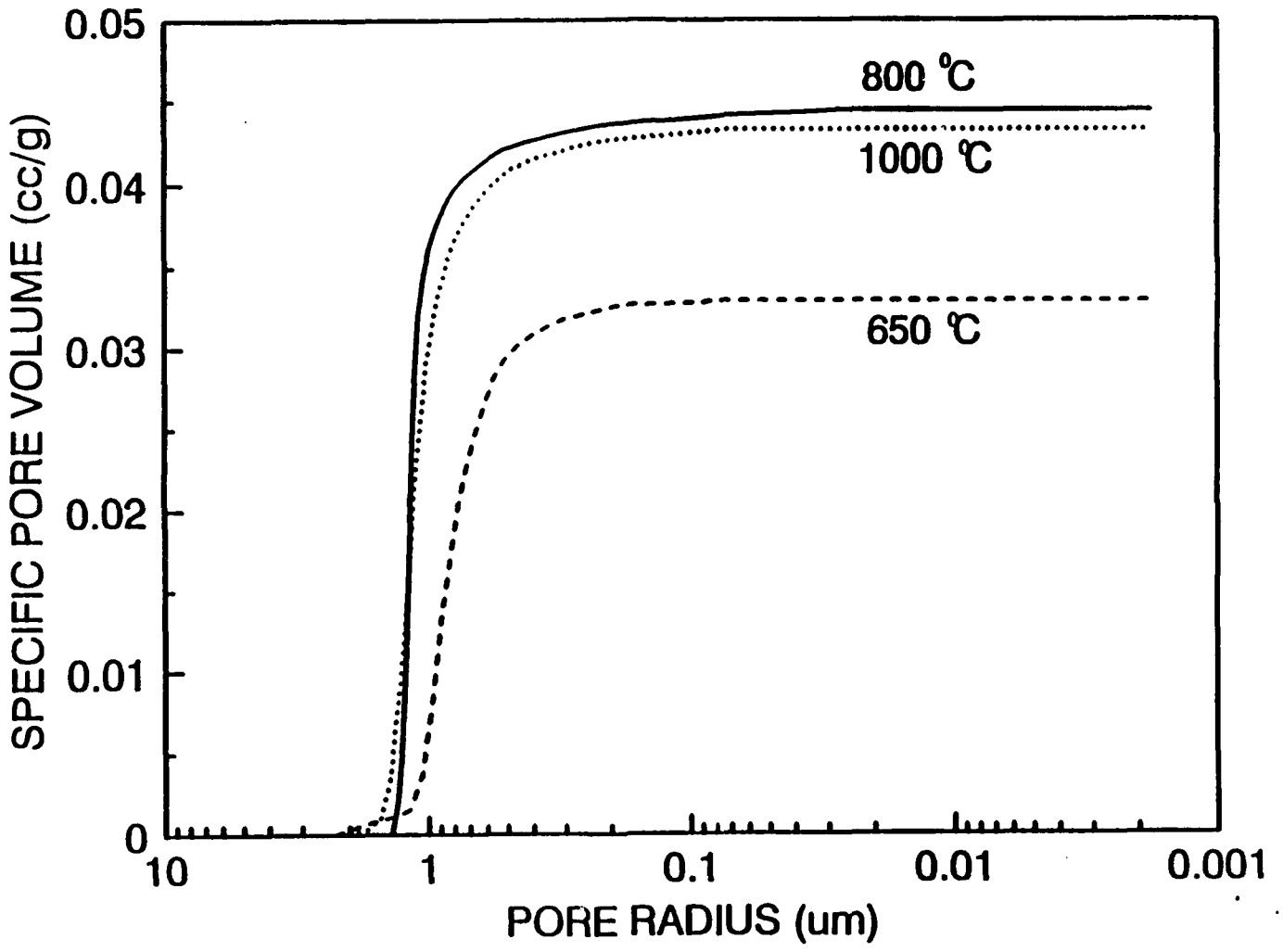

Figure 31 Plots of Specific Pore Volume vs. Pore Radius (Obtained by Mercury Porosimetry) for Samples with Two Carbon Precursor Infiltration/Pyrolysis Cycles Using Varying Pyrolysis Temperatures

small pores that are not accessible to penetration during the Archimedes open porosity measurement. The same trend in open porosity and apparent density with pyrolysis temperature is observed in Table 16 from Archimedes measurements carried out on samples which have received two infiltration/pyrolysis treatments. It is also noted that the bulk densities are increased and the apparent densities and open porosities are decreased relative to the values after the first infiltration/pyrolysis cycle. This reflects the increased content of carbonaceous material in the SiC preform after two infiltration/pyrolysis treatments.

Mercury porosimetry measurements were made on the samples which had received two infiltration/pyrolysis treatments. The results are consistent with the Archimedes measurements in the sense that the 800- and 1000°C-pyrolyzed samples have similar amount of open porosity, while the 650°C-pyrolyzed sample has a lower amount of open porosity. However, as discussed earlier in regards to Table 14, a smaller amount of porosity is accessible to mercury penetration (i.e., compared to water penetration). Therefore, the amount of open porosity measured by mercury porosimetry is much less than that measured by the Archimedes method (Table 16).

The differences in the pore volume and pore size shown in Figure 31 and Table 16 are probably not the primary reason for the differences in carbon precursor infiltration rate shown in Figure 30. Instead, it is believed that the differences arise primarily from differences in the size of the fine pores (~40 Å or less) which are not detected by mercury porosimetry. It is interesting to note ~50% of the weight gained during infiltration of the 650°C-pyrolyzed sample occurs within ~30-60 seconds. According to Figure 28, such rapid infiltration is consistent with the presence of large pores in the preform (i.e., the micron-size pores detected by mercury porosimetry). The ~50 wt% gain in the initial seconds of the infiltration process is consistent with the fact the large pores only comprise a fraction of the total porosity. Table 16 shows that the large pores (accessible by mercury porosimetry) are only ~62% of the "total" open porosity measured by the Archimedes method[2]. Table 16 shows that the 800- and 1000°C-pyrolyzed samples also contain a large fraction of open pores that are not accessible to mercury porosimetry penetration (e.g., ~36%). However, Figure 30 showed that a much greater percentage of the porosity was penetrated rapidly in these samples during the second carbon precursor infiltration. A possible explanation for this behavior is that the size of the finest pores (i.e., those not detected by mercury porosimetry) is substantially larger in the samples pyrolyzed at the higher temperature. This is reasonable based on previous studies [Fit70] which show that heat treatment significantly increases the pore sizes in "glassy" carbons.

Based on criteria of short infiltration time, large weight gain, and low cost, the optimum pyrolysis temperature appears to be 800°C for samples used in this study. However, for very thick samples, it may be beneficial to use pyrolysis at 1000°C because of the higher infiltration rate (Figure 30 and Table 15).

---

2 In fact, the total porosity may be somewhat higher than that measured by the Archimedes measurement (i.e., some pores may be inaccessible even to water penetration). Therefore, the larger pores probably comprise a little less than the ~62% value cited above.

Infiltration of Combined Precursors

Combined successive infiltrations using both carbon and ceramic precursors were carried out to explore the possibility of obtaining improved SiC yield. Table 17 summarizes the infiltration conditions and Archimedes measurement results.

In sample H, the first infiltration/pyrolysis treatment was carried out with the carbon precursor and the second treatment was carried out with the ceramic precursor. The weight gain after the second treatment was much lower than the theoretical value (given in parentheses in Table 17). This is probably due to poor filling of the vinyl silazane during the infiltration process. There may have been difficulting in penetrating the relatively large vinyl silazane molecules into the ultrafine pores (i.e., those that cannot be detected by mercury porosimetry) created after infiltration/pyrolysis of the carbon precursor. It is also possible that the vinyl silazane does not wet the carbon-infiltrated SiC preform as well as an uninfiltrated preform.

In contrast to sample H, both infiltration/pyrolysis treatments yielded weight gains close to the theoretical values for sample J. However, a large number of closed pores formed, which is evident from the significant decrease in both open porosity and apparent density values measured by the Archimedes immersion method. A large amount of closed porosity is obviously harmful to both further precursor infiltrations and the final siliconization process.

Table 17 Infiltration Conditions and Archimedes Measurement Results for Combined Infiltrations with Carbon and Ceramic Precursors

Sample	H	J
Uninfiltrated		
Open Porosity	37.0	34.3
Bulk Density	2.02	2.10
App. Density	3.20	3.20
Infil. 1		
Precursor	Carbon	Silazane
Time (hr)	5	2
Pyrolysis Temp.(°C)	800	1000
Open Porosity	26.6	24.3
Bulk Density	2.21	2.31
App. Density	3.01	3.06
Wt Gain	9.4(11.1)	10.0(9.8)
Infil. 2		
Precursor	Silazane	Carbon
Time (hr)	8	15
Pyrolysis Temp.(°C)	1000	800
Open Porosity	23.0	5.3
Bulk Density	2.27	2.46
App. Density	2.95	2.60
Wt Gain	2.7(7.2)	6.2(6.4)
Cumul. Gain	11.8	16.7

Characterization of Siliconized SiC Composites

Siliconized SiC with Infiltration of Carbon Precursor

Both infiltrated and uninfiltrated samples were siliconized to determine the effect of SiC content on mechanical and optical properties. Infiltrated samples prepared under various processing conditions (i.e., varying pyrolysis temperature, number of infiltrations) were siliconized to determine effect on the amount of SiC formed.

Table 18 gives the properties of siliconized SiC composites with different number of carbon precursor infiltration/pyrolysis cycles. Open Porosity, bulk density, and apparent density were determined by the Archimedes immersion method. The volume of "free" (unreacted) silicon was calculated using the "rule of mixtures" (equation 11). The last column in Table 18 gives measured free silicon values determined by quantitative microscopy. These values show good agreement with the values calculated from the Archimedes density data. This, together with the very low open porosity for samples with up to two carbon precursor infiltrations, indicates that fully dense siliconized SiC composites were obtained.

Table 19 shows apparent density results for siliconized flexural strength test bars. Also shown are several calculations regarding the free silicon content of the siliconized composites, the "new" SiC formed during siliconization process, and the weight loss of carbon during siliconization. For comparison, results for the samples in Table 18 are also included. The free silicon content was determined using the measured apparent density and equation 11. The other calculations in Table 19 are discussed in more detail below. Figure 32 plots the change in average bulk density and average SiC content with the number of infiltrations for the samples in Table 18 and 19. It is clear that infiltration with the carbon precursor results in significant increases in density and SiC content.

The new SiC formed during siliconization (column six of Table 19) was calculated by subtracting the free silicon content from the open porosity of the original porous SiC preform. These calculations show that new SiC is formed much more efficiently with the carbon precursor infiltration/pyrolysis

Table 18 Properties of Siliconized SiC Samples Prepared with Different Number of Carbon Precursor Infiltration/Pyrolysis Cycles*

Name	Infil. Times	Open Pore (%)	Bulk Density (g/cm^3)	Apparent Density (g/cm^3)	Free Si Calculated (%)	Free Si Measured (%)
X	0	0.3	2.89	2.90	34.5	33.6
N	1	0.0	3.03	3.03	19.5	18.8
K	2	0.0	3.13	3.13	8.0	8.9
M	3	6.1	2.60	2.70		

* Characteristics of samples N, K, and M prior to siliconization are given in Table 11.

Table 19 Silicon Content and "New" SiC Formed for Siliconized Samples*

Name	Number of Infiltration	Bulk Density (g/cm^3)	Apparent Density (g/cm^3)	Free Si[1] Content (%)	New SiC[2] Formed (%)	New SiC[3] Expected (%)	Carbon[4] Loss (%)
X		2.89	2.90	34.5			
N1	0	2.90	2.90	34.5			
N2		2.89	2.89	35.6			
N		3.03	3.03	19.5	14.7	18.9	22.2
N6	1	3.03	3.03	19.5	14.5	18.9	23.2
N7		3.03	3.03	19.5	14.7	18.7	21.4
K		3.13	3.13	8.0	26.2	30.3	13.5
N4	2	3.14	3.14	6.9	27.2	31.4	13.4
N8		3.12	3.12	9.2	25.1	30.3	17.2

Note:

1. Silicon contents were calculated by "rule of mixture" (equation 11).
2. New SiC content equals the open porosity of the original SiC preform minus the free Si content calculated using the "Rule of Mixtures" (equation 11).
3. New SiC expected was calculated using equation (15), assuming no carbon loss above 800°C (i.e., L=0).
4. Carbon loss % = 100 x [1 - (New SiC formed/New SiC expected)].

* Characteristics of samples N6, N7, N4, and N8 prior to siliconization are given in Table 12.

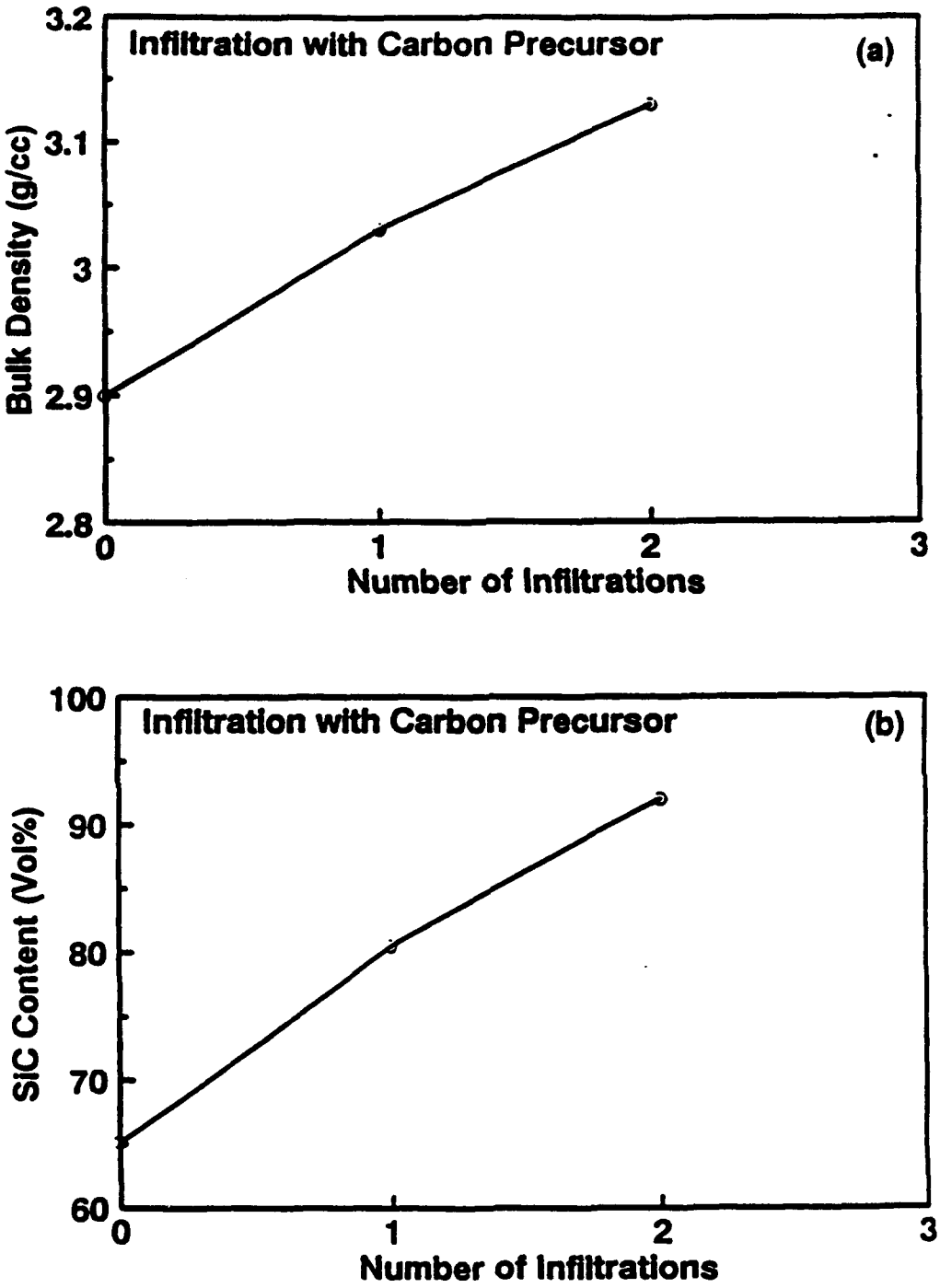

Figure 32 Plots of (a) Bulk Density and (b) SiC Content for Siliconized Samples as a Function of the Number of carbon Precursor Infiltration/Pyrolysis Cycles

process compared to the results achieved with the vinyl silazane precursor. As discussed in section 1.3 (Table 8), only 5-10 vol% new SiC is formed in samples given three or four infiltration/pyrolysis treatments with the vinyl silazane. However, with only one carbon precursor infiltration/pyrolysis cycle, ~14-15 vol% new SiC is formed during siliconization process (Table 19). With two carbon precursor infiltration/pyrolysis cycles, more than 25 vol% new SiC is produced and the residual silicon content is less than 10 vol%.

Table 19 also shows calculations of the expected amount of new SiC that would form if all the carbon present in the infiltrated/pyrolyzed samples was converted to SiC. This volume fraction of new SiC, V_{NSiC}, is given by

$$V_{NSiC} = \text{volume of new SiC/volume of bulk sample}$$

$$= 3.3417 d_b W(1-L)/d_{th} \qquad (16)$$

where

- d_b = bulk density of the original porous SiC preform
- W = fractional weight gain after the infiltration/pyrolysis process
- L = fractional weight loss of carbon that occurs between the pyrolysis process and the siliconization process
- d_{th} = theoretical density of SiC (3.2 g/cm^3)

The factor 3.3417 is used to convert from carbon to SiC and is obtained using the formula:

$$1 + (W_{Si}/W_C) \qquad (17)$$

where W_{Si} is the atomic weight of silicon and W_C is the atomic weight of carbon. The derivation of equation 16 is similar to that of equation 12. The calculated amounts of new SiC formed during siliconization (column seven of Table 19) are based on the assumption that the weight loss between pyrolysis temperature 800°C and siliconization temperature (>1500°C), L, is zero. However, from TG analysis (Figure 24), it is known that the pyrolyzed carbon precursor continues to lose weight above 800°C in nitrogen. This is why the amount of new SiC determined from the density measurements (column six of Table 19) is less than the values calculated from equation 16 using L=0 (column seven of Table 19). Nevertheless, if accurate values for L were available, equation 16 would be accurate for predicting the amount of new SiC formed.

The carbon loss during siliconization (in the range 13-24% according to Table 19) is much larger than expected from the TGA data shown in Figure 24 (i.e., ~6.5% between 800 and 1575°C). The difference in weight loss behavior was also observed in a bulk carbon precursor sample which was first pyrolyzed at 800°C for 2 hours and then heat treated to 1650°C for 1 hour. The weight loss during the second heat treatment was only 3.5 wt%. Possible reasons for the larger carbon loss observed during siliconization of infiltrated samples include: (1) Carbon reacts with silica (reaction 10) as discussed in section 1.2. (2) The pyrolysis behavior of the carbon precursor confined to small pores in the SiC preforms may be different from that observed for bulk samples. (3) Residual products for the carbon precursor after pyrolysis may not be pure. Consequently, the amount of the new SiC calculated from equation 16 (column seven of Table 19) may be overestimated.

Table 19 also shows that percent carbon weight loss is greater for samples receiving only one infiltration/pyrolysis treatment (21-24 wt%) compared to samples receiving two infiltration/pyrolysis treatments (13-17 wt%). A possible reason is that the pyrolysis product obtained after the first infiltration/pyrolysis treatment may lose additional weight during the second pyrolysis treatment. Therefore, the percent weight loss of the first pyrolysis product may be reduced during siliconization. This would lower the overall percent weight loss for the twice-infiltrated/pyrolyzed

samples. Another possible reason is that the latter samples have less open porosity compared to the samples receiving only one infiltration/pyrolysis treatment. It may be more difficult for volatile products to escape from the twice-infiltrated/pyrolyzed samples prior to silicon infiltration.

Table 18 shows that a sample (M) prepared with three carbon precursor infiltrations has low bulk and apparent density values and 6 vol% open porosity after siliconization. Microstructure analysis (see Figure 33(a)) shows that a thin (~200 μm) dense layer,which consists of SiC and a small amount of isolated silicon or carbon, is formed on all sample surfaces. In contrast, the interior of the sample retains the porous structure of the SiC/C preform (see Figure 33 (b)). This microstructure development can be explained by "reaction choking", a mechanism which occurs during the siliconization process if excess carbon is present in the porous preform. Whether reaction choking occurs, depends on the relative values of the volume of open pores available in the original SiC preform and the volume of the new SiC, V_{NSiC}, that is expected to form (calculated from equation 15) based on the amount of carbon present. If V_{NSiC} is larger than the available open pore volume, two possibilities arise: (1) The reaction to form SiC will continue to occur until pore channels become blocked. The reaction "chokes off" as molten silicon cannot reach the interior of the sample to react with available carbon. Thus, the sample contains unfilled pore channels and unreacted carbon. (2) The material will expand. In the present case, the sintered SiC preform cannot expand. Therefore, reaction choking, as indicated by Figure 33(b), occurs.

It should be noted that reaction choking is not expected in samples given one or two infiltration/pyrolysis treatments because the amount of new SiC formed (14-27 vol% according to Table 19) is considerably less than the initial open pore volume (~34-36%). In contrast, the amount of carbon in the thrice-infiltrated/pyrolyzed sample (M) is sufficient to form 41.8 vol% of new SiC, according to equation 15. This calculation was made assuming that L=0 (i.e., no carbon loss during siliconization). In reality, some additional loss of carbon occurs during siliconization. If one assumes a relatively high weight loss of 15%, the calculated volume of new SiC (35.5 vol%) is still too close to the open pore volume of preform (36.7%) to avoid the reaction choking problem.

Another way to determine if reaction choking will occur is to calculate the bulk density of the carbonaceous material in the preform. Theoretical calculations show that a bulk density less than 0.963 is needed to avoid to formation of carbon inclusions. For the samples in this study, the carbon bulk density is calculated by assuming that the carbon bulk volume is equivalent to the open pore volume in the original porous preform. Thus, the carbon bulk density, d_c, is given by

$$d_c = d_o W (1-L)/P \qquad (18)$$

where

- d_o = bulk density of the original preform
- P = open pore volume fraction of the original preform
- W = fractional weight gain after the infiltration/pyrolysis process
- L = fractional weight loss of carbon that occurs between the pyrolysis process and the siliconization process

If L = 0, then d_c = 1.09 for sample M, i.e., well above the threshold for reaction choking. When a relatively high weight loss is assumed (L = 0.15), the d_c value (0.93) is still too close to the reaction choking threshold.

Figure 34 shows X-ray diffraction patterns obtained from siliconized samples prepared with and without carbon precursor infiltrations. Both samples consist of silicon, α-SiC and β-SiC. However, the silicon peak intensities are much weaker in the sample with two carbon precursor infiltrations. This is, of course, consistent with the increased SiC content and decreased Si content that develops in siliconized samples that were infiltrated with carbon.

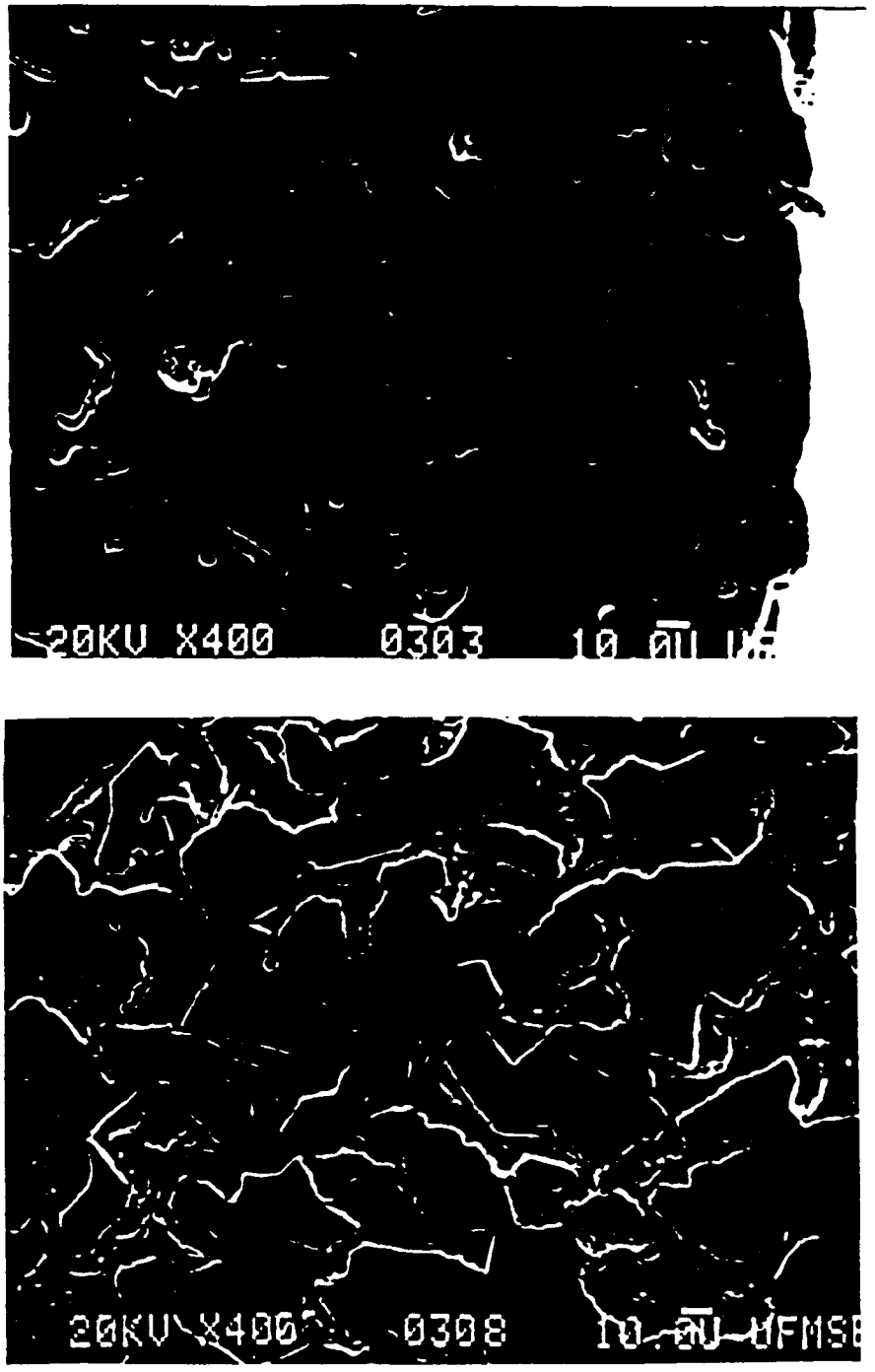

Figure 33 Scanning Electron Micrographs of the (a) Surface and (b) Interior of Sample (M) Prepared with Three Carbon Precursor Infiltration/Pyrolysis Cycles

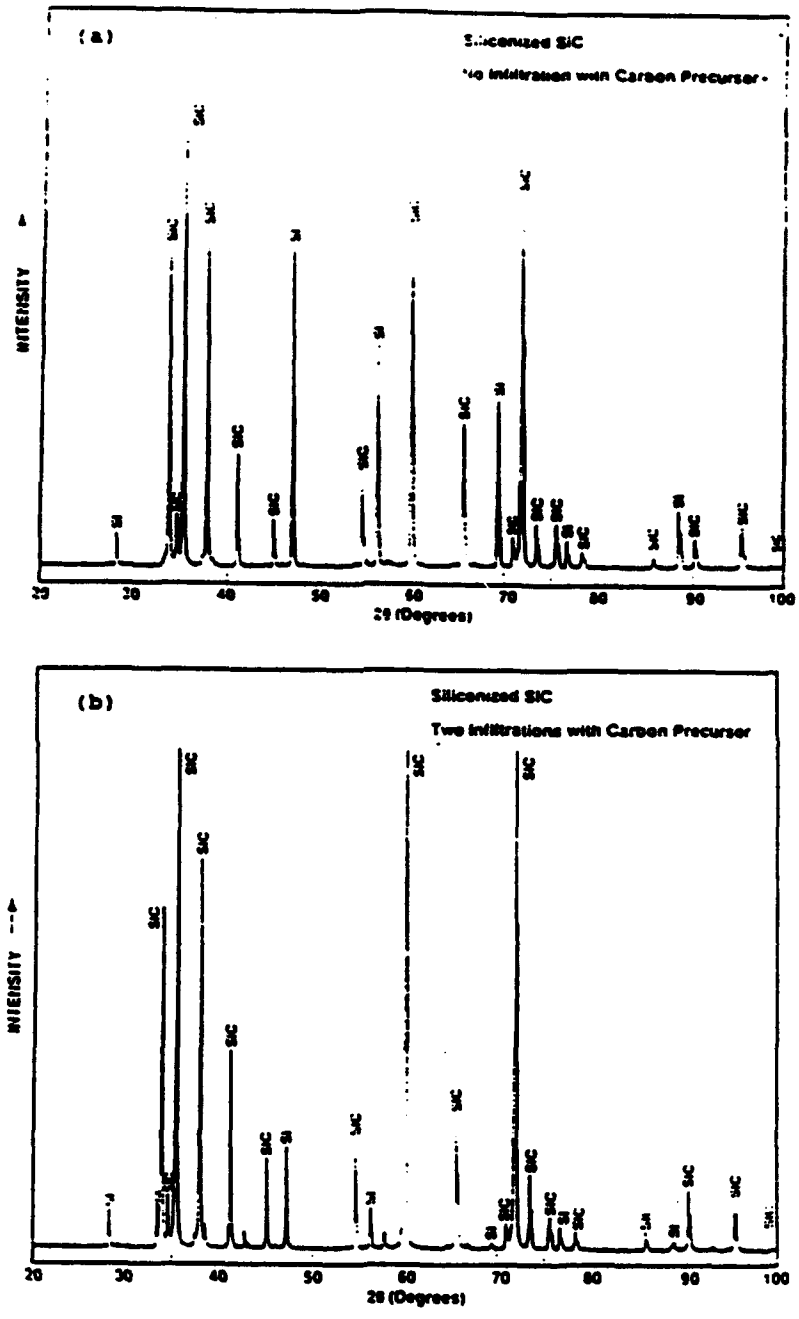

Figure 34 X-Ray Diffraction Patterns for the Samples (a) without Carbon Precursor Infiltration (Sample X) and (b) with Two Carbon Precursor Infiltrations (Sample K)

Siliconized SiC with Combined Infiltrations

Table 20 shows the properties of siliconized samples prepared with combined infiltrations of both ceramic and carbon precursors. The Si content values in column six are calculated using the "rule of mixtures" (equation 11). The increases in bulk density and SiC content for these samples were considerably lower than that for sample K with two carbon precursor infiltrations (Tables 18 and 19) and was even somewhat lower than that for sample N which had only one carbon precursor infiltration (Tables 18 and 19). The Si content values in last column are predicted using equations 12 and 16. They are 3-4% lower than the values calculated using the "rule of mixtures" equation. Possible reasons are as follows: (1) Both calculations have some assumptions which may not be accurate. (2) The actual weight loss during siliconization is higher than assumed.

Table 20 Density Results and Free Si Content for Siliconized SiC with Combined Infiltrations

Name	Infiltration Sequence	Open Pore (%)	Bulk Density (g/cm^3)	Apparent Density (g/cm^3)	Silicon Content (%)	Silicon Content Predicted
H	1st carbon 2nd silazane	0.1	3.01	3.01	21.8	18.7
J	1st silazane 2nd carbon	0.2	3.00	3.01	21.8	17.3

Microstructure Evolution

SiC Preform after Carbon Precursor Infiltration

Figure 35 shows typical SEM micrographs for a porous SiC preform after carbon precursor infiltration and low temperature (140°C) heat treatment to remove solvent. The carbon precursor appears to be uniformly distributed within the porous SiC preform. This is, of course, desirable for obtaining a uniform final microstructure of the siliconized SiC composites.

The carbon obtained from pyrolysis of phenolic resins is referred to as "glassy," or "vitreous" carbon, due to its glass-like appearance and glass-like fracture characteristics. In fact, glassy carbon is not truly an amorphous material, but has a disordered graphite structure with a small crystallite size (15-50 Å). Jenkins [Jen73; Rob86] developed a model for the structure of glassy carbon which is shown in Figure 36. The model consists of entangled ribbons of graphitic polymeric molecules which can explain the low density and the high porosity of glassy carbon. X-ray diffraction patterns obtained in this study did not reveal any significant difference between uninfiltrated SiC and samples which were infiltrated with carbon precursor and pyrolyzed at 800°C. This indicates that the carbon formed at this stage is essentially amorphous to X-rays under the scanning conditions used.

Siliconized SiC with Carbon Precursor Infiltrations

Figure 37(a) and (b) are SEM micrographs for siliconized SiC composites with one and two carbon precursor infiltrations, respectively. The darker phase in the micrographs is SiC and the lighter phase

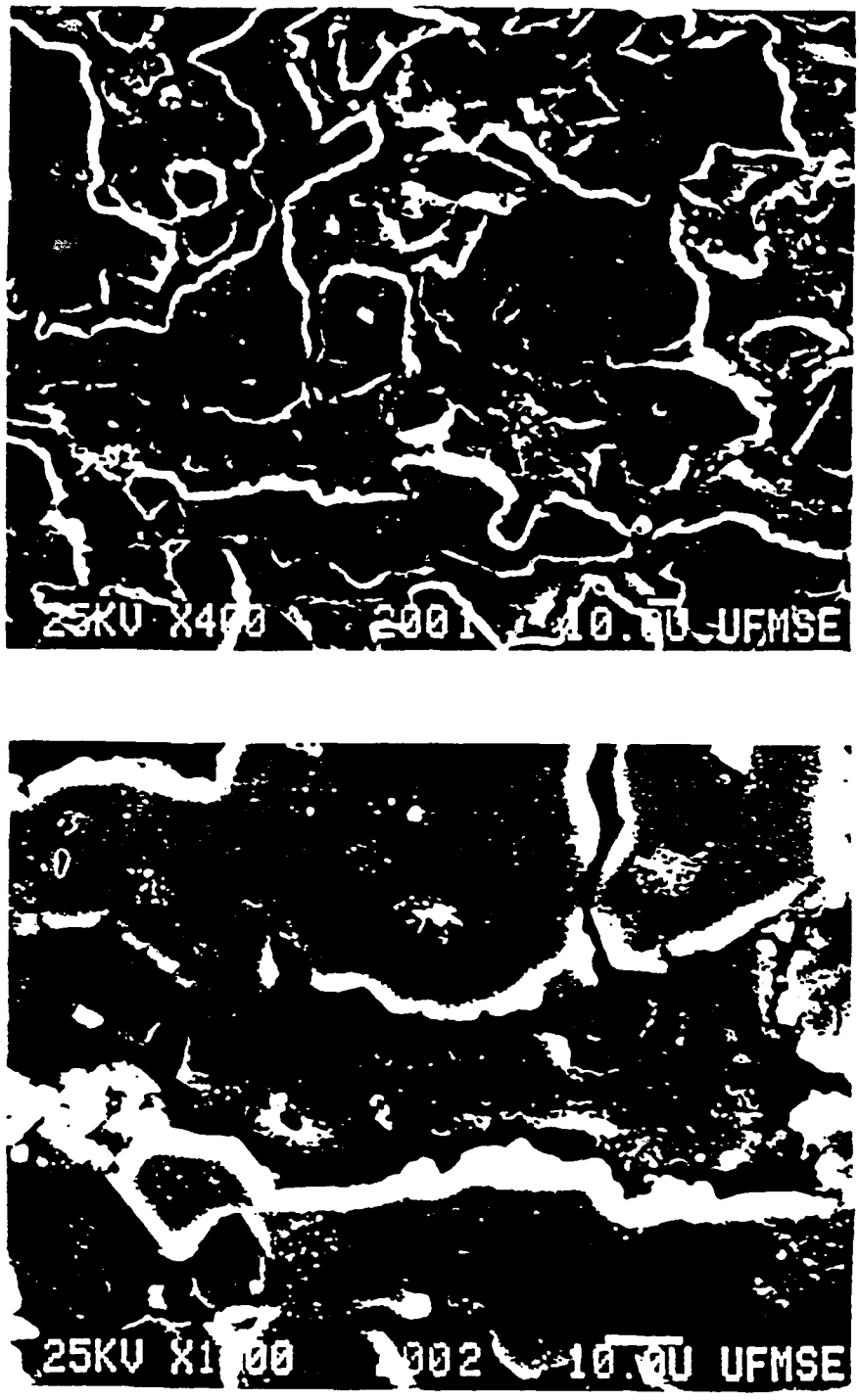

Figure 35 Scanning Electron Micrographs at (a) Low and (b) High Magnification of an SiC Porous Preform after One Carbon Precursor Infiltration

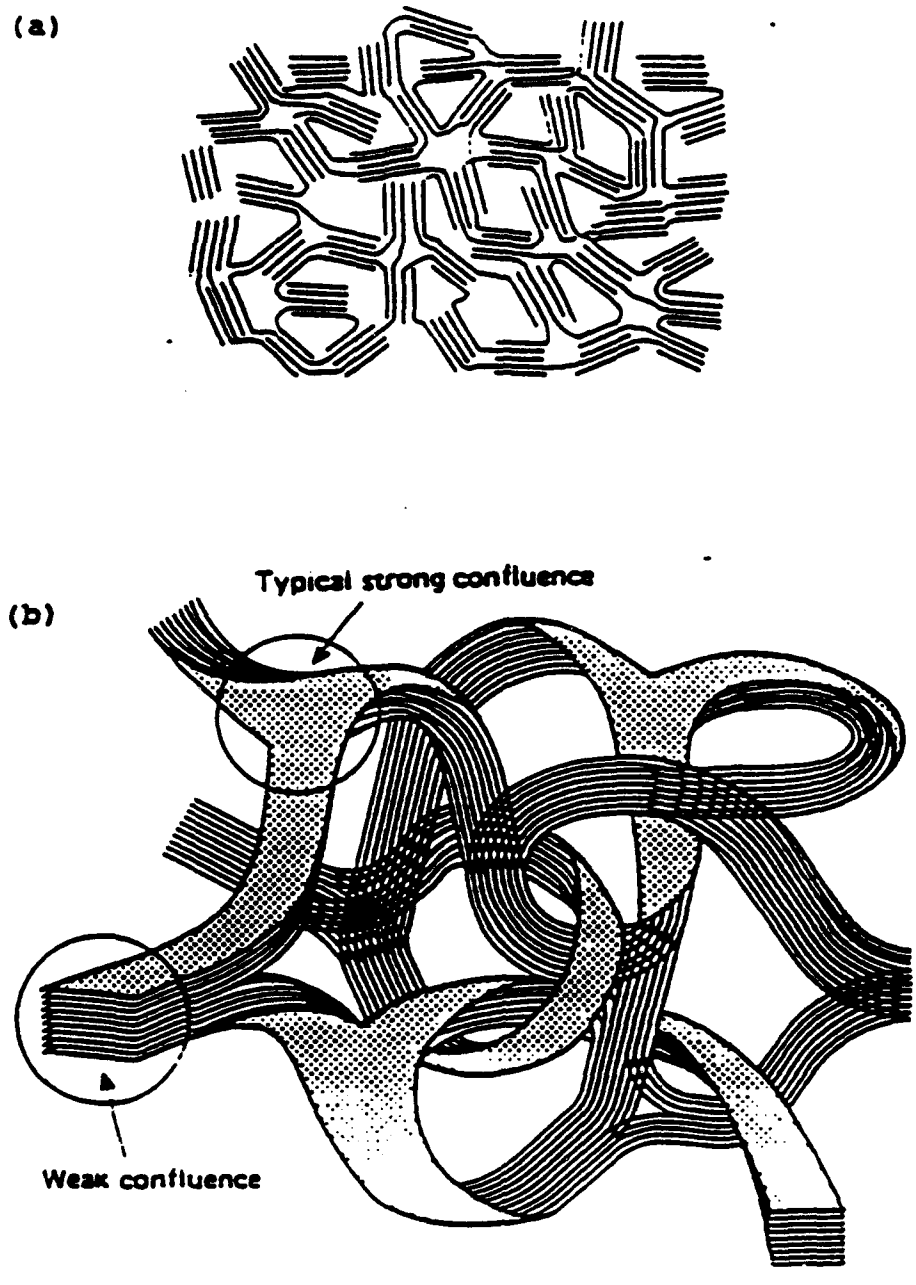

Figure 36 (a) Two-Dimensional and (b) Three-Dimensional Models of the Structure of Glassy Carbon Proposed by Jenkins [Jen73; Rob86]

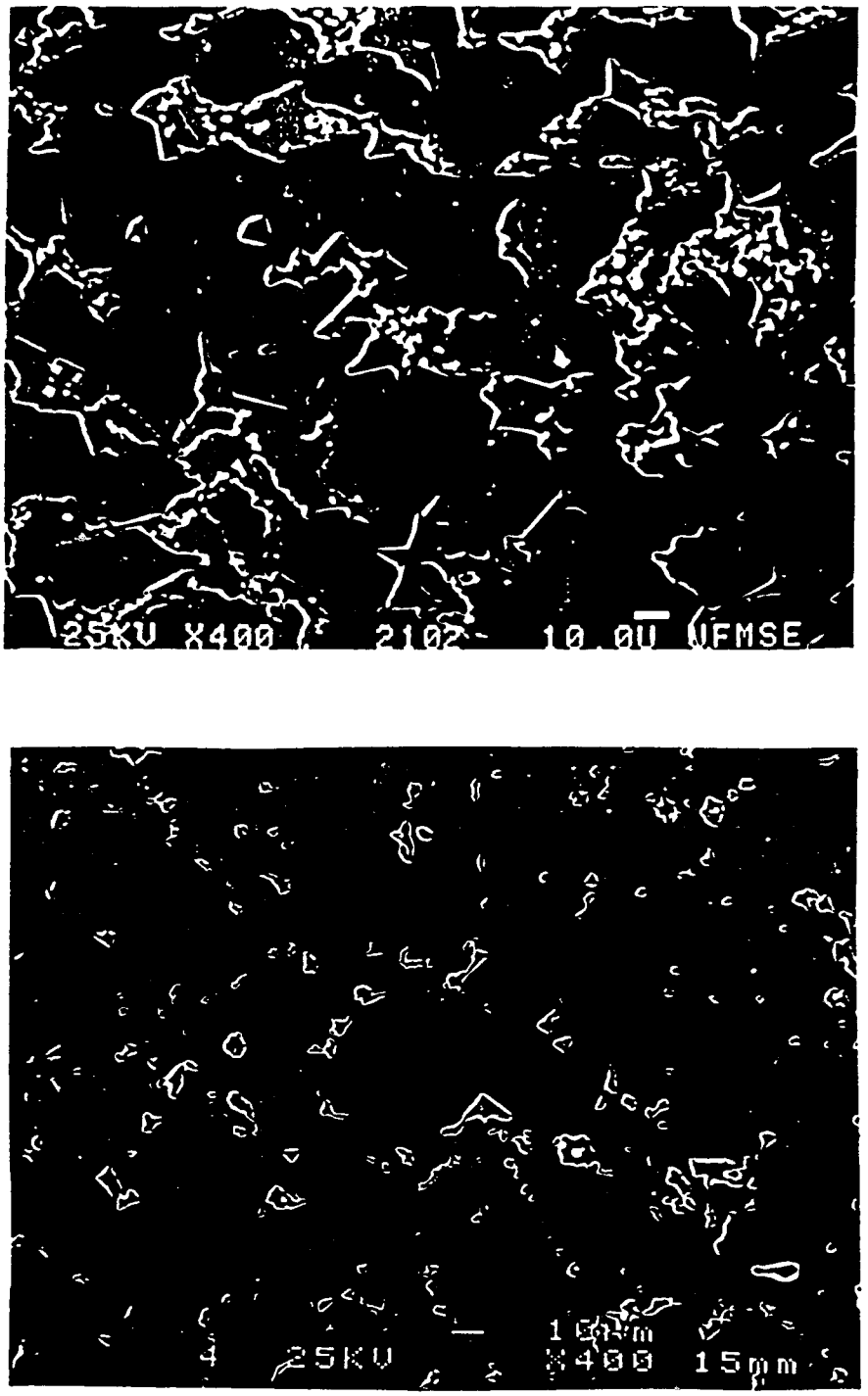

Figure 37 Scanning Electron Micrographs of Siliconized SiC Samples Prepared with (a) One and (b) Two Carbon Precursor Infiltration/Pyrolysis Cycles

is silicon. In comparison with samples prepared without infiltration (see Figure 19(a)) or even with multiple preceramic infiltrations(Figure 19(b)), the siliconized SiC composites prepared with the carbon precursor show a much greater SiC content. This was, of course, expected based on the Archimedes density measurements. For composites prepared with two carbon precursor infiltrations, not only does the SiC volume fraction increase significantly, but the average size of the free silicon phase regions is much smaller. The silicon phase is restricted to isolated pockets with relatively small dimensions, i.e., instead of having the continuous structure associated with the microstructure shown in Figure 19(a). Samples with this type of microstructure should have improved high-temperature mechanical properties which would make the material more useful for a variety of structural applications. Also, these samples are expected to show improved polishability which is important for optical mirror applications.[3]

Occasionally, a large carbon inclusion was detected with a dense SiC layer around it (Figure 38). This kind of defect is probably associated with bubbles incorporated in the green body during the original forming process. After sintering at >2050°C, large pores of 100-200 μm were formed as a result of these bubbles. These pores would be filled with the carbon precursor during infiltration, resulting in a very high local carbon density after pyrolysis. During siliconization process, silicon reacts with the large carbon inclusion to form a layer of dense SiC which will prevent further reaction between silicon and carbon.

Infiltration and Reaction mechanism

In samples Prepared without precursor infiltration, siliconization is a relatively simple process involving only liquid penetration through a porous structure. The infiltration kinetics have been described by relatively simple models, such as those based on the modified Washburn equation 14 or by a model developed by Beltran et al. [Bel88; Bel89]. In addition, more sophisticated models, such as developed by Scheidegger [Sch74], have also been utilized.

The case in which the preceramic precursor is first infiltrated into the porous preform is somewhat more complicated because precursor decomposition, densification, and crystallization reactions are not usually completed prior to siliconization, i.e., unless a high pyrolysis temperature (e.g., ~1650°C) is used.

If carbon exists in preforms, the siliconization process will involve the conceptually independent processes of infiltration and the reaction to form SiC: Si(l) + C(s) = SiC(s). In practice, however, these processes are not separable. The reaction tends to close infiltration pore channels, thereby making continued infiltration of silicon into the preform difficult. For preforms with one or two carbon precursor infiltration/pyrolysis cycles, there is sufficient excess porosity such that a nearly continuous infiltration path (open porosity) exists even after all carbon is consumed by the reaction. For the sample (M) with three infiltration/pyrolysis cycles, however, the preform contains too much carbon content and too little open porosity. Another concern in samples with multiple infiltrations is that concentration gradients may develop, such that excess carbon is found at the surface of the sample. This could lead to the formation of a dense layer of SiC which would prevent further silicon infiltration. Therefore, there exists a maximum infiltration depth which is possible before "reaction-choking" occurs. Reaction-choking is analogous to the "freeze-choking" phenomenon in metal-matrix composites processing which occurs when a melt is infiltrated into a cold preform.

The liquid-phase reactive infiltration process is further complicated by spatially varying temperature due to the exothermic reaction: Si + C = SiC. Also, the reaction results in a net decrease in volume of about 25-35% (with the exact change depending on the density of the starting carbon).

---

3 In fact, this was confirmed in tests conducted at United Technologies Optical Systems [Bro91]

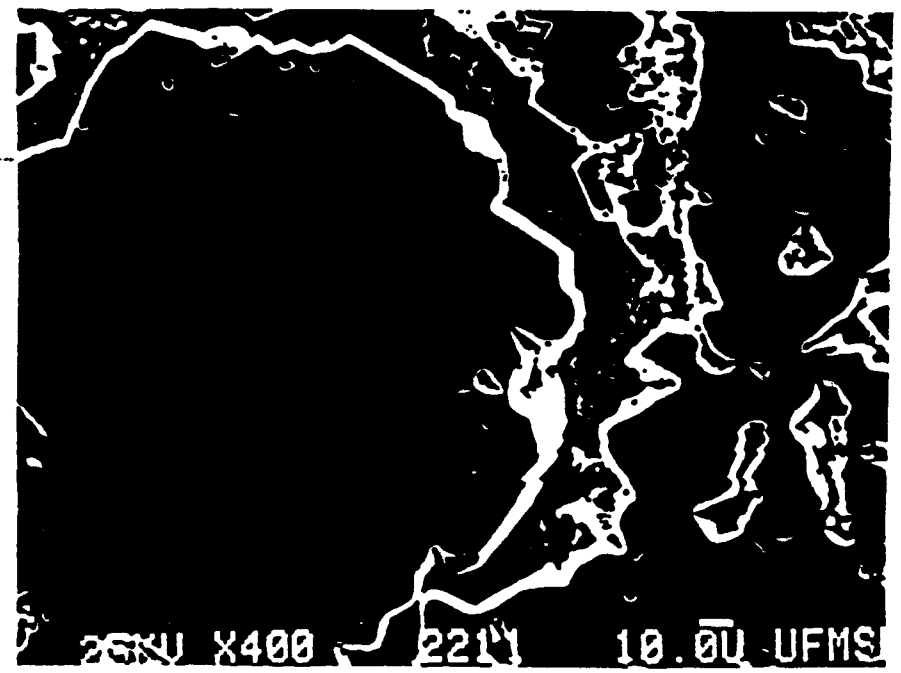

Figure 38 Scanning Electron Micrograph of a Large Carbon Inclusion in a Siliconized SiC Sample Prepared with Carbon Precursor Infiltrations (The free Si was etched away with $HF\text{-}HNO_3$ acid solution.)

As a result, obtaining dense materials requires continued infiltration of silicon as the reaction proceeds.

A complete model of reactive infiltration kinetics requires a detailed knowledge of the evolution of the preform microstructure as the reaction proceeds, as well as a solution to the combined heat and mass transfer problem. Messner and Chiang [Mes90] presented a simple model which treated the reactive infiltration process as a special case of porous-media infiltration, in which the permeability of the preform varies with both time and distance. They obtained the ultimate infiltration length l_f at which reaction-choking occurs.

If the siliconization process is controlled by interface-reaction kinetics, then

$$l_f = [(2\beta\delta P r_o^6)/5\eta K]^{1/2} \quad (19)$$

and if the siliconization process is controlled by diffusion limited kinetics, then

$$l_f = [(2\beta\delta P r_o^6/15\eta K'^2]^{1/2} \quad (20)$$

where

- β = $1/(8r_o^2)$ for the Hagen-Poisseuille model
- δP = infiltration capillary pressure
- r_o = initial radius of cylindrical pores comprising the porous preform
- η = viscosity of liquid silicon
- K = linear reaction rate constant
- K' = the parabolic reaction rate constant

It is clear from these equations that increasing the ultimate infiltration depth requires increasing pore radius r_o and capillary pressure δP and decreasing viscosity η of liquid silicon and reaction rate constant K or K'. The viscosity η and reaction rate constant K depend largely on temperature. With increasing temperature, the latter increases while the former decreases. Therefore, the proper temperature should be chosen after careful temperature-dependent studies of the viscosity and reaction rate constant. Usually, the reaction rate constant is much more temperature-dependent than the melt viscosity. Further, l_f is inversely proportional to $\eta^{1/2}$ and K' in the case of diffusion-limited kinetics. Therefore, a lower siliconization temperature may be favorable for maximizing the ultimate infiltration depth.

Microstructure of Siliconized SiC with Surface Carbon Precursor Infiltrations

To improve the polishability of siliconized SiC materials, a layer of SiC can be deposited on the surface of the SiC/Si composite by chemical vapor deposition (CVD), a process known as "CVD-SiC cladding". The CVD-SiC layer can be polished to an extremely good finish. However, CVD processes are relatively expensive and slow. Also, some defects are usually observed at the interface between siliconized SiC composite and the CVD-SiC layer. An alternative to CVD-SiC cladding is to infiltrate the surface of the porous SiC preform with the carbon precursor prior to the siliconization process.

As expected, the multiple surface carbon precursor infiltrations can modify the microstructure of siliconized SiC significantly. A dense and >95% SiC layer could be formed in the surface portion of samples with three or four surface infiltrations (see Figures 39 and 40). With two surface infiltrations, the surface layer showed less SiC (i.e., compared to the samples in Figures 39 and 40), although the SiC/Si ratio was clearly larger than in the interior of sample. In contrast, a large proportion of carbon remained at the surface portion of a sample with five surface infiltrations. Figures 39, 40, and 41 show the microstructure of both the cross section and the surface portion for samples with 3, 4, 5 surface infiltrations, respectively.

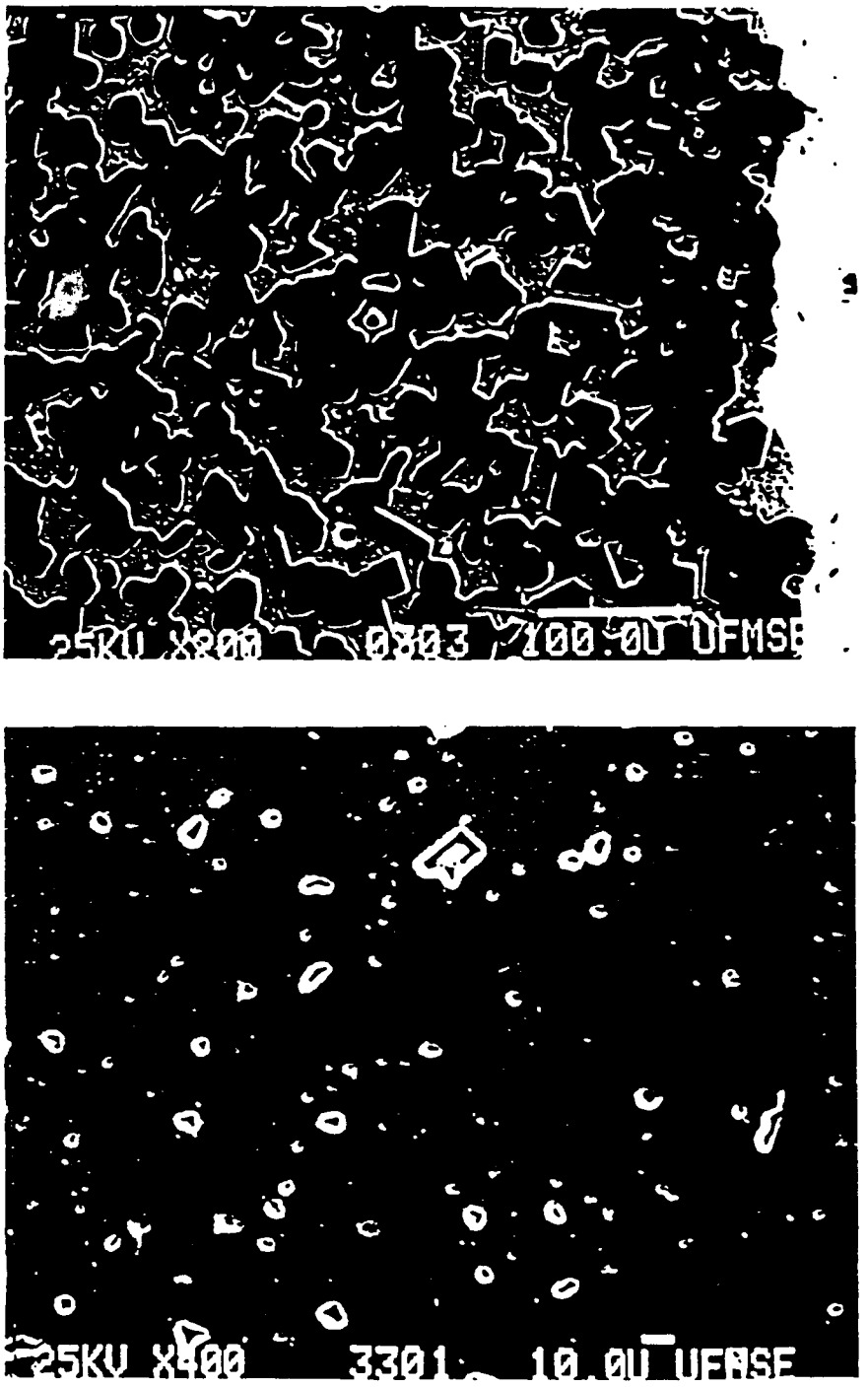

Figure 39 Scanning Electron Micrographs of the (a) Cross-Section and (b) Surface Region of Siliconized SiC Samples Prepared with Three Surface Carbon Precursor Infiltration/Pyrolysis Cycles

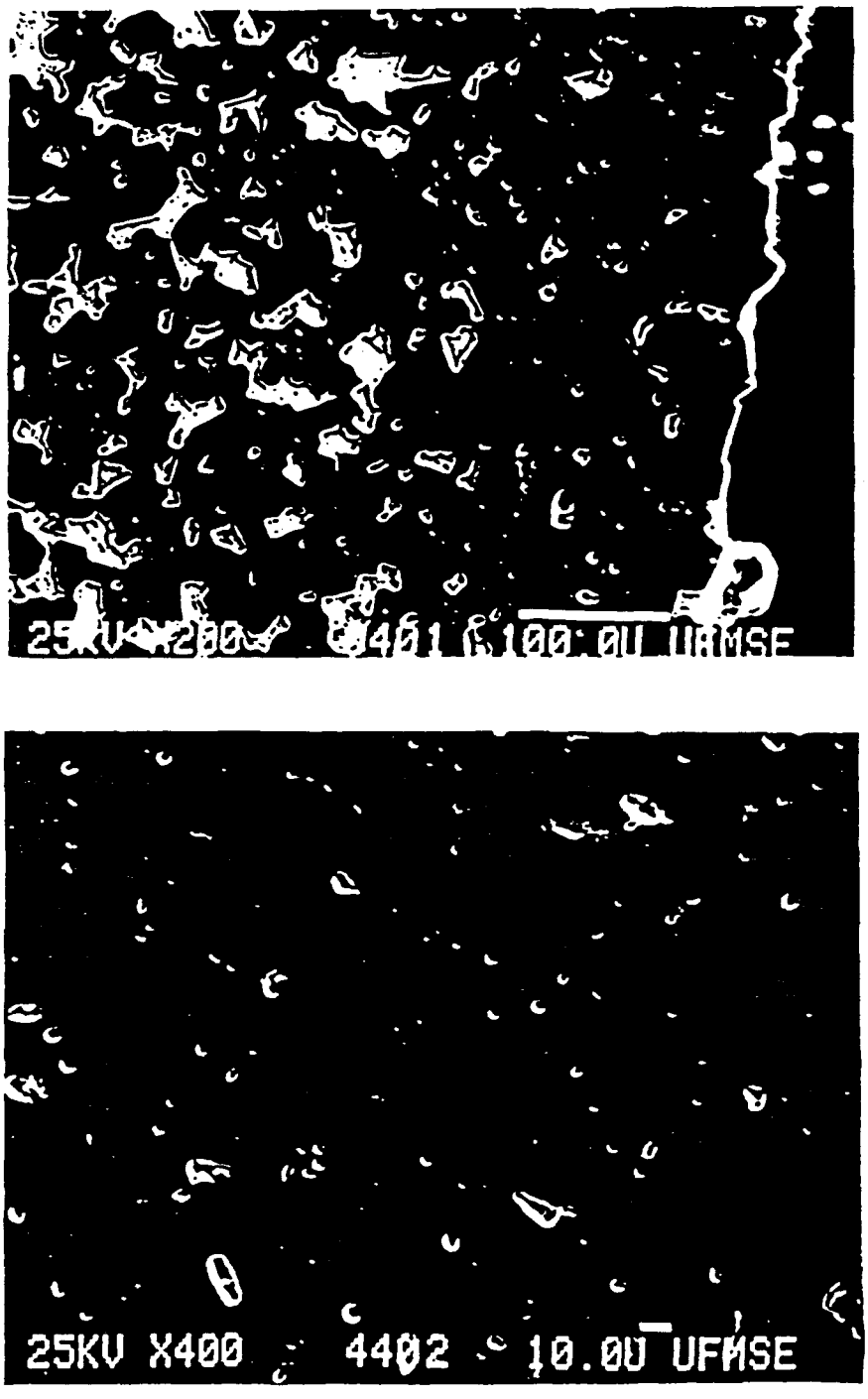

Figure 40 Scanning Electron Micrographs of the (a) Cross-Section and (b) Surface Region of Siliconized SiC Samples Prepared with Four Surface Carbon Precursor Infiltration/Pyrolysis Cycles

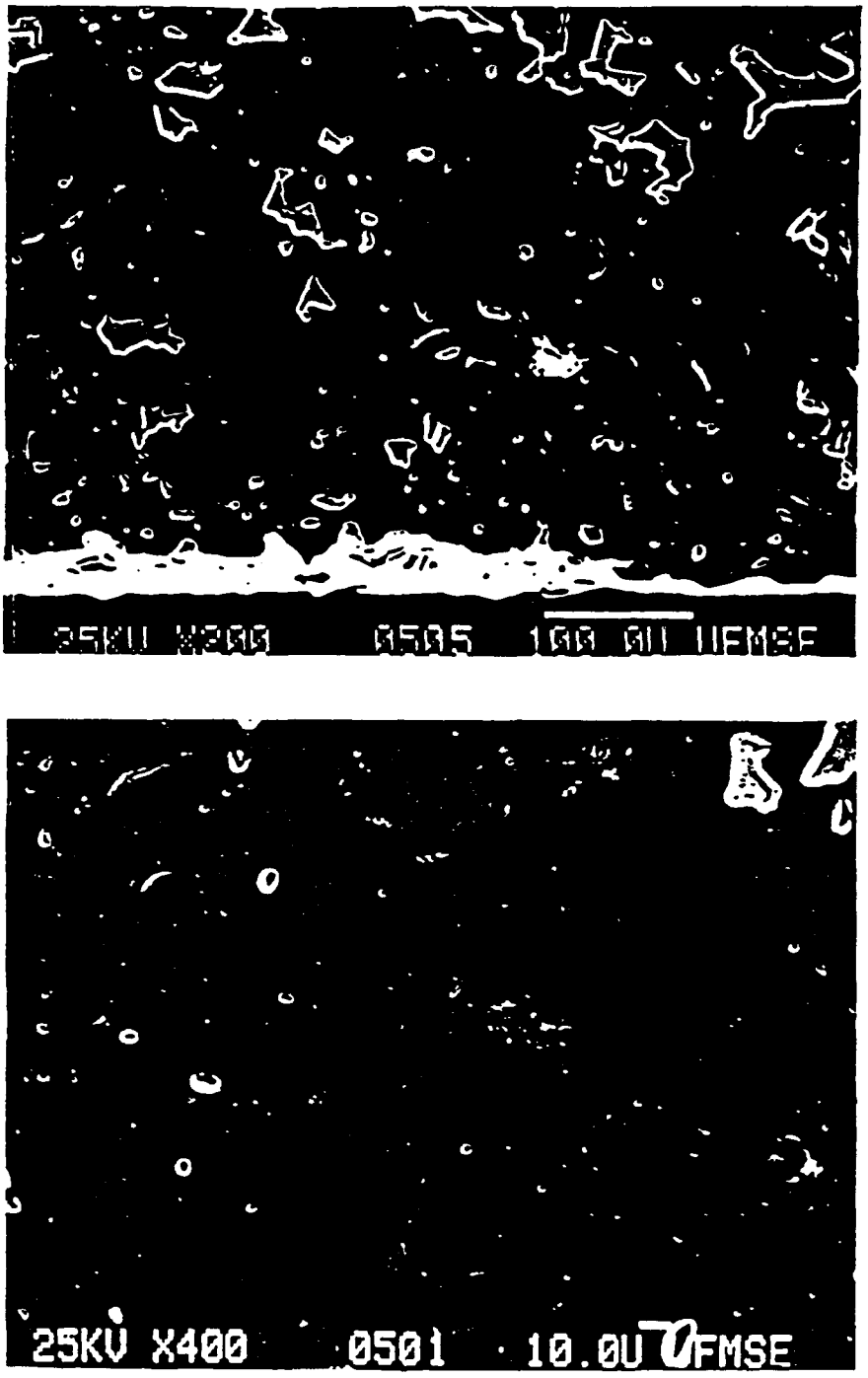

Figure 41 Scanning Electron Micrographs of the (a) Cross-Section and (b) Surface Region of Siliconized SiC Samples Prepared with Five Surface Carbon Precursor Infiltration/Pyrolysis Cycles

Compared with CVD-SiC cladding methods for creating a dense SiC surface layer, the use of the carbon precursor surface infiltration method is relatively simple and economical. However, some problems still remain to be solved. For example, the thickness of the dense SiC layer was not uniform along the sample length. Also, for the sample with 3 surface infiltrations, the dense layer may be too thin, while for the sample with 4 surface infiltrations some carbon inclusions were detected. These problems probably result from insufficient control over the surface infiltration parameters used, as well as the rough surface and non-uniform pore channels of the SiC preform. Further research work should be directed at optimizing the surface infiltration parameters, such as infiltration time, number of infiltrations, pyrolysis temperature and, probably, concentration of precursor solution. In addition, efforts to improve the smoothness of the surface and the uniformity of the microstructure of the porous preform would be beneficial.

Mechanical Properties of Siliconized SiC Composites

Mechanical properties of siliconized SiC composites (including strength, fracture toughness, elastic modulus, hardness, creep, fatigue and so on) are very important not only for structural applications, but also for electronic, optical and thermoelectric applications. The results of mechanical property measurements are summarized in Table 21. The effects of carbon precursor infiltrations on the four-point flexural strength, Young's elastic modulus, hardness and fracture toughness values are reported in the following sections.

Flexural strength

The effect of the number of infiltrations on flexural strength (measured by four-point bending) is illustrated in Figure 42(a). The strength increases by ~23 % with one carbon precursor infiltration and by ~45% with two carbon precursor infiltrations. Recall that in Figure 32, the SiC content was shown to increase by approximately same percentages with succeeding infiltrations. Thus, it is reasonable to attribute the increase in strength to the increase in silicon carbide fraction since silicon carbide is stronger and tougher than silicon. The linear increase in strength with number of infiltrations is expected because the samples already have an SiC skeleton and the SiC content increases linearly with the number of infiltrations.

For some applications requiring a light weight structure, the specific strength (i.e., strength/bulk density) is more important than strength itself. Figure 42(b) shows the specific strength also increases linearly with number of infiltrations.

Table 21 Mechanical Property Data

No. of Infiltrations	0	1	2	Porous SiC Preform
Flexural Strength (MPa)	193±21	237±21	279±32	58±9
No of Measurements	7	6	8	12
Vickers Hardness (GPa)	15.8±4.8	20.4±4.2	24.2±2.6	
No of Measurements	114	73	73	
Fracture Toughness (MPa $m^{1/2}$)	3.0±0.3	3.7±0.4	4.0±0.4	
No of Measurements	6	7	6	

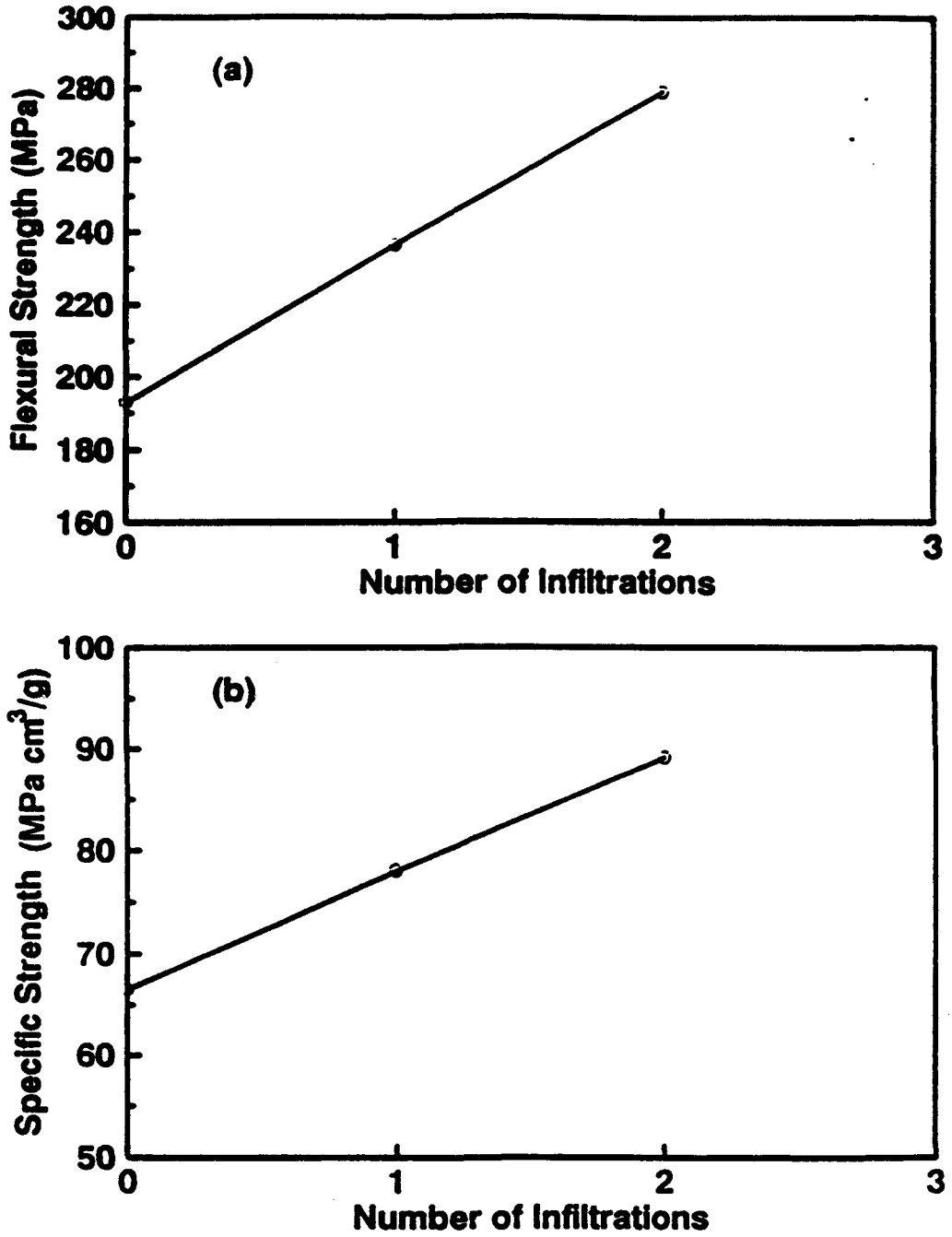

Figure 42 Plots of (a) Four-Point Flexural Strength and (b) Specific Strength vs. Number of Carbon Precursor Infiltration/Pyrolysis Cycles for Siliconized Samples

Young's Elastic Modulus

The modulus data plotted in Figure 43(a) were calculated from the stress-strain data obtained during four-point bending tests. Although these values are not very accurate (e.g., compared to other methods for determining elastic modulus, such as the sonic pulse-echo technique), they do give a good evaluation of the relative relationship between elastic modulus and the number of infiltrations. Like flexural strength, Young's elastic modulus increases with the number of infiltrations. This increase is also attributed to the increase of silicon carbide content. Of course, silicon carbide has much higher elastic modulus than silicon.

Similar to the specific strength, the specific stiffness (i.e., elastic modulus/bulk density) is important for some applications requiring light weight, e.g., mirrors or other structural components for aerospace applications. Figure 43(b) shows that the specific stiffness increases with the number of infiltrations. Increases of ~12% and ~41% in specific stiffness are obtained for siliconized SiC samples prepared with one and two carbon precursor infiltrations, respectively.

Hardness

Figure 44(a) shows the relationship between Vickers hardness and number of infiltrations and Figure 44(b) gives the corresponding change in the standard deviation. Compared to the value for siliconized SiC without any carbon precursor infiltrations, the hardness increases ~29% and ~53% for siliconized SiC composites with one and two carbon precursor infiltrations, respectively, while the standard deviation decreases ~13% and ~45%, respectively. The decrease in the standard deviation of the hardness is not surprising based on the changes in microstructural features shown in Figures 19(a) and 37. Siliconized SiC composites without carbon precursor infiltrations exhibit a microstructure having a very coarse mixture of the Si and SiC phase and, therefore, there is a very large amount of scatter in the hardness values. On the other hand, siliconized SiC composites show a much finer-scale microstructure (especially after two carbon precursor infiltrations, see Figure 37(b)) and, thus, give smaller standard deviation values.

Higher hardness makes the material more scratch resistant and impact damage resistant which are crucial properties for optical mirror applications. The finer-scale SiC/Si microstructure improves the polishability of the material which is also essential for high-performance mirror applications.

Fracture Toughness

Figure 45 shows the fracture toughness (K_{IC}) as a function of the number of infiltrations. Similar to other mechanical properties, the average fracture toughness of siliconized SiC composites increases with the number of infiltrations. The toughness increases by ~23% with one carbon precursor infiltration and by ~34% with two carbon precursor infiltrations.

From the Griffith's relations, the fracture strength, σ_f, can be correlated with fracture toughness, K_{IC}, as follows:

$$K_{IC} = Y\sigma_f(a_e)^{1/2} \qquad (21)$$

where a_e is maximum flaw size and Y is a geometrical factor. For a semicircular flaw with the bend test geometry, Y = 1.23. Therefore, the maximum flaw size can be estimated if the toughness and strength are measured.

Table 22 gives the calculated maximum flaw size for samples with different number of infiltrations. The maximum flaw size is about 150 μm and is independent of number of carbon precursor infiltrations. The large size flaws are believed to result from bubbles incorporated in the green body during the original forming process (see Figure 38). Thus, more processing control is needed during the initial forming process to avoid bubbles so as to improve the fracture strength. For example,

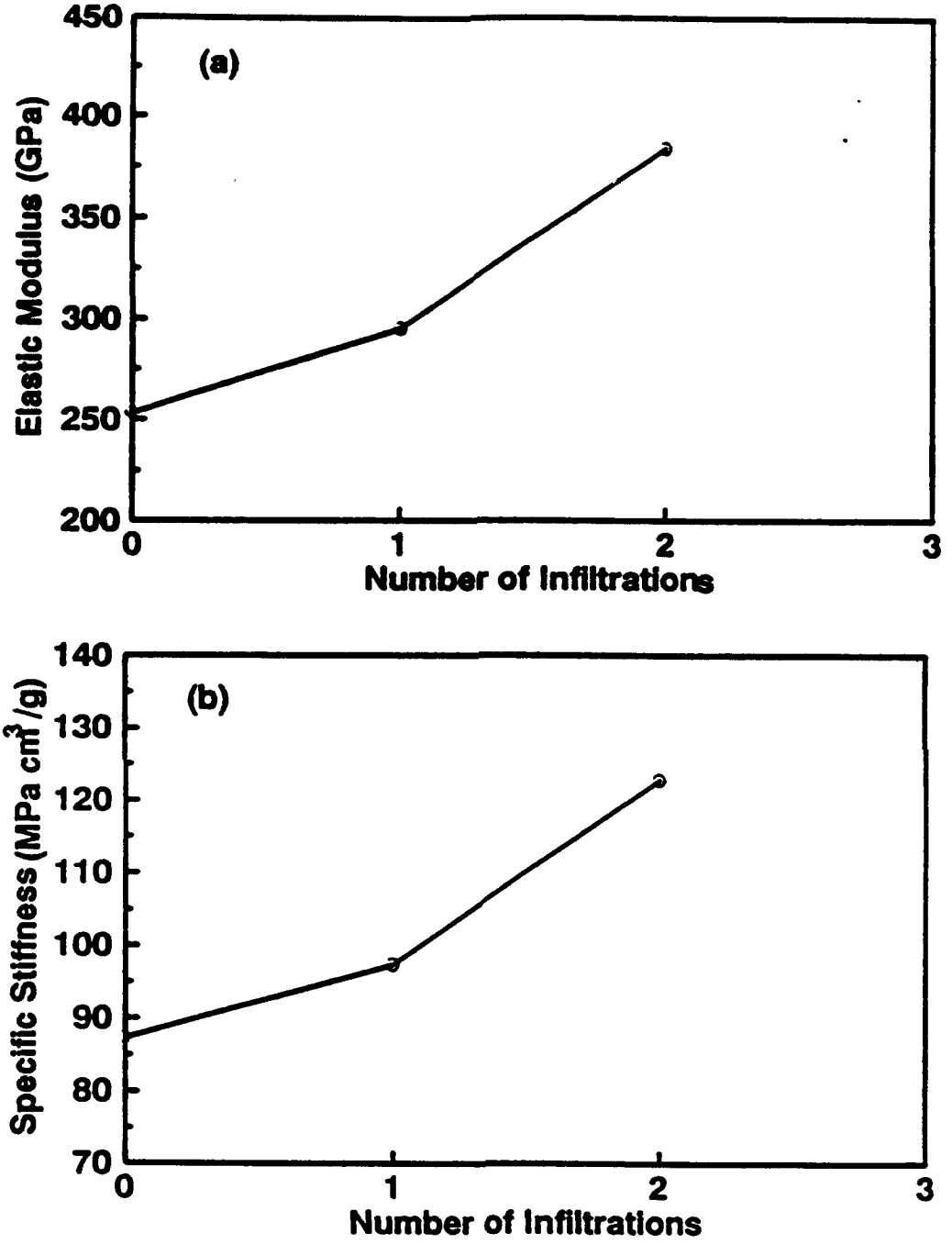

Figure 43 Plots of (a) Elastic Modulus and (b) Specific Stiffness vs. Number of Carbon Precursor Infiltration/Pyrolysis Cycles for Siliconized Samples

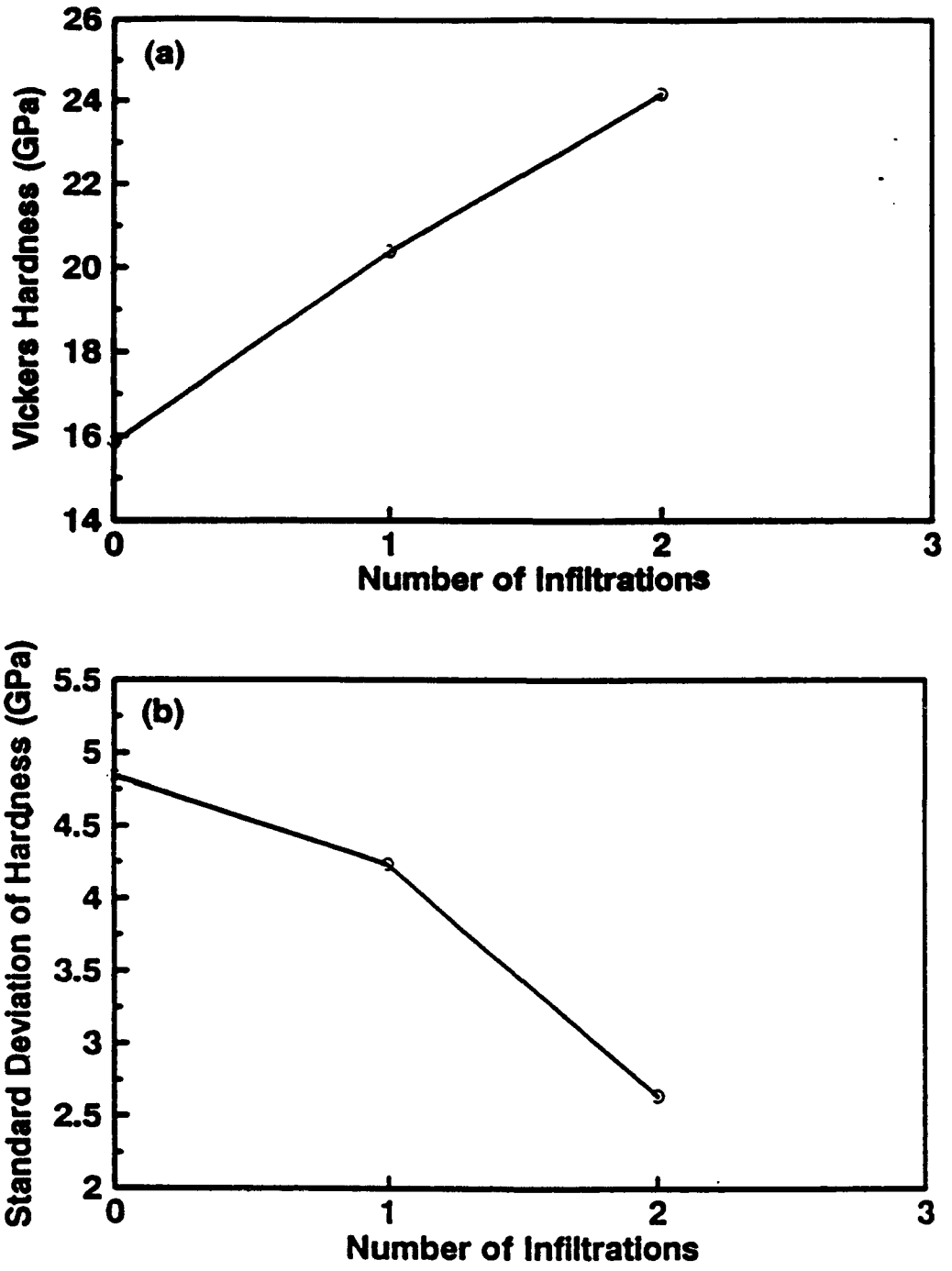

Figure 44 Plots of (a) Vickers Hardness and (b) Standard Deviation vs. Number of Carbon Precursor Infiltration/Pyrolysis Cycles for Siliconized Samples

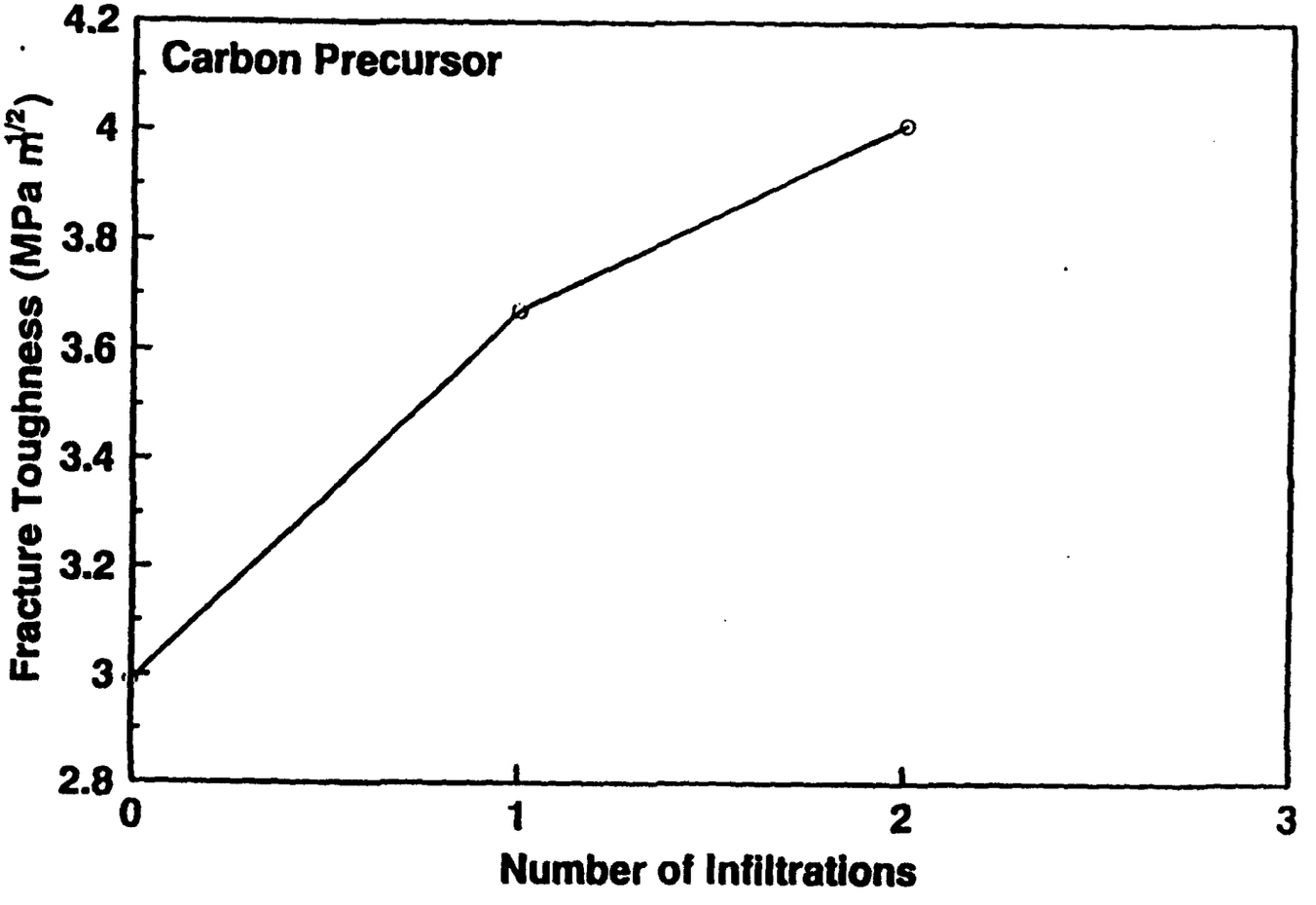

Figure 45 Plot of Fracture Toughness (MPa $m^{1/2}$) vs. Number of Carbon Precursor Infiltration/Pyrolysis Cycles for Siliconized SiC Samples

a degassing step may be added during the initial forming process. If the maximum flaw size is limited to 25 μm (i.e., the approximate size of the coarse SiC particles shown in Figure 16), the fracture strength will be increased by more than 100%. (The calculated values are shown in Table 22.) Therefore, avoiding large processing flaws is very important if a high strength material is needed. Furthermore, if very high strength (larger than the values in last column in Table 22) is desirable, the maximum grain size of starting SiC powders should be reduced.

Table 22 Calculation Values of Maximum Flaw Size

Number of Infil.	Measured K_{IC}(MPam$^{1/2}$)	Measured σ_f (MPa)	Calculated a_c (μm)	Calculated σ_f ($a_c = 25\mu$m)
0	2.99	193	160	486
1	3.67	234	160	597
2	4.01	280	140	652

REFERENCES

[Bel88] V. Beltran, A. Escardino, C. Feliu and M.D. Rodrigo, "Liquid Suction by Porous Ceramic Materials," Br. Ceram. Trans. J. 87, 64-69 (1988).

[Bel89] V. Beltran, A. Barba, M.D. Rodrigo and A. Escardino, "Liquid Suction by Porous Ceramic Materials: 2. -Influence of Pressing Conditions," Br. Ceram. Trans. J. 88, 219-222 (1989).

[Cha85] M.W. Chase, Jr., C.A. Davies, J.R. Downey,Jr., D.J. Frurip, R.A. McDonald and A.N. Syverad, JANAF Thermochemical Table, Third Edition, 14 (1985).

[Fit70] E. Fitzer and W. Schaffer, "The Effect of Crosslinking on the Formation of Glasslike Carbon from Thermosetting Resin," Carbon 8, 353-364 (1970).

[Jen73] G.M. Jenkins, In Physics and Chemistry of Carbon, Vol. 11, Edited by P.L. Walker, M. Dekker, New York (1973).

[Lee90] H.D. Lee, "Validity of Using Mercury Porosimetry to Characterize the Pore Structures of Ceramic Green Compacts," J. Am. Ceram. Soc. 73 [8], 2309-2315 (1990).

[Low84] S. Lowell and J.E. Shields, P. 216 in Powder Surface Area and Porosity, Second Edition, Published by Chapman and Hall, London (1984).

[Mes90] R.P. Messner and Y.M. Chiang, "Liquid-Phase Reaction Bonding of Silicon Carbide Using Alloyed Si-Mo Melts," J. Am. Ceram. Soc. 73 [5], 1193-1200 (1990).

[Mil79] P.D. Miller, J.G. Lee and I. B. Cutler, "The Reduction of Silica with Carbon and Silicon Carbide," J. Am. Ceram. Soc. 62 [3-4], 147-149 (1979).

[Pul66] W.W. Pultz and W. Hertl, "SiO_2 + SiC Reaction at Elevated Temperature: I," Trans. Faraday Soc., 62 [9], 2499-2504 (1966).

[Rob86] J. Robertson, "Amorphous Carbon," Advances in Physics 35 [4], 317-374 (1986).

[Sch74] G.W. Scheidegger, The Physics of Flow Through Porous Media, 3rd ed., University of Toronto Press, Toronto, Canada (1974).

[Tor90] W. Toreki, C.D. Batich, M.D. Sacks and A.A. Morrone, "Synthesis and Applications of a Vinylsilazane Preceramic Polymer," Proc. 14th Annual Conference on Composites and Advanced Ceramics, Cocoa Beach, FL (January 14-17, 1990).

[Wea74] R.C. Weast, Handbook of Chemistry and Physics, 55th Edition, CRC Press, Boca Raton (1974-1975).

BOOK III

Section 1

Processing

of

$BaO\text{-}Al_2O_3\text{-}2SiO_2$ Fibers

Principal Investigator: D.E. Clark

Processing of $BaO \cdot Al_2O_3 \cdot 2SiO_2$ - A High Temperature Matrix Material

Principal Investigator: **D.E. Clark**

Abstract

The crystallization kinetics of the celsian phase from $BaO \cdot Al_2O_3 \cdot 2SiO_2$ glass was examined. The Celsian phase is desirable as a composite matrix material because of its high potential use temperature ($>1500°C$) and its low coefficient of thermal expansion ($2.2 \times 10^{-6}/°C$). The parent glass ($BaO \cdot Al_2O_3 \cdot 2SiO_2$) was prepared by the sol-gel process. A second composition of $(Sr_{0.15},Ba_{0.85})O \cdot Al_2O_3 \cdot 2SiO_2$ also has been produced using sol-gel techniques in order to evaluate the effect of strontium on the formation of the monoclinic celsian phase. Several different seed materials also were investigated to determine their potential for promoting formation of the monoclinic phase. Stabilization of the gel was performed in a Deltec conventional furnace while densification and crystallization were performed in a Raytheon QMP 2101B-6 microwave oven operating at 2.45 GHz as well as in the conventional furnace.

Introduction

Barium aluminosilicate glass-ceramics are being investigated as matrix materials in high-temperature ceramic composites for structural applications. There are several reasons for choosing $BaO \cdot Al_2O_3 \cdot 2SiO_2$ as a matrix material. The potential maximum use temperature in air is $>1500°C$, higher than the lithium aluminosilicates and the calcium aluminosilicates and comparable to the upper use temperature of mullite which is in the range of 1600°C as determined from the phase diagram. Another appealing characteristic is its resistance to thermal shock, due primarily to its low coefficient of thermal expansion ($\alpha = 2.29 \times 10^{-6}/°C$ from RT to 1000°C). This low thermal expansion (lower than SiC at $\alpha = 4.3\text{-}5.6 \times 10^{-6}/°C$ from RT to 1000°C [1]) would put the matrix in compression during cool down and could increase the strength of the composite. Other advantages include good resistance to oxidation and formability (net shaping) prior to crystallization.

Celsian, the monoclinic phase, is stable at temperatures $<1590°C$ and is the crystalline phase of interest. However, hexacelsian, the high-temperature, hexagonal phase, often is the primary phase that nucleates even at low temperatures. The hexagonal phase is undesirable because of its higher coefficient of thermal expansion ($\alpha = 8 \times 10^{-6}/°C$) and because it transforms at 300 °C to the orthorhombic phase, accompanied by a 3 percent

volume change. Hot pressed composites of celsian with 20 volume percent of SiC fiber reinforcement produced samples of > 90 percent of the calculated density and ultimate flexural strengths above 500 MPa[2]. No physical testing results at high temperatures have been reported for this system. Bahat examined the heterogeneous nucleation of $BaO \cdot Al_2O_3 \cdot 2SiO_2$ with several nucleating agents [3]. He reported that hexacelsian still was the primary phase to crystallize. Bahat continued work in the $BaO \cdot Al_2O_3 \cdot 2SiO_2$ system with a kinetic study of the hexacelsian-celsian phase transformation [4]. He found that the complete transformation often took days. Seeding the hexacelsian with 5 percent celsian reduced the transformation time to a few hours.

Glass-ceramics are pore free, fine-grained, polycrystalline ceramics produced by controlled crystallization of glass. The small crystallites apparently provide a barrier to the propagation of cracks initiated at the surface. This phenomenon can make glass-ceramics significantly tougher than the glasses from which they were formed. In general, glass-ceramics possess low coefficients of thermal expansion, high elastic moduli and have strengths considerably higher than the parent glasses from which they are derived.

Ceraming, the process by which glasses are transformed into glass-ceramics, can be achieved by two means. The traditional process consists of the conventional melting of the raw materials followed by a rapid cooling to the glassy state, bypassing the formation of any crystalline phases. The glass then is subjected to controlled heat-treatment to bring about nucleation and crystallization of the desired phase(s). When a reinforcing phase, such as SiC, is added the process becomes more complicated. Due to the high melting temperature of the raw materials, the glass must first be fritted so that a second phase can be added before forming, densifying and crystallizing the end product.

Many researchers have used the traditional method with hot pressing or hot isostatic pressing for the nucleation, crystallization and densification in the production of celsian [2,5]. The melting of $BaO \cdot Al_2O_3 \cdot 2SiO_2$ glass requires temperatures in excess of 2100°C. Thus, sophisticated furnaces are necessary. The major problems associated with this technique are (a) contamination from the molybdenum electrode in amounts up to one weight percent; (b) uncontrolled heterogeneous nucleation influenced by the impurities and the walls of the container; and (c) the hexagonal phase, although thermodynamically unstable, is the first phase to crystallize.

Other research groups have pursued a low-temperature sol-gel method for the formation of the parent glass [6-8]. Although the parent glass is synthesized readily by the sol-gel process, to date only hexacelsian has been crystallized. In the traditional processing method, substitution of strontium for barium has produced the direct crystallization of the celsian phase [9].

The use of microwave energy to process ceramic materials is still in the early stages of development. One of the objectives of this study addresses the use of microwave energy to study the densification, nucleation and crystallization of $BaO \cdot Al_2O_3 \cdot 2SiO_2$ glass.

Microwave processing is fundamentally different from conventional heating. Microwave heating depends upon the dielectric properties and the heat transfer characteristics of the material, and allows a uniform heating throughout the entire body. This uniform processing capability reduces significantly the thermal stresses that can cause microcracking in the ceramic.
The power absorbed by a material is described by the equation

$$P_{abs} = 2\pi f \epsilon_0 \epsilon''_{eff} |E|^2 V \quad (1)$$

where

P_{abs}	=	power absorbed
f	=	frequency
ϵ_0	=	permittivity of free space
ϵ''_{eff}	=	effective dielectric loss factor
$\|E\|$	=	internal electric field strength
V	=	volume of material

and the resulting temperature rise brought about by this absorption is

$$\Delta T = \frac{P_{abs} \Delta t}{\rho C_p} \quad (2)$$

where

ΔT	=	temperature rise
Δt	=	time of exposure
ρ	=	density of material
C_p	=	specific heat

The kinetics of bulk crystallization involve a combination of nucleation and growth, both of which require energy to be added to the system. In addition to thermal energy, microwave radiation also adds energy of an electrical and magnetic nature. Therefore, microwave processing is a good candidate for investigating crystallization kinetics.

It has been reported that microwaves interact with glass modifiers and enhance their diffusion in glass[10]. Figure 1 illustrates an interdiffusion enhancement of K^+ for Na^+ in a sodium aluminosilicate glass composition having a molar ratio of alumina to sodium oxide equal to 1. Although it is unproven, it is believed that the rapid reversal of the electromagnetic field may be increasing the local temperature of the ion, making the ionic jump out of the potential well easier.

Since crystallization is a diffusion controlled process, any enhancement in the diffusion would result in increased crystallization kinetics. The same author also has shown that crystallization in lithium disilicates can be carried out at lower temperatures and shorter times in a microwave field [11]. The microwave heat treatments described here have been shown to enhance crystallization at lower temperatures and produce more uniform microstructures. This observation is significant in light of the results found in reference 8

where the author reported increased porosity in samples, possibly due to Ostwald ripening of the early nucleating crystallites.

It is difficult to heat celsian with stand alone (microwave heating only) due to its low dielectric loss. However, we have demonstrated that other low loss materials (such as Al_2O_3) can be heated with a combination of microwaves and conventional methods. This combination, referred to as microwave hybrid heating (MHH), results in more volumetric heating of the material and translates into more uniform microstructures throughout the sample. In the case of celsian, we expect more uniform crystallization with MHH than with conventional heating. Further, the addition of a strong microwave absorbing reinforcement phase (such as SiC) may provide the same results using stand-alone microwaves.

Project Goal

The goal of this investigation is to produce a high-temperature ($>1500\,°C$) matrix that has a coefficient of thermal expansion similar to or lower than a suitable reinforcement phase and that is chemically and physically compatible with reinforcement preferred agents.

Project Objectives (July 1, 1993 - June 30, 1994)

(1) Evaluate $BaO \cdot Al_2O_3 \cdot 2SiO_2$ as a potential matrix material.

(2) Investigate sol-gel as an alternative processing route to traditional glass-ceramic processing.

(3) Investigate the use of microwave energy for processing glass-ceramics.

Experimental Procedure

Glass Preparation

Gels were prepared by the sol-gel process with two compositions, $BaO \cdot Al_2O_3 \cdot 2SiO_2$ and $(Sr_{0.15},Ba_{0.85})O \cdot Al_2O_3 \cdot 2SiO_2$. The precursor materials used were tetraethylorthosilicate (TEOS), aluminum-sec-butoxide, (ASB) barium acetate and strontium acetate.

In the first step, a dilute solution of TEOS in ethanol was partially hydrolyzed by adding 1/4 of the theoretical water needed for full hydrolysis and a few drops of HCl this solution was refluxed at 60°C for three hours. Step two was the slow addition of a dilute solution of ASB in isopropanol to the cooled TEOS/ethanol mixture. This solution was allowed to react overnight. Step three consisted of dissolving barium acetate in 3.75 times the amount of water needed to fully hydrolyze the TEOS and enough acetic acid to lower the pH below

4. This solution was added slowly to the TEOS/ASB mixture with sufficient excess acetic acid to clear the sol. The resulting sol was stirred for 20 minutes before casting. Gelation normally occurred within 30 minutes of casting.

The second composition was identical to the first with the exception of the partial substitution of strontium acetate for barium acetate.

The gels were dried to a powder at several temperatures (50, 200 and 800°C). The dried gels were characterized using differential thermal analysis (DTA) to obtain information such as organic burnout and Tg needed for vitrification of the gels. X-ray diffraction analysis also was performed on the DTA samples to determine the crystalline phases present, if any. X-ray diffraction indicated that the gels were amorphous up to at least 900°C.

Seeding

Several seed materials with the potential to promote forming the monoclinic phase also were investigated. Monoclinic zirconia, copper oxide and strontium aluminosilicate (produced by the sol-gel process and crystallized at 1300°C for four hours) were used in amounts ranging from 0.1wt% to 10wt%. The temperatures investigated (1050 to 1300°C) included those below and above the zirconia monoclinic → tetragonal phase transformation. The gel powders were cold pressed into discs at 4000 psi for the vitrification study.

Vitrification

Vitrification was carried out in a conventional furnace at temperatures extracted from the processing "window"provided by the DTA results in Figure 4. The temperatures used for vitrification were 800, 900, 950, 1020 and 1050°C. The glasses were screened using XRD to evaluate the extent of crystallization, if any, that occurred during heat treatments.

Archimedes density measurements were performed on the vitrified samples to determine the bulk density of the glass before crystallization. This was done on samples of approximately three grams with water as the liquid medium.

Crystallization

In the next phase of the study, the glass samples were heat treated using conventional and MHH. Temperatures investigated ranged from 1050 to 1300°C. The time allowed for crystallization was 3 hours in the conventional furnace and ninety minutes at 1100°C in the microwave furnace.

Crystallized samples were analyzed using x-ray diffraction analysis and the bulk densities

were determined by the Archimedes method.

Results & Discussion

$Li_2O \cdot 2SiO_2$

The $Li_2O \cdot 2SiO_2$ system was chosen as the lead-in material for $BaO \cdot Al_2O_3 \cdot 2SiO_2$ for several reasons. $Li_2O \cdot 2SiO_2$ is a simple material that readily crystallizes and its crystallization kinetics have been well documented.

Rods of lithium disilicate were nucleated at 450°C for 3 hours in a conventional furnace. The bars then were cut into discs and crystals were grown over a range of temperatures using both microwave and conventional heating. X-ray diffraction analysis was performed on the samples to determine the crystalline phases present. Peak intensities were compared to determine the relative percent crystallinity due to differing heat treatments. The effect of the heat-treatment parameters using both microwave and conventional heating on the extent of crystallization were investigated.

Glass samples were prepared from TiO_2-free silica and reagent grade Li_2CO_3. A batch of SiO_2 + 33.3 mol% Li_2O was melted at 1350°C for 72 hours in a covered platinum crucible. The glass was cast as rods (75 mm long and 13 mm in diameter) and annealed at 300°C for 12 hours. Nucleation was performed at 450°C for 4 hours on all of the rods simultaneously to ensure consistency. Discs 4 mm thick were cut from the rods and polished with an emery cloth until optically clear. Samples containing seeds were discarded.

The growth process was performed isothermally with the time being measured from when the sample was inserted in the furnace or microwave cavity. Growth temperatures ranged from 500 to 600°C, inclusive. The samples then were ground into a fine powder with a mortar and pestle. Specimens for x-ray diffraction were prepared and analyzed in a Phillips ADP 3720 x-ray diffractometer. The relative fraction of crystallinity in each of the specimens was determined by comparing the intensities of all peaks observed to the peak intensities of the sample heat-treated in the microwave at 600°C for 10 minutes. All of the peaks encountered during x-ray diffraction analysis corresponded to the orthorombic phase of lithium disilicate. The effect of temperature on the crystallization of Li_2O-SiO_2 are listed in Table 1. There was considerable difference in the crystallization kinetics between the two processes. Heat treating the discs for 10 minutes using microwave energy was sufficient to fully crystallize the samples at temperature as low as 580°C. Table 2 is the effect of time and temperature on the relative crystallinity of the samples heat-treated using microwave energy. It was determined that significant crystallization could be achieved at temperatures as low as 500°C using microwave energy. Figure 2 indicates the relative percent crystallinity as a function of time for samples heat-treated in the microwave. Figure 3 shows x-ray diffraction patterns of samples (MHH) heated at 540°C at different times. This demonstrates the development of the crystalline phase with time for a given temperature.

$BaO \cdot Al_2O_3 \cdot 2SiO_2$

The DTA for a gel dried at 50°C is shown in Figure 4. The two peaks below 200°C were attributed to elimination of the alcohols and pore water of the gel. The exotherm at 400°C can be attributed to burning out the remaining organic materials. The small endotherm slightly below 1200°C was confirmed by x-ray diffraction to be due to the crystallization of the hexagonal phase. Table 3 provides the x-ray diffraction results of the unseeded glasses after crystallization in both the conventional and microwave furnaces.

Differential thermal analysis also was performed on various seeded samples. The substitution of strontium for barium in the gel crystallized only the hexagonal phase. Zirconia, when added as a seed in amounts of one and ten weight percent, crystallized as the hexagonal phase at both 1050°C and 1250°C. Monoclinic strontium aluminosilicate ($SrO \cdot Al_2O_3 \cdot 2SiO_2$) was used as a seed in two, five and ten weight percents additions. This resulted in the formation of the hexagonal phase. Results for the samples seeded with CuO were more promising. At 1050°C, a 10 wt% addition of CuO exhibited a small amount of monoclinic phase among the hexagonal phase. At 1300°C, a one percent addition of CuO also showed signs of the monoclinic phase. Figure 4c is the DTA for the sample with 10 wt% CuO added. The range from 900 to 1250°C is expanded in Figure 8 to elucidate the crystalline peaks. X-ray diffraction performed on samples heated below 1100°C, between 1100 °C and 1200 °C, and above 1200 °C provided confirmation of the phases described in the DTA plot. The sample exhibited peaks corresponding primarily to the monoclinic celsian phase with a small number of low intensity peaks corresponding to the hexagonal phase. Seeding with the crystalline phase formed upon heating at 1300°C with a one percent CuO addition did not enhance monoclinic crystallization in any sample.

Samples seeded with one, five and ten weight percent $SrO \cdot Al_2O_3 \cdot 2SiO_2$ and CuO also were heat-treated using microwave energy. All of the samples seeded with $SrO \cdot Al_2O_3 \cdot 2SiO_2$ crystallized as the hexagonal phase. A one percent CuO addition also crystallized as the hexagonal phase. The x-ray diffraction pattern of the sample containing five weight percent of CuO exhibited peaks corresponding to both the monoclinic and hexagonal phases. Semi-quantitative analysis indicated and equal amount of both phases. Under the same conditions, a ten weight percent addition of CuO contained a 70/30 mix of the monoclinic and hexagonal phases. Table 4 shows the results of the effects of seeding on the phases crystallized.

The bulk density was measured for samples with various amounts of seed material heat-treated at 950°C for 20 hours and then at 1300°C for 4 hours.

Conclusions

Powders of the composition $BaO \cdot Al_2O_3 \cdot 2SiO_2$ can be produced using the sol-gel process.

Low temperature heat-treatments of the pressed powders did not increase the bulk density of the samples. During crystallization, only the sample with ten weight percent CuO added and heated in the microwave for 15 minutes exhibited noticeable densification. Crystallization of the monoclinic celsian phase was achieved with the addition of CuO as a seed material. A five weight percent addition of CuO produced a significant amount of the monoclinic phase. A completely monoclinic material was achieved with a ten weight addition of CuO. Relying on the limited results obtained, it appeared that the use of microwave energy for the crystallization process did not decrease either the temperature or the amount of seed material needed to produce the monoclinic phase when compared to the samples heat-treated in conventional furnace. Only in the case of the ten weight percent CuO addition sample heated to 1050°C using microwaves was the formation of the thermodynamically stable monoclinc phase at lower temperatures using microwave energy consistent with the results obtained for the lithium disilicate glasses.

Future Work

- Modify the gel formation process to produce a gel that can be densified without external pressure during forming.
- Continue investigation of time, temperature and seeding on the crystallization of the celsian phase.
- Study the enhancement of crystallization as a function of microwave energy input.
- Prepare samples for high temperature mechanical testing.
- Determine the effect of CuO additions on the high temperature behavior of the matrix.
- Proceed with the addition of SiC as a second phase and perform a compatibility study.

The present work was presented at the American Ceramic Society Meeting and Exposition, Cincinnati, OH [12]. The basic science developed in this work has led to new initiatives in microwave processing. A proposal on waste remediation using microwave energy has been submitted to ARPA under the Technology Reinvestment Program.

With support of this project, Zak Fathi will graduate with a doctoral degree in december 1993. Mr Fathi's work was supported primarily by DARPA since 1989. Alex Cozzi has left the DARPA project to accept a graduate fellowship from the High Temperatures Materials Laboratory at Oak Ridge National Lab.

References

(1) W.J. Lackey, D.P. Stinton, G.A. Cerny, L.L. Fehrenbacher and A.C. Schaffhauser, "Ceramic Coatings for Heat Engine Materials - Status and Future Needs," Proc. Int. Symp. on Cer. Components for Heat Engines, Oct. 1983.

(2) N.P. Bansal, J.A. Setlock and C.H. Drummond, III, "Celsian Glass-Ceramic Composites," Hi-Temp Review, NASA, cp-10039, pp. 62.1 - 62.12 1989).

(3) D. Bahat, "Heterogenous Nucleation of Alkaline Earth Feldspar Glasses," J. Mat. Sci., **4**, pp. 847-854 (1969).

(4) D. Bahat, "Kinetic Study of the Hexacelsian-Celsian Phase Transformation," J. Mat. Sci., **5**, pp. 805-810 (1970).

(5) C.H. Drummond III, W.E. Lee, N.P. Bansal and M.J. Hyatt, "Crystallization of a Barium Aluminosilicate Glass," Ceram. Eng. Sci. Proc., **10**, [9-10], pp. 1485-1502 (1989).

(6) W.K. Treadway and S.H. Risbud, "Gel Synthesis of Glass Powders in the $BaO \cdot Al_2O_3 \cdot 2SiO_2$ System," J. Non-Cryst. Solids, **100**, pp. 278-283 (1988).

(7) V.S.R. Murthy, Li Jie and M.H. Lewis, "Interfacial Microstructure and Crystallization in SiC-Glass Ceramic Composites," Ceram. Eng. Sci. Proc., **10** [7-8], pp. 938-951 (1989).

(8) M. Chen, W.E. Lee and P.F. James, "Preparation and Characterization of Alkoxide-Derived Celsian Glass Ceramic," to be published in JNCS.

(9) N.P. Bansal and M.J. Hyatt, "Crystallization and Properties of Sr-Ba Aluminosilicate Glass-Ceramic Matrices," Ceram. Eng. Sci. Proc., **12**, [7-8], pp. 1222-1234 (1991).

(10) Z. Fathi, I. Ahmad, J.H. Simmons, D.E. Clark and A.R. Lodding, "Surface Modification of Sodium Aluminosilicate Glasses Using Microwave Energy," Ceramic Transactions, Microwaves: Theory and Application in Materials Processing, Vol. 21, pp. 612-630, (D.E. Clark, F.D. Gac and W.H Sutton, eds.) The American Ceramic Society, Inc., Westerville, OH (1991).

(11) A.D. Cozzi, Z. Fathi, R.L. Schr ıd D.E. Clark, " Nucleation and Crystallization of Li_2O-$2SiO_2$ in a 2.45 GHz Microwave Field", presented at the 17th Annual Conference on Composites and Advanced Ceramics, January 10-15, 1993, Cocoa Beach, Florida (to be published).

(12) A.D. Cozzi, Z Fathi and D.E. Clark, "Crystallization of Sol-Gel Derived Barium

Aluminosilicate in a 2.45 GHz Microwave Field", presented at the American Ceramic Society Meeting and Exposition, Cincinnati, OH, April, 1993 (to be published).

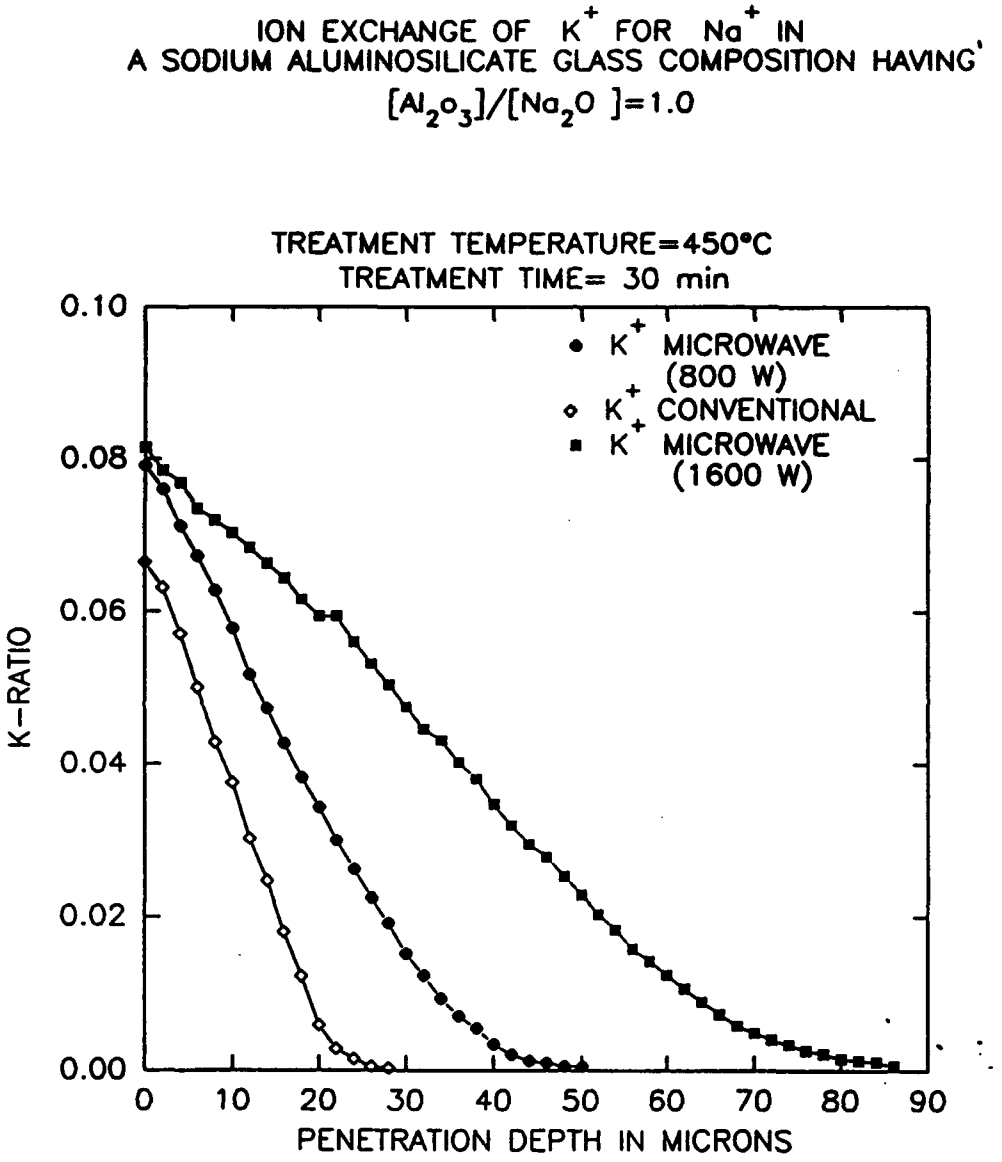

Figure 1. Penetration depth (in microns) of K^+ ions into a sodium aluminosilicate glass.

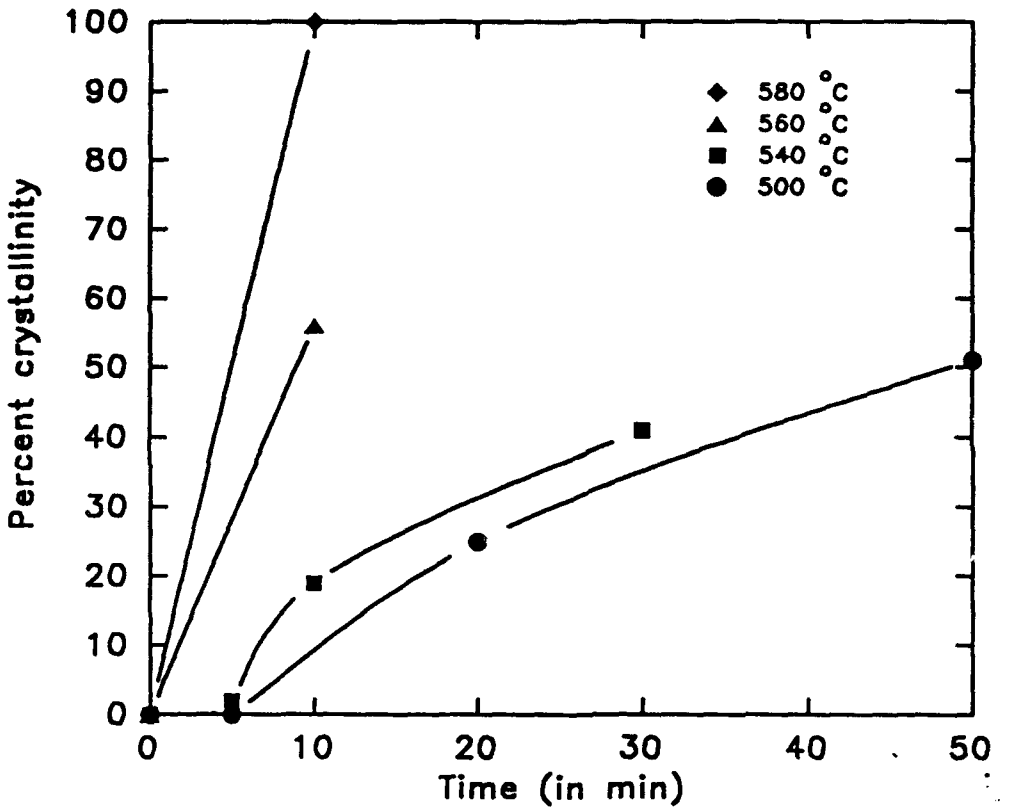

Figure 2. Relative percent crystallinity vs. time for Li_2O-$2SiO_2$ heated using microwave energy.

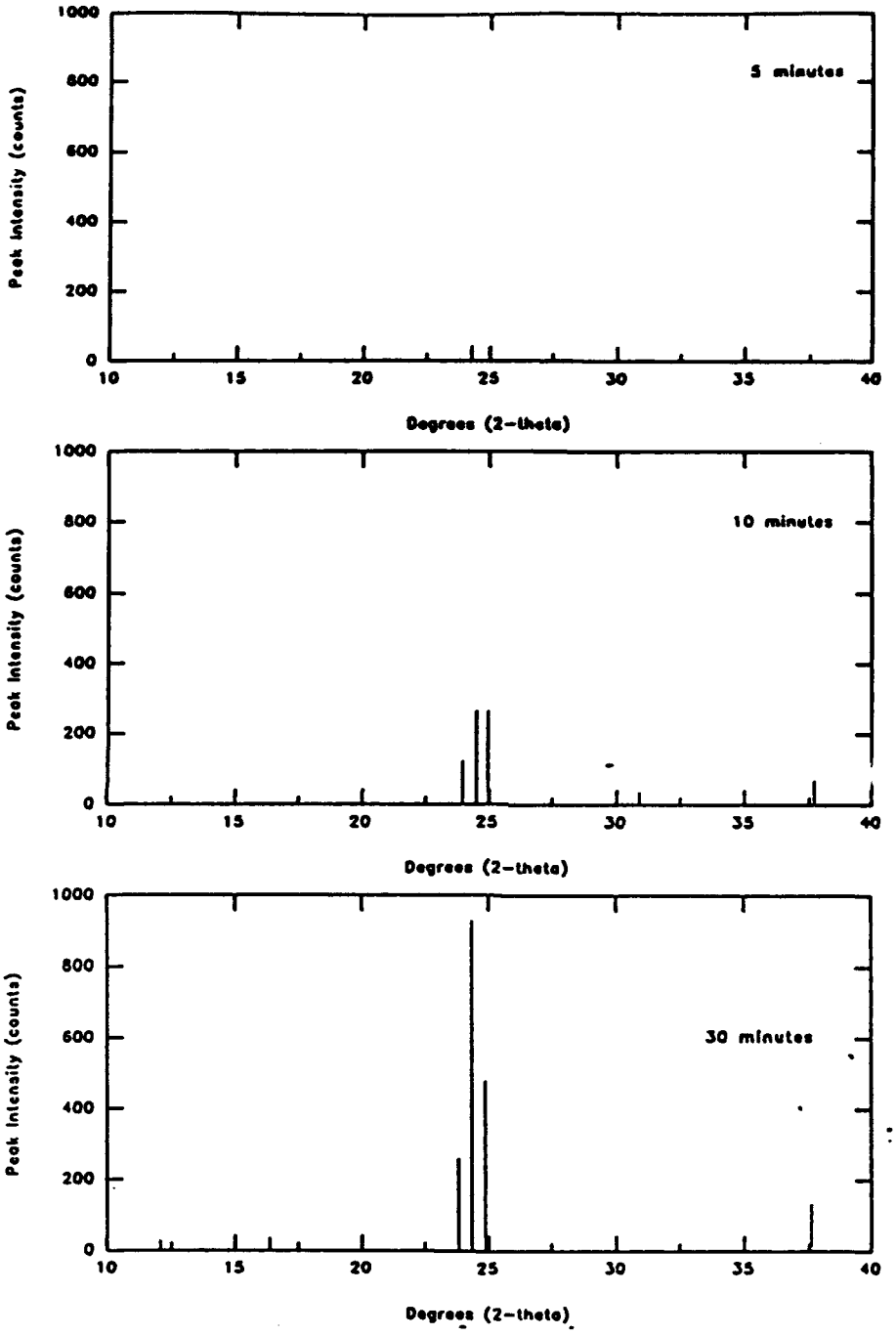

Figure 3. X-ray diffraction patterns for specimens heat treated at 450°C using microwaves.

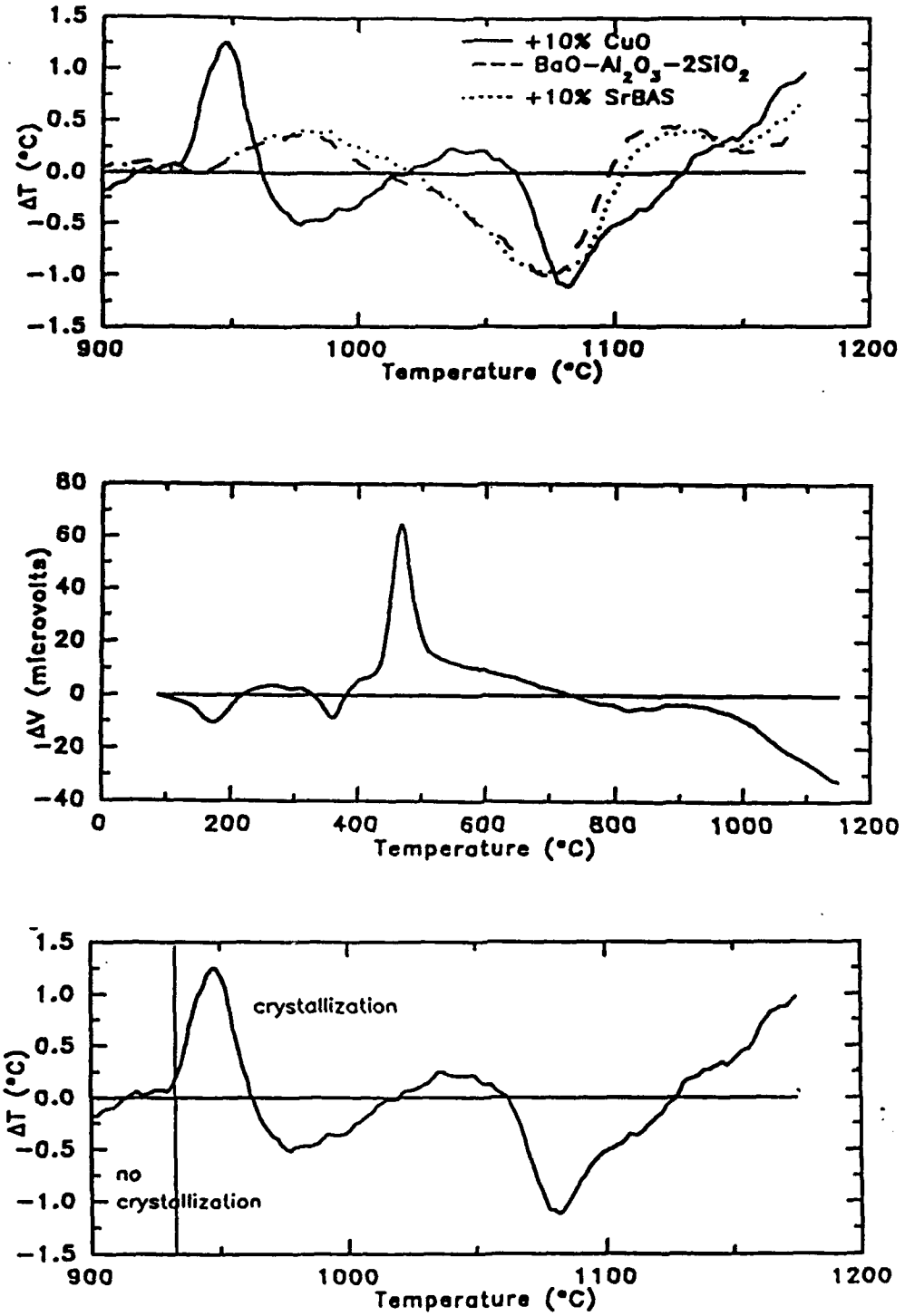

Figure 4. 4a. DTA plot of the unseeded and seeded $BaO\text{-}Al_2O_3\text{-}2SiO_2$ glass-ceramics.
4b. DTA plot of $BaO\text{-}Al_2O_3\text{-}2SiO_2$ gel derived at 50°C.
4c. DTA plot of $BaO\text{-}Al_2O_3\text{-}2SiO_2$ with 10 wt% CuO added.

Table 1. Effect of Temperature on the Relative Crystallization of Li_2O-$2SiO_2$

Heating method	Temperature (°C)	Time (minutes)	Percent crystallinity
microwave	600	10	100
conventional	600	10	6
microwave	580	10	100
conventional	580	10	0
microwave	560	10	56
conventional	560	10	0
microwave	540	10	19
conventional	540	10	0

Table 2. Effect of Time and Temperature on the Relative Crystallinity of Samples Heat-treated Using Microwave Energy.

Heating method	Temperature (°C)	Time (minutes)	Percent crystallinity
microwave	540	5	2
microwave	540	10	19
microwave	540	30	41
microwave	540	5	0
microwave	540	20	25
microwave	540	50	51

Table 3. X-ray Diffraction Results of Unseeded $BaO \cdot Al_2O_3 \cdot 2SiO_2$ After Crystallization Using Conventional and Microwave Energy.

Material	First Temp	First Time	Second Temp	Second Time	Phases Detected
Conventional					
$BaO \cdot Al_2O_3 \cdot 2SiO_2$	800°C	20 hrs	none		none
$BaO \cdot Al_2O_3 \cdot 2SiO_2$	800°C	20 hrs	1300 °C	4 hrs	hexagonal
$BaO \cdot Al_2O_3 \cdot 2SiO_2$	900°C	20 hrs	none		none
$BaO \cdot Al_2O_3 \cdot 2SiO_2$	900°C	20 hrs	1300 °C	4 hrs	hexagonal
$BaO \cdot Al_2O_3 \cdot 2SiO_2$	1050°C	20 hrs	none		hexagonal
$BaO \cdot Al_2O_3 \cdot 2SiO_2$	1050°C	20 hrs	none		hexagonal
$BaO \cdot Al_2O_3 \cdot 2SiO_2$	1300°C	4 hrs	none		hexagonal
$BaO \cdot Al_2O_3 \cdot 2SiO_2$	1300°C	72 hrs	none		hexagonal
$BaO \cdot Al_2O_3 \cdot 2SiO_2$	1500°C	4 hrs	none		hexagonal
Microwave					
$BaO \cdot Al_2O_3 \cdot 2SiO_2$	900°C	3 hrs	none		none
$BaO \cdot Al_2O_3 \cdot 2SiO_2$	1100°C	1.5 hrs	none		hexagonal

Table 4. X-ray Diffraction Results of Seeding of $BaO \cdot Al_2O_3 \cdot 2SiO_2$ Glass Crystallized Using Conventional and Microwave Energy.

Seed Material wt% unless noted	Heat Treatment Temp	Time	Phases Detected
Conventional			
(1) 5 mol% Sr → Ba	1050°C	20 hrs	hexagonal
(2) 5 mol% Sr → Ba	1250°C	20 hrs	hexagonal
(3) 15 mol% Sr → Ba	1050°C	20 hrs	hexagonal
(4) 15 mol% Sr → Ba	1250°C	20 hrs	hexagonal
(5) 1% ZrO_2	1050°C	20 hrs	hexagonal
(6) 1% ZrO_2	1250°C	20 hrs	hexagonal
(7) 10% ZrO_2	1050°C	20 hrs	hexagonal
(8) 10% ZrO_2	1250°C	20 hrs	hexagonal
(9) 1% CuO	1050°C	20 hrs	hexagonal
(10) 1% CuO	1250°C	20 hrs	hex, mono
(11) 10% CuO	1050°C	20 hrs	hex, mono
(12) 10% CuO	1250°C	20 hrs	mono, tr. hex
(13) 0.1% CuO	1300°C	4 hrs	hexagonal
(14) 0.1% CuO + 0.5% (10)	1300°C	4 hrs	hexagonal
(15) 0.1% CuO + 1% (10)	1300°C	4 hrs	hexagonal
(16) 0.1% CuO + 5% (10)	1300°C	4 hrs	hexagonal
(17) 0.5% CuO	1300°C	4 hrs	hexagonal
(18) 0.5% CuO + 0.5% (10)	1300°C	4 hrs	hexagonal
(19) 0.5% CuO + 1% (10)	1300°C	4 hrs	hexagonal
(20) 0.5% CuO + 5% (10)	1300°C	4 hrs	hexagonal
(21) 1% CuO	1300°C	4 hrs	mono, hex
(22) 1% CuO + 0.5% (10)	1300°C	4 hrs	mono, hex
(23) 1% CuO + 1% (10)	1300°C	4 hrs	mono, hex

(24) 1% CuO + 5% (10)	1300°C	4 hrs	mono, hex

Table 4 continued.

Seed Material	Heat Treatment Temp	Time	Phases Detected
Microwave			
1% CuO	1100°C	1.5 hrs	hexagonal
5% CuO	1100°C	1.5 hrs	50 hex/50 mono
10% CuO	1100°C	1.5 hrs	30 hex/ 70 mono
1% $SrO \cdot Al_2O_3 \cdot 2SiO_2$	1100°C	1.5 hrs	hexagonal
5% $SrO \cdot Al_2O_3 \cdot 2SiO_2$	1100°C	1.5 hrs	hexagonal
10% $SrO \cdot Al_2O_3 \cdot 2SiO_2$	1100°C	1.5 hrs	hexagonal